NONLINEAR FINITE ELEMENT ANALYSIS AND DESIGN OF FLEXIBLE PAVEMENTS

By

Ming-Shan Yeh

A DISSERTATION

Submitted to
Michigan State University
in partial fulfillment of the requirements
for the degree of

DOCTOR OF PHILOSOPHY

Department of Civil and Environmental Engineering

1989

ABSTRACT

NONLINEAR FINITE ELEMENT ANALYSIS AND DESIGN OF FLEXIBLE PAVEMENTS

By

Ming-Shan Yeh

A nonlinear finite element program called MICH-PAVE has been developed for use on personal computers to aid the routine design of flexible pavements. Three major achievements have been accomplished in this research. First, a new concept of utilizing a flexible boundary in pavement analysis has been introduced, and its characteristics fully investigated. Second, an extremely "user-friendly" nonlinear finite element program for pavement analysis and design has been implemented on personal computers. Third, two empirical equations to predict fatigue life and rut depth have been developed for use with nonlinear finite element analysis.

In the MICH-PAVE program, the pavement is represented by an axisymmetric finite element model, and the resilient modulus model together with the Mohr-Coulomb failure criterion is used to characterize the nonlinear material response of granular and cohesive soils. Extrapolation and interpolation techniques have been used to improve stresses and strains at layer boundaries. Results from a variety of analyses have been compared with exact solutions (when available), and with the results from existing computer programs. Extensive sensitivity analyses have also been performed to explore the capabilities and limitations of the program.

ACKNOWLEDGMENTS

The author would like to express his deepest gratitude to his major advisor Prof. Ronald Harichandran and co-advisor Prof. Gilbert Baladi for their guidance and encouragement throughout this research. Gratitude is also expressed to the doctoral committee members Professors Robert Wen and David Yen for their useful comments. The auther expresses special thanks to his colleague C.M. Lee for his valuable suggestion during the early development of the finite element program, and to his wife, Seok Yan Yeh, for her many encouragements, support, and help during this study.

Finally, the author gratefully acknowledges the financial support provided by the Michigan Department of Transportation for this research.

TABLE OF CONTENTS

LIST OF TABLES

TABLE

LIST OF FIGURES

FIGURE

CHAPTER 1

INTRODUCTION

In recent years pavement design is being done more and more based on mechanistic analysis. The migration from empirical methods to mechanistic analysis has been facilitated by the availability of relatively inexpensive microcomputers that can be used in daily practice. Early mechanistic analysis computer programs (such as CHEV5L, BISAR, ELSYM5, etc.) modeled pavemments as being composed of linear elastic layers, and computed deflections, stresses, and strains within a pavement arising from a single circular wheel load. Each pavement layer is assumed to extend infinitely in the horizontal directions, allowing the three-dimensional problem to be reduced to an axisymmetric two-dimensional problem. Due to the linear elastic assumption, multiple wheel loads can be analyzed by superposing the results due to single wheel loads.

The main drawbacks of the linear elastic layer programs are that: (a) they cannot represent the nonlinear resilient behavior of granular and cohesive soils; (b) they normally assume weightless material; (c) they may yield tensile stresses in granular material, which cannot physically occur; and (d) they do not represent "locked-in" stresses due to compaction during construction. In order to overcome these shortcomings, nonlinear analysis programs based on the finite element method have been developed (e.g. ILLI-PAVE, etc.). However, due to the large memory and computational effort requirements, they have been implemented on mainframe computers. Further, the interaction of the user

with these programs, in terms of data input and interpretation of the output, are not "friendly" precluding their use in daily practice.

For most state highway agencies, a "user-friendly" flexible pavement program can be used for the design or rehabilitaion of flexible pavements in daily practice is desired. And this program should consider all the major factors affecting the design or rehabilitation of the flexible pavements. In order to achieve this, the main goal of this research was to review existing analysis and design methods, and then to develop a "user-friendly" program that can be used on personal computers in daily practice. Since current personal computers have limited memory capacities, the traditional finite element method which requires large amount of memory cannot be suitably implemented on them for nonlinear pavement analysis. In order to overcome this, Harichandran and Yeh (1988) proposed a new technique of placing a relatively shallow finite element mesh on a flexible boundary. This technique substantially reduces the memory and computational requirements of the nonlinear finite element method, without significantly sacrificing accuracy. In this research, this technique is implemented together with extremely user-friendly input and output features, to develop a nonlinear finite element flexible pavement analysis program on personal computers, for daily use by state highway agencies. The program has been named MICH-PAVE.

Chapter 2 contains a review of relevant design methods and material models for designing flexible pavements. In general, there are two different design approaches, empirical methods, and mechanistic-empirical (rational) methods. The former are developed on the basis of functional failure criteria, while the latter are based upon various

structural failure criteria.

Three empirical methods are briefly reviewed at the beginning. These are the AASHTO, the National Stone Association (NSA), and the California methods of design. Following this, eight mechanistic-empirical analysis and design computer programs are briefly reviewed. These are the Chevron, CHEV5L, ELSYM5, CHEVIT, BISAR, DAMA, VESYS-II, and ILLI-PAVE programs. The advantages and disadvantages/limitations of each design method/program is discussed.

Four material models such as the hyperbolic stress-strain relationship, the resilient modulus model, shear and volumetric stress-strain relationship (also called contour method), and the third order hyperelastic model are briefly reviewed. The advantages and disadvantages/limitations of these material models are also discussed.

Chapter 3 presents an overview of linear finite element analysis. The advantages and disadvantages of four finite element models are discussed here. They are the sandwich plate theory model, the plane strain model, the three dimensional finite element model, and the axisymmetric model. The reasons for selecting the axisymmetric model for implementation in the MICH-PAVE program are also outlined.

The first part of this chapter discusses the formulation of the axisymmetric element stiffness matrix, assembling of the global stiffness matrix, formulation of the edge loads, and the solution of the stiffness equations. The second part covers the new concept of locating a flexible boundary at the bottom of the finite element mesh. The technical representation of the flexible boundary is discussed, and results obtained by utilizing it in linear analyses are compared with other linear methods. Finally, the sensitivity of the linear analysis

results to the location of the flexible boundary, the tire pressure, and the wheel load is investigated.

Chapter 4 deals with nonlinear finite element analysis including: (a) the selection of suitable material models; (b) use of the Mohr-Coulomb failure criterion to modify the principal stresses in the granular layers and roadbed soil (Raad et al., 1980); (c) sensitivity studies of the results of nonlinear analysis to the location of the flexible boundary, and magnitude of the tire pressure and wheel load; (d) the automatic generation of the finite element mesh; (e) the incorporation of the gravity stress and lateral "locked-in" stress due to compaction; (f) recovery of the global stresses from the modified principal stresses; (g) the use of interpolation and extrapolation to improve the accuracy of stresses and strains at layer interfaces.

In chapter 5, the linear elastic part of the MICH-PAVE program is validated by comparison of its results with those obtained from the commercial finite element program, SAP-IV (Bathe, et al.,1973). The results are also compared with those obtained from the linear elastic layer program, CHEV5L. In addition, the nonlinear part of MICH-PAVE program is compared with the nonlinear finite element program, ILLI-PAVE. A method of estimating "equivalent resilient moduli" for granular layers and roadbed soil based on nonlinear finite element analysis is introduced, These equivalent moduli can subsequently be used in linear analysis programs such as CHEV5L.

In Chapter 6, two empirical equations for estimating the fatigue life and rut depth of flexible pavements based on the results obtained from mechanistic analysis are presented (Baladi, 1989). The sensitivity of the fatigue life and rut depth due to variations in key properties

and response values, such as the tensile strain at the bottom of the asphalt concrete layer, the compressive strain at the top of the roadbed soil, and the surface deflection, etc., are examined.

The final chapter, Chapter 7, presents the conclusions of the research and recommendations for future work in this area.

CHAPTER 2

LITERATURE REVIEW

2.1 : GENERAL

The classical definition of flexible pavements, as stated by Yoder and Witczak (1975), includes those pavements that have an asphalt concrete surface. An asphalt pavement may consist of a thin wearing surface course built over a base course, subbase course, and compacted roadbed soil. Thus, the term pavement herein implies all the layers (courses) in the pavement structure. The load carrying-capacity of a flexible pavement is brought about by the load distribution characteristics of the layered system. The highest quality layer is placed at or near the surface. Hence, the strength of the pavement is the result of building up thick layers and, thereby, distributing the load over the relatively weak roadbed soil (Yoder, et al. 1975).

The structural design of flexible pavements is an evolutionary process which is continually changing as new data becomes available. This process involves the design of the supporting foundation (roadbed soil), subbase, base (may be asphalt treated), and the asphalt course. In the early stages of development, design and/or evaluation of flexible pavements consisted of rule-of-thumb procedures based on judgement and past experience. In the 1920's, the U.S. Bureau of Public Road (BPR)[1] developed a soil classification system based upon field observation of soil behavior under highway pavements (Baladi, et al., 1989). This system, in conjunction with the accumulated data, helped the highway

1. The Bereau of Public Road is now known as the Federal Highway administration.

engineer to correlate pavement performance with roadbed soil types.

After World War II, highway engineers were faced with the need to design and predict the performance of pavement systems subjected to greater loads and frequencies than they had ever experienced (Yoder, et al., 1975; Baladi, et al, 1989). Therefore, new empirical/rational pavement design procedures were introduced and implemented in the early 1950's that resulted in a better pavement design process, although severe breakup was still a common phenomenon on some highways (Yoder, et al., 1975; Baladi, et al, 1989).

Beginning in the early 1960's, new analytical pavement design techniques started to emerge. Elastic and viscoelastic layered pavement models and finite element models were developed, and are slowly being tried across the country. These new structural models provide the pavement engineer with a better understanding of pavement behavior and performance. One drawback (as perceived by some engineers) is that the models require new types of data to be collected prior to their use. Consequently, combinations of analytical, empirical, and statistical pavement design methods were developed and implemented by some highway agencies. Other agencies adopted a standard cross-section for the design of flexible pavements. Still others directed their engineers and researchers to look for better solutions (Baladi, et al, 1989).

2.2 : DESIGN METHODS FOR FLEXIBLE PAVEMENT STRUCTURE

In general, two classes of pavement failure and/or distress can be found: structural and functional. The former is associated with the inability of the pavement to carry the design load. The latter deals mainly with ride quality (a smooth and comfortable ride at the posted

speed limits) and safety (loss of skid resistance and hydroplaning due to rutting) issues (Baladi, et al., 1989). Pavements that exhibit structural distress and/or failure (e.g. severe alligator cracking) will also exhibit functional distress and/or failure. Functionally distressed and/or failed pavements (e.g. very rough) may nevertheless be structurally sound. Each class (functional or structural) of pavement distress and/or failure usually contains several types of distress and/or failure (e.g. fatigue failure, rutting, block cracking, etc.) (Baladi, et al.,1989).

Beginning in the early 1950's, several rational and empirical pavement design methods were developed. The former were based upon various structural failure criteria, while the empirical methods were developed on the basis of functional failure criteria. Efforts to perfect both empirical and rational design methods have been focused in two areas. The first of these is a proper characterization of the paving materials. The second is based on limiting the deflections and strains in the pavement structure. Further, in order to calculate the stresses, strains, and deflections of the pavement layers, several theoretical analysis methods were developed. These include : elastic, viscoelastic, transfer function, and nonlinear finite element methods.

A brief literature review of the empirical and theoretical pavement design methods are presented in the subsequent sections.

2.2.1 : Empirical Methods

As noted above, several empirical methods for the design of flexible pavements were developed. Each method has its own philosophy and is based upon certain assumptions, experience, and criteria. Hence, it is

not uncommon, for the same input variables, to obtain different layer thicknesses using different methods. Nevertheless, three of these methods: the AASHTO, the National Stone Association (NSA), and the California method of design are briefly reviewed.

The major advantage in using empirical mehtods is that they tend to be simple and easy to use. Unfortunately, they are usually only accurate for the exact conditions for which they have been developed. They may be invalid outside the range of variables used in the development of the methods.

2.2.1.1 : AASHTO Flexible Pavement Design

The AASHO flexible pavement design procedure is based upon the results of the AASHO Road Test conducted in Ottawa, Illinois, in the late 1950's and early 1960's. Based upon the Road Test results, the AASHO Committee on Design published an Interim Design Guide in 1961 and issued a revised edition in 1972. A new revision of the AASHTO Design Guide was published in 1986.

The current guide retains modified AASHO Road Test performance prediction equations as the basic models for use in pavement design. Major flexible pavement design procedure changes have been made in several areas including:

1. Incorporation of a design reliability factor, based upon a variation in the magnitude of the design traffic to allow the designer to use the concept of risk analysis for various classes of highways.
2. Replacement of the soil support number with the resilient modulus (AASHTO T274) to provide a rational testing procedure for

defining material properties.

3. Use of the resilient modulus test for assigning layer coefficients to both stabilized and unstabilized material.
4. Provision of guidance for the construction of subsurface drainage systems and modifications to the design equations to take advantage of improvements in performance that result from good drainage.
5. Replacement of the subjective regional factor with a rational approach to the adjustment of designs to account for environmental conditions such as moisture and temperature variations.

The 1986 AASHTO flexible pavement design method considers the following general design variables: time constraints (include performance and analysis periods), traffic, reliability, environmental impacts, and performance criteria.

1. Time constraints - The selection of various performance and analysis periods forces the designer to consider several design strategies which range from a low-maintenance structure to staged construction options. The performance period is the period of time that elapses as a new or rehabilitated pavement structure deteriorates from its initial serviceability to its terminal serviceability and requires rehabilitation. The designer must select minimum and maximum allowable bounds on the performance period. The analysis period is the period of time that any design strategy must cover. The analysis period may be identical to the selected performance period. However, realistic practical performance limitations for some pavement designs may necessitate

the consideration of staged construction or planned rehabilitation to achieve the desired analysis period. The AASHTO design guide recommends that the analysis period be selected to include at least one rehabilitation of the pavement.

2. Traffic - The AASHTO Flexible pavement design methods are based on the cumulative number of expected 18-kip equivalent single-axle loads (ESAL), during the analysis period.
3. Reliability - Design reliability refers to the degree of certainty that a given design alternative will last for the entire analyis period. The AASHTO design-performance reliability is controlled through the use of a reliability factor that is multiplied by the design period traffic prediction to produce design load applications for use in the design equations. For a given reliability level, the reliability factor is a function of the overall standard deviation which accounts for standard variation in material properties and construction practices, the probable variation in the traffic prediction, and the normal variation in pavement performance for a given design traffic.
4. Environmental Impacts - Temperature and moisture changes have substantial effects on the strength, durability, and load-carrying capacity of the pavement and roadbed materials through the mechanics of swelling soils, frost heave, and other phenomena. Criteria for modifying the input requirements and for adjusting the pavement performance period due to environmental conditions are provided in the AASHTO design guide.
5. Performance criteria - The serviceability of a pavement is defined as its ability to serve the type of traffic that uses the

facility. The primary measure of serviceability used by the AASHTO procedures is the present serviceability index (PSI), which ranges from a minimum of 0 (representing impossible conditions) to a maximum of 5 (representing perfect conditions). The AASHTO flexible pavement design equation is given below:

$$\log_{10}W_{18} = Z_R*S_o + 9.36*\log_{10}(SN+1) - .20 + \frac{\log_{10}(\Delta PSI/(4.2-1.5))}{.4 + 1094/(SN+1)^{5.19}} + 2.32*\log_{10}(MR) - 8.07 \qquad \text{(Eq.2-1)}$$

Where :

W_{t18} = the number of 18-kip single-axle load repetitions;

SN = the structural number;

ΔPSI = the design serviceability loss;

Z_R = reliability factor;

S_o = standard deviation; and

MR = effective roadbed soil resilient modulus.

In addition, the AASHTO flexible pavement design procedure provides means to adjust the layer coefficients to take into account the effects of certain levels of drainage on pavement. Therefore, the structural number equation modified for drainage becomes :

$$SN = a_1h_1 + a_2h_2m_2 + a_3h_3m_3 \qquad \text{(Eq.2-2)}$$

Where:

a_1, a_2, a_3 = layer coefficients for surface, base, and subbase, respectively;

h_1, h_2, h_3 = layer thicknesses for surface, base, and subbase, respectively;

m_2, m_3 = drainage modifying factors for base, and subbase, respectively.

A set of nomographs and computer program (DNPS86) were developed to aid the pavement designer in evaluating the influence of design

variables on the final thickness and to examine the various design (AASHTO, 1986).

The 1986 AASHTO design procedures have several limitations including (ERES, 1987; Baladi, et al., 1989) :

1. Limited Materails and Subgrade - The AASHO Road Test used a specific set of pavement materials and one roadbed soil. The extrapolation of the performance of these specific materials to general applications may be dangerous.
2. No Mixed Traffic - The AASHTO Road Test accumulated traffic on each test section by operating vehicles with identical axle loads and axle configurations. In-service pavements are exposed to many different axle configurations and loads.
3. Short Road Test Performance Period - The number of years and heavy axle load applications upon which the design procedure is based represents only a fraction of the design age and load applications that many pavements must endure.
4. Load Equivalency Factors - The load equivalency factors used to determine cumulative 18-kip ESAL pertain specifically to the road test materials, pavement composition, climate and subgrade soils. The accuracy of extrapolating them to other regions, material and environment, is not known.
5. Variability - A serious limitation of the AASHTO design procedure is that it is based upon very short pavement sections where construction and material quality were highly controlled. Typical highway projects are normally several miles in length and contain much greater construction and material variability.

6. Lack of Guidance on Some Design Input - Structural coefficients and drainage modifying factors are very significant in influencing flexible pavement layer thickness and there is very little guidance given in the guide.

Successful use of the AASHTO Guide requires considerable experience and knowledge of the assumptions and underlying basis for design. It is strongly recommended that the resulting design be checked using other procedures and mechanistic analysis (Baladi, et al., 1989).

2.2.1.2 : National Stone Association Design Method

The National Stone Association (NSA, 1972) design method is based upon the U.S. Corps of Engineers (1961) pavement design procedure which uses a modified California Bearing Ratio (CBR) to determine the strength of roadbed soil (Baladi, et al., 1989). The NSA method incorporates crushed stone-base course as a part of the pavement system. The basis of the method is to provide adequate thickness and material quality to prevent repetitive shear deformation within any layer and to minimize the effects of frost-action.

The NSA design method uses only two basic input criteria to determine the total thickness of the pavement structure. The first is the strength of the roadbed soil as determined by its CBR. The second is the amount of traffic (18-kip ESAL applications) estimated to travel the roadway over a twenty year design life. The total pavement thickness is obtained from a design table using the CBR and Traffic values. The total thickness is then divided into asphalt concrete (AC) and granular base layers. A minimum thickness of AC is required for each particular level

of traffic.

The advantages of this method are (Baladi, et al., 1989):

1. The method is simple to use.
2. The input requirements are minimal and usually easy to obtain.
3. The method has been revised as necessary through long-term monitoring of performance of in-service pavements.

The disadvantages of this method are:

1. The strength properties of each layer above the roadbed soil are not considered.
2. The time and temperature dependence of the AC layer is ignored.
3. A stabilized base layer is not an option using this method.
4. Uncertainty and variability in performance may result from the application of a generalized design procedure to a site-specific condition.
5. The minimum thickness of AC is not always sufficient to withstand the design traffic.

2.2.1.3 ; California Method of Design

The California method of design is based on two properties of the paving materials: Cohesion which is obtained using a cohesionmeter, and stabilometer resistance value (R) obtained using a stabilometer. The R value is used along with equivalency factors to design the pavement structure (Baladi, et al., 1989).

The required thickness of gravel equivalent (GE) above each material is determined using the following equation:

$$GE = 0.0032(TI)(100-R) \qquad \text{(Eq.2-3)}$$

where

GE = gravel equivalent;

TI = traffic index which is a function of the amount of equivalent 5 kip wheel loads;

R = stabilometer value.

The actual thickness of each layer is then determined by dividing the GE by an appropriate equivalency factor.

The advantages of this method is that it is simple and easy to use. However, the simple form becomes a drawback because the AC properties are neglected. Another disadvantage of this method is that the equivalent 5 kip wheel load is far less than the current wheel loads on the highways (Baladi, et al., 1989).

2.2.2 : Mechanistic-Empirical Methods

The basic components of mechanistic-empirical or rational methods consist of a structural analysis of the pavement system and the incorporation of distress or performance functions into the method.

Structural analysis refers to the calculation of stress, strain, and deflection developed in a pavement section due to traffic loads, temperature, and/or moisture. Once these values are determined at critical locations in the pavement structure, comparisons can be made with the maximum allowable values obtained from experimental or theoretical studies based on predictions of pavement distress such as cracking, rutting, or roughness. The pavement can then be designed by adjusting the different layer thicknesses so that the calculated stresses, strains, and deflections are less than the maximum allowable values.

Mechanistic flexible pavement design procedures are typically based on the assumption that a pavement can be modeled as a multi-layered elastic or visco-elastic structure on an elastic or visco-elastic foundation. Assuming that pavements can be modeled in this manner, it is possible to calculate the stress, strain, or deflection due to traffic loadings and environmental conditions at any point within or below the pavement structure. However, researchers have recognized that pavement performance is influenced by a number of factors that cannot be precisely modeled by mechanistic methods. Therefore, these methods were calibrated using field observations of pavement performance. Thus, the methods are referred to as a mechanistic-empirical design procedures.

An important advantage of this design philosophy is the ability to analyze a pavement for several different failure modes such as cracking and permanent deformation (rutting). This allows the engineer to adjust the pavement design and to produce a cost-effective pavement section that does not fail prematurely.

The main disadvantage of this design method is that it requires more comprehensive and sophisticated data than empirical design mehtods. Extensive laboratory and field testing may be required to determine the design parameters such as the resilient modulus, creep compliance, and others.

Nevertheless, most of the mechanistic-empirical design methods have been computerized. Several of these methods are presented in the subsequent sections.

2.2.2.1 : Chevron Program

The Chevron program (developed by the Chevron Oil Company) is based on Burmister's linear layered elastic solution. The basic assumptions behind Burmister's theory in relation to pavement structures are:

1. Single-wheel loads that are vertical, uniformly distributed over a circular area, and statically applied.
2. Each pavement layer consists of a homogeneous, isotropic, and linear elastic material.
3. There is continuous contact between each interface of the layered pavement.
4. Each layer is infinite in the horizontal directions and has a finite depth, except for the bottom layer which has an infinite depth.
5. Deformations of the pavement are small.
6. Temperature effects are neglected.
7. The pavement is weightless.

The Chevron program has been widely used in the analysis and design of flexible pavement structures. The program is relatively easy to use and requires little computer time. The disvantages of the Chevron program include:

1. It neglects the effects of the pavement weight.
2. It cannot model the nonlinear behavior of the granular layers and roadbed soil.
3. It is limited to a single wheel load.

Several modifications of the Chevron program were made. These include:

1. The CHEV5L program which is capable of handling dual loads and up to 5 layers.
2. The ELSYM5 program which is designed for a microcomputer, and can handle up to 5 layers and 10 wheel loads (Kopperman, et al., 1985).
3. The CHEVIT program which includes iterative procedures to determine the stress-dependent moduli of pavement materials and a superposition subroutine for multiple-wheel loads (Chou, 1976). However, the CHEVIT program assumes that the material moduli in the horizontal direction are constant. This is true if the applied stresses are small such as in the roadbed soil. In the base layer where the stresses are high, the assumption leads to a certain degree of error.

2.2.2.2 : The Shell Method

The shell method uses a set of design charts for the design of the flexible pavement structures (Claessen, et al., 1977). The charts include combinations of AC and unbound base layers thicknesses for various mean annual temperatures, mixes of AC, and roadbed soil moduli.

The shell method for flexible pavement design has been computerized (BISAR), and calculates stresses, strains, and deflections at any point in the pavement under vertical and/or horizontal surface loads. In concept, the shell method program is similar to the Chevron method, except that it is capable of applying horizontal surface loads and assuming partial or zero friction at the interface between the layers (De Jong, et al., 1973).

The BISAR program incorporates several primary and secondary criteria in the design of pavement structures. The primary criterion is based on limiting the compresive strain at the top of the roadbed soil and the horizontal tensile strain at the bottom of the AC course. The second criterion is based on limiting stresses in the cemented base layers, permanent deformation of the AC, and others.

2.2.2.3 : The Asphalt Institute Design

The Asphalt Institute design procedure can be used to design an asphalt pavement composed of various combinations of asphalt surface and base, emulsified asphalt surface and base, and untreated aggregate base and subbase.

The original Asphalt Institute design methodology was an empirical approach based upon data from the AASHO Road Test, and other various state and local test road sections. The procedure was completely revised in 1981 and the current procedure uses multi-layer linear elastic theory for the determination of the required pavement thickness (ERES, 1987; Baladi, et al., 1989).

A computer program DAMA was used in the development of the design procedure to examine two critical stress-strain conditions (The Asphalt Institute, 1983). The first is the maximum vertical compressive strain induced at the top of the roadbed soil due to a wheel load. The second is the maximum horizontal tensile strain induced at the bottom of the AC layer. For a given set of design variables, either the vertical compressive strain at the top of the roadbed soil or the horizontal tensile strain at the bottom of the AC course governs the required

pavement thickness (The Asphalt Institute, 1981)

The major design considerations required for the structural design of flexible pavements using the Asphalt Institute procedure include the selection of design variables for traffic, roadbed soil strength, material properties, and environmental conditions.

1. Traffic - The traffic analysis procedure used by the Asphalt Institute is based on the load equivalency factor developed at the AASHO Road Test. The traffic variable required for design is the total number of ESAL applications that the pavement structure will sustain over the pavement design period.
2. Roadbed soil strength - The roadbed soil is characterized by the resilient modulus (MR). The value of the resilient modulus used in this design procedure is that under unfrozen conditions, excluding periods when the roadbed soil is frozen or when it is undergoing thaw.
3. Material Properties - The properties of the paving material are characterized by the elastic modulus and Poisson's ratio.
4. Environmental conditions - The Ashalt Institute method considers the effects of temperature and seasonal variations on pavement thickness design by adjusting the asphalt concrete modulus, the roadbed soil resilient modulus, and the modulus of the granular materials. The effects of moisture and drainage on pavement design are not considered directly in the method.

The Asphalt Institute design procedure consists of the following steps:

1. Determination of the roadbed soil resilient modulus.
2. Selection of material types to be used in the design of the surface and base layers.

3. Determination of the equivalent single-wheel load (ESWL) to be carried by the pavement over the design period.

4. Determination of layer thicknesses by using various design charts.

The major limitation of the Asphalt Institute procedure is that it does not consider environmental effects directly in the procedure. While there is an attempt to account for environmental effects in the roadbed soil resilient modulus and in the asphalt grade to be used, it does not accurately account for major climatic considerations such as seasonal variation in moisture.

Another problem lies in the limited environmental applicability of the design charts. They contain a mean annual air temperature of only 60°F, which accurately represents only a portion of the United States.

2.2.2.4 ; VESYS (Visco-Elastic System) II Computer Program

The VESYS II program developed at the Massachusetts Institute of Technology (Soussou, et al., 1973) consists of five subsystems: structural, maintenance, cost, decision, and optimization. The VESYS II program models the pavement structure using a three-layer system. The upper two layers have finite thicknesses while the third layer is infinite. All layers have infinite dimensions in the horizontal directions. Each layer may have elastic and/or viscoelastic properties.

The VESYS structural subsystem consists of a primary response model, a damage model, and a serviceability model. In the primary response model, variations in matertial properties are accounted for using Monte Carlo techniques. A closed form probabilistic solution of the response of the layered system to an axisymmetric stationary or moving load applied at the surface is obtained. The probabilistic estimates of

stresses, strains and deflections, the loading characteristic, and the temperature history are used as inputs to the damage model to obtain the extent of rut depth, roughness or slope variance, and the extent of cracking. The distress indicators obtained from the damage model are combined using the AASHO equation to provide a subjective measure of the Present Serviceability Index (PSI). VESYS II was modified and the new version is capable of analyzing an N-layered viscoelastic system (Huffred, et al., 1978)

The advantages of the VESYS computer program include:

1. It models both the elastic and viscoelastic responses of the pavement structure.
2. It considers variations in material properties, environmental factors, and wheel loads.
3. The program is capable of conducting cost analysis of various pavement sections, which results in the design of a structurally sound and cost effective pavement section. Thus, the program considers various aspects of pavement design.

The main disadvantages of the VESYS computer program is that it requires complex material input data that are not readily available at most state highway agencies.

2.2.2.5 : Nonlinear Finite Element Method

Raad and Figueroa (1980) used the Mohr-Coulomb failure criterion to modify the stresses calculated using a finite element method (FEM) at the end of each iteration so that the principal stresses in the granular and roadbed soil layers do not exceed the strength of the material as defined by the Mohr-Coulomb envelope.

Thompson (1986) used the above algorithm to develope the ILLI-PAVE program which is a nonlinear FEM.

The features of the ILLI-PAVE program include:

1. It uses nonlinear material models.
2. It uses the Mohr-Coulomb failure criterion to modify the computed principal stresses such that the radial stresses within the granular material or roadbed soils are always compressive.
3. The analysis time (convergence to the final solution) is faster than other nonlinear FEM programs.
4. The program uses a very deep mesh to represent the infinitely deep roadbed soil. Hence, it requires a large amount of computer memory.
5. The program does not account for the viscoelastic response and temperature effects on the AC material.
6. The program assumes axisymmetric loading.

2.3 : MATERIAL CHARACTERIZATION

Regardless of the mechanistic design procedure used in the pavement design, the accuracy and adequacy of the design are functions of the employed material model.

Linear material models have been used for a period of time. However, field data, shows that most paving materials have nonlinear behavior. In general, two kinds of nonlinearity can be found: geometric, and material. Since the deformations of pavements are small compared to their depth, it is not necessary to consider geometric nonlinearity. Only stress-strain nonlinearity needs to be considered. The essential computational problem of material nonlinearity is that equilibrium

equations must be written in terms of material properties which are dependent on the induced strains and stresses, which are not known in advance.

Dehlen and Monismith (1970) applied an approximate nonlinear elastic analysis to a full-depth asphalt pavement overlaying a sandy clay. Their results showed that , for engineering purposes, linear elastic theory could be used with some degree of confidence for full-depth asphalt concrete but not for pavement systems which have non-cohesive soils (granular materials) close to the surface. Hence, several nonlinear material behavior models were developed. A summary of some of these models is presented below.

2.3.1: Hyperbolic Stress-Strain Relationship

The original hyperbolic stress-strain relationship was developed by Duncan and Chang (1970). The model uses a constant value of Poisson's ratio and the tangent value of the elastic modulus (E_t) which varies with the magnitude of the applied stress. More recently the accuracy of the model has been improved by using values of the bulk modulus which varies with the confining stress.

The hyperbolic stress-strain relationship, which was developed for the incremental analysis of soil deformations, may be expressed as

$$\sigma_1-\sigma_3 = \frac{\epsilon}{\frac{1}{E_i} + \frac{\epsilon}{(\sigma_1-\sigma_3)_{ult}}} \qquad \text{(Eq.2-4)}$$

where

σ_1 = the major principal stress (psi);

σ_3 = the minor principal stress (psi);

ϵ = the axial or major principal strain (in./in.);

E_i = the initial tangent modulus (psi);

$(\sigma_1-\sigma_3)_{ult}$ = the asymptotic value of stress difference (psi).

The initial tangent modulus (E_i) can be expressed in terms of the minor principal stresses using the relation suggested by Janbu (1963).

$$E_i = K \times P_a(\sigma_3/P_a)^n \qquad \text{(Eq.2-5)}$$

where

K,n = modulus constants;

P_a = atmospheric pressure (psi).

The value of the asymptotic stress $(\sigma_1-\sigma_3)_{ult}$ is often found to be somewhat larger than the stress difference at failure, $(\sigma_1-\sigma_3)_f$, these two values may be related as follows:

$$(\sigma_1-\sigma_3)_f = R_f(\sigma_1-\sigma_3)_{ult} \qquad \text{(Eq.2-6)}$$

where

$(\sigma_1-\sigma_3)_f$ = the compressive stress difference at failure;

R_f = the failure ratio which is always smaller than unity, and varies from 0.5 to 0.9 for most soils.

The variation of soil strength $(\sigma_1-\sigma_3)_f$ with σ_3 using the Mohr-Coulomb failure criterion can be expressed as:

$$(\sigma_1-\sigma_3)_f = \frac{2c\cos\phi + 2\sigma_3\sin\phi}{1-\sin\phi} \qquad \text{(Eq.2-7)}$$

where

c = cohesion (psi);

ϕ = the friction angle (degrees).

The expression of the tangent modulus E_t can be obtained from Eq. (2-4) by differentiation with respect to ϵ as follows:

$$E_t = \frac{\partial\ (\sigma_1 - \sigma_3)}{\partial\ \epsilon} = \frac{1/E_i}{[1/E_i + R_f\epsilon/(\sigma_1 - \sigma_3)_f]^2} \qquad \text{(Eq.2-8)}$$

Equation 2-8 can be simplified by using Eq.(2-4) to express ϵ in terms of stresses $(\sigma_1-\sigma_3)$, and substituting E_i and $(\sigma_1 - \sigma_3)_f$ from Eq.(2-5) and (2-7),respectively.

$$E_t = \left[1 - \frac{R_f(1 - \sin\phi)(\sigma_1 - \sigma_3)}{2c\cos\phi + 2\sigma_3 \sin\phi}\right] K\ P_a\ (\sigma_3/P_a)^n \qquad \text{(Eq.2-9)}$$

This equation can be used to calculate the appropriate value of the tangent modulus for any stress conditions[σ_3, and $(\sigma_1 - \sigma_3)$], if the values of the parameters K, n, c, ϕ, and R_f are known (Chen, et al., 1982).

The limitations of the hyperbolic stress-strain relationship include:

1: The relationships must be suitable for analysis of stresses and strains prior to failure. When elements have already failed, the results will no longer be reliable. In most elastic analysis of pavement structures, the granular layer will fail in tension. Therefore, the model cannot be used without modification. Also, the model is more appropriate for monotonic loading conditions than for repeated loadings that are encountered in pavement analysis.

2: The hyperbolic relationships do not include volume changes due to changes in shear stresses or "shear dilatancy".

2.3.2 : The Resilient Modulus

Hicks and Monismith (1972) developed nonlinear models that expresses the resilient modulus of granular material in term of

confining pressure (lateral stress) and of cohesive soils in term of the deviatoric stress (the principal stress difference $\sigma_1 - \sigma_3$).

The resilient modulus is a dynamic test response defined as the ratio of the repeated axial deviator stress to the recoverable axial strain as follow:

$$M_r = \frac{\sigma_d}{\epsilon_a} \qquad \text{(Eq.2-10)}$$

where
M_r = the resilient modulus (psi);

σ_d = the repeated axial deviator stress (psi);

ϵ_a = the recoverable axial strain (in./in.).

For granular materials, the resilient modulus can be expressed either in terms of the bulk stress or lateral stress as follows (Young, et al. , 1977):

$$M_r = K_1(\theta)^{K_2} \qquad \text{(Eq.2-11)}$$

or

$$M_r = K_1'(\sigma_3)^{K_2'} \qquad \text{(Eq.2-12)}$$

where

M_r = resilient modulus (psi);

σ_3 = confining pressure (psi);

θ = bulk stress ($= \sigma_1+\sigma_2+\sigma_3$) (psi); and

K_1, K_2, K_1', K_2' = experimental test constants.

As with static testing on granular materials, M_r modulus values increase with increasing density, decreasing saturation and increasing angularity of the particles.

For fine-grained soils, the resilient modulus can be expressed as

$$M_r = K_2 + (K_1 - \sigma_d)K_3, \text{ for } \sigma_d < K_1 \qquad \text{(Eq.2-13a)}$$

or

$$M_r = K_2 + (\sigma_d - K_1)k_4, \text{ for } \sigma_d > K_1 \qquad \text{(Eq.2-13b)}$$

where

K_1, K_2, K_3, K_4 = material constants determined by least squares curve fitting methods; and

σ_d = deviator stress ($\sigma_1 - \sigma_3$) (psi).

For granular material, Equation 2-11 was found to be more accurate than equation 2-12. Analysis of test data revealed a higher correlation coefficient and a lower standard error for (Eq.2-11) than for (Eq.2-12). The explanation for this is believed to be that (Eq.2-11) accounts for all 3 principal stresses, whereas (Eq.2-12) accounts for only 2 principal stresses.

Some limitations of using the resilient modulus models in the pavement analysis include:

1. It only considers a very limited range of stress paths.
2. The models may not be suitable for a three dimensional system, since they are based on laboratory tests with only a two dimensional state of stress.

2.3.3 : Shear and Volumetric Stress-Strain Relationship

To overcome the first limitation of the resilient modulus models and to be able to account for the effects of shear and volumetric strains, Brown and Pappin introduced shear and volumetric stress-strain relationships (Brown, et al., 1981). Their relationships can more accurately simulate the deformation and stresses within pavements. However, these relationships require seven material constants in order to compute the shear and volumetric strains. For most state highway

agency laboratories, the lack of sophisticated equipment to control the stress paths in order to estimate all the constants, has resulted in a very limited application of these relationships.

2.3.4 ; Third Order Hyperelastic model.

Ko and Mason (1976) used a complete three-dimensional third-order hyperelastic model to simulate the behavior of medium-loose Ottawa sand under loading. This classical continuum mechanics model accounts for material nonlinearity, its dependence on the hydrostatic stress, and its dilatancy and stress-induced anisotropy. The model requires nine material constants that are difficult to estimate in practice. Hence, its application remain very limited.

2.4 ; PAVEMENT EVALUATION METHODS

Several in-service pavement structural evaluation methods were developed based on nondestructive deflection testing. These include transfer functions and back-calculation of layer moduli.

2.4.1 ; Transfer Function Theory

Although transfer function theory has been applied for some time by mechanical and electrical engineers, Swami, et al. (1970) were the first to use transfer functions to characterize the time-dependent behavior of asphalt concrete in the laboratory. Boyer (1972), Highter, et al. (1974), and Baladi (1979) applied transfer function theory to in-service pavements. They measured the pavement surface deflection due to moving wheel loads and calculated the transfer function of various air field and highway pavements. They showed that the parameters of the

transfer function represented the pavement global properties that are independent of the type of load input and that the temperature of the pavement had the greatest single effect on the transfer function. Due to the nature of the transformation, however, the nonlinear behavior of the pavement materials was not accounted for.

2.4.2 Back-calculation Methods

Recently many methods for the back-calculation of layer moduli using nondestructive deflection testing have been developed. Some of the methods use the elastic layer theory while others use the finite element method. Conceptually, all methods are based on iterative routines whereby layer moduli are assumed and the the pavement surface deflection is computed. If the computed values match the field measured ones, then the calculation is terminated. It should be noted that (for most methods) the calculated layer moduli are not unique, they depend on the assumed values of the seed moduli. Moreover, various combinations of layer moduli values may exist such that the calculated deflections match the measured ones. Nevertheless, the methods are still in the developmental stage and they can be used to estimate the material properties of each layer of an existing flexible pavement.

2.5 SUMMARY

Two basic methods are currently being used to determine the required layer thicknesses for flexible pavement structures: empirical, and mechanistic-empirical or rational methods.

Empirical methods are derived from experience or observation, often without regard to system behavior or pavement theory. The advantage of

using empirical models is that they tend to be simple and easy to use. Unfortunately, they are usually only accurate for the exact conditions under which they were developed.

Mechanistic-empirical design methods utilize calculated stresses, strains, and deflections and pavement distress or performance prediction models. Mechanistic approaches are, in general, capable of analyzing a pavement structure using several different failure modes. One disadvantage is that they typically require more comprehensive and sophisticated data inputs than empirical design methods.

Several factors influence the response of pavements including temperature, material properties, water table, tire pressure and magnitude of the applied load. Several pavement design procedures were developed and computerized whereby one or several of these factors were accounted for. Each program has it own advantages and limitations.

The main limitation of the Chevron, CHEV5L, ELSYM5, and BISAR programs is that they do not account for nonlinear material responses. The CHEVIT program attempts to partially account for nonlinearities, but suffers from the drawback that any given sublayer must have the same modulus even though stresses vary with radial distance away from the load. The ILLI-PAVE program, is perhaps the only one that is capable of reasonably representing nonlinear materials. However, the large number of finite elements required for a typical analysis requires a significant amount of memory and computational time.

Four nonlinear material models can be found: the hyperbolic stress-strain, the resilient modulus, the shear and volumetric stress-strain, and the third order hyperelastic models.

The principal objectives of flexible pavement thickness design are to minimize compressive strains in the roadbed soils and to minimize the tensile strains at the bottom of the asphalt layer.

CHAPTER 3

LINEAR FINITE ELEMENT ANALYSIS

3.1 ; GENERAL

A comprehensive analysis of flexible pavements should include soil overburden, inelastic behavior of granular and cohesive material, the finite width of the pavement, and the lack of bonding between the asphalt and granular layers. Four kinds of finite element methods that may be applied in the analysis of flexible pavements are reviewed here. None of these models, however, is capable of incorporating all the above effects, therefore the method that incorporates the most important factors should be chosen.

One approach is to use a sandwich plate model of an asphalt layer with a granular base. Its main advantage is its capatility of modeling the finite width of the pavement (i.e., the edge effect). Since the nodes of the plate elements lie in the center of the thickness, it is difficult to connect them to the nodes of the brick elements representing the granular base. The unbound behavior of the granular base cannot be easily represented in this method. Kujawski and Wiberg (1982) used this technique to study rigid pavements. They assumed that the displacement vector $u = u(x,y)$ can be expressed by the sum of zero order components which are constant along the z-direction, and two angles of rotation due to pure bending and shear deformations of the plate. They also found the interaction between the plate and the three dimensional element. The vertical displacements based on their approach showed good accuracy but the horizontal displacements did not.

Furthermore, the elastic modulus of asphalt is only about one fifth of that of concrete, making this model less suitable for flexible pavements.

Another approach is to use a two dimensional plane strain model of the pavement cross section, in which both the edge effect and inelastic behavior can be modeled. However, the wheel loading would have to be considered as infinitely long in the longitudinal (out of plane) direction. This would be unrealistic because most trucks have few axles with fairly wide spacings, rather than many closely spaced axles. The problem is therefore three dimensional and cannot be simplified to a two dimensional problem if all the conditions to be investigated are retained.

The most comprehensive approach would be one that uses three-dimensional finite element (FE) analysis. In a three dimensional model, suitable boundary conditions must be imposed at some reasonable distance away from the loaded region in all three directions. Ioannides and Donnelly (1988) used the radius of relative stiffness for a slab on an elastic foundation (l_e) to decide the vertical and lateral subgrade extent. From Barkdales and Hicks's (1973) report, the tranverse distance of one side from the loading should be about 90 inches. Assuming the distance between the two wheels to be 72 inches, and allowing 90 inches outside the wheel loads, the total transverse distance is 252 inches.

$$l_e = \left[\frac{E\, h^3\, (1-\mu_s)^2}{6(1-\mu^2)\, E_s} \right]^{1/3}$$

where E : Young's modulus of slab
h : Slab thickness
μ_s : Poisson's ratio for elastic foundation
μ : Poisson's ratio for slab
E_s : Young's modulus of elastic foundation

Using a depth of 270 inches, and dividing this region into eight-node brick elements results in approximately 3240 degrees-of-freedom (d.o.f.) per 10-inch length of pavement. Dysli and Fontana (1982) used a three dimensional model to simulate a field excavation which had 3153 d.o.f.. This 3-D model was processed on a VAX 11-780 computer with 2 Mbytes of core storage and the computation required over 30 hours of CPU time. Therefore, from a pratical point of view, the use of a three dimensional model is time consuming and uneconomical. Furthermore, it should be noted that the solution of an inelastic system by the FE method requires many iterative or incremental solutions of linear problems with the stiffness matrix having to be reassembled many times. This makes the problem even longer. Thus, unless supercomputers become readily accessible, a 3-D FEM. model cannot be used for day-to day design.

The most commonly used 2-D model is the axisymmetric one. This model assumes that the pavement geometry and loading are both axisymmetric. With these assumptions, a three dimensional problem can be reduced to a two dimensional one. However, the asphalt surface must be assumed to be infinitely wide and therefore the edge effect cannot be considered. Although non-axisymmetric multiple wheel loads can be analyzed by superposition for linear elastic material, this cannot be done for nonlinear materials. Apart from multiple wheel loads and consideration of the edge effect, all other effects can be included. In comparison to the other three approaches, the axisymmetric model has significant advantages in the analysis of flexible pavements.

3.2 : AXISYMMETRIC FINITE ELEMENT ANALYSIS

3.2.1 : Formulation of Axisymmetric Element Stiffness Matrix

Cook (1981) formulates the plane linear isoparametric element which can be revised to obtain the axisymmetric element. Bathe and Wilson (1976) outline a computer program (called subroutine QUADS) which can implement plane stress, plane strain, and axisymmetric analysis. The geometry and shape of a four-node element is shown in Figures (3-1) and (3-2). The global coordinates (radial and vertical), and the corresponding displacements at an internal point can be related to the corresponding nodal quantities through shape functions:

$$\begin{Bmatrix} r \\ z \end{Bmatrix} = [N]\{C\} \text{ and } \qquad \begin{Bmatrix} u \\ w \end{Bmatrix} = [N]\{U\} \qquad \text{(Eq.3-1)}$$

where $\{C\}^T = \{r_i \; z_i \; r_j \; z_j \; r_k \; z_k \; r_m \; z_m\}$ are the coordinates of the nodes and $\{U\}^T = \{u_i \; w_i \; u_j \; w_j \; u_k \; w_k \; u_m \; w_m\}$ are the nodal displacements.

The shape function matrix is

$$[N] = \begin{bmatrix} N_i & 0 & N_j & 0 & N_k & 0 & N_m & 0 \\ 0 & N_i & 0 & N_j & 0 & N_k & 0 & N_m \end{bmatrix}$$

Sometimes it is convenient to write Equation (3-1) in the form

$$\begin{aligned} r &= \Sigma N_I \, r_I & u &= \Sigma N_I \, u_I \\ z &= \Sigma N_I \, z_I & w &= \Sigma N_I \, w_I \end{aligned} \qquad \text{(Eq.3-2)}$$

where I = i, j, k, m

The individual shape functions are

$$\begin{aligned} N_i &= 0.25(1-\xi)(1-\eta) \\ N_j &= 0.25(1+\xi)(1-\eta) \\ N_k &= 0.25(1+\xi)(1+\eta) \end{aligned} \qquad \text{(Eq.3-3)}$$

$N_m = 0.25(1-\xi)(1+\eta)$

If ϕ is some function of r and z, then applying the chain rule of differentiation yields

$$\frac{\partial \phi}{\partial \xi} = \frac{\partial \phi}{\partial r}\frac{\partial r}{\partial \xi} + \frac{\partial \phi}{\partial z}\frac{\partial z}{\partial \xi}$$

$$\frac{\partial \phi}{\partial \eta} = \frac{\partial \phi}{\partial r}\frac{\partial r}{\partial \eta} + \frac{\partial \phi}{\partial z}\frac{\partial z}{\partial \eta}$$

$$\text{or } \begin{Bmatrix} \phi,_\xi \\ \phi,_\eta \end{Bmatrix} = [J]\begin{Bmatrix} \phi,_r \\ \phi,_z \end{Bmatrix} \qquad \text{(Eq.3-4)}$$

Where [J] is the Jacobian matrix

$$[J] = \begin{bmatrix} \frac{\partial r}{\partial \xi} & \frac{\partial z}{\partial \xi} \\ \frac{\partial r}{\partial \eta} & \frac{\partial z}{\partial \eta} \end{bmatrix} = \begin{bmatrix} J_{11} & J_{12} \\ J_{21} & J_{22} \end{bmatrix} \qquad \text{(Eq.3-5)}$$

The inverse relations of equation (3-5) is

$$\begin{Bmatrix} \phi,_r \\ \phi,_z \end{Bmatrix} = [\Gamma]\begin{Bmatrix} \phi,_\xi \\ \phi,_\eta \end{Bmatrix} \qquad \text{(Eq.3-6)}$$

$$\text{where } [\Gamma] = \begin{bmatrix} \Gamma_{11} & \Gamma_{12} \\ \Gamma_{21} & \Gamma_{22} \end{bmatrix} = \frac{1}{J_{11}J_{22}-J_{21}J_{12}} \begin{bmatrix} J_{22} & -J_{12} \\ -J_{21} & J_{22} \end{bmatrix} \qquad \text{(Eq.3-7)}$$

$$J_{11} = r,_\xi = N_{i,\xi}\, r_i + N_{j,\xi}\, r_j + N_{k,\xi}\, r_k + N_{m,\xi}\, r_m \qquad \text{(Eq.3-8)}$$

There are similar expressions for J_{12}, J_{21}, and J_{22}, where

$N_{i,\xi} = -0.25(1-\eta)$

$N_{i,\eta} = -0.25(1-\xi)$ ...etc. (Eq.3-9)

The relationships between the strain and displacement vectors are

$$\begin{Bmatrix} \epsilon_r \\ \epsilon_\theta \\ \epsilon_z \\ \gamma_{rz} \end{Bmatrix} = \begin{Bmatrix} \partial u/\partial r \\ u/r \\ \partial w/\partial z \\ \partial u/\partial z + \partial w/\partial r \end{Bmatrix} \qquad \text{(Eq.3-10)}$$

It is convenient to treat the tangential strain ϵ_θ separately.

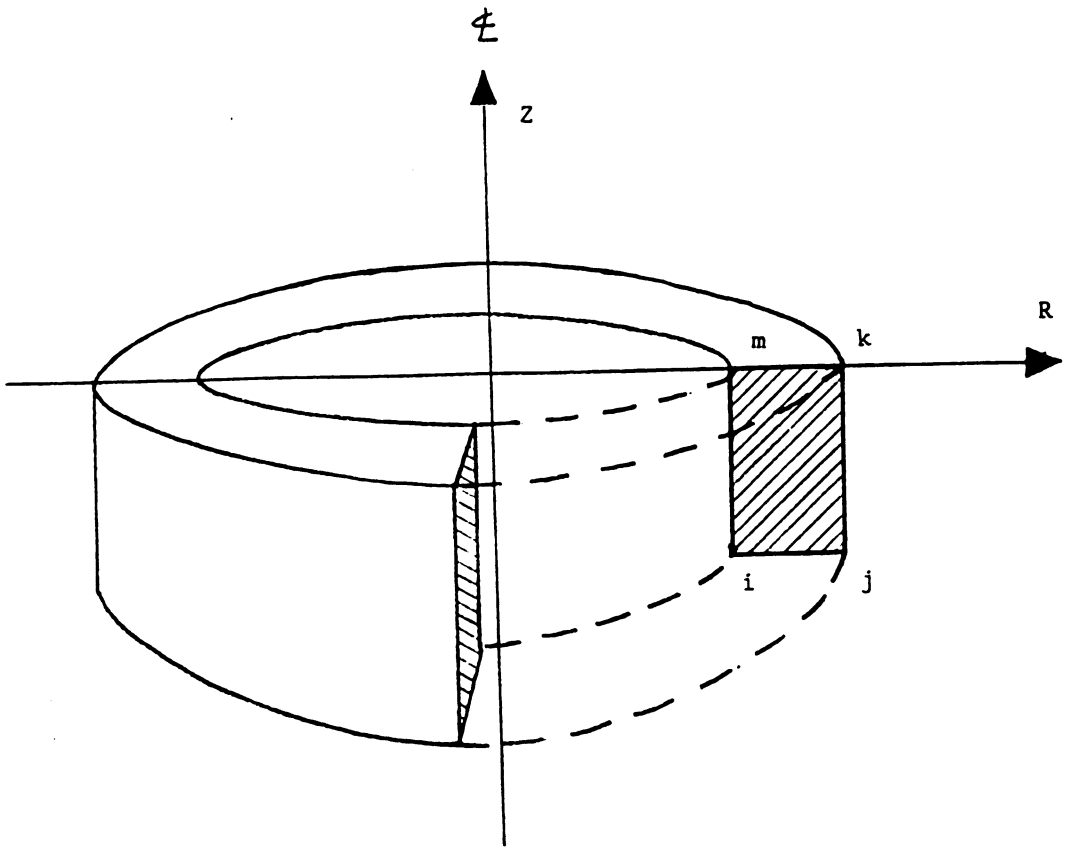

Figure 3-1 : A Typical Axisymmetric Finite Element

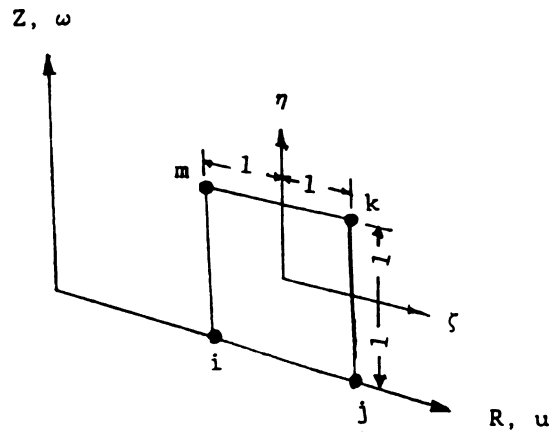

Figure 3-2 : The Four-Node Isoparametric Element

Considering ϵ_r, ϵ_z and γ_{rz} only, the strain-displacement relations can be expressed as

$$\{\epsilon\} = \begin{Bmatrix} \epsilon_r \\ \epsilon_z \\ \epsilon_{rz} \end{Bmatrix} = \begin{bmatrix} 1 & 0 & 0 & 0 \\ 0 & 0 & 0 & 1 \\ 0 & 1 & 1 & 0 \end{bmatrix} \begin{Bmatrix} u,_r \\ u,_z \\ w,_r \\ w,_z \end{Bmatrix} \qquad \text{(Eq.3-11)}$$

The displacement derivatives in the global coordinates can be related to those in the local isoparametric coordinates through

$$\begin{Bmatrix} u,_r \\ u,_z \\ w,_r \\ w,_z \end{Bmatrix} = \begin{bmatrix} \Gamma_{11} & \Gamma_{12} & 0 & 0 \\ \Gamma_{21} & \Gamma_{22} & 0 & 0 \\ 0 & 0 & \Gamma_{11} & \Gamma_{12} \\ 0 & 0 & \Gamma_{21} & \Gamma_{22} \end{bmatrix} \begin{Bmatrix} u,_\xi \\ u,_\eta \\ w,_\xi \\ w,_\eta \end{Bmatrix} \qquad \text{(Eq.3-12)}$$

Finally, the displacement derivatives in the local coordinates are expressed in term of the derivatives of the shape functions and the nodal displacements, as

$$\begin{Bmatrix} u,_\xi \\ u,_\eta \\ w,_\xi \\ w,_\eta \end{Bmatrix} = \begin{bmatrix} N_{i,\xi} & 0 & N_{j,\xi} & 0 & N_{k,\xi} & 0 & N_{m,\xi} & 0 \\ N_{i,\eta} & 0 & N_{j,\eta} & 0 & N_{k,\eta} & 0 & N_{m,\eta} & 0 \\ 0 & N_{i,\xi} & 0 & N_{j,\xi} & 0 & N_{k,\xi} & 0 & N_{m,\xi} \\ 0 & N_{i,\eta} & 0 & N_{j,\eta} & 0 & N_{k,\eta} & 0 & N_{m,\eta} \end{bmatrix}_{4x8} \{U\} \qquad \text{(Eq.3-13)}$$

Combining equations (3-11), (3-12) and (3-13), we obtain the strain-displacement relations

$$\{\epsilon\} = [B]\{U\}$$

Matrix [B] is the product of the three succesive rectangular matrices in equations (3-11) through (3-13). The tangential strain may also be expressed in terms of the shape functions and nodal displacements, as

$$\epsilon_\theta = [N]\{U\}/r \qquad \text{(Eq.3-14)}$$

where $r = N_i r_i + N_j r_j + N_k r_k + N_m r_m$

Thus, incorporating ϵ_θ into the strain-displacement relations, we can

write

$$\{\epsilon\} = \begin{Bmatrix} \epsilon_r \\ \epsilon_\theta \\ \epsilon_z \\ \gamma_{rz} \end{Bmatrix} = \begin{bmatrix} B_{11} & B_{12} & B_{13} & B_{14} & B_{15} & B_{16} & B_{17} & B_{18} \\ B_{21} & B_{22} & B_{23} & B_{24} & B_{25} & B_{26} & B_{27} & B_{28} \\ B_{31} & B_{32} & B_{33} & B_{34} & B_{35} & B_{36} & B_{37} & B_{38} \\ B_{41} & B_{42} & B_{43} & B_{44} & B_{45} & B_{46} & B_{47} & B_{48} \end{bmatrix}_{4x8} \{U\} \qquad \text{(Eq.3-15)}$$

where

$$B_{11} = \Gamma_{11}N_{i,\xi} + \Gamma_{12}N_{i,\eta} = B_{42}$$

$$B_{13} = \Gamma_{11}N_{j,\xi} + \Gamma_{12}N_{j,\eta} = B_{44}$$

$$B_{15} = \Gamma_{11}N_{k,\xi} + \Gamma_{12}N_{k,\eta} = B_{46}$$

$$B_{17} = \Gamma_{11}N_{m,\xi} + \Gamma_{12}N_{m,\eta} = B_{48}$$

$$B_{21} = N_i/r \; ; \; B_{23} = N_j/r \; ; \; B_{25} = N_k/r \; ; \; B_{27} = N_m/r$$

$$B_{32} = \Gamma_{21}N_{i,\xi} + \Gamma_{22}N_{i,\eta} = B_{41}$$

$$B_{34} = \Gamma_{21}N_{j,\xi} + \Gamma_{22}N_{j,\eta} = B_{43}$$

$$B_{36} = \Gamma_{21}N_{k,\xi} + \Gamma_{22}N_{k,\eta} = B_{45}$$

$$B_{38} = \Gamma_{21}N_{m,\xi} + \Gamma_{22}N_{m,\eta} = B_{47}$$

and $B_{12}=B_{14}=B_{16}=B_{18}=B_{22}=B_{24}=B_{26}=B_{26}=B_{31}=B_{33}=B_{35}=B_{37}= 0.$

The element stiffness matrix is

$$[k_e] = \int\int\int_V [B]^T[D][B]r\,dr\,d\theta\,dz \qquad \text{(Eq.3-16)}$$

$$= 2\pi \int\int [B]^T[D][B]r\,dr\,dz$$

$$[k_e] = 2\pi \int_{-1}^{1}\int_{-1}^{1} [B]^T[D][B]r\,|[J]|\,d\xi\,d\eta \qquad \text{(Eq.3-17)}$$

where the matrix of elastic constants [D] is

$$[D] = \frac{E}{1+\nu}\begin{bmatrix} d & b & b & 0 \\ b & d & b & 0 \\ b & b & d & 0 \\ 0 & 0 & 0 & 0.5 \end{bmatrix} \qquad \text{(Eq.3-18)}$$

The constants in the above matrix are:

$$d = \frac{1-\nu}{1-2\nu} \; ; \; b = \frac{\nu}{1-2\nu}$$

where E = elastic modulus, and ν = Poisson's ratio

Equation (3-17) must be integrated numerically. Using Gauss quadrature in two dimensions, the integral of a function $\phi(\xi,\eta)$ can be expressed as

$$[k_e] = \int_{-1}^{1}\int_{-1}^{1} \phi(\xi,\eta)d\xi d\eta = \sum\sum W_{i_i} W_{j_j} \phi(\xi_i,\eta_j) \qquad \text{(Eq.3-19)}$$

where W_i and W_j are weights associated with the Gauss-points (ξ_i,η_j).

3.2.2 ; Assembling the Global Stiffness Matrix

The global stiffness matrix is usually a banded matrix where all the nonzero elements cluster about the diagonal. For efficiency in storage and computation the zeros outside the band need not be stored or processed. Since the global stiffness matrix is also symmetric,it is only necessary to store the elements on the diagonal and on one side of the diagonal.

The semibandwidth of a symmetric banded matrix BW, can be found by the following scheme: (a) find the column number j of the last nonzero entry in row i of [K] and compute $b_i = 1+(j-i)$; (b) repeat this for all rows and indentify the largest b_i as BW. The elements in the upper semibandwidth can be stored into a compressed matrix by shifting rows to the left. 1 space for row 2; 2 spaces for row 3; and i-1 spaces for row i. Thus all diagonal coefficients of the matrix appear in the first column of the matrix.

The entire information content of a symmetric banded matrix resides in the (N × BW) coefficients of the semiband, where N is the total d.o.f.. In pratice, N may greatly exceed BW, so there is obvious merit in storing (N × BW) coefficients rather than all N^2 matrix coefficients.

There are other efficient methods to assemble the global stiffness matrix, such as the skyline method which stores the nonzero elements of the matrix (Bathe, et al., 1976)in a one-dimensional array. However, the semibandwidth method is both easy implement and sufficient for the problem being considered.

3.2.3 : Formulation of the Edge Loads

At the upper edge of an element $\eta = 1$, and the shape functions reduce to

$N_1 = 0.5(1 - \xi)$

$N_2 = 0.5(1 + \xi)$

$N_{1,\xi} = -0.5$

$N_{2,\xi} = +0.5$

The edge loads applied along the upper edge of an element need to be transformed into equivalent nodal loads. This is performed by integrating along the surface S

$$f_S = 2\pi r \int_S N^T S \, dS \qquad \text{(Eq.3-20)}$$

f_S is the forces along surface.

Changing to the ξ coordinate, the radial and vertical nodal loads can be expressed as (see figure (3-3))

$$P_{ri} = 2\pi r \int_{-1}^{1} N_i \left\{ P_t \frac{\partial r}{\partial \xi} - P_n \frac{\partial z}{\partial \xi} \right\} d\xi \qquad \text{(Eq.3-21)}$$

$$P_{zi} = 2\pi r \int_{-1}^{1} N_i \left\{ P_n \frac{\partial r}{\partial \xi} + P_t \frac{\partial z}{\partial \xi} \right\} d\xi \qquad \text{(Eq.3-22)}$$

where P_n is the normal load, and P_t is the tangential load.

In pavement analysis, wheel loads are considered to act vertically and hence $P_t = 0$. Therefore equations (3-21) and (3-22) reduce to

$$P_{ri} = 2\pi r \int_{-1}^{1} N_i \left\{ - P_n \frac{\partial z}{\partial \xi} \right\} d\xi = 0 \qquad \text{(Eq.3-22)}$$

Since $\partial z/\partial \xi = 0$ for local and global axes in the same direction (as in this case).

$$P_{zi} = 2\pi r \int_{-1}^{1} N_i \left\{ P_n \frac{\partial r}{\partial \xi} \right\} d\xi \qquad \text{(Eq.3-23)}$$

Using Gaussian quadrature, one dimensional integration of a function $\phi(\xi)$ becomes

$$P_z = \sum_i W_i \, \phi(\xi_i) \qquad \text{(Eq.3-23a)}$$

where W_i is the weight associated with the Gauss-point ξ_i

The sum of the nodal forces at the same node from the adjacent elements is the equivalent nodal load due to the tire pressure (See Figure 3-4).

3.2.4 : Gauss Elimination for the Solution of the Stiffness Equations

In the Gauss elimination of the stiffness equations $[K]\{U\} = \{R\}$ the first equation is symbolically solved for the unknown U_1, then substituted into the subsequent equations. The second equation is similarly treated, then the third, and so on. This forward reduction process alters $\{R\}$ and changes $[K]$ to an upper triangular form, with 1's on the diagonal. Finally, the unknown displacements are found by back-substitution, so that the numerical value of U_1 is found last.

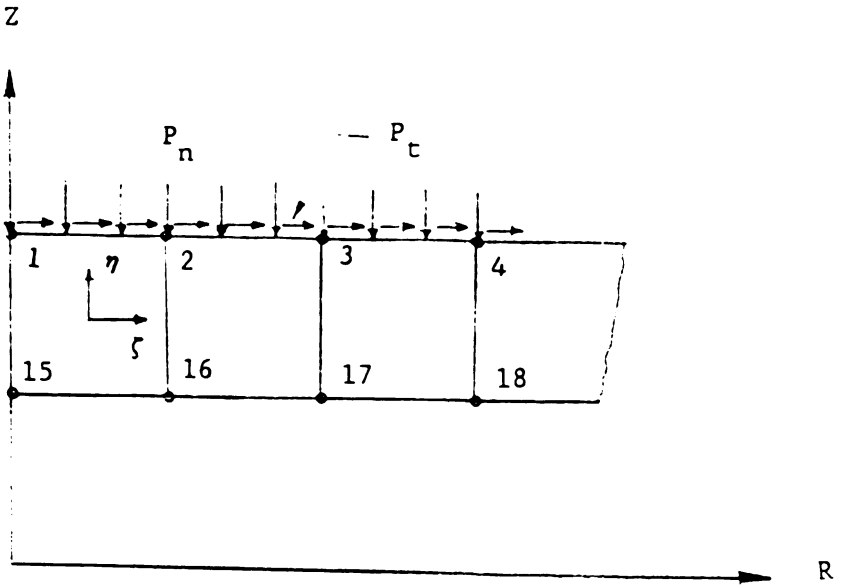

Figure 3-3 : Normal and Tangential Loads/unit Length Applied to an Isoparametric Element

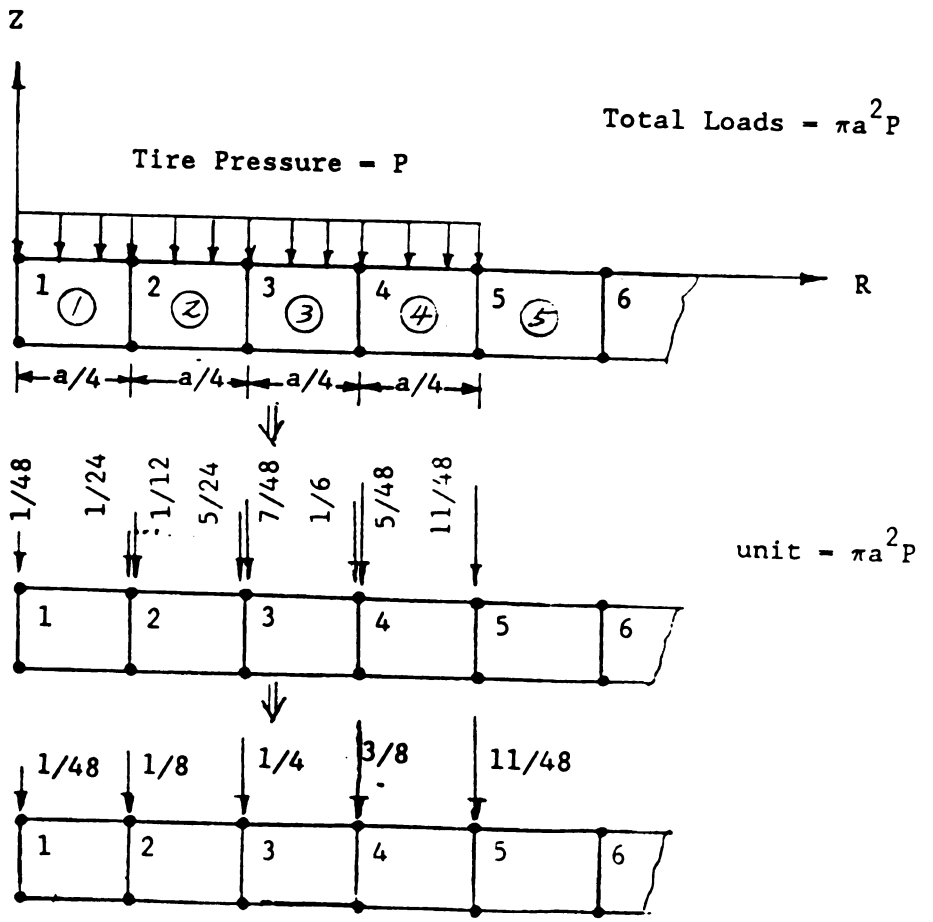

Figure 3-4 : Typical Conversion of Tire Pressure into Node Forces

3.3 : USE OF FLEXIBLE BOTTOM BOUNDARY

3.3.1 : Introduction

In pavement analysis, very deep finite element meshes need to be used to satisfactorily model the infinitely deep subgrade layer. Due to this, and the general nature of the finite element approach, programs tend to require large amounts of computer memory and computational time. These are the main factors prohibiting the use of finite element programs in day-to-day design.

In attempts to implement finite element programs on personal computers, efficient techniques are necessary. Harichandran and Yeh (1988) initiated the concept of a flexible boundary to overcome the computational burden imposed by the requirement of a deep bottom boundary in the finite element analysis of pavements. A flexible boundary, which accounts for displacements that occur beneath it, is used with finite elements above it.

Finite elements are used to model the soil in the vicinity of the loaded area. In addition, the bottom boundary is placed at a depth below which displacements and stresses are not of interest. Further, the bottom boundary is assumed to be flexible, and the half-space below the boundary is assumed to be composed of linear elastic, layered material. (Usually the boundary will be placed at some depth within the subgrade, in which case the half-space below the boundary will be homogenous.) Displacements that occur in the soil below the boundary are therefore considered in the analysis.

When dealing with nonlinear soil, the bottom boundary must be placed at a depth below which it is reasonable to neglect nonlinearities. The

highly stressed, and therefore significantly nonlinear, soil in the vicinity of the loaded area can be modeled by finite elements. This technique, while being computationally efficient, should yield sufficiently accurate results.

3.3.2 : Modeling of Flexible Boundary

Figure (3-5) illustrates the modeling of a pavement system. One circular wheel load is assumed, and the problem therefore reduces to an axisymmetric one, The main region of interest under the load is divided into finite elements. The finite element mesh rests on a half-apace consisting of elastic layered strata. The coupling between the finite elements and the half space occur at the d.o.f. along the bottom boundary which are shown in the figure (3-5).

In order to account for the coupling between the flexible boundary and the finite elements it is necessary to determine the stiffness matrix of the half-space corresponding to the d.o.f. along the boundary. It is illuminating at this point to consider the physical meaning of such a stiffness matrix. Due to the axisymmetric nature of the problem, the d.o.f. along the boundary are really the vertical and radial displacements of the rings shown in figure (3-6). At the origin the ring degenerates to a point. If there are n rings as shown in figure, there will be (2n-1) d.o.f. since there is no radial d.o.f. at the origin (the radial displacement at the origin is zero due to symmetry). The stiffness matrix will then have dimensions of [(2n-1) x (2n-1)]. The element k_{ij} (i^{th} row and j^{th} column) of the stiffness matrix K, is the total force required along the ring at d.o.f. i when d.o.f. j is displaced by a unit amount while all other d.o.f. are held fixed. The

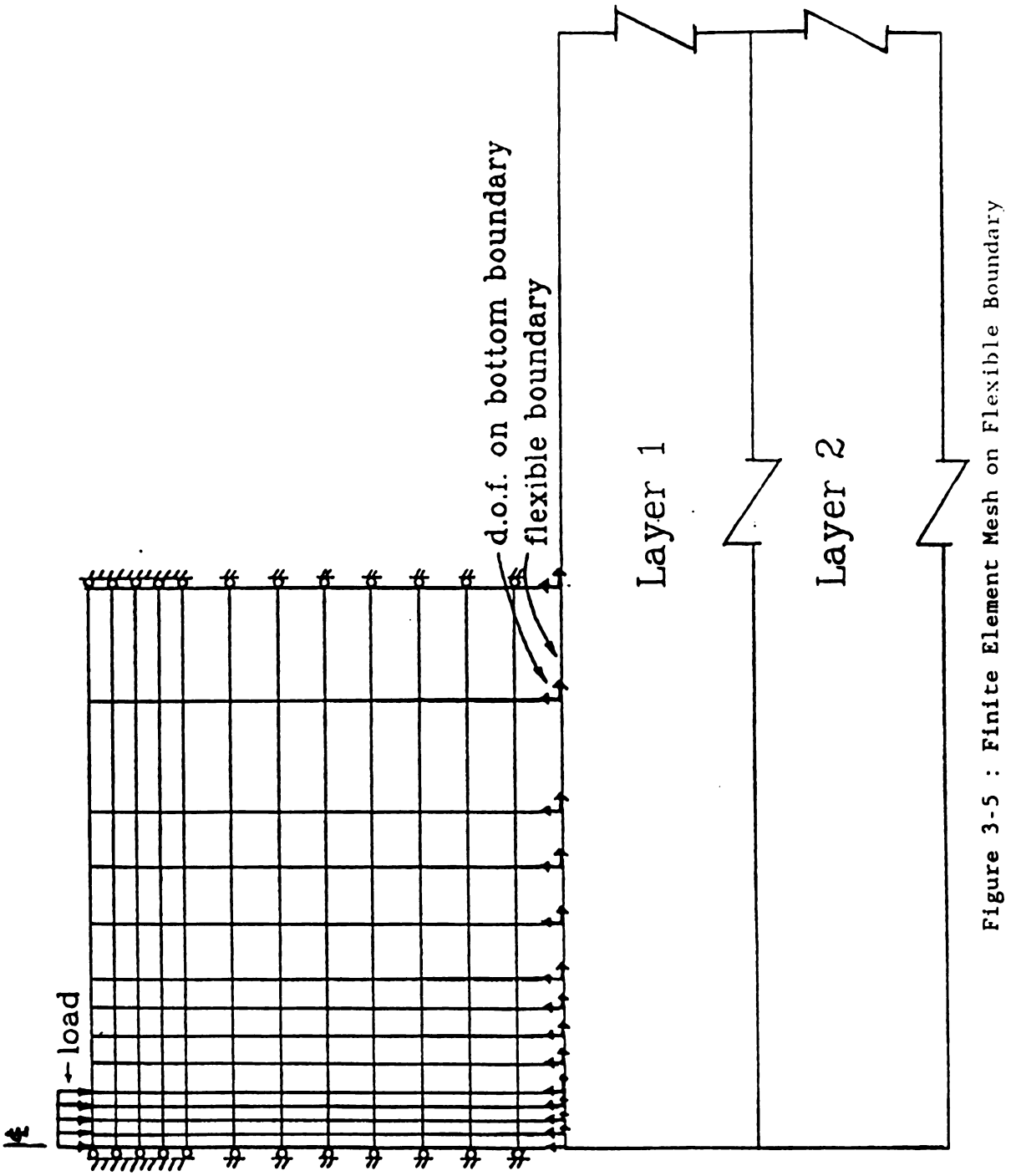

Figure 3-5 : Finite Element Mesh on Flexible Boundary

elements of the stiffness matrix are extremely difficult to compute directly. However, the inverse of the stiffness matrix, commonly known as the flexibility matrix, can be easily computed. The element f_{ij} of the flexibility matrix F, is the displacement along d.o.f. i due to a unit total uniform ring load along d.o.f. j (vertical and radial uniform ring loads are depicted in figure (3-6)). This displacement can be obtained from an elastic layer program such as CHEV5L. If the boundary is placed within the subgrade, as will be most common, then the half-space will be homogeneous and analytical results can be used to determine the flexibility coefficients.

There is one problem of incompatibility between finite element modeling and elastic layer modeling. If finite element are used to model the half-space beneath the boundary, concentrated ring loads (load per unit arc length) can be applied at nodes and all displacements on the boundary will be finite and can be computed. When the half-space is modeled by elastic layer theory, however, concentrated ring loads will produce finite displacements at all points on the boundary except directly under the load. On the ring where the load is placed the displacements will tend to infinity. This, of course, is the true behavior since it is known that plastic deformation will occur under the concentrated load. In order to link together the finite elements and the elastic half-space, however, some approximation is necessary to compute the diagonal elements of the flexibility matrix (these f_{jj} elements are the displacements directly under the ring loads). One physically appealing approximation is to assume that the load is uniformly distributed over the annular surface halfway from the loaded ring to the two adjacent rings.

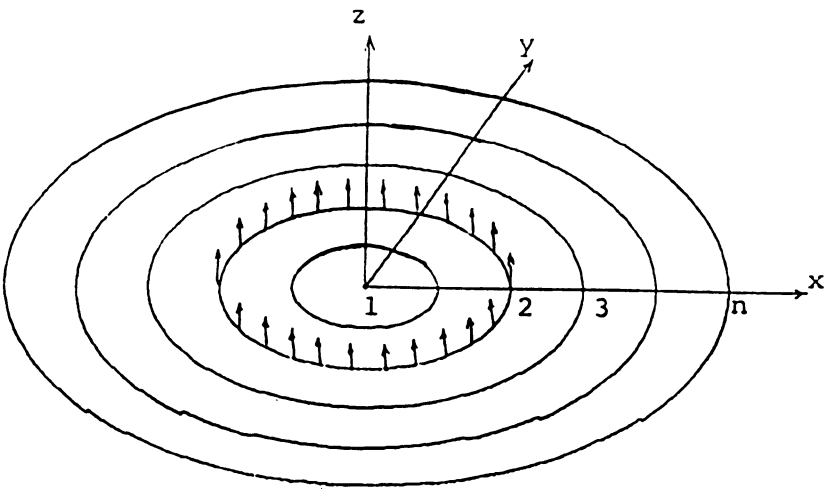

Figure 3-6(a) : Vertical Ring Loads

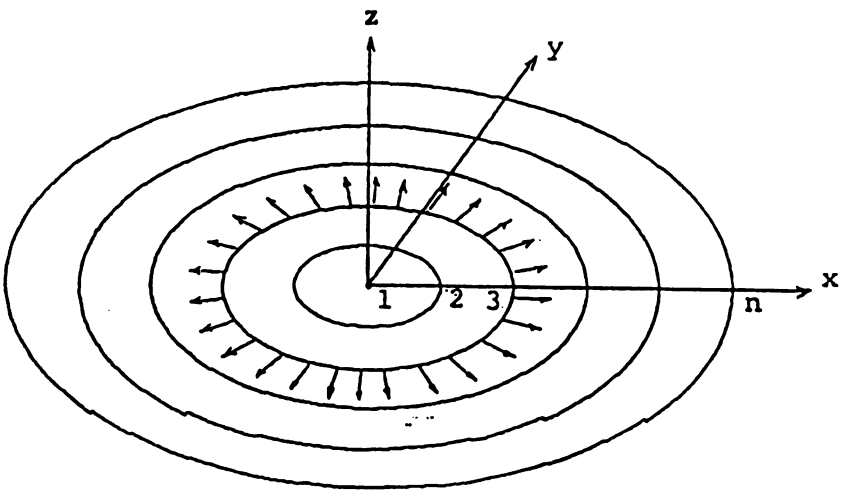

Figure 3-6(b) : Radial Ring Loads

Once the flexibility matrix of the half-space has been estimated it can be inverted to obtain the corresponding stiffness matrix. The d.o.f. along the bottom boubdary are usually of the order of 30 or so and the inversion of a 30x30 symmetric matrix presents no problem. The stiffness matrix of the finite elements are computed one by one and assembled as usual. This matrix, denoted by K_{FE}, may be partitioned as follows:

$$K_{FE} = \begin{bmatrix} K_{FF} & K_{FB} \\ K_{BF} & K_{BB} \end{bmatrix} \qquad \text{(Eq.3-24)}$$

Where the (2n-1) x (2n-1) matrix K_{BB} corresponds to the d.o.f. along the bottom boundary. The stiffness matrix of the half-space is denoted by K_{HS} (also a (2n-1) x (2n-1) matrix). It should be noted that K_{BB} will have many zero elements (since K_{FE} is usually a banded matrix), but K_{HS} will be fully populated. The stiffness matrix of the combined system is then

$$K = \begin{bmatrix} K_{FF} & K_{FB} \\ K_{BF} & K_{BB} + K_{HS} \end{bmatrix} \qquad \text{(Eq.3-25)}$$

If the nodal displacements D are partitioned corresponding to K as

$$D = \begin{Bmatrix} D_F \\ D_B \end{Bmatrix} \qquad \text{(Eq.3-26)}$$

Then the solution of the stiffness equations

$$KD = Q \qquad \text{(Eq.3-27)}$$

will yield the displacement at all nodes, including those at the boundary, D_B.

3.3.3 : Flexibilities for Homogeneous Half-Space

As mentioned earlier, in most cases the bottom boundary will be within the subgrade and the half-space beneath the boundary will be homogeneous. For this case it is possible to use analytical expressions

to evaluate the flexibilities of the half-space. Analytical solutions for vertical and radial ring loads may be derived, but in the absence of simple expressions, it is necessary to resort to numerical integration. Elegant closed form solutions, however, exist for uniform vertical loads and linearly varying radial loads on a circular area. These can be utilized to estimate the required flexibility coefficients. For a uniform vertical upward load p applied to a circular area of radius r_o the vertical (upward) and radial (outward) surface displacements are (Poulos, et al., 1974):

$$w_V(r;r_o;p) = \begin{cases} F(0.5,-0.5;1;(r/r_o)^2)\ \dfrac{2(1-\nu^2)}{E}\ pr_o, & \text{for } r < r_o \\ \dfrac{4(1-\nu^2)}{\pi E}\ pr_o, & \text{for } r = r_o \\ F(0.5,0.5;2;(r_o/r)^2)\ \dfrac{(1-\nu^2)}{Er}\ pr_o^2, & \text{for } r > r_o \end{cases} \quad \text{(Eq.3-28)}$$

and

$$u_V(r;r_o;p) = \begin{cases} \dfrac{(1+\nu)\ (1-2\nu)}{2E}\ pr, & \text{for } r \le r_o \\ \dfrac{(1+\nu)\ (1-2\nu)}{2Er}\ pr_o^2, & \text{for } r > r_o \end{cases} \quad \text{(Eq.3-29)}$$

respectively, where

r = horizontal distance from the center of the load;

E, ν = Elastic modulus and Poisson's ratio of half-space.

$F(\alpha,\beta;\gamma;x)$ is the Hypergeometric function with parameters α, β and γ, the series representation of which is

$$F(\alpha,\beta;\gamma;x) = 1 + \frac{\alpha\beta}{(1)\gamma}\,x + \frac{\alpha(\alpha+1)\ \beta(\beta+1)}{(1)\ (2)\ \gamma(\gamma+1)}\,x^2 + \ldots \quad \text{(Eq.3-30)}$$

For a radial (outward) load varying linearly from zero at the center to p at distance r_o, acting on a circular area of radius r_o, the vertical and radial displacements are:

$$W_R(r;r_o;p) = \begin{cases} \dfrac{(1+\nu)(1-2\nu)}{2E}\left[1-\left(\dfrac{r}{r_o}\right)^2\right] pr_o, & \text{for } r < r_o \\ 0, & \text{for } r \geq r_o \end{cases} \quad \text{(Eq.3-31)}$$

and

$$u_R(r;r_o;p) = \begin{cases} F(1.5,-0.5;2;(r/r_o)^2)\ \dfrac{(1-\nu^2)}{E}\ pr, & \text{for } r < r_o \\ \dfrac{4(1-\nu^2)}{3\pi E}\ pr_o, & \text{for } r = r_o \\ F(1.5,0.5;3;(r_o/r)^2)\ \dfrac{p(1-\nu^2)}{4E}\left(\dfrac{r_o^3}{r^2}\right), & \text{for } r > r_o \end{cases} \quad \text{(Eq.3-32)}$$

respectively.

Consider now the two boundary nodes shown in Figure (3-7), with d.o.f i and j at node A, and d.o.f. k and ℓ at node B. By approximating the vertical ring load at k by a uniform vertical load over a very thin annulus of width 2ϵ (see Figure 3-8), the flexibility coefficients f_{ik}, f_{jk} and $f_{\ell k}$ can be estimated as follows:

$$f_{ik} = w_V(r_1;\ r_2+\epsilon;\ p_1) - w_V(r_1;\ r_2-\epsilon;\ p_1) \quad \text{(Eq.3-33)}$$

$$f_{jk} = u_V(r_1;\ r_2+\epsilon;\ p_1) - u_V(r_1;\ r_2-\epsilon;\ p_1) \quad \text{(Eq.3-34)}$$

$$f_{lk} = u_V(r_2;\ r_2+\epsilon;\ p_1) - u_V(r_2;\ r_2-\epsilon;\ p_1) \quad \text{(Eq.3-35)}$$

$$\text{where } p_1 = \frac{1}{4\pi\epsilon r_o} \quad \text{(Eq.3-36)}$$

With p_1 defined as in equation (3-35), the total load on the annulus is unity. As long as ϵ is small, these coefficients are not sensitive to the exact magnitude of ϵ. Due to the Maxwell-Betti reciprocal theorem $f_{ki} = f_{ik} = f_{kj} = f_{jk}$ and $f_{k\ell} = f_{\ell k}$.

This technique cannot be used to estimate f_{kk} or $f_{\ell\ell}$. These flexibilities are very sensitive to the magnitude of ϵ. In fact, as mentioned before, as $\epsilon \to 0$, $f_{kk} \to \infty$ and $f_{\ell\ell} \to \infty$. To estimate the

diagonal flexibilities, therefore, we assume that a uniform load (with unit total load) is applied in an annulus from midway between nodes A and B to midway between nodes B and C in Figure (3-7). The loading approximations used for the vertical and radial loads are illustrated in Figure (3-9) and (3-10).

$$f_{kk} \approx w_V(r_2;(r_2+r_3)/2;p_2) - w_V(r_2;(r_1+r_2)/2;p_2) \qquad \text{(Eq.3-37)}$$

and

$$f_{\ell\ell} \approx u_R(r_2;(r_2+r_3)/2;p_4) - u_R(r_2;(r_1+r_2)/2;p_3) \qquad \text{(EQ.3-38)}$$

where

$$p_2 = \frac{1}{\pi[(r_2+r_3)^2 - (r_1+r_2)^2]} \qquad \text{(Eq.3-39)}$$

$$p_3 = \frac{6(r_1+r_2)}{\pi[(r_2+r_3)^3 - (r_1+r_2)^3]} \qquad \text{(Eq.3-40)}$$

and

$$p_4 = p_3 \frac{(r_2+r_3)}{(r_1+r_2)} \qquad \text{(Eq.3-41)}$$

The expression for p_2, p_3 and p_4 given above ensure the load patterns illustrated in Figure (3-9) and (3-10), with the total load in each case being unity. All the diagonal terms of the flexibility matrix can be estimated as in equations (3-37) and (3-38).

3.4 : COMPARISON OF THE FLEXIBLE BOUNDARY WITH OTHER LINEAR METHODS

Analysis using the flexible boundary were performed for homogeneous and multilayered (Three-layered) half-spaces. in both cases, a load of 100 psi was applied on a circular area of redius 10", and the flexible boundary was placed at a depth of 50", above which a finite element mesh was used. The side boundary was placed at 100" from the centerline (10 times the radius of the loaded area) for both cases. The material

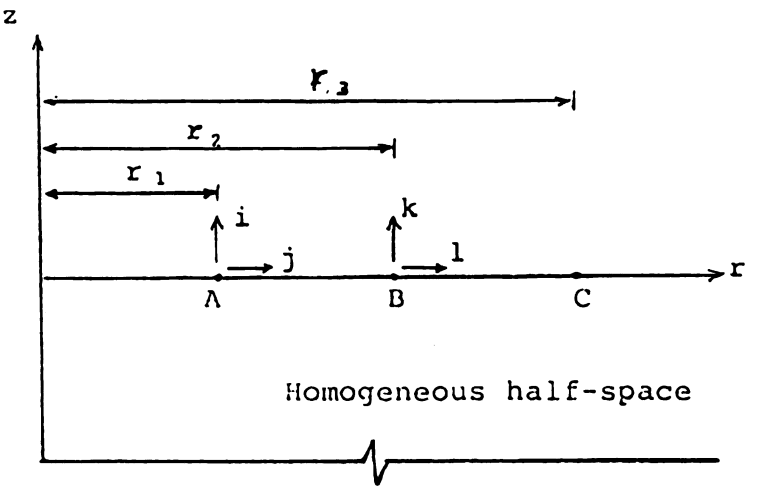

Figure 3-7 : Typical Nodes and Degree-of-Freedom

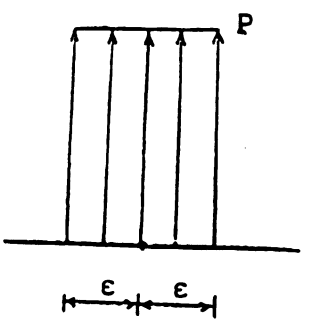

Figure 3-8 : Vertical Load on Thin Annulus

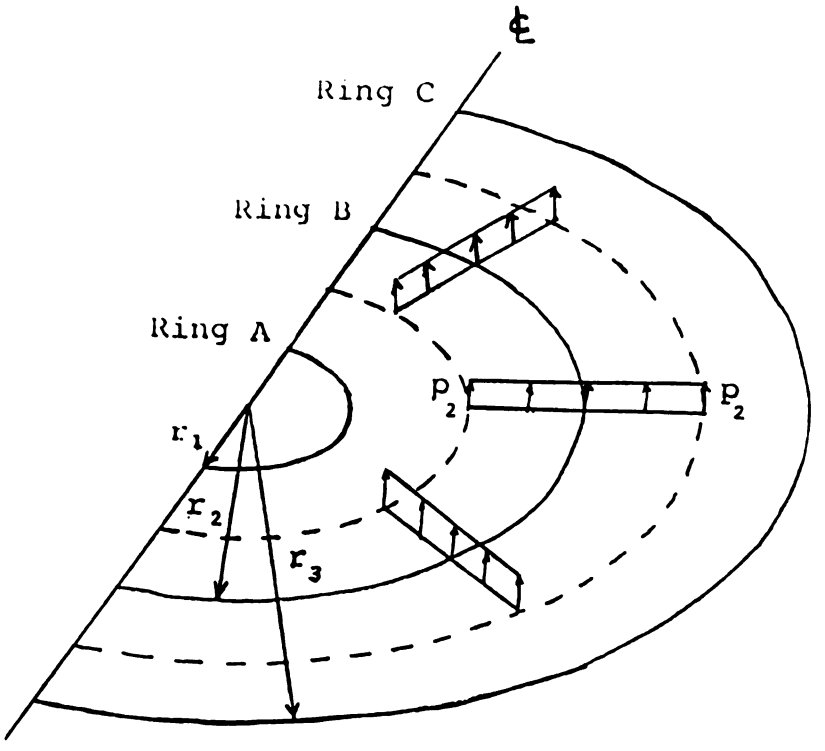

Figure 3-9 : Uniform Vertical Loading to Estimate f_{kk}

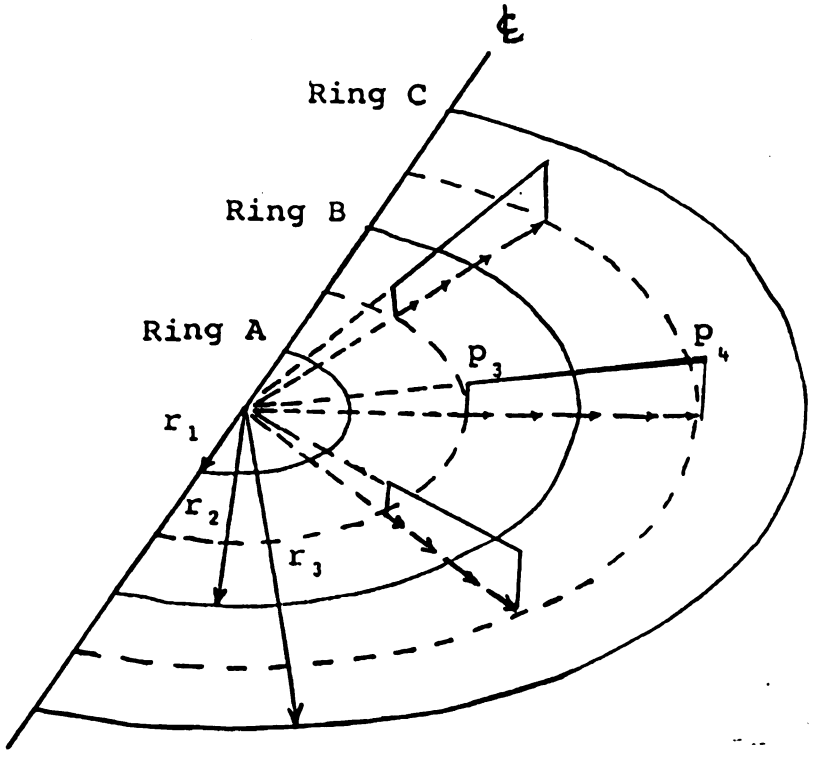

Figure 3-10 : Linear Radial Load to Estimate f_{11}

properties were as follows:

Homogeneous : E = 5000 psi; υ = 0.45.
Multilayer :
layer 1 (asphalt) - E = 200,000 psi; υ = 0.35; depth = 10";
layer 2 (base) - E = 15,000 psi; υ = 0.40; depth = 20";
layer 3 (roadbed soil)- E = 5,000 psi; υ = 0.45; infinite depth.

In order to compare the results with the traditional finite element approach, a mesh of depth 510" was uesed with a fixed boundary. (As noted by Duncan et. al. (1968) a deep mesh is required in traditional finite element analysis.) The number of elements was kept the same in both meshes to facilitate a direct comparison, while keeping the computational effort approximately the same. This meant that in the traditional mesh the deeper elements had very large length to width ratios. The mesh used with the flexible boundary and the traditional mesh (finite element only) are shown in Figures 3-11 and 3-12, respectively. The same meshes were used for the homogeneous and multilayered cases.

The vertical displacements along the top free surface and the variation of the vertical dsiplacement with depth beneath the center of the loaded area shown in Figures 3-13 and 3-14. The percentage errors in both finite element approaches, as compared with the exact results, are tabulated in Tables 3-1 and 3-2. (The abbreviations "FE+FB" and "FE only" are used to denote "finite elements plus flexible boundary" and "finite elements only", respectively, in the figures and tables.) It is apparent that use of the flexible boundary gives significantly better results, especially for the multilayered case where displacements within the subgrade contribute significantly toward the total displacements. The flexible boundary approach is more accurate for the homogeneous case than for the multilayered case, but in both cases it is more accurate than traditional finite element approach.

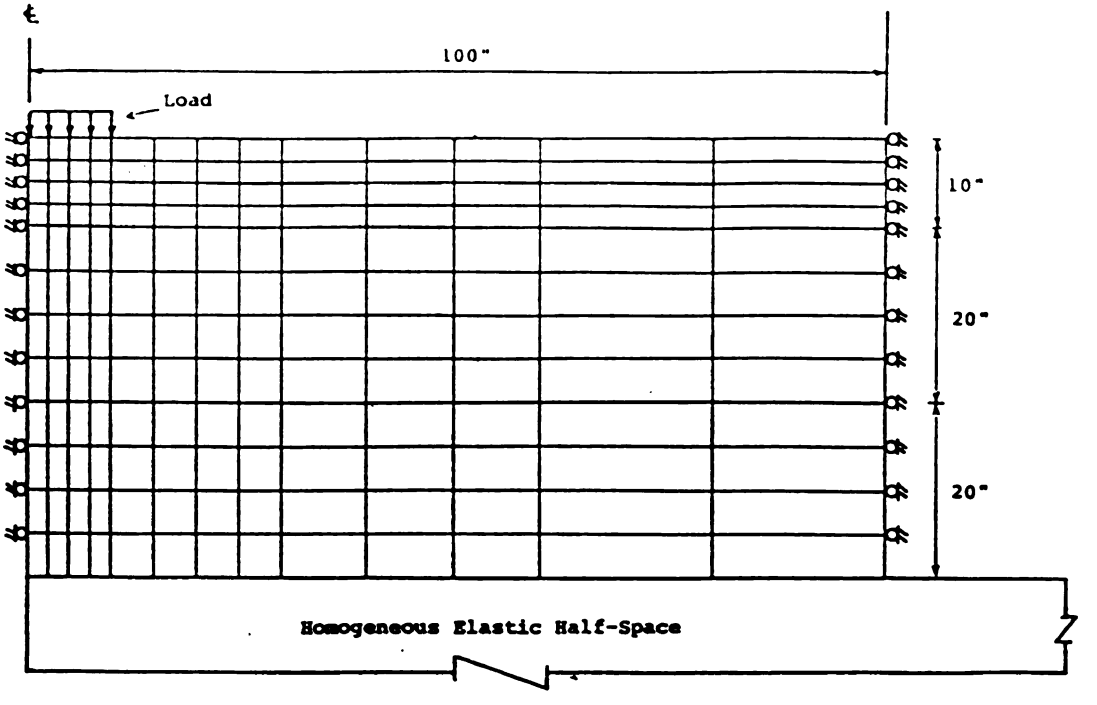

Figure 3-11 : Finite Element Mesh used with Flexible Boundary

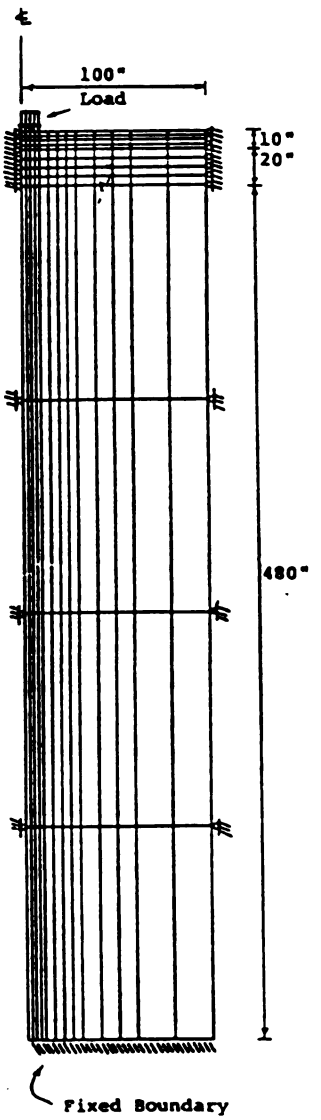

Figure 3-12 : Traditional Finite Element Mesh

The variation of vertical and radial stresses with depth beneath the center of the loaded area are presented in Figures 3-15 and 3-16, respectively. The percentage errors, as compared with exact results, are tabulated in Tables 3-3 and 3-4. Again, use of the flexible boundary gives better results than the tranditional approach. The differences in the stresses, however, are less significant than those in the displacements. For the homogeneous case, at depths below 30" the actual radial stresses are very small. Due to this, a comparison of the percentage errors (which were very large) are somewhat meaningless and have been omitted from Table 3-4. For the same reason, the percentage errors are very large for the tranditional approach at large depths. The percentage errors should be compared with the value of the actual stresses in mind.

One point worth noting is the lack of accuracy of the finite element method (both with and without the flexible boundary) when stresses are evaluated near the corners of elements (i.e., near nodes). Stresses are most accurate at the middle of elements and are reasonable at the middle of element edges, but not accurate near element cornors. For homogeneous material the stresses from finite element solutions are not continuous across element boundaries (as they should be). This is the reason for the large errors in the radial stresses at depths of 10" and 30" (see Table 3-4). These depths represent the interfaces between layers for the multilayered case. Also, when elements with very large aspect ratios (such as the deeper element in the traditional mesh (Figure 3-12) are used, the results tend to be poor. A better mesh than the one in Figure 3-12 would require many more elements and hence would result in a much greater computational effort.

A number of case studies were performed using the flexible boundary approach, varying the moduli and thicknesses of the base and subbase layers. In all cases the results compared favorably with the exact solutions.

Table 3-1 : Errors in surface deflections

Radial Dist. (inches)	Homogeneous			Multilayer		
	Exact displ. (inch)	Percentage Error		Exact displ. (inch)	Percentage Error	
		FE + FB	FE only		FE + FB	FE only
0	.3190	-1.9	-9.3	.0807	-6.6	-17.4
2.5	.3140	-2.6	-10.1	.0802	-6.8	-17.6
5	.2980	-3.3	-11.1	.0788	-6.9	-17.9
7.5	.2677	-4.6	-13.1	.0763	-7.1	-18.3
10	.2031	-6.8	-17.7	.0725	-7.5	-19.0
15	.1136	-2.5	-19.8	.0653	-8.0	-20.2
20	.0825	-2.8	-23.6	.0592	-8.4	-20.9
25	.0652	-2.5	-25.4	.0537	-8.7	-21.4
30	.0539	-3.0	-25.1	.0488	-8.9	-21.5
40	.0401	-4.6	-24.4	.0406	-9.1	-21.0
50	.0321	-5.6	-21.9	.0342	-8.9	-19.4
60	.0266	-4.7	-17.8	.0292	-7.3	-16.0
80	.0201	-4.8	-12.0	.0220	0.9	-4.6
100	.0160	6.4	3.1	.0173	19.3	15.2

Table 3-2 : Errors in vertical displacements beneath center of load

Depth (inches)	Homogeneous			Multilayer		
	Exact displ. (inch)	Percentage Error		Exact displ. (inch)	Percentage Error	
		FE + FB	FE only		FE + FB	FE only
0	.3190	-1.9	-9.3	.0807	-6.6	-17.4
1.25	.3134	-2.5	-10.3	.0810	-6.7	-17.5
3.75	.2916	-2.4	-11.1	.0809	-6.6	-17.5
6.25	.2620	-2.3	-12.3	.0803	-6.7	-17.7
8.75	.2314	-1.9	-13.6	.0792	-6.8	-18.0
10	.2171	-2.0	-14.5	.0784	-6.8	-17.2
12.5	.1913	-0.6	-15.2	.0749	-6.7	-18.5
17.5	.1516	-0.4	-19.4	.0691	-7.0	-19.9
22.5	.1239	-0.6	-23.9	.0646	-7.1	-20.9
27.5	.1042	-0.8	-26.1	.0608	-7.2	-20.9
30	.0964	-1.4	-26.4	.0588	-7.1	-20.5
32.5	.0897	-0.9	-22.2	.0563	-6.8	-18.0
37.5	.0785	-0.6	-14.1	.0518	-6.3	-13.3
42.5	.0698	-0.4	-6.7	.0480	-5.8	-9.1
47.5	.0628	0.0	0.0	.0447	-4.9	-5.2
50.	.0598	0.0	+2.7	.0433	-4.5	-3.4

Table 3-3 : Errors in vertical stresses beneath center of load

Depth (inches)	Homogeneous			Multilayer		
	Exact stress (psi)	Percentage Error		Exact stress (psi)	Percentage Error	
		FE + FB	FE only		FE + FB	FE only
1.25	99.81	-3.2	-3.0	97.62	-4.5	-4.4
3.75	95.67	-2.0	-1.8	80.43	-1.3	-0.7
6.25	85.11	0.0	0.6	53.54	1.1	2.7
8.75	71.45	1.8	2.9	30.11	15.3	19.7
10	64.64	-2.3	-0.5	24.62	10.7	16.9
12.5	52.39	2.3	5.2	20.26	-2.3	6.3
17.5	34.55	1.7	8.6	13.68	-4.6	10.7
22.5	23.69	-0.6	11.8	9.25	-6.2	16.8
27.5	17.00	-2.7	11.7	6.44	-6.8	17.9
30	14.62	-1.6	-25.5	5.65	-6.1	-18.2
32.5	12.69	-3.7	-110.	5.13	-10.3	-112.
37.5	9.79	-3.9	-109.	4.30	-11.3	-109.
42.5	7.76	-4.6	-107.	3.66	-13.0	-106.
47.5	6.30	-14.9	-103.	3.15	-23.6	-100.
50.	5.71	22.8	-101.	2.94	1.1	-97.

Table 3-4 : Errors in radial stresses beneath center of load

Depth (inches)	Homogeneous			Multilayer		
	Exact stress (psi)	Percentage Error		Exact stress (psi)	Percentage Error	
		FE + FB	FE only		FE + FB	FE only
1.25	77.11	-4.5	-7.6	169.9	-2.2	-7.8
3.75	46.25	-3.3	-7.0	69.39	-3.7	-9.7
6.25	25.59	7.9	3.6	-19.36	3.0	-1.7
8.75	13.79	31.1	27.5	-111.	-1.8	-7.3
10 (+)	10.15	159.0	158.5	-163.5	9.9	3.7
10 (-)	10.15	176.0	181.	2.05	-217.	-128.
12.5	5.58	62.2	68.6	.54	25.7	352.
17.5	1.83	46.4	145.	-1.63	-9.3	150.
22.5	.65	-9.7	602.	-3.66	-8.9	103.
27.5	.23	-95.3	3197.	-6.27	-9.0	-97.2
30 (+)	.13			-8.04	-8.6	121.
30 (-)	.13			3.28	-131.	-165.
32.5	.07			.28	6.4	-821.
37.5	.00			.22	25.1	-949.
42.5	-.03			.17	44.6	
47.5	-.04			.14	-106.	
50.	-.04			.12	403.	

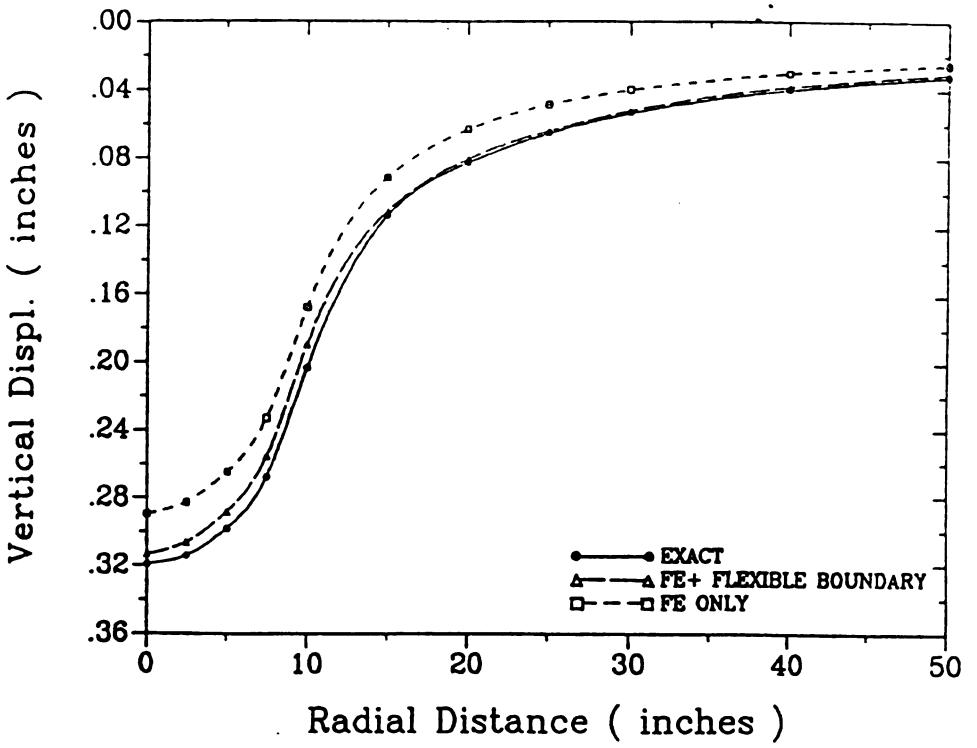

Figure 3-13a : Comparison of Surface Deflections with and without Flexible Boundary for the Homogeneous Material

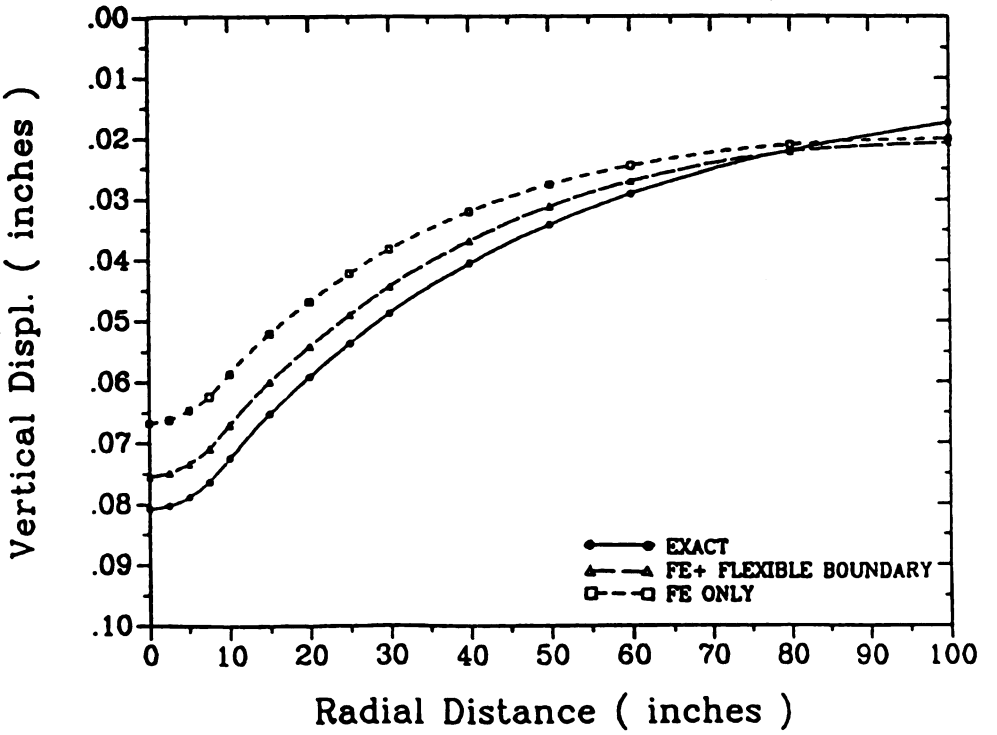

Figure 3-13b : Comparison of Surface Deflections with and without Flexible Boundary for the Multilayer Pavement

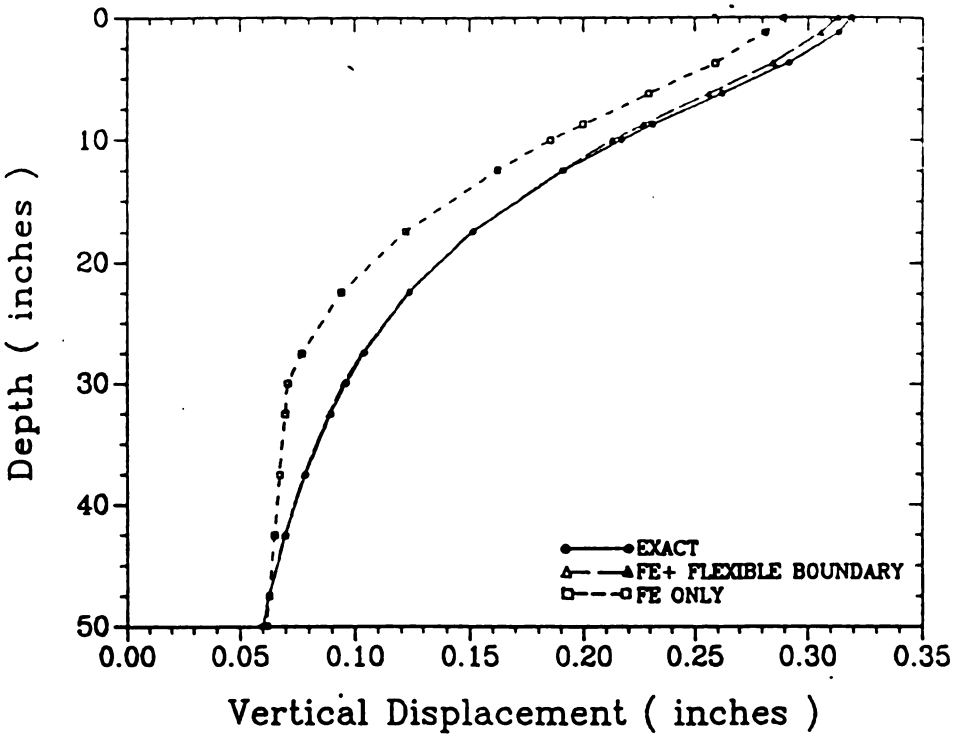

Figure 3-14a : Comparison of Vertical Displacements beneath Center of Load with and without Flexible Boundary for the Homogeneous Material

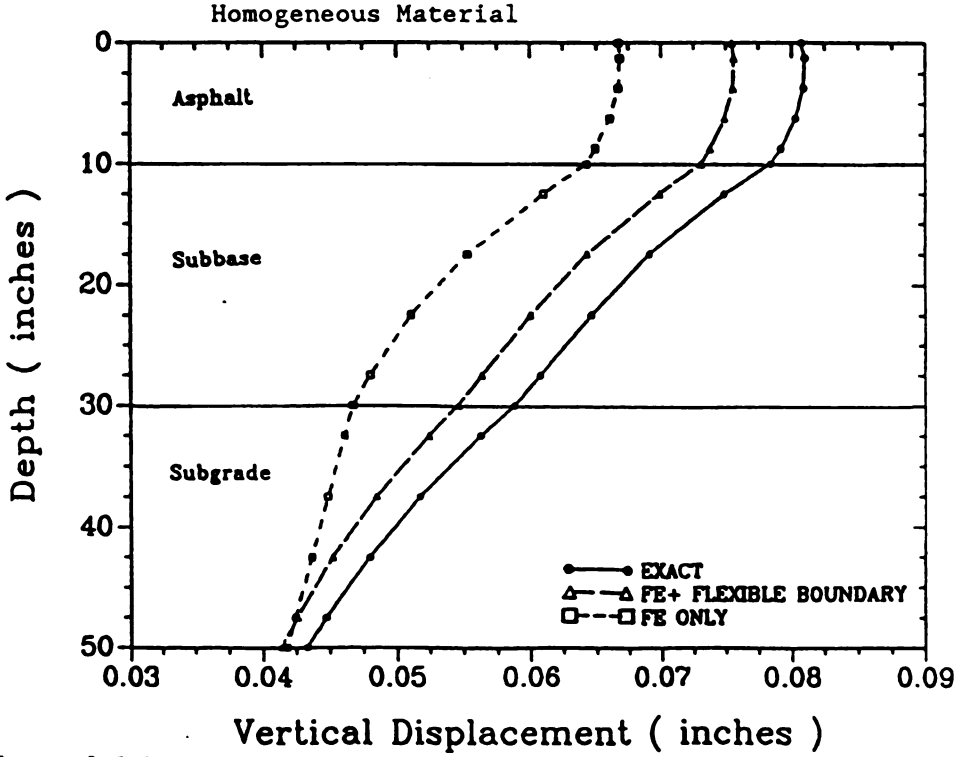

Figure 3-14b : Comparison of Vertical Displacements beneath Center of Load with and without Flexible Boundary for the Multilayer Pavement

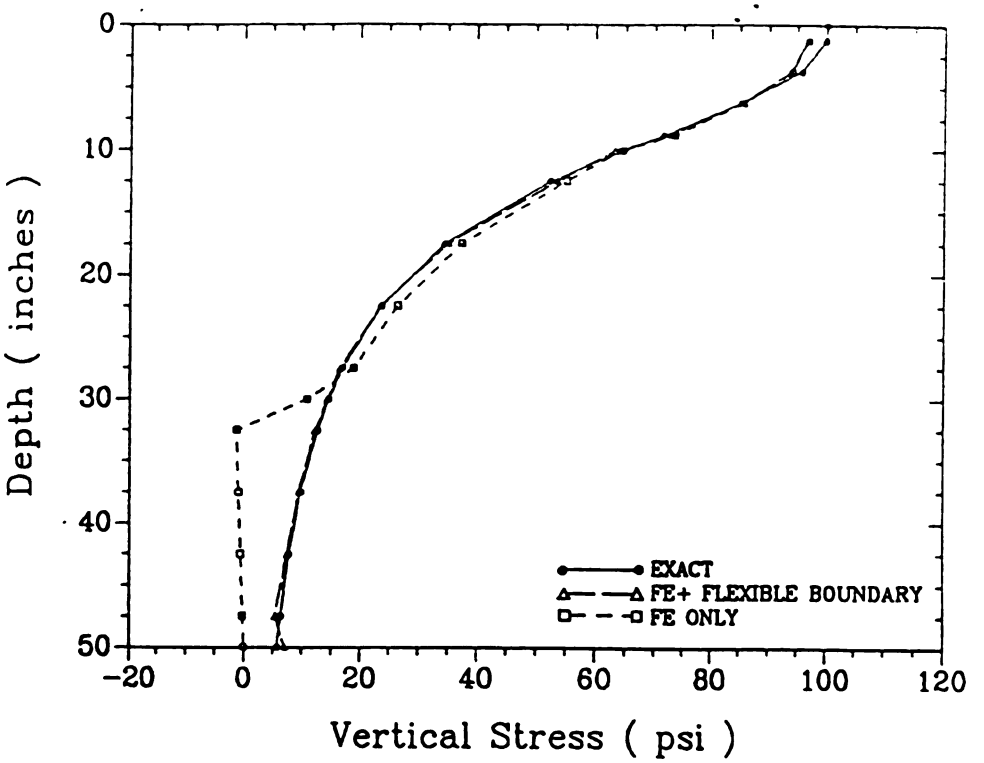

Figure 3-15a : Comparison of Vertical Stresses beneath Center of Load with and without Flexible Boundary for the Homogeneous Material

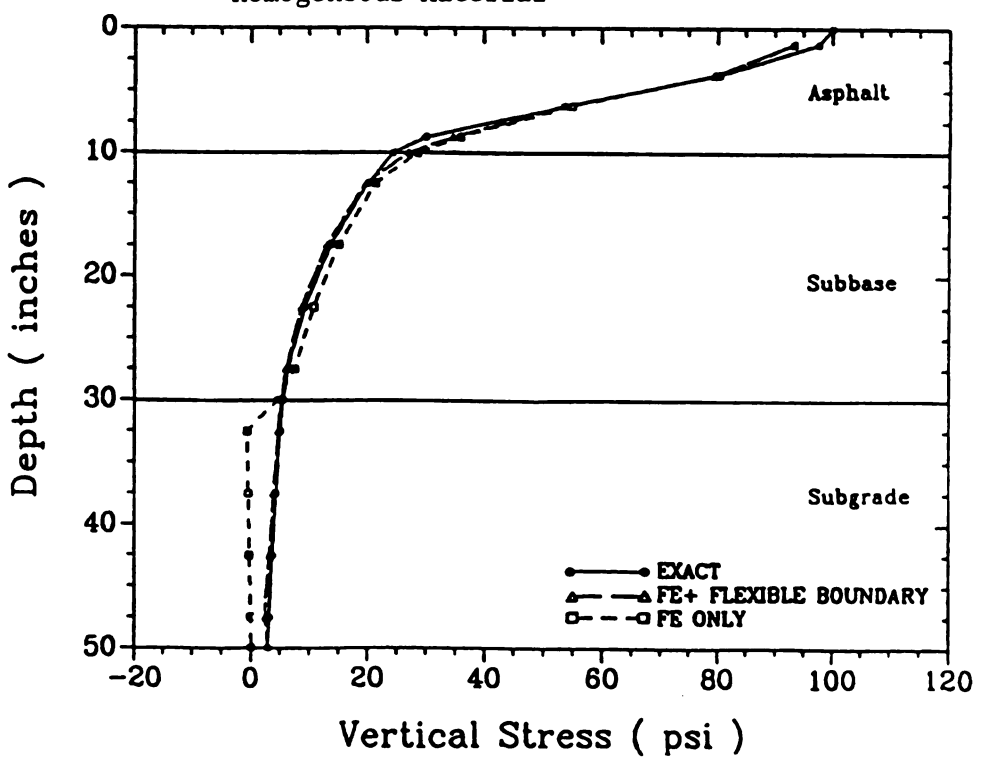

Figure 3-15b : Comparison of Vertical Stresses beneath Center of Load with and without Flexible Boundary for the Multilayer Pavement

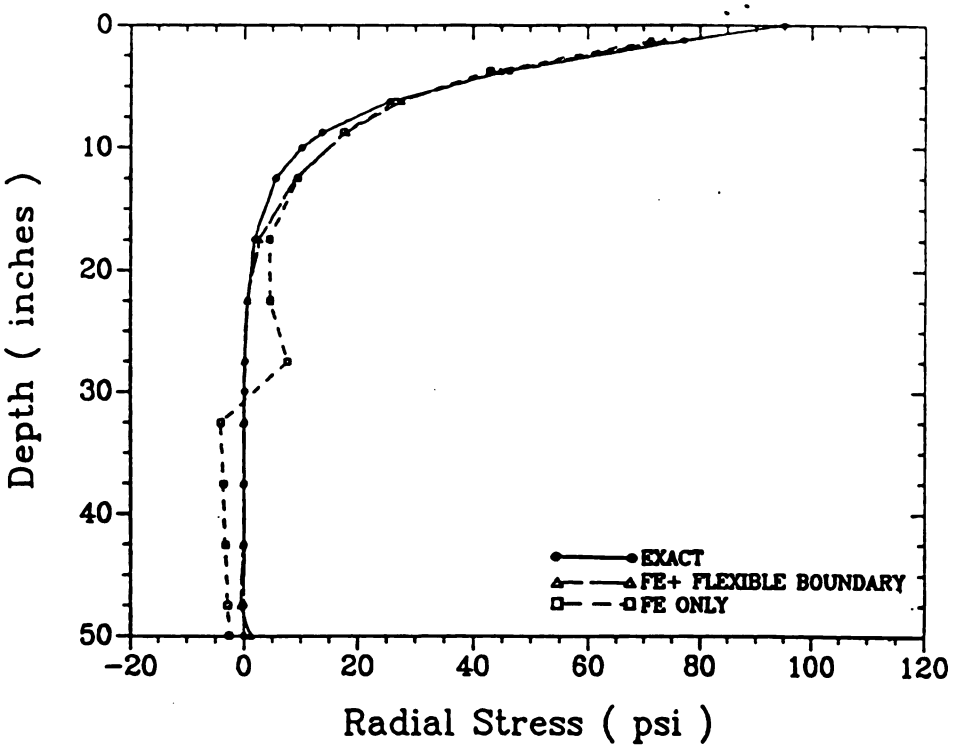

Figure 3-16a : Comparison of Radial Stresses beneath Center of Load with and without Flexible Boundary for the Homogeneous Material

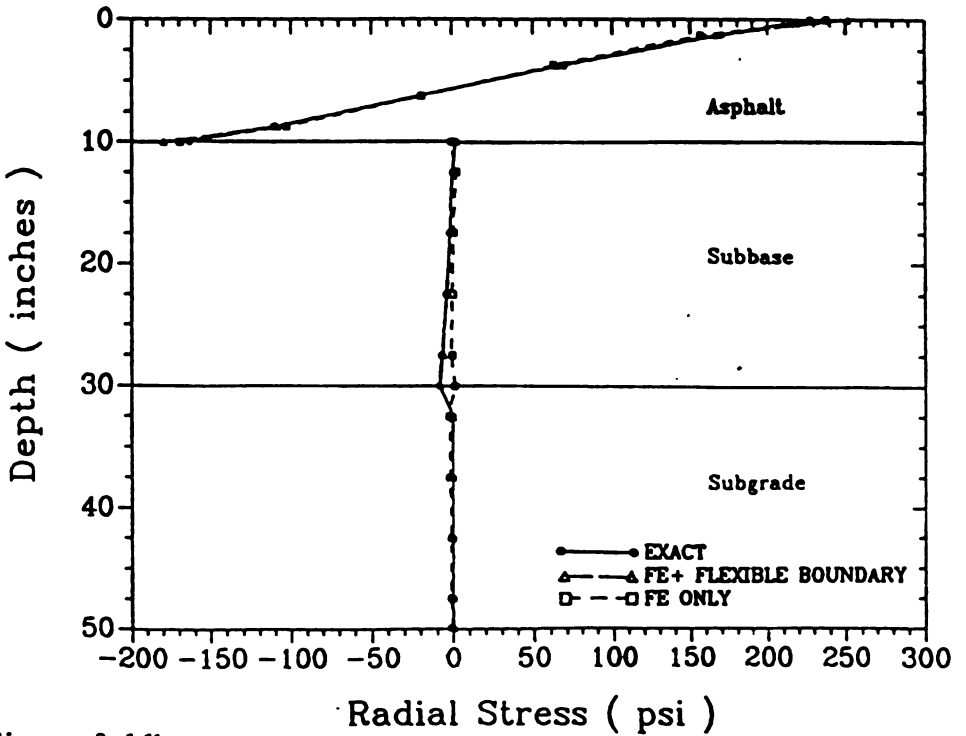

Figure 3-16b : Comparison of Radial Stresses beneath Center of Load with and without Flexible Boundary for the Multilayer Pavement

3.5 : SENSITIVITY OF FLEXIBLE BOUNDARY IN LINEAR ANALYSIS

In this section, a typical pavement section is selected to analyze the sensitivity of the flexible boundary with respect to the depth, tire pressure, and the magnitude of wheel loads. The material properties of the pavement section are chosen to be

layer 1 (Asphalt) - E = 500,000 psi; υ = .4 ; depth = 6";

layer 2 (Base) - E = 30,000 psi; υ = .38; depth = 12";

layer 3 (roadbed soil)- E = 5,000 psi; υ = .45; infinite depth.

Comparison of the results of the CHEV5L program with the results using the flexible boundary placed at different depths and under different tire pressure and wheel loads are discussed in the following sections. Unless otherwise mentioned, the pavement structure is subjected to a 9 kip of wheel load with 100 psi of tire pressure.

3.5.1 : Effect of the Depth of the Flexible Boundary

In cases 1, 2, and 3, the flexible boundary is placed at depths of 12", 35", and 85" beneath the surface of the roadbed soil, respectively. Comparison of surface deflections, and radial and vertical stresses between these three cases and CHEV5L program are given in Tables 3-5, to 3-7, and Figures 3-17 to 3-19.

Table 3-5 : Sensitivity of surface deflections to the depth of the flexible boundary

radial dist. (inches)	Surface Deflection (inch)			
	Case 1	Case 2	Case 3	CHEV5L
0	.02521	.02567	.02847	.02695
0.67	.02515	.02561	.02841	.02693
2.	.02495	.02541	.02821	.02674
3.3	.02457	.02503	.02784	.02636
4.7	.02395	.02442	.02723	.02576
6.7	.02288	.02335	.02616	.02439
9.4	.02158	.02207	.02489	.02317
12	.02042	.02092	.02376	.02198
14.7	.01934	.01985	.02271	.02075
18.7	.01791	.01845	.02134	.01904
24.1	.01628	.01686	.01980	.01698
29.4	.01499	.01561	.01860	.01521
37.5	.01375	.01443	.01747	.01293
48.2	.01283	.01357	.01667	.01055

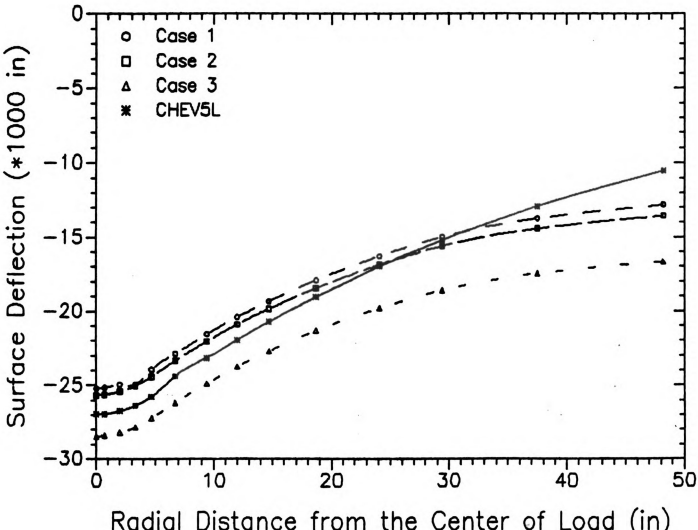

Figure 3–17: Sensitivity of Surface Deflection to the Depth of the Flexible Boundary

Table 3-6 : Sensitivity of radial stresses to the depth of the flexible boundary (at a radial distance of .67" from the center of the loaded area)

Depth (inches)	Radial Stresses (psi)			
	Case 1	Case 2	Case 3	CHEV5L
0	-232.56	-231.11	-229.16	-242.60
0.5	-194.11	-192.86	-191.16	-200.4
1.5	-117.21	-116.35	-115.14	-123.10
2.5	-50.69	-50.69	-49.48	-55.03
3.5	9.69	9.80	10.05	7.43
4.5	69.45	69.19	68.96	69.58
5.5	135.54	134.90	134.20	137.70
6. (+)	168.59	167.76	166.81	176.2
6. (-)	.61	.53	.41	.32
7.	.99	.90	.79	.98
9.	1.74	1.64	1.53	2.13
11.	2.53	2.41	2.29	3.25
13.	3.49	3.33	3.21	4.52
15.	4.75	4.57	4.43	6.08
17.	6.48	6.27	6.11	8.12
18. (+)	7.35	7.13	6.95	9.39
18. (-)	-.28	-.38	-.62	-.21
19.	-.29	-.40	-.63	-.20
21.	-.32	-.45	-.66	-.18
23.	-.34	-.48	-.69	-.17
25.	-.36	-.51	-.72	-.17
27.	-.37	-.54	-.76	-.15
29.	-.33	-.57	-.81	-.14
30.	-.32	-.58	-.83	-.13

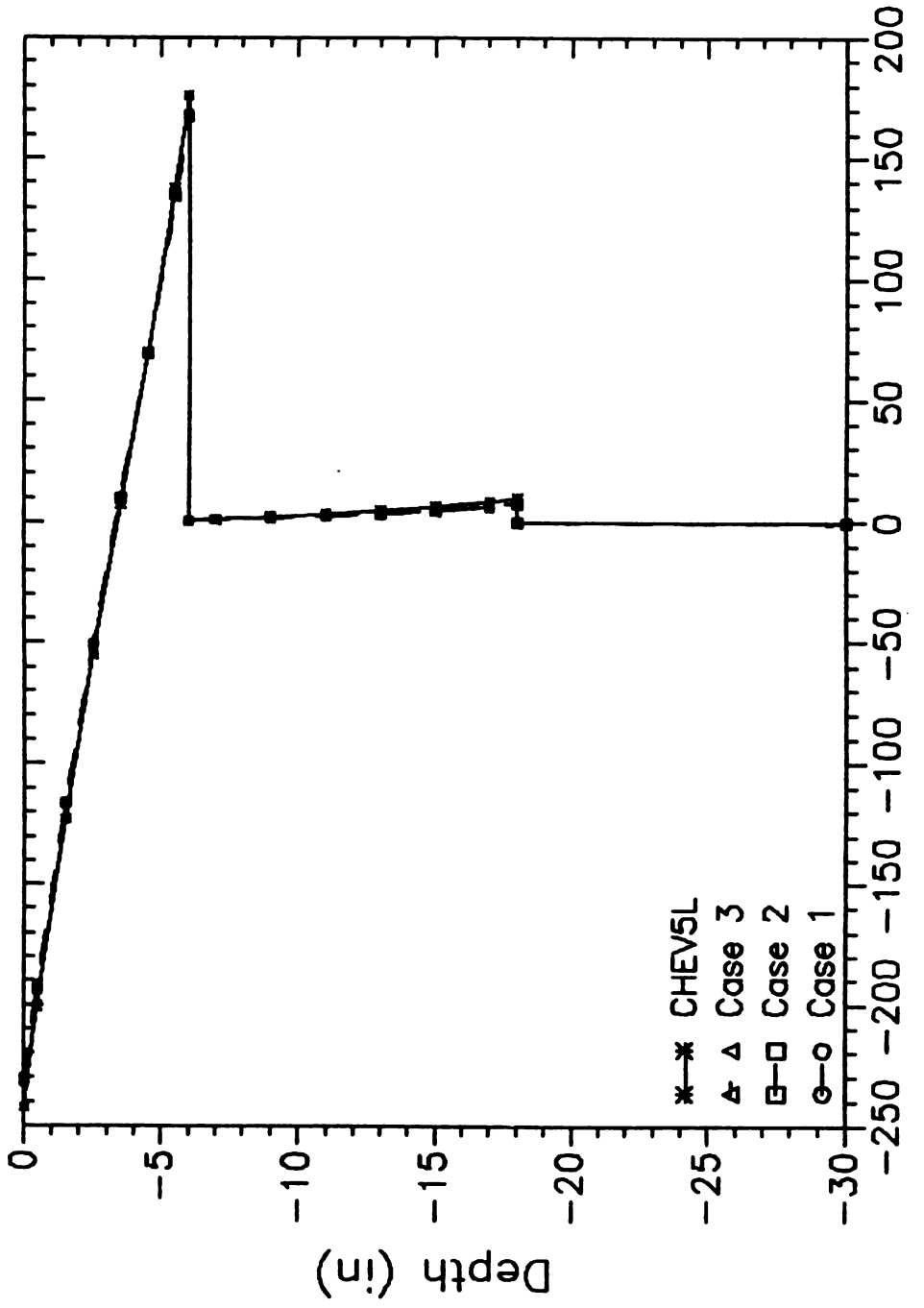

Figure 3-18: Sensitivity of Radial Stress to the Depth of the Flexible Boundary(R=.67")

Table 3-7 : Sensitivity of vertical stresses to the depth of the flexible boundary (at a radial distance of .67" from the center of the loaded area)

Depth (inches)	Vertical Stresses (psi)			
	Case 1	Case 2	Case 3	CHEV5L
0	100.	100.	100.	99.7
0.5	98.72	98.72	98.71	98.9
1.5	90.43	90.44	90.44	90.14
2.5	73.96	73.97	74.00	73.9
3.5	53.34	53.37	53.42	53.67
4.5	33.53	33.56	33.65	34.10
5.5	20.22	20.26	20.37	20.26
6.	17.49	17.54	17.66	17.3
7.	14.03	14.08	14.21	14.82
9.	10.19	10.25	10.42	10.9
11.	7.33	7.41	7.62	7.94
13.	5.21	5.29	5.53	5.73
15.	3.67	3.76	4.02	4.10
17.	2.71	2.80	3.09	3.07
18.	2.49	2.58	2.88	2.8
19.	2.26	2.34	2.65	2.64
21.	2.01	2.09	2.41	2.37
23.	1.80	1.88	2.21	2.14
25.	1.62	1.71	2.04	1.95
27.	1.47	1.56	1.89	1.79
29.	1.29	1.43	1.75	1.64
30.	1.20	1.35	1.60	1.58

Table 3-5 and Figure 3-17, show that the flexible boundary placed at about 3 feet beneath the surface of the roabed soil yields the most accurate surface deflections. However, Tables 3-6 to 3-7 and Figures 3-18 to 3-19, indicate that the radial and vertical stresses are relatively insensitive to the location of the flexible boundary. For linear analysis, it is recommended that the flexible boundary be placed at about 3 feet beneath of the surface of the roadbed soil, unless stresses and displacements are required beneath this depth.

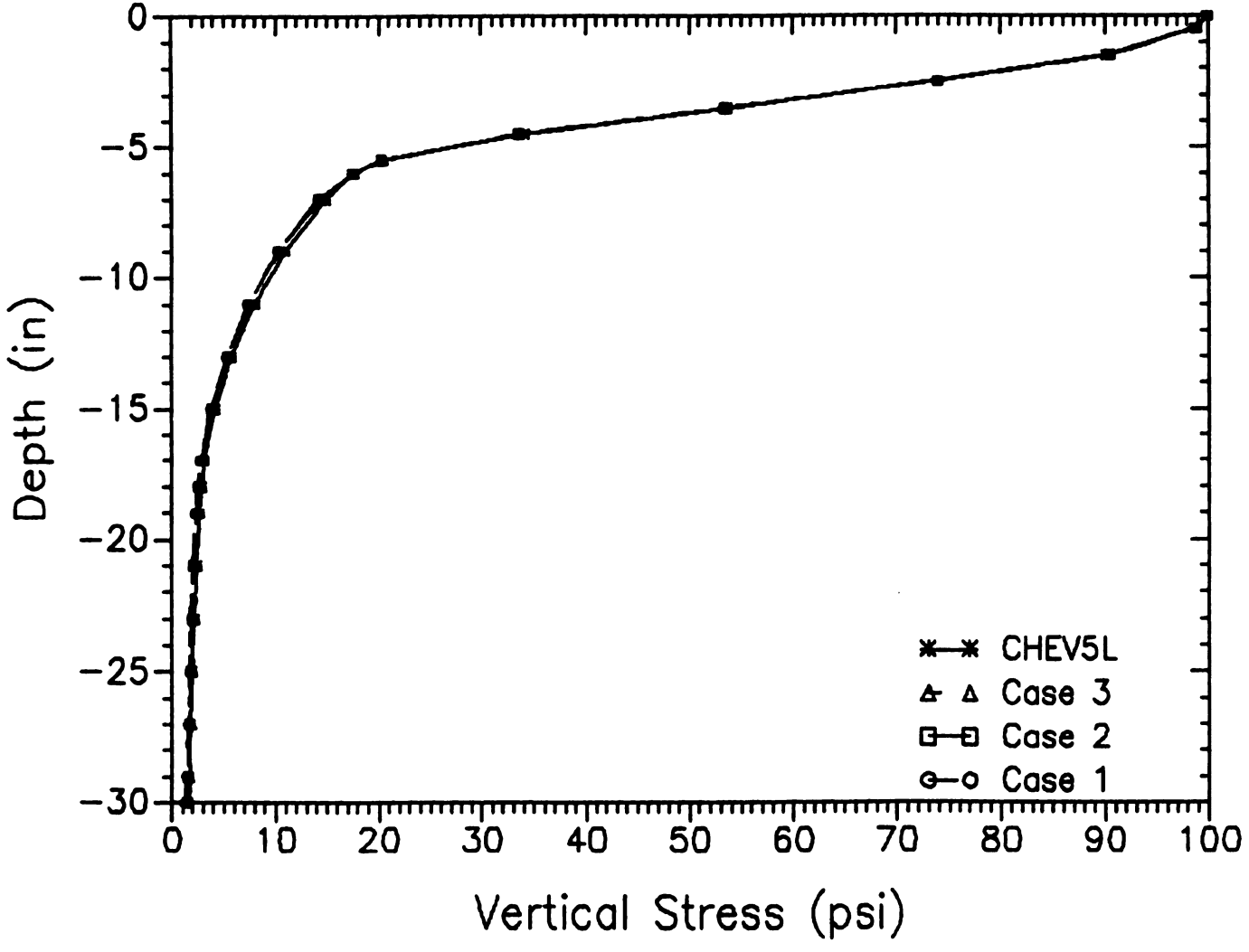

Figure 3-19: Sensitivity of Vertical Stress to the Depth of the Flexible Boundary (R=.67")

3.5.2 ; Effect of the Tire Pressure on the Location of the Flexible Boundary

Here all input parameters are kept the same except the tire pressure, which is increased from 100 psi to 120 psi. Comparisons of the surface deflections, and the radial and vertical stresses between the three cases and the CHEV5L program are presented in Tables 3-8 to 3-10, and Figures 3-20 to 3-22, respectively.

Table 3-8 : Sensitivity of surface deflections to increase in the tire pressure from 100 to 120 psi.

radial dist. (inches)	Surface Deflection (inch)			
	Case 1	Case 2	Case 3	CHEV5L
0	.02598	.02664	.03016	.02736
0.6	.02593	.02658	.03010	.02734
1.8	.02574	.02639	.02991	.02717
3.1	.02538	.02603	.02955	.02679
4.3	.02478	.02544	.02896	.02622
6.1	.02374	.02440	.02793	.02476
8.6	.02252	.02320	.02674	.02355
11	.02145	.02214	.02569	.02246
13.4	.02045	.02115	.02471	.02135
17.1	.01913	.01985	.02344	.01972
22.	.01760	.01836	.02199	.01775
26.9	.01639	.01719	.02086	.01602
34.2	.01522	.01607	.01978	.01380
44.	.01436	.01526	.01901	.01141

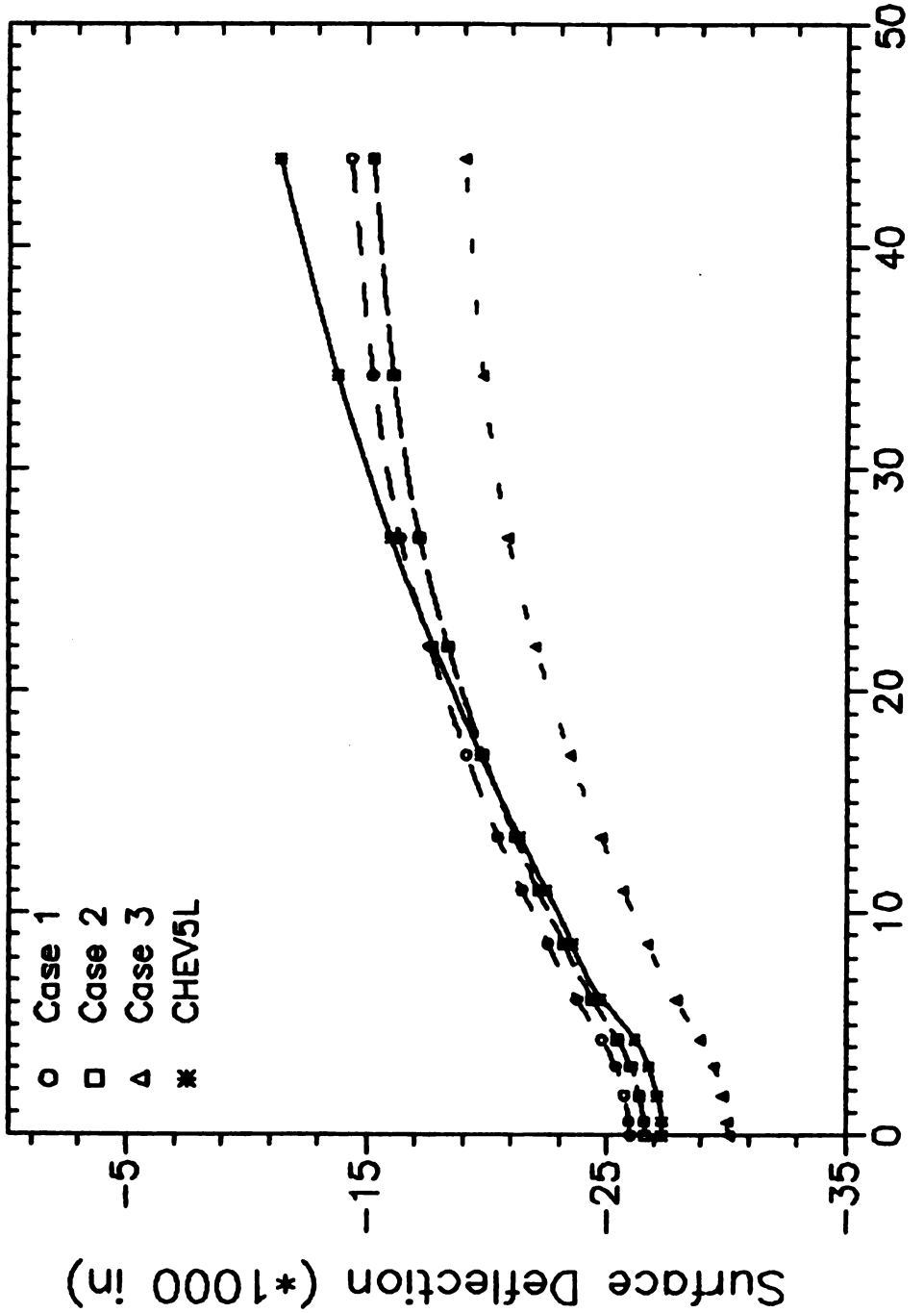

Figure 3–20: Sensitivity of Surface Deflection to Increase in the Tire Pressure from 100 to 120 psi

Table 3-9 : Sensitivity of the radial stresses to increase in the tire pressure from 100 to 120 psi (at a radial distance of .61" from the center of the loaded area)

Depth (inches)	Radial Stresses (psi)			
	Case 1	Case 2	Case 3	CHEV5L
0	-251.90	-250.35	-248.57	-265.20
0.5	-209.30	-207.96	-206.41	-217.60
1.5	-124.10	-123.17	-122.07	-131.60
2.5	-52.41	-51.88	-51.22	-57.63
3.5	11.06	11.19	11.42	8.58
4.5	73.35	73.08	72.87	73.45
5.5	142.92	142.24	141.60	146.40
6. (+)	177.70	176.82	175.96	188.10
6. (-)	.68	.60	.48	.48
7.	1.00	.91	.79	1.09
9.	1.64	1.52	1.42	2.17
11.	2.32	2.19	2.10	3.25
13.	3.19	3.04	2.94	4.50
15.	4.38	4.20	4.10	6.05
17.	6.06	5.85	5.74	8.09
18. (+)	6.90	6.68	6.55	9.37
18. (-)	-.38	-.51	-.77	-.22
19.	-.40	-.54	-.78	-.21
21.	-.43	-.59	-.81	-.20
23.	-.46	-.64	-.85	-.18
25.	-.48	-.68	-.88	-.17
27.	-.50	-.71	-.92	-.16
29.	-.46	-.74	-.97	-.16
30.	-.45	-.75	-1.00	-.15

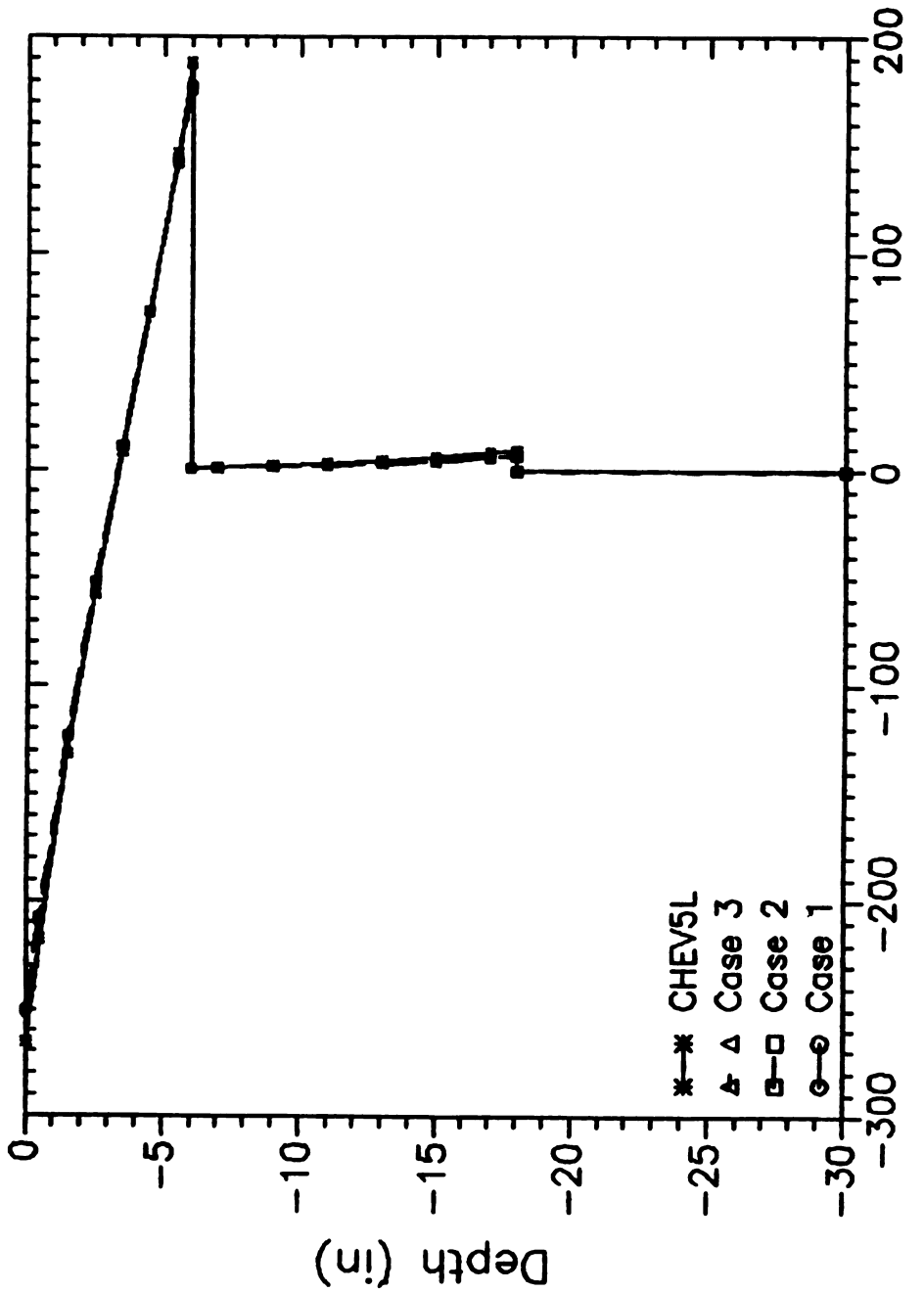

Figure 3-21: Sensitivity of the Radial Stress to Increase in the Tire Pressure from 100 to 200 psi (at R=.61")

Table 3-10 : Sensitivity of vertical stresses to increase in the tire pressure from 100 to 120 psi (at a radial distance of .61" from the center of the loaded area)

Depth (inches)	Vertical Stresses (psi)			
	Case 1	Case 2	Case 3	CHEV5L
0	120.	120.	120.	119.6
0.5	118.39	118.40	118.39	118.7
1.5	108.11	108.12	108.13	108.1
2.5	87.62	87.64	87.67	87.97
3.5	62.18	62.22	62.27	62.81
4.5	38.06	38.10	38.19	38.67
5.5	21.94	21.99	22.10	21.77
6.	18.73	18.79	18.92	18.19
7.	14.65	14.72	14.86	15.48
9.	10.51	10.61	10.79	11.23
11.	7.51	7.63	7.85	8.13
13.	5.31	5.44	5.69	5.83
15.	3.72	3.86	4.15	4.15
17.	2.74	2.87	3.19	3.08
18.	2.52	2.65	2.98	2.81
19.	2.28	2.41	2.75	2.65
21.	2.03	2.15	2.51	2.38
23.	1.82	1.94	2.32	2.15
25.	1.65	1.77	2.15	1.96
27.	1.50	1.63	2.01	1.79
29.	1.32	1.50	1.89	1.65
30.	1.24	1.42	1.74	1.58

When the tire pressure is increased from 100 to 120 psi, the flexible boundary placed at about 3 feet from the surface of roadbed soil still has the most accurate surface deflections. As before, the radial and vertical stresses are quite close for these three cases and the CHEV5L method. Thus the optimal location of the flexible boundary is not sensitive to the tire pressure, and placement at a depth of about 3 feet still yields the best results.

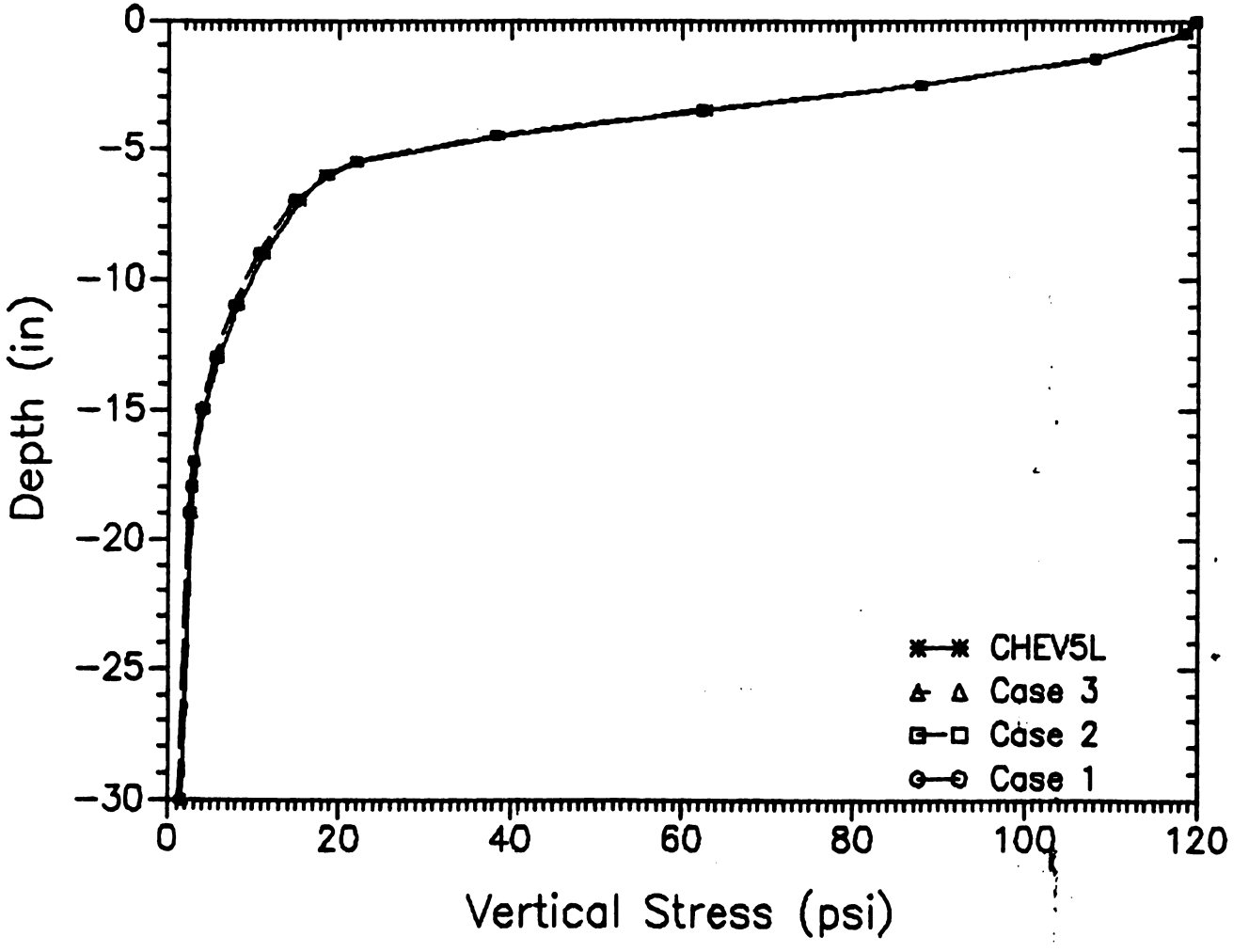

Figure 3-22: Sensitivity of the Vertical Stress to Increase in the Tire Pressure from 100 to 120 psi (at R=.61")

3.5.3 : Effect of the Wheel Load on the Location of the Flexible Boundary

Here all input parameters are kept the same except the wheel load which is increased from 9,000 to 12,000 pounds. Comparisons of the surface deflections, and the radial and vertical stresses between the three cases and the CHEV5L program are presented in Tables 3-11 to 3-13, and Figures 3-23 to 3-25, respectively.

Table 3-11 : Sensitivity of surface deflections to increase in the wheel load from 9 to 12 kips.

radial dist. (inches)	Surface Deflection (inch)			
	Case 1	Case 2	Case 3	CHEV5L
0	.03246	.03278	.03532	.03523
0.8	.03237	.03269	.03523	.03519
2.3	.03206	.03239	.03493	.03491
3.9	.03151	.03183	.03438	.03434
5.4	.03064	.03096	.03352	.03351
7.7	.02910	.02943	.03200	.03181
10.8	.02719	.02754	.03013	.02999
13.9	.02544	.02581	.02843	.02811
17.0	.02383	.02422	.02687	.02631
21.6	.02172	.02215	.02486	.02386
27.8	.01932	.01981	.02260	.02096
34.0	.01745	.01800	.02089	.01848
43.3	.01565	.01629	.01929	.01541
55.6	.01434	.01506	.01814	.01231

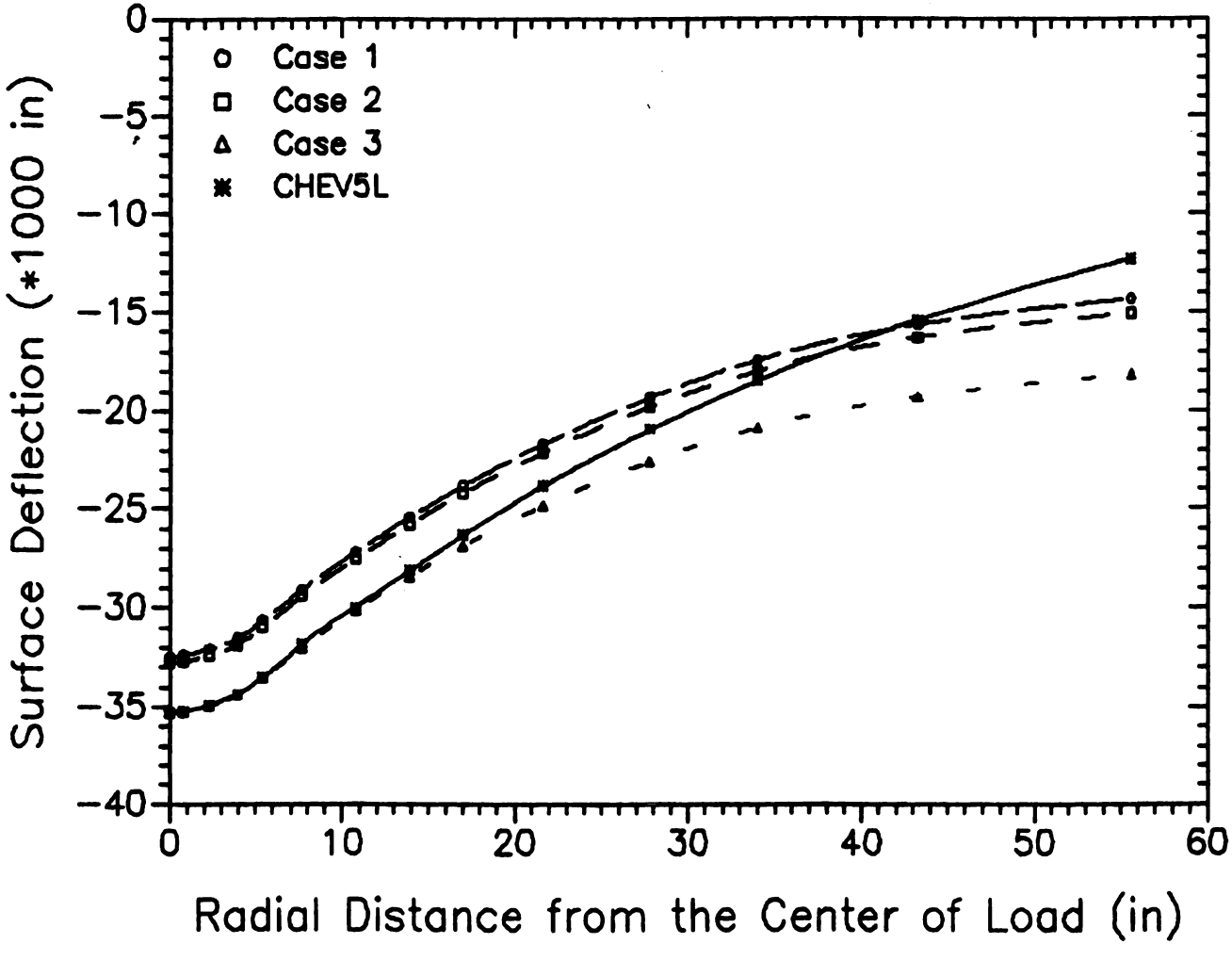

Figure 3–23: Sensitivity of Surface Deflection to Increase in the Wheel Load from 9 to 12 kips

Table 3-12 : Sensitivity of radial stresses to increase in the wheel load from 9 to 12 kips (at a radial distance of .77" from the center of the loaded area)

Depth (inches)	Radial Stresses (psi)			
	Case 1	Case 2	Case 3	CHEV5L
0	-273.71	-272.18	-269.48	-282.30
0.5	-229.73	-228.40	-226.04	-234.90
1.5	-141.76	-140.84	-139.16	-147.10
2.5	-63.13	-62.62	-61.59	-67.34
3.5	10.37	10.49	10.86	7.87
4.5	83.85	83.57	83.29	83.35
5.5	163.92	163.25	162.30	164.70
6. (+)	203.96	203.08	201.81	209.50
6. (-)	.59	.53	.39	.10
7.	1.21	1.13	.98	1.06
9.	2.44	2.32	2.17	2.70
11.	3.67	3.52	3.35	4.28
13.	5.09	4.91	4.70	6.01
15.	6.88	6.66	6.43	8.10
17.	9.27	9.02	8.74	10.80
18. (+)	10.47	10.20	9.90	12.40
18. (-)	-.24	-.33	-.59	-.27
19.	-.25	-.34	-.61	-.25
21.	-.26	-.38	-.63	-.23
23.	-.28	-.41	-.67	-.21
25.	-.29	-.44	-.71	-.19
27.	-.29	-.47	-.75	-.17
29.	-.24	-.49	-.81	-.16
30.	-.22	-.51	-.84	-.15

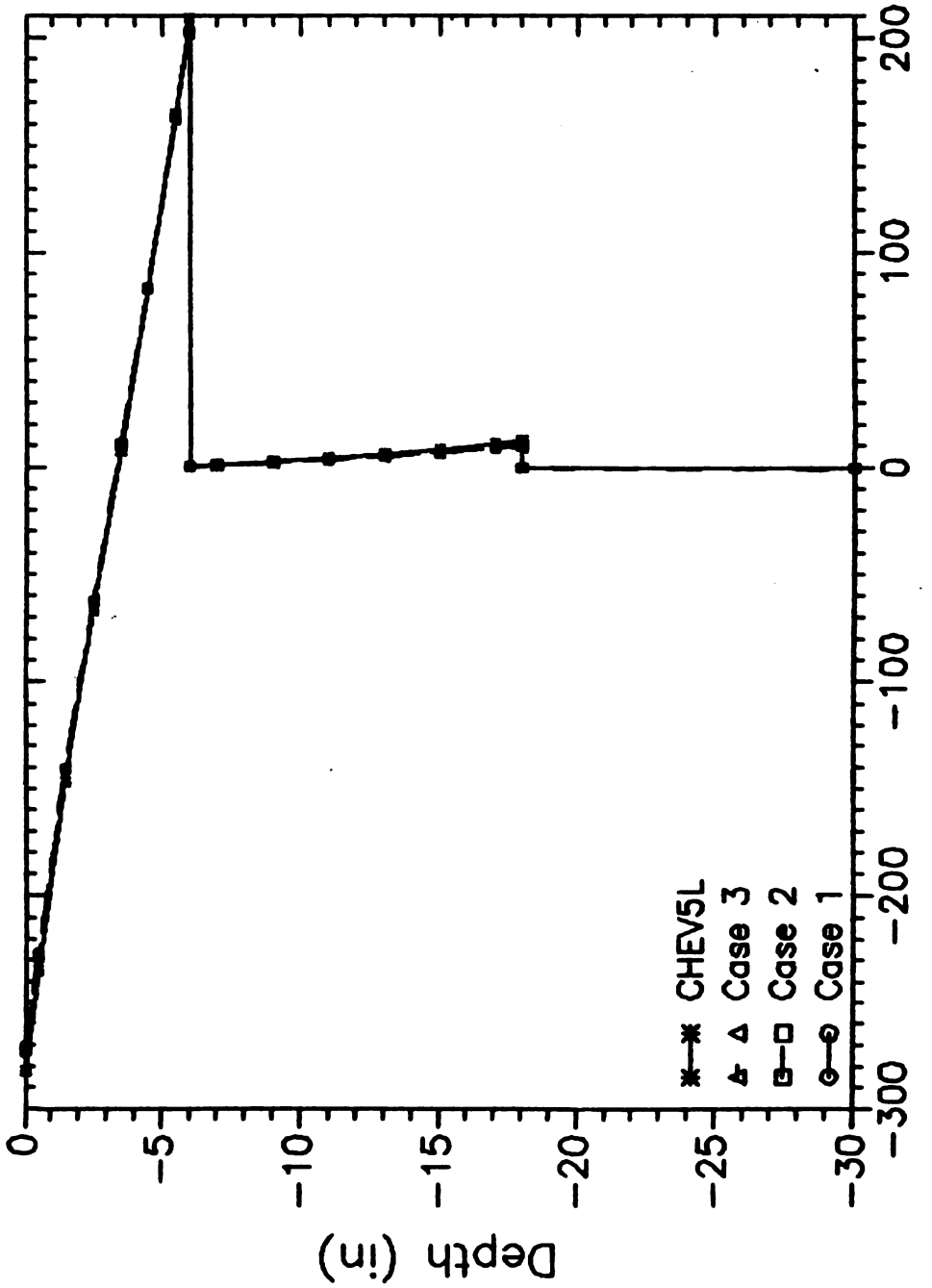

Figure 3-24: Sensitivity of Radial Stress to Increase in the Wheel Load from 9 to 12 kips (at R=.77")

Table 3-13 : Sensitivity of vertical stresses to increase in the wheel loads from 9 to 12 kips (at a radial distance of .77" from the center of the loaded area)

Depth (inches)	Vertical Stresses (psi)			
	Case 1	Case 2	Case 3	CHEV5L
0	100.	100.	100.	99.70
0.5	98.75	98.75	98.75	98.83
1.5	90.78	90.79	90.79	90.12
2.5	75.09	75.10	75.13	74.66
3.5	55.46	55.48	55.53	55.58
4.5	36.42	36.43	36.51	37.08
5.5	23.66	23.68	23.79	23.96
6.	20.88	20.90	21.01	21.00
7.	17.33	17.35	17.49	18.27
9.	12.82	12.86	13.04	13.70
11.	9.37	9.42	9.62	10.14
13.	6.73	6.78	7.02	7.40
15.	4.79	4.85	5.12	5.36
17.	3.58	3.64	3.93	4.05
18.	3.31	3.36	3.66	3.71
19.	3.00	3.05	3.36	3.51
21.	2.67	2.72	3.04	3.16
23.	2.39	2.45	2.78	2.86
25.	2.16	2.22	2.55	2.60
27.	1.95	2.02	2.34	2.39
29.	1.70	1.85	2.16	2.20
30.	1.58	1.73	1.95	2.11

When the pavement structure is subjected to high wheel loads (such as 12 kips), Table 3-11 and Figure 3-23 shows that the deeper flexible boundary results in the most accurate surface deflections.

The above tables and figures, show that when flexible boundary is placed deeper, the radial stresses decrease slightly, and the vertical stresses increase slightly. The radial and vertical stresses from the CHEV5L program are always slightly higher than the results of the finite element plus flexible boundary solution.

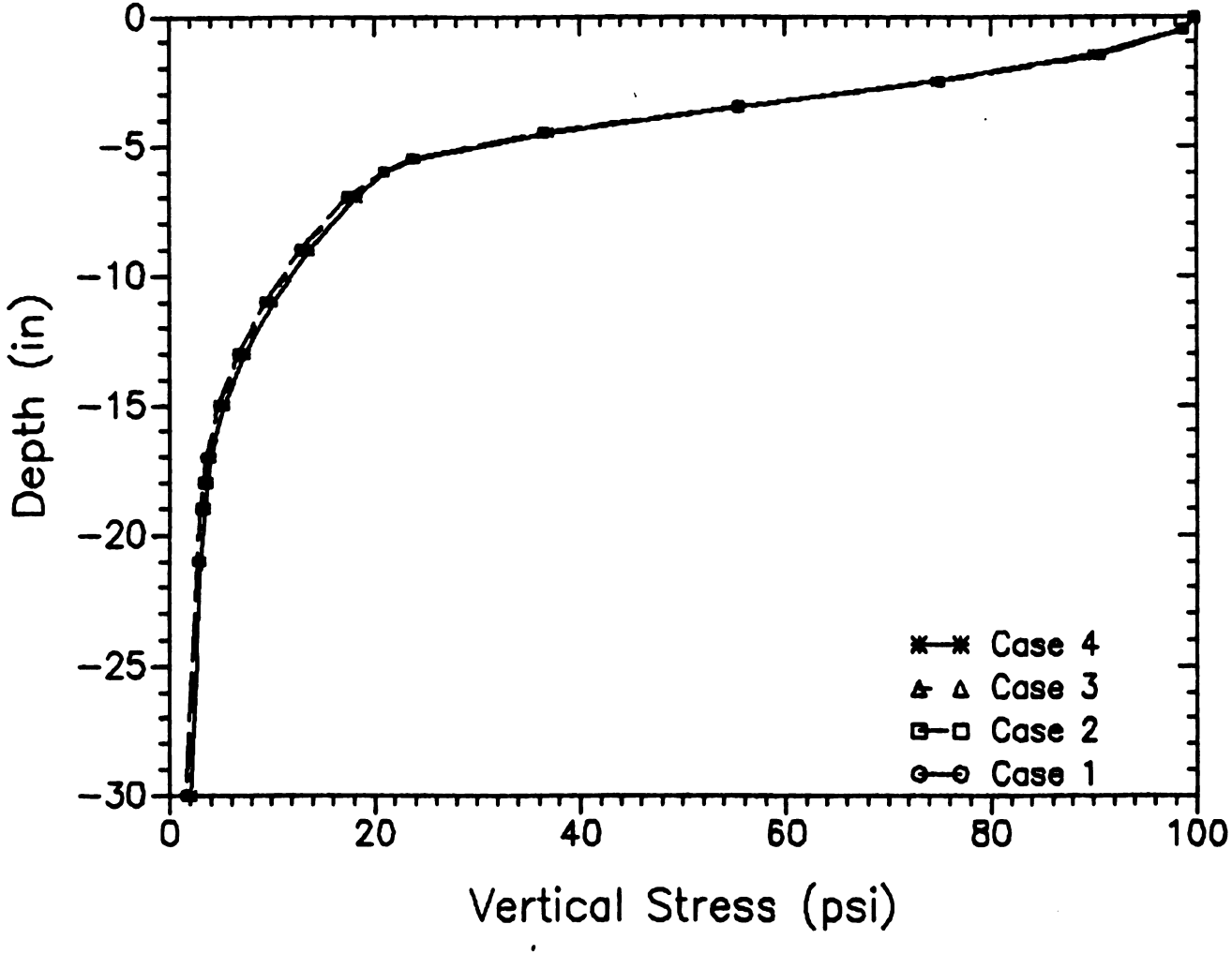

Figure 3-25: Sensitivity of Vertical Stress to Increase in the Wheel Load from 9 to 12 kips (at R=.77")

3.6 DISCUSSION AND SUMMARY

Four FE methods are reviewed to ascertain which ones are capable of simulating the behavior of asphalt pavements observed in the field and the laboratory. While a 3-D FEM is the most suitable technique, present computational capabilities limit its use in practice. Table 3-14 summarizes the effects that can and cannot be accounted for by each of the four models.

Table 3-14 : Capabilities of the Finite Element Models

	Sandwich plate theory model	Plane strain model	3-D FE model	Axisymmetric model
Soil overburden	Yes	Yes	Yes	Yes
Inelastic behavior of granular and cohesive material	Yes	Yes	Yes	Yes
Edge effect	Yes	Yes	Yes	No
Unbound behavior between asphalt and granular layer	No	No	No	No
Economical CPU time	No	Yes	No	Yes
Accuracies of computational results	Not good	Not good	Good	Good

From the above table, the major disadvantages of the sandwich plate theory which is sometimes used for the analysis of rigid pavements, is that it cannot accurately calculatethe horizontal displacements of pavement. Also it is not well suited for the analysis of flexible

pavements. The major disadvantage of the two dimensional plane strain model is that it assumes an infinitely long loading which is unrealistic. The 3-D FE model is the most versatile but needs large storage and a large amount of computation time. At present, due to their limitations, it is practically impossible to implement this model on personal computers. The obvious disadvantages of the axisymmetric model are that it cannot consider the edge effect of pavements and multiple-wheel loadings in nonlinear problems. Nevertheless, the axisymmetric model appears to be the most suitable at the present time.

If flexible pavements can be assumed to be composed of linear elastic material, the Chevron series programs are perhaps the best. These can quickly and accurately compute the required displacements and stresses. However, the Chevron series programs cannot be used to model the inelastic behavior of granular or cohesive material.

The axisymmetric finite element model is selected as the basic foundation for the development of a nonlinear finite element program to be implemented on personal computers. The validation of this with the general purpose SAP IV program, will be discussed in Chapter 5.

A flexible boundary concept is used in the static finite element analysis of pavements. Such modeling enables the bottom boundary to be placed at any depth below which displacements and stresses are not of interest, while accurately representing the displacements occuring in the material below the boundary. The principal advantage of this new technique is its computational efficiency, especially when used with nonlinear finite element approaches requiring iterative solutions.

CHAPTER 4

NONLINEAR FINITE ELEMENT ANALYSIS

4.1 : INTRODUCTION

In a pavement, repeated vehicle loads cause permanent deformations as well as resilient (recoverable) deformations. At the present time, the computational capacity to follow the stress-strain curve through millions of load repetitions is not readily available. In practice, mechanistic models are used only to compute stresses and resilient strains, while permanent (plastic) deformation is empirically related to the resilient strains, magnitude of load, number of load applications, material properties, etc. (see chapter 6). The resilient response is characterized by the resilient modulus of the material (see Figure 4-1), which is defined as the ratio of the repeated axial deviator stress to the recoverable axial strain as in Eq.2-10.

4.2 : MATERIAL NONLINEARITY

There are many nonlinear material models that may be used in the finite element analysis. Four suitable models, the hyperbolic, the resilient modulus, the shear and volumetric stress-strain (also called the contour model), and the third hyperelastic models are reviewed here. The advantages and limitations of each model is briefly discussed, and the reasons for choosing the resilient modulus model with the Mohr-Coulomb failure criterion are discussed.

The advantage of the hyperbolic model is that it is simple and easy to use (Duncan, et al., 1970). However, it is primarily suited for

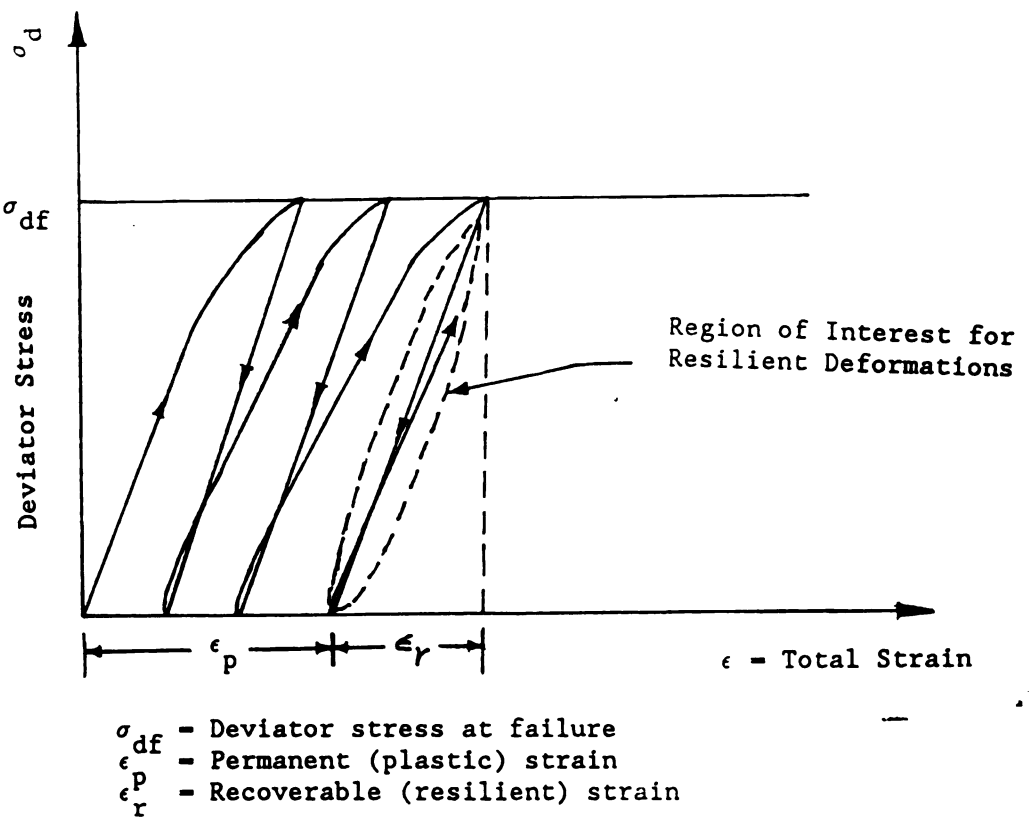

Figure 4-1: **Complete Pavement Response**

monotomic loading problems than for repeated loading problems. It is therefore unsuitable in estimating pavement responses under repeated loads.

The contour model is an advanced and sophisticated model which can successfully predict the nonlinear responses of granular materials, and is especially suited to three dimensional problem (Brown, et al., 1981). However, due to the limitation of laboratory equipment in most state highway agencies, it is difficult to estimate the necessary material constants. Therefore, the model is unsuitable for the development of a daily design program for the state highway departments.

The advantages of the hyperelastic model are that it can simulate the nonlinearity, shear dilatancy, stress-induced anisotropy, effect of the confining stress, and the effect of the third stress invariant of soils. However, the limitations of the model include (Chen, et al., 1982):

1. Best results from the model are generally expressed at low stress levels below failure.
2. Although the nine material constants required for the model can be estimated, it is still not easy to apply. In addition, the nine material constants have no direct physical interpretation.
3. If monotonic loading without unloading or reloading is applied, then the model satisfies all the requirements such as uniqueness, stability, and continuity. However, when the unloading or reloading occurs, it fails to satisfy continuity at or near material loadings. Actually, pavement structures are subjected to many loadings and reloadings. Therefore, the model is not very suitable to simulate the granular materials and roadbed soil in

the pavement structure.

The advantages of the resilient modulus model include:

1. The model reduces the complicated nonlinear response to a simple form and is easy to use.
2. The resilient moduli of granular materials and roadbed soil can be determined by most state highway agencies.
3. The granular materials and roadbed soil still maintain their resilient behavior under repeated loads even after the occurrence of large permanent deformations (Haynes, et al., 1963; Seed, et al., 1962).

However, there are some limitations of the resilient modulus model:

1. The model does not consider the loading and unloading stress paths and the shear dilatancy of granular materials and roadbed soil.
2. The model is accurate only in the range of relatively low stresses.

Due to practical constraints, the resilient modulus model is selected in this study.

If only the FEM with the resilient modulus model is used, it will converge extremely slowly. Therefore, Raad and Figueroa (1980) applied the resilient modulus model with the Mohr-Coulomb failure criterion. The Mohr-Coulomb failure criterion was used to modify the principal stresses of each element in the granular layers and roadbed soil after each iteration such that the Mohr-Coulomb envelope was not exceeded.

Before introducing the Mohr-Coulomb criterion, the resililent moduli of granular materials and roadbed soil are briefly reviewed.

For granular materials, the resilient modulus can be expressed as

$$M_r = K_1(\theta)^{K_2} \quad \text{(Eq.2-11)}$$

or

$$M_r = K_1'(\sigma_3)^{K_2'} \quad \text{(Eq.2-12)}$$

Where

M_r = resilient modulus (psi);

θ = bulk stress (= $\sigma_1+\sigma_2+\sigma_3$) (psi);

σ_3 = confining pressure (psi);

K_1, K_2, K_1', K_2' = material constants.

The relationship between the bulk stress and the resilient modulus is shown in Figure 4-2.

Since the regression equation expressed in equation 2-11 is found to be more accurate than that expressed in equation 2-12. The former is chosen for this analysis.

For fine-grained soils subjected to repeated deviatoric stresses at low values of confining pressure, the resilient modulus can be expressed as

$$M_r = K_2 + K_3[K_1 - (\sigma_1 - \sigma_3)]; \quad \text{for } K_1 > (\sigma_1 - \sigma_3) \quad \text{(Eq.2-13a)}$$

and

$$M_r = K_2 + K_4[(\sigma_1 - \sigma_3) - K_1]; \quad \text{for } K_1 < (\sigma_1 - \sigma_3) \quad \text{(Eq.2-13b)}$$

where

$(\sigma_1 - \sigma_3)$ = deviator stress (psi);

K_1, K_2, K_3, K_4 = material constants determined by linear regression.

The relationship between the resilient modulus and the deviator stress is shown in Figure 4-3.

The nonlinear FE analysis of the flexible pavement structure can be divided into the following steps:

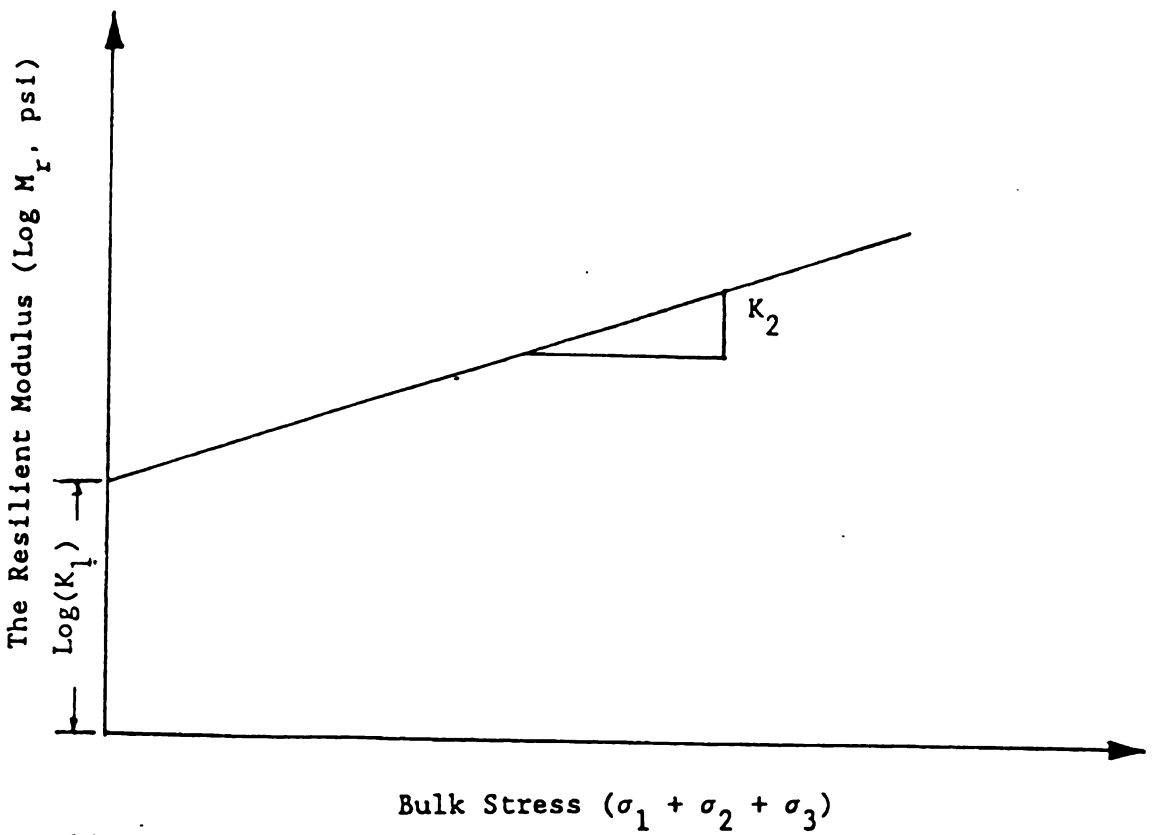

Figure 4-2 : Typical Variation of Resilient Modulus with Repeated Stress for Granular Material

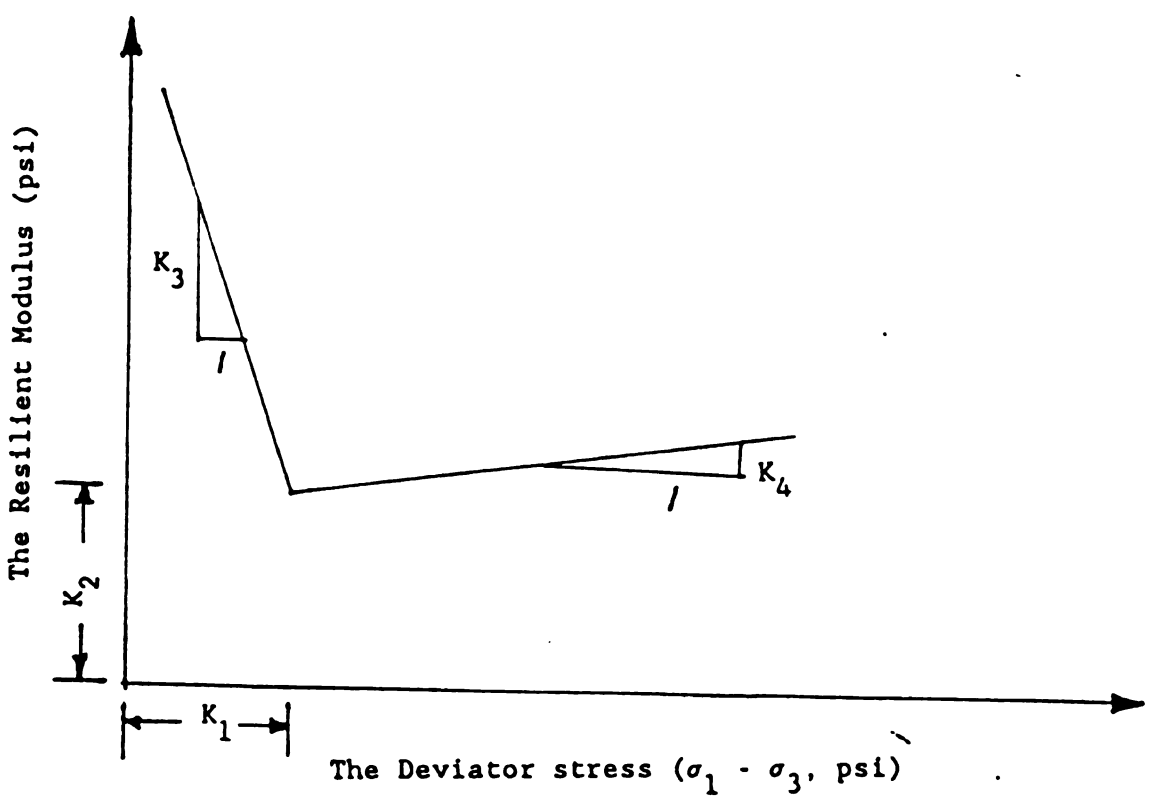

Figure 4-3 : Typical Variation of Resilient Modulus with Repeated Stress for Roadbed Soil (cohesive soil)

1. The pavement is discretized into a set of elements connected at nodal points.
2. Nonlinear properties of the granular materials and roadbed soil are included by means of successive iteration.
3. The principal stresses in the granular layers and roadbed soil are modified at the end of each iteration so that they do not exceed the strength of the material as defined by the Mohr-Coulomb envelope. At the end of each iteration, the maximun and minimum allowable principal stresses in each element are calculated as

$$(\sigma_1)_{max} = \sigma_v \tan^2\left(45 + \frac{\phi}{2}\right) + 2c \tan\left(45 + \frac{\phi}{2}\right) \qquad \text{(Eq.4-1)}$$

$$(\sigma_3)_{min} = \sigma_v \tan^2\left(45 - \frac{\phi}{2}\right) + 2c \tan\left(45 - \frac{\phi}{2}\right) \qquad \text{(Eq.4-2)}$$

where

$(\sigma_1)_{max}$ = maximum allowable principal stress (psi);

$(\sigma_3)_{min}$ = minimum allowable principal stress (psi);

σ_1, σ_3 = major and minor principal stress, respectively (psi);

σ_v = vertical stress which includes gravity (psi);

c, ϕ = cohesion and angle of friction (degrees) of the soil, respectively.

However, σ_1 should not be greater than σ_1', the major principal stress associated with σ_3 at failure (see Fig.4-4).

where

$$\sigma'_1 = \sigma_3 \tan^2\left(45 + \frac{\phi}{2}\right) + 2c \tan\left(45 + \frac{\phi}{2}\right) \qquad \text{(Eq.4-3)}$$

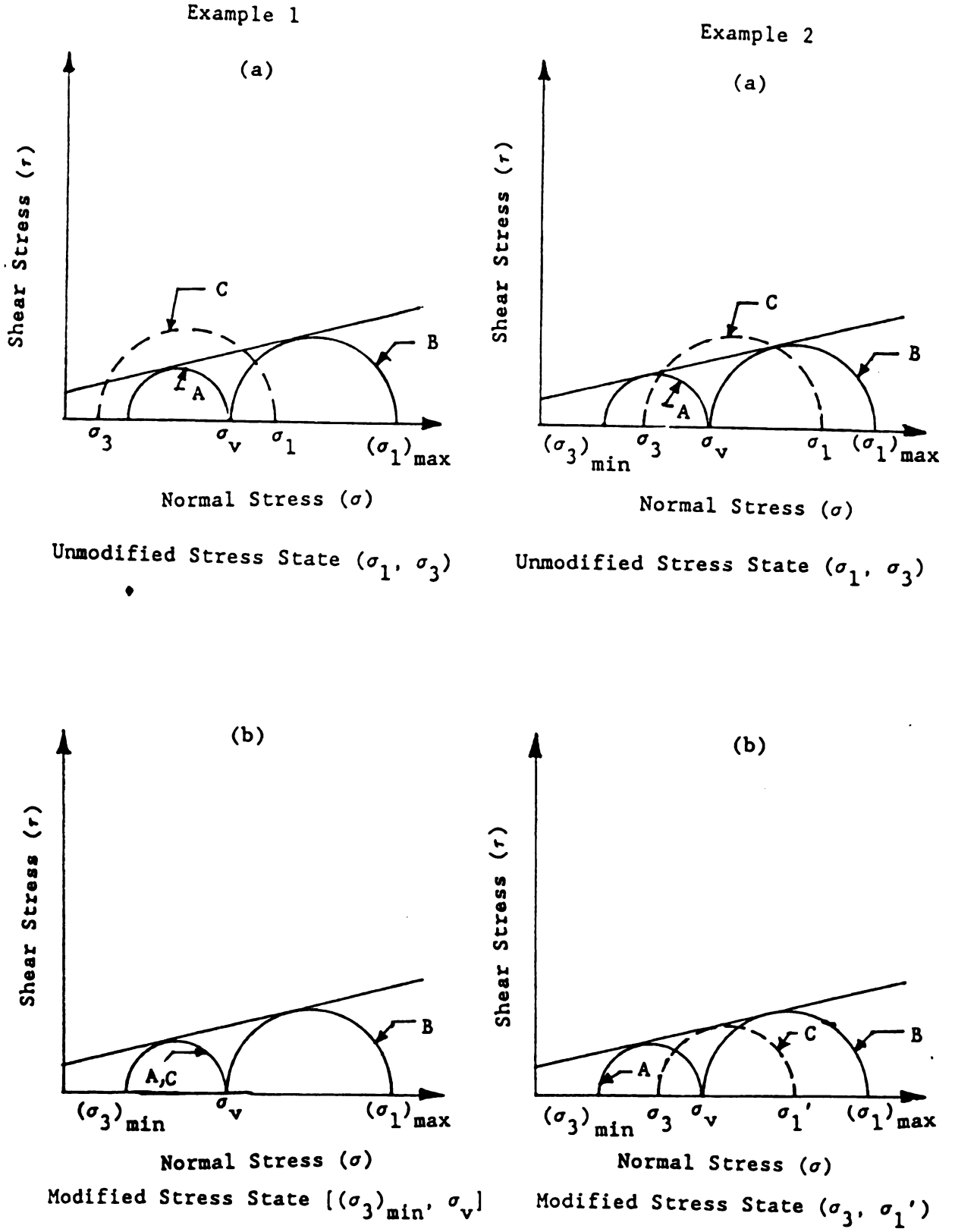

Figure 4-4 : Examples for Stress Modification at End of Iteration

The tensile stress that can be resisted by cohesive soils is

$$\sigma'_T = -2c \tan^2\left(45 - \frac{\phi}{2}\right) \qquad \text{(Eq.4-4)}$$

If the maximum and/or minimum principal stresses exceed these limits then they are set to the corresponding extreme value. Figure 4-4a illustrates typical principal stresses before modification, and Figure 4-4b illustrates the modified principal stresses.

4. For the next iteration, the stresses determined in the preceeding iteration are used to calculate the resilient moduli (using Eq. 2-11 and Eqs. 2-13a, 2-13b) of elements in the granular layers and the roadbed soil. Furthermore, the strains, and resilient deformation of the pavement structure are determined.

5. The convergence error in each iteration can be expressed as (Brown, et al., 1981):

$$\varepsilon = \sum (E_n - E_o) / \sum E_n^2 \qquad \text{(Eq.4-5)}$$

Where

E_o = the current value of resilient modulus (psi);

E_n = the resilient modulus from the previous iteration (psi);

$\sum$ = summation over all nonlinear elements.

If the convergence error between the two successive iterations is smaller than .001, then the iterations are terminated.

A detailed flow chart of how the principal stresses, σ_1 and σ_3, are modified is illustrated in Figure 4-5.

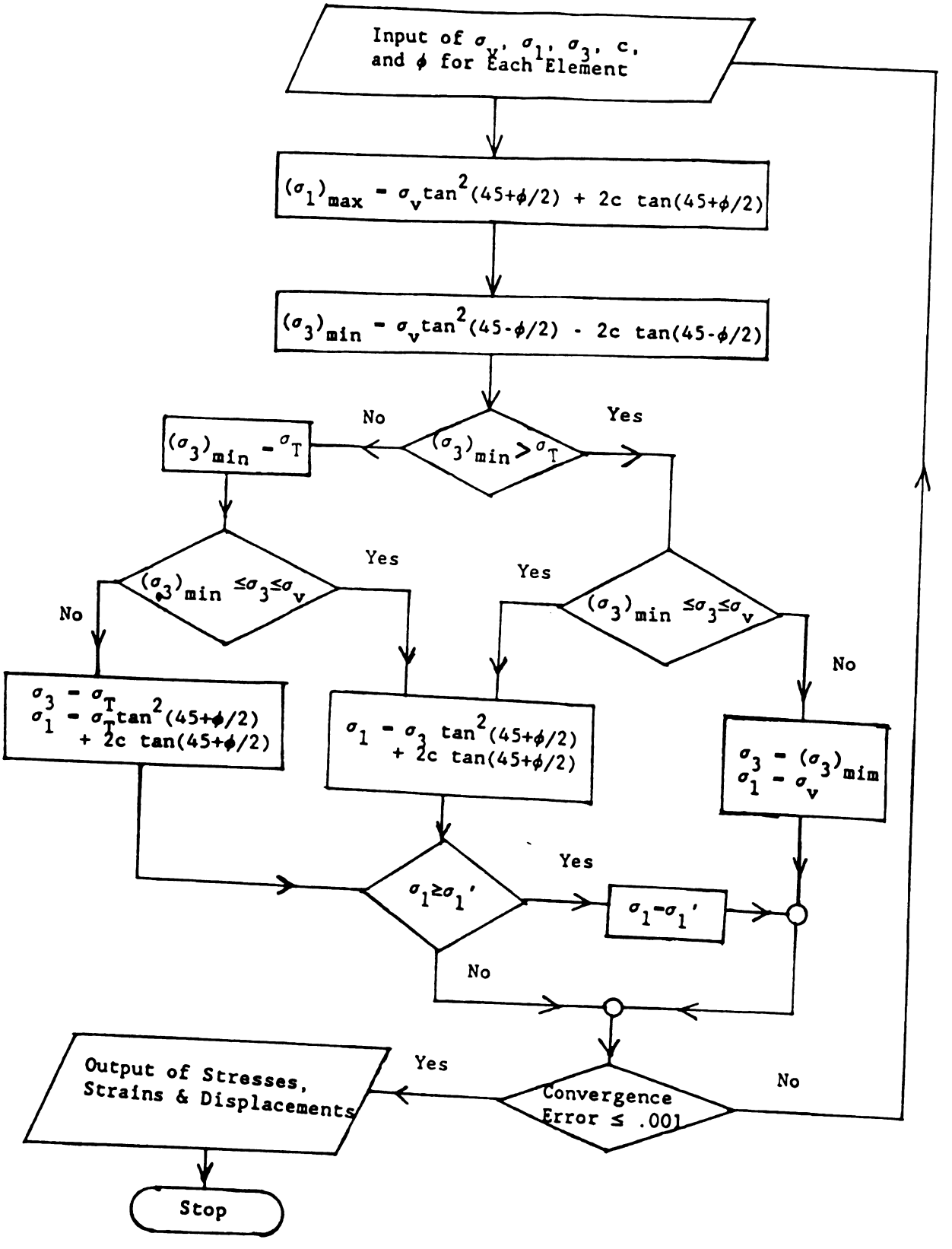

Figure 4-5 : Stress Modification Procedures for Given Iteration

4.3 : SENSITIVITY OF FLEXIBLE BOUNDARY IN NONLINEAR ANALYSIS

When the flexible boundary is used in nonlinear analysis, the nonlinear properties of the material above the boundary may be accounted for through the use of finite elements, but the halfspace below the boundary is assumed to be linear elastic. The boundary should therefore be placed at a sufficient depth below which material nonlinearities can be neglected due to low stresses. The depth at which the boundary is placed should depend on the strength of the upper layers of the pavement section, as well as on the magnitude of the wheel load, since these factors affect the stresses in the roadbed soil. Some reasonable method of obtainng an equivalent modulus for the halfspace beneath the boundary must also be developed. In this section, the sensitivity of the displacements and stresses with respect to the location of the flexible boundary is studied for pavements with nonlinear materials. The estimation of the equivalent modulus of the halfspace is also discussed.

4.3.1 ; Equivalent Modulus for Halfspace below Flexible Boundary

It is necessary to find an equivalent modulus for the halfspace below theflexible boundary in order to approximately account for the displacements below it. A typical section is given in Table 4-2, and two approaches of estimating an equivalent modulus are discussed. In the first, the equivalent modulus for the halfspace is calculated by averaging the resilient moduli of all elements immediately above the boundary; in the second, the equivalent modulus is calculated by averaging the resilient moduli of all bottom elements except for the three elements which are closest to the right vertical boundary.

The resilient moduli of elements just above the flexible boundary are tabulated in Table 4-1. The change in the modulus becomes sharp close to the right vertical boundary, indicating that the boundary has an undersirable effect on the estimated moduli. In order to minimize the influence of the boundary, it is suggested that the last three elements be excluded when estimating an equivalent modulus of the halfspace as the average modulus of the elements immediately above the halfspace.

Table 4-1 : Resilient moduli of elements just above flexible boundary

Element*	1	2	3	4	5	6	7	8
Modulus (psi)	8300	8300	8300	8310	8320	8310	8320	8360
Distance+ (inch)	0.5	1.5	2.5	3.5	4.5	5.5	7.5	10.5
Element*	9	10	11	12	13	14	15	
Modulus (psi)	8410	8440	8520	8660	8780	8950	8920	
Distance+ (inch)	13.5	16.5	21	27	33	42	54	

* Elements are numbered sequentially in the outward radial direction starting at r = 0;

+ Distance is to the center of element.

4.3.2 : Effect of the Depth of the Flexible Boundary

The sensitivity of the depth of the flexible boundary with respect to surface deflections and stresses is discussed below. Results obtained with the flexible boundary placed at depths of 12, 35 and 85 inches beneath the surface of roadbed soil are compared with the results obtained using the ILLI-PAVE program (see Tables 4-3, 4-4 and Figures 4-

6 to 4-8). The ILLI-PAVE program uses finite elements extending to large depths and has a fixed boundary at the bottom.

The properties of the pavement section are given in Table 4-2

Table 4-2 : The properties of the pavement section

Layer	Thick. (in)	E (psi)	υ	Den. (pcf)	K_0	K_1	K_2	K_3	K_4
AC	3	500,000	.4	150	.67				
Base	12		.38	140	.60	5000	.5		
R.S.*	285		.45	115	.82	6.2	3021	1110	-178

* R. S. = Roadbed soil

The cases with the flexible boundary at depth of 12, 35 and 85 inches are henceforth denoted as cases 1, 2 and 3, respectively.

Based on the comparisons for linear material, it would be expected that a deep fixed boundary would still give rise to smaller surface deflections than an exact solution, with the flexible boundary solution being closer to the exact solution (see Figures 3-13 and Table 3-1 in section 3.4). Thus, the surface deflection computed with ILLI-PAVE being smaller than those estimated with the flexible boundary in Table 4-3 and Figure 4-6 is not surprising.

Table 4-3 : Sensitivity of the surface deflections to the depth of the flexible boundary

Rad. Dist. (in)	Surface Deflection (in)			Rad. Dist. (in)	Surf. Def.	% of Diff. (Case 2 - ILLI) / ILLI-PAVE
	Case 1	Case 2	Case 3		ILLI-PAVE	
0.	.03852	.03515	.03515	0	.03184	10.4
.5	.03843	.03506	.03506	1	.03175	
1.5	.03813	.03476	.03477	2	.03137	
2.5	.03758	.03422	.03423	3	.03074	
3.5	.03678	.03344	.03346	4	.02986	
4.5	.03575	.03242	.03245	5	.02876	
5.5	.03449	.03117	.03122	6	.02742	
7.5	.03172	.02845	.02853	7.5	.02533	12.3
10.5	.02771	.02454	.02468	9	.02335	
13.5	.02407	.02102	.02124	12	.01966	
16.5	.02092	.01801	.01830	15.8	.01583	
21.	.01722	.01456	.01495	19.5	.01296	
27.	.01339	.01106	.01156	27	.00936	18.2
33.	.01080	.00878	.00938	42	.00549	28.4
42.	.00871	.00705	.00776	57	.00360	
54.	.00729	.00592	.00671	72	.00306	

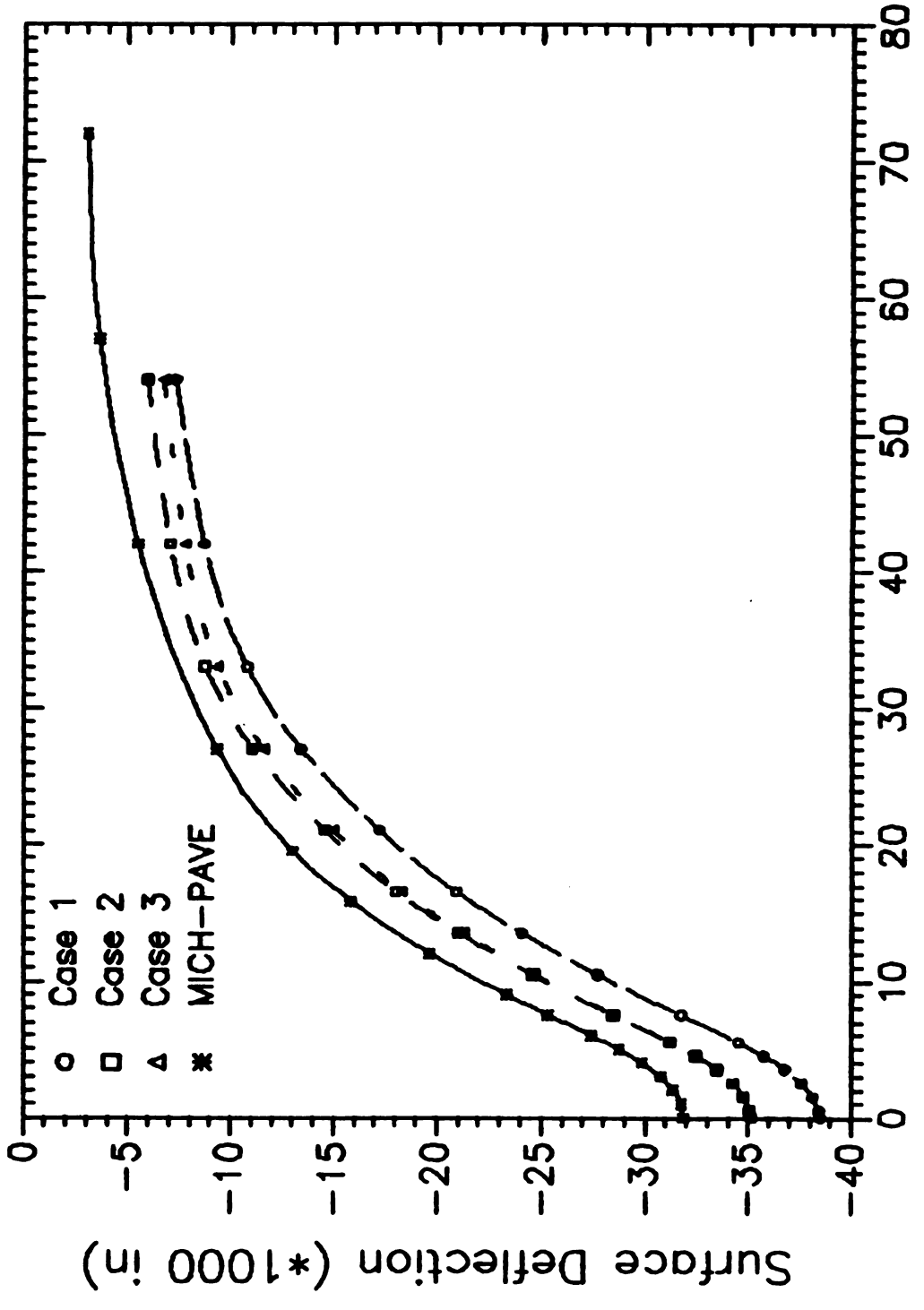

Figure 4-6: Sensitivity of the Surface Deflection to the Depth of the Flexible Boundary

Table 4-4 : Sensitivity of the radial and vertical stresses to the depth of the flexible boundary (at a redial distance of .5" from the center of loaded area)

Depth (in)	Case 1		Case 2		Case 3		LLI-PAVE	
	σ_r	σ_z	σ_r	σ_z	σ_r	σ_z	σ_r	σ_z
0.	-360.78	79.6	-354.95	79.6	-350.47	79.6		
.75	-200.68	72.6	-197.24	72.6	-194.59	72.8	-185.	70.9
2.25	119.5	53.6	118.18	53.7	117.18	54.1	108.	51.7
3(+)	279.59	48.1	275.89	48.2	273.07	48.7		
3(-)	-7.57	48.1	-7.59	48.2	-7.7	48.7		
4	-6.67	38.2	-6.7	38.4	-6.81	39.	-6.11	35.6
6	-4.85	27.8	-4.9	28.1	-5.03	28.9	-4.58	26.7
8	-3.47	19.9	-3.53	20.3	-3.65	21.	-3.36	19.6
10	-2.50	14.4	-2.56	14.7	-2.68	15.5	-2.5	14.6
12	-1.84	10.7	-1.9	11.	-2.01	11.6	-1.91	11.1
14	-1.45	8.4	-1.5	8.7	-1.57	9.1	-1.54	8.95
15(+)	-1.25	8.1	-1.3	8.1	-1.36	8.1		
15(-)	-2.94	8.1	-2.92	8.1	-2.57	8.1		
16.5	-2.7	7.6					-2.5	7.69
19.5	-2.22	6.6					-2.46	6.84
22.5	-2.02	6.0	-2.32	6.2				
25.5	-1.78	5.3						
27	-1.66	4.9						

From Table 4-3 and Figure 4-6, the increase the depth of the flexible boundary from 35 to 85 inches does not change the surface deflections significantly. Therefore, from the surface deflection point of view, the flexible boundary located about 3 feet beneath the surface of roadbed soil is recommended. Furthermore, from Table 4-4, and Figures 4-7 and 4-8, the radial and vertical stresses are similar for all three cases. Therefore, from the stress point of view, the flexible boundary located deeper than 1 foot beneath the surface of the roadbed soil is adequate.

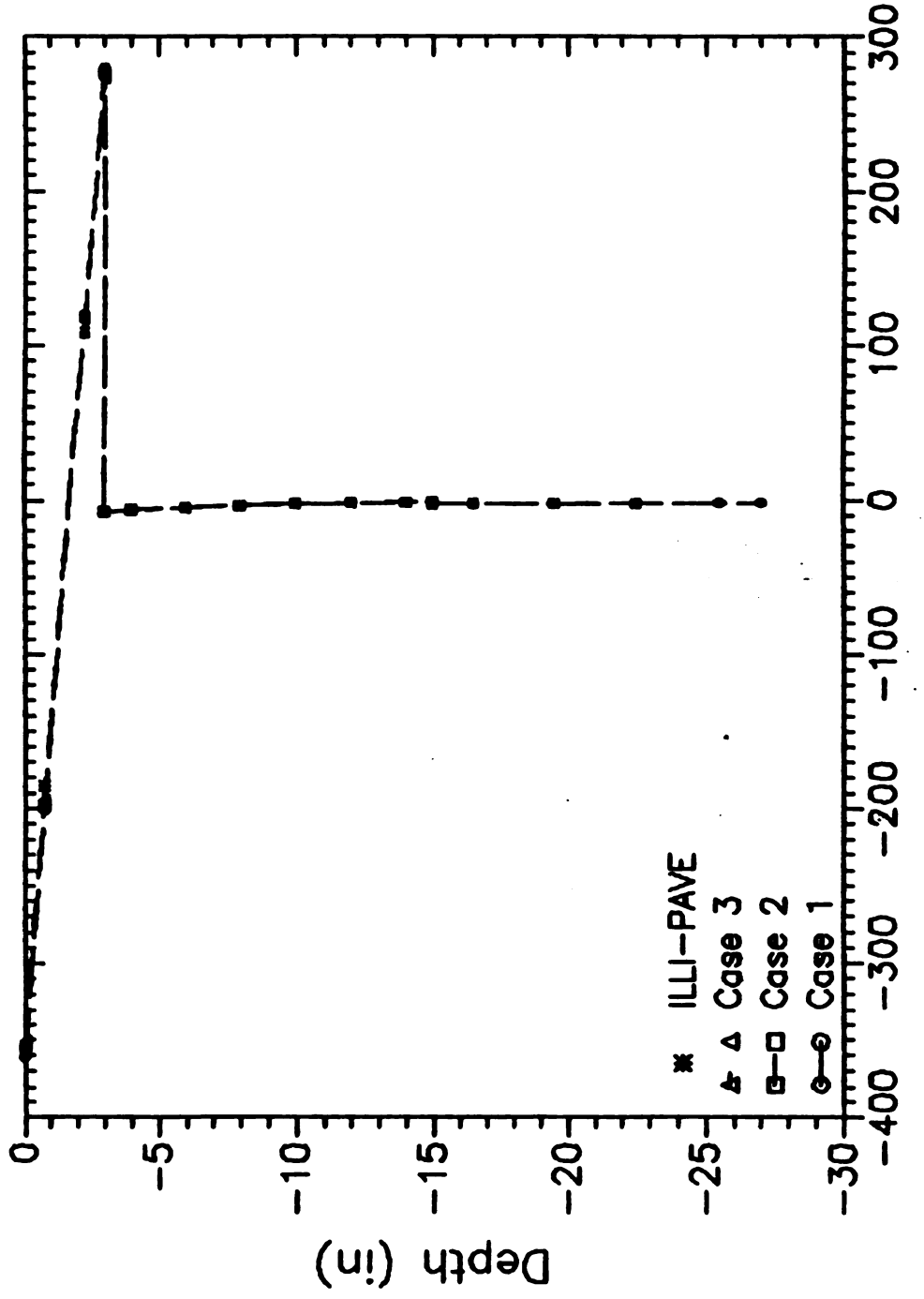

Figure 4-7: Sensitivity of the Radial Stress to the Depth of the Flexible Boundary (at R=.5")

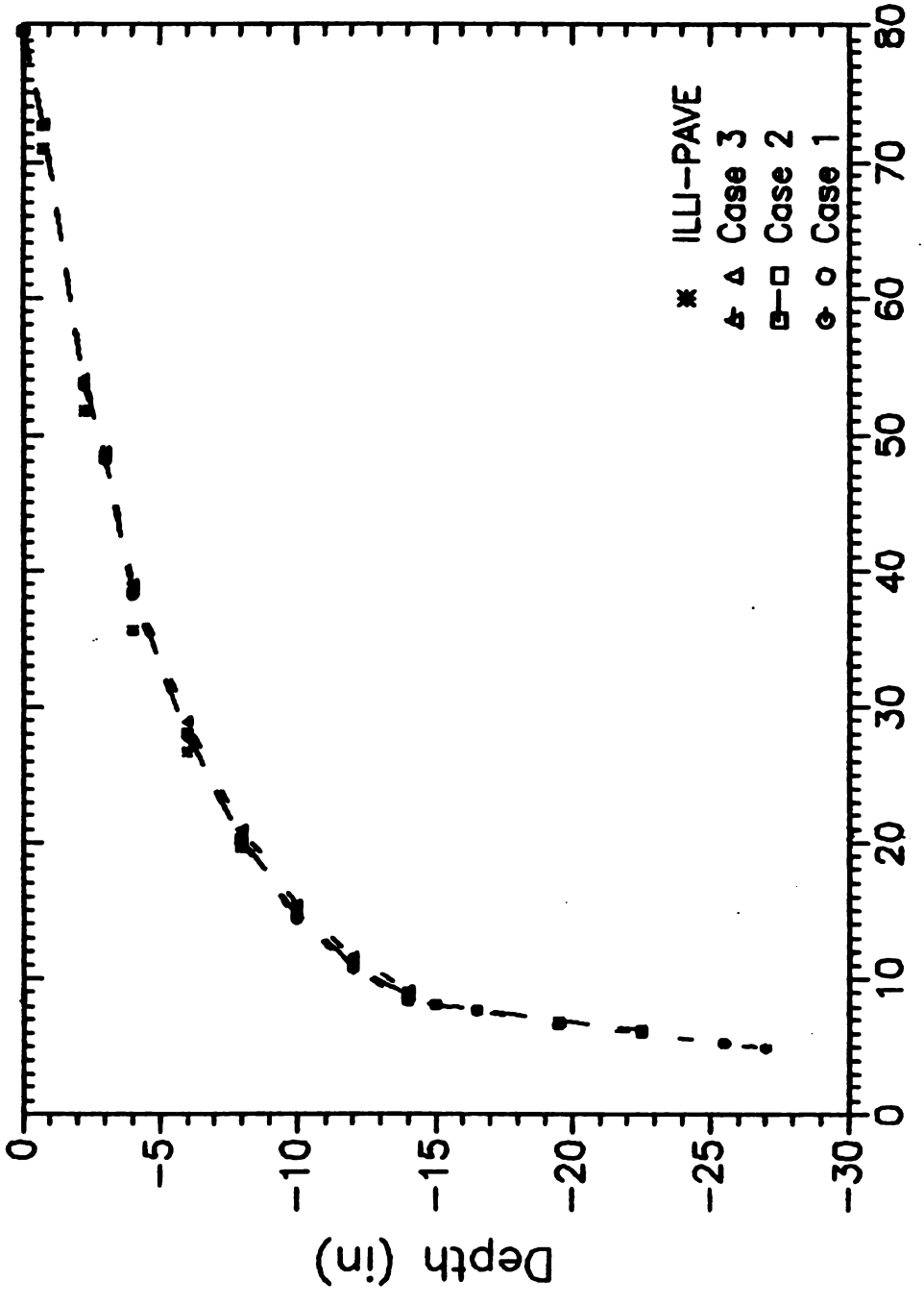

Figure 4–8: Sensitivity of the Vertical Stress to the Depth of the Flexible Boundary (at R=.5")

4.3.3 ; Effect of the Wheel Load on the Location of the Flexible Boundary

Here all input parameters are kept the same except the wheel load which is increase from 9,000 to 11,000 pounds. Comparisons of the surface deflections, and radial and vertical stresses along the three cases are presented in Tables 4-5, 4-6 and Figures 4-9 to 4-11.

Table 4-5 : Sensitivity of surface deflections to increase in the wheel load from 9 to 11 kip

Rad. Dist. (in)	Surface Deflection (in)		
	Case 1	Case 2	Case 3
0.	.04816	.05054	.04359
.7	.04791	.05029	.04335
2.2	.04710	.04948	.04255
3.7	.04566	.04804	.04113
5.2	.04358	.04597	.03909
7.4	.03987	.04227	.03546
10.4	.03502	.03742	.03075
13.3	.03058	.03301	.02651
16.3	.02670	.02915	.02287
20.7	.02211	.02463	.01870
26.6	.01731	.01994	.01447
32.5	.01403	.01679	.01173
41.4	.01137	.01431	.00968
53.3	.00956	.01267	.00837

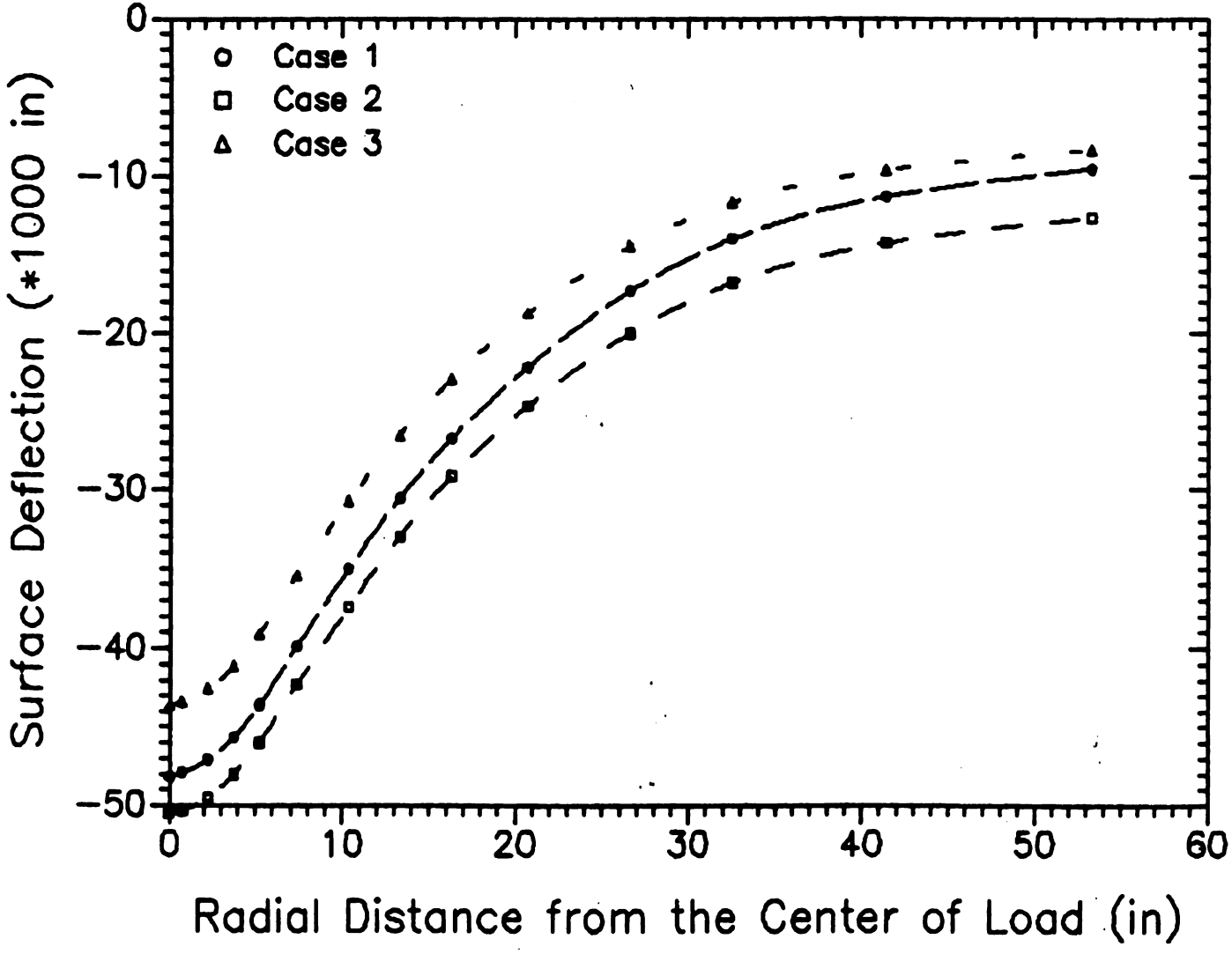

Figure 4–9: Sensitivity of Surface Deflection to Increase in the Wheel Load from 9 to 11 kips

Table 4-6 : Sensitivity of the radial and vertical stresses to increase in the wheel load from 9 to 11 kips (at a redial distance of .74" from the center of loaded area)

Depth (in)	Case 1		Case 2		Case 3	
	σ_r	σ_z	σ_r	σ_z	σ_r	σ_z
0.	-456.70	100	-456.18	100	-447.65	100
0.5	-322.05	97.1	-321.71	97.1	-315.33	97.1
1.5	-52.75	82.6	-52.78	82.6	-50.70	82.6
2.5	211.24	65.0	210.83	65.0	208.67	65.1
3.(+)	343.23	59.3	342.63	59.3	338.35	59.4
3.(-)	-10.26	59.3	-10.26	59.3	-10.27	59.4
4.	-8.94	50.0	-8.94	50.0	-8.97	50.2
6.	-6.29	35.3	-6.29	35.3	-6.36	35.7
8.	-4.34	24.4	-4.34	24.4	-4.42	24.9
10.	-2.99	16.9	-2.99	17.0	-3.08	17.5
12.	-2.09	11.9	-2.09	12.0	-2.19	12.6
14.	-1.57	9.1	-1.57	9.1	-1.68	9.7
15.(+)	-1.31	10.5	-1.31	9.9	-1.42	10.4
15.(-)	-5.76	10.5	-4.89	9.9	-5.31	10.4
16.	-4.92	12.0	-4.26	10.8	-4.70	11.1
18.	-3.24	9.0	-3.03	8.4	-3.50	8.9
20.	-2.66	7.8	-2.53	7.3	-3.10	8.0
22.	-2.38	7.0	-2.25	6.6	-2.93	7.4
24.	-2.14	6.4	-2.03	6.1	-2.88	6.9
26.	-1.87	5.7	-1.83	5.6	-2.88	6.5
27.	-1.73	5.4	-1.73	5.5	-2.88	6.2

Table 4-5 and Figure 4-9 shows that when the location of the flexible boundary is moved from 35" (Case 2) to 85" (Case 3) there is a reduction in the surface deflections. This can be attributed to the larger elements being used in the bottom region, which results in inaccurate stresses consequence of which the equivalent modulus for the halfspace below the flexible boundary becomes too large (the equivalent modulus increases from 5112 to 8446 psi). However, the radial and vertical streses upto a depth of 27 inches are similar for the three cases (see Figures 4-10, 4-11). Therefore, for the nonlinear FE analysis of flexible pavements, the flexible boundary located about 3 feet beneath the surface of the roadbed soil is recommended.

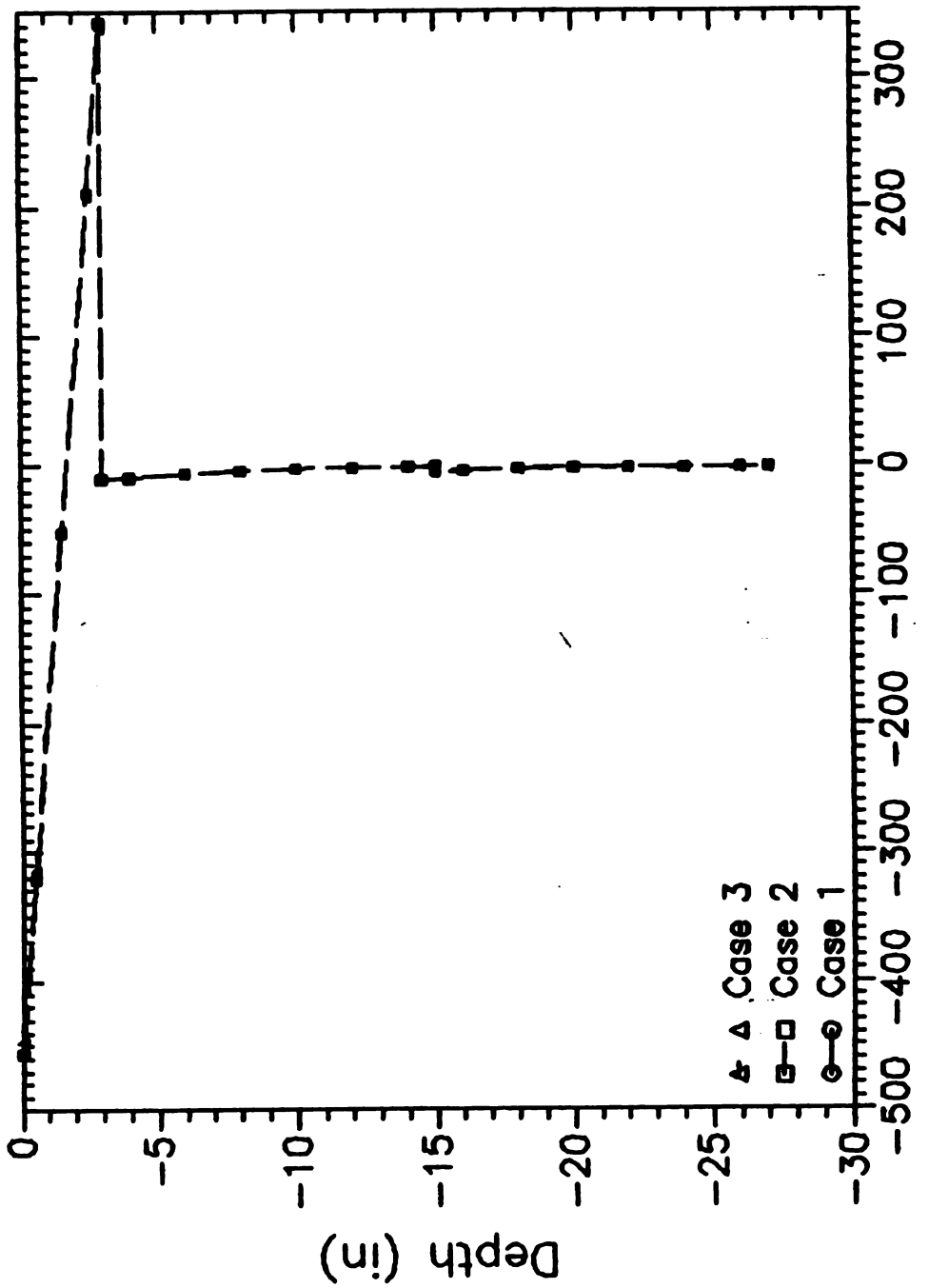

Figure 4–10: Sensitivity of Radial Stress to Increase in the Wheel Load from 9 to 11 kips (at R=74")

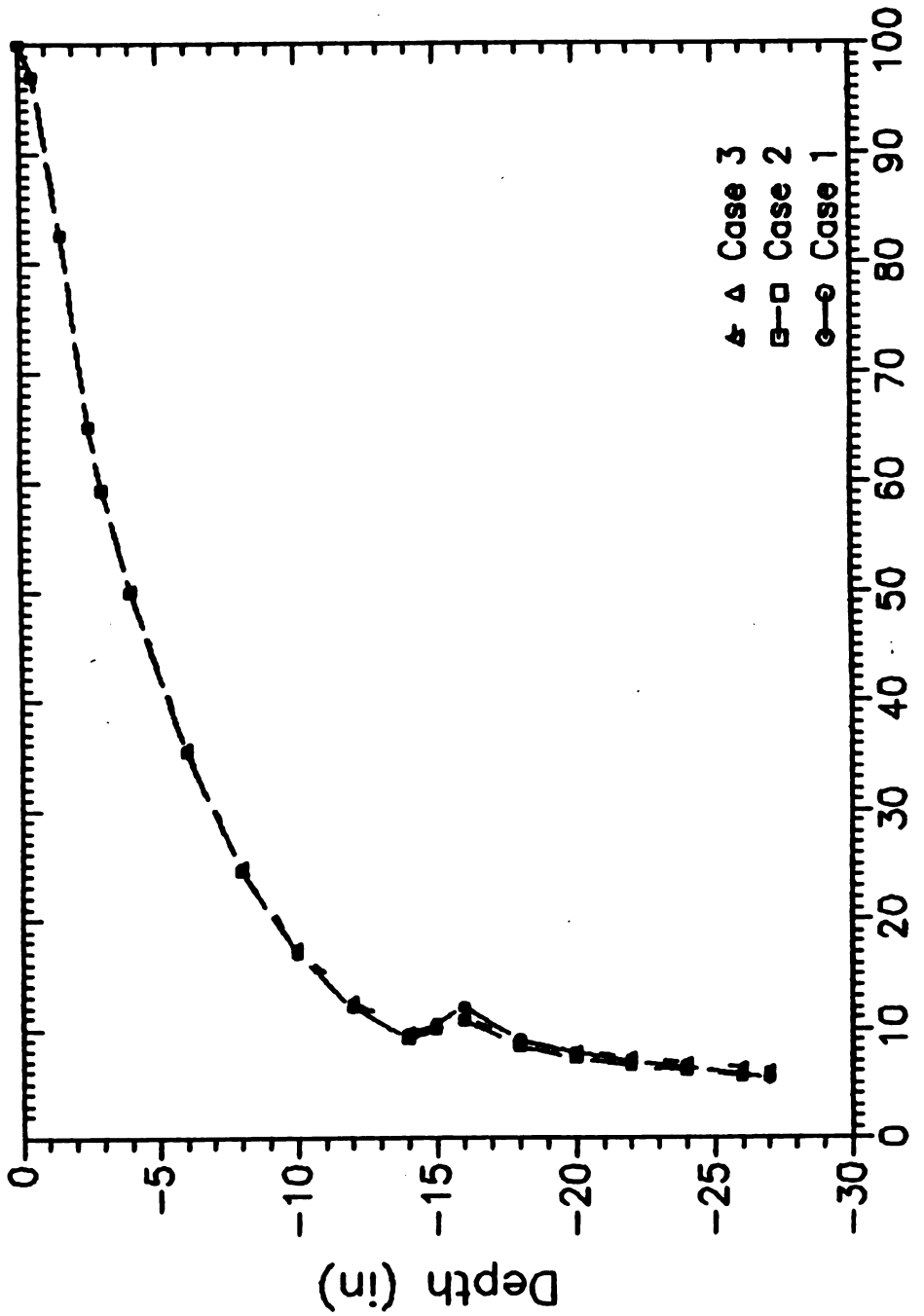

Figure 4-11: Sensitivity of Vertical Stress to Increase in the Wheel Load from 9 to 11 kips (at R=.74")

It should be noted that when the wheel load was increased up to 12,000 pounds, the program did not converge even after 25 iterations. This indicates that this pavement section becomes significantly nonlinear at this very high load, and is too weak for practical purposes. It also indicates that the algorithm being used converges well only for moderate levels of nonlinearity and may not converge for strongly nonlinear problems. This, however, should not be a cause for concern in normal practice.

4.4 : THE MICH-PAVE PROGRAM

The nonlinear FE program with the flexible boundary developed in this work is named MICH-PAVE. Details such as the choice of the FE mesh, effects of gravity and compaction ("locked-in") stresses of pavement materials, the modification of stresses, and the interpolation and extrapolation of stresses at layer boundaries, that are employed in this program are discussed below.

4.4.1 : Mesh Generation

The FEM needs to satisfy some basic requirements as far as the mesh is concerned, such as how far the vertical and bottom boundaries should be located, the size and shape of elements, and the distribution of elements in the various regions. Duncan and Monismith (1968) showed comparisons between displacements and stresses computed using the FEM and those computed using elastic half-space and layered system analysis to establish criteria for locating the boundaries in the FEM.

For an elastic half-space subjected to a uniform circular load, displacements and stresses computed by the FEM compare well with those

determined from the Boussinesq solution when the boundary nodal points in the FEM are fixed at a depth of about 18 radii of the loaded area for the bottom boundary, and constrained from moving radially on the vertical side boundary at a distance of about 12 radii from the center. However, to obtain a reasonable comparison between the two procedures for a three-layered system, it was necessary to move the bottom boundary in the FEM to a depth of about 50 radii while maintaining the same radial constraint as for the half-space analysis for the side boundary.

From previous experience, stresses based on quadrilateral elements will be accurate provided that the length-to-width ratio for the elements do not exceed five to one. Furthermore, smaller elements may be used close to the loaded area, and progressively larger elements may be used in the regions away from the loaded region.

Based on the above considerations and experience, the following mesh generation rules were used. In the radial direction, a mesh with a total width of 10 radii was divided into four zones. The first zone, which is between 0 and 1 radius, is equally divided into four elements; the second zone which is between 1 radius and 3 radii, is equally divided into four elements; the third zone which is between 3 radii and 6 radii, is equally divided into three elements; the fourth zone that is between 6 radii and 10 radii, is equally divided into 2 elements. The MICH-PAVE program will automatically generate the default values of the finite element mesh along the radial and vertical direction (see Figure 4-11, 4-12).

In the MICH-PAVE program, a flexible boundary is used instead of a fixed bottom boundary. Therefore, it does not need a mesh that is 50 radii deep. Normally when a mesh depth of about 10 radii is used, it

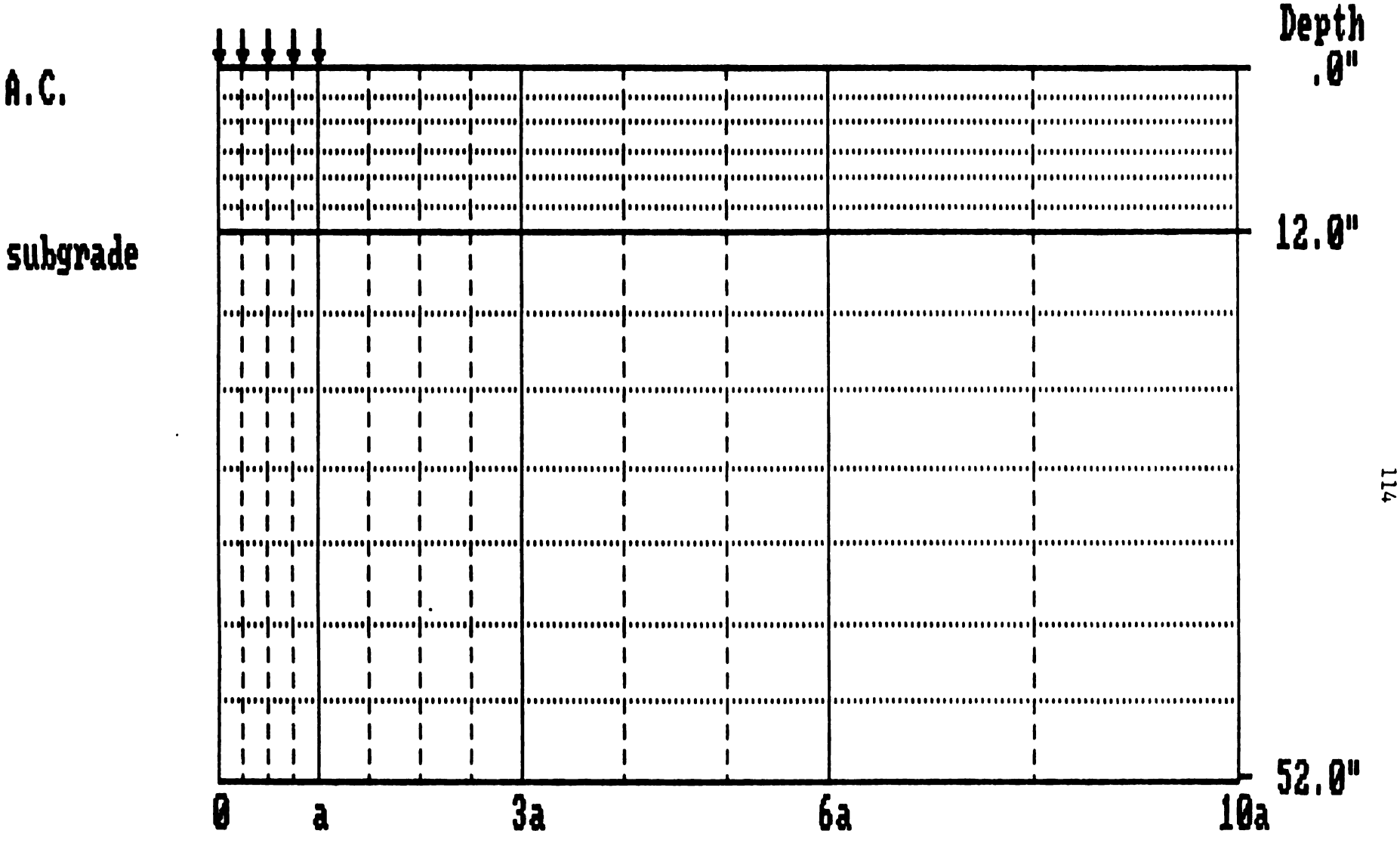

Radial Distance in Radii (Radius of Loaded Area, a = 6 in)
Figure 4-12 : Finite Element Mesh for section 1

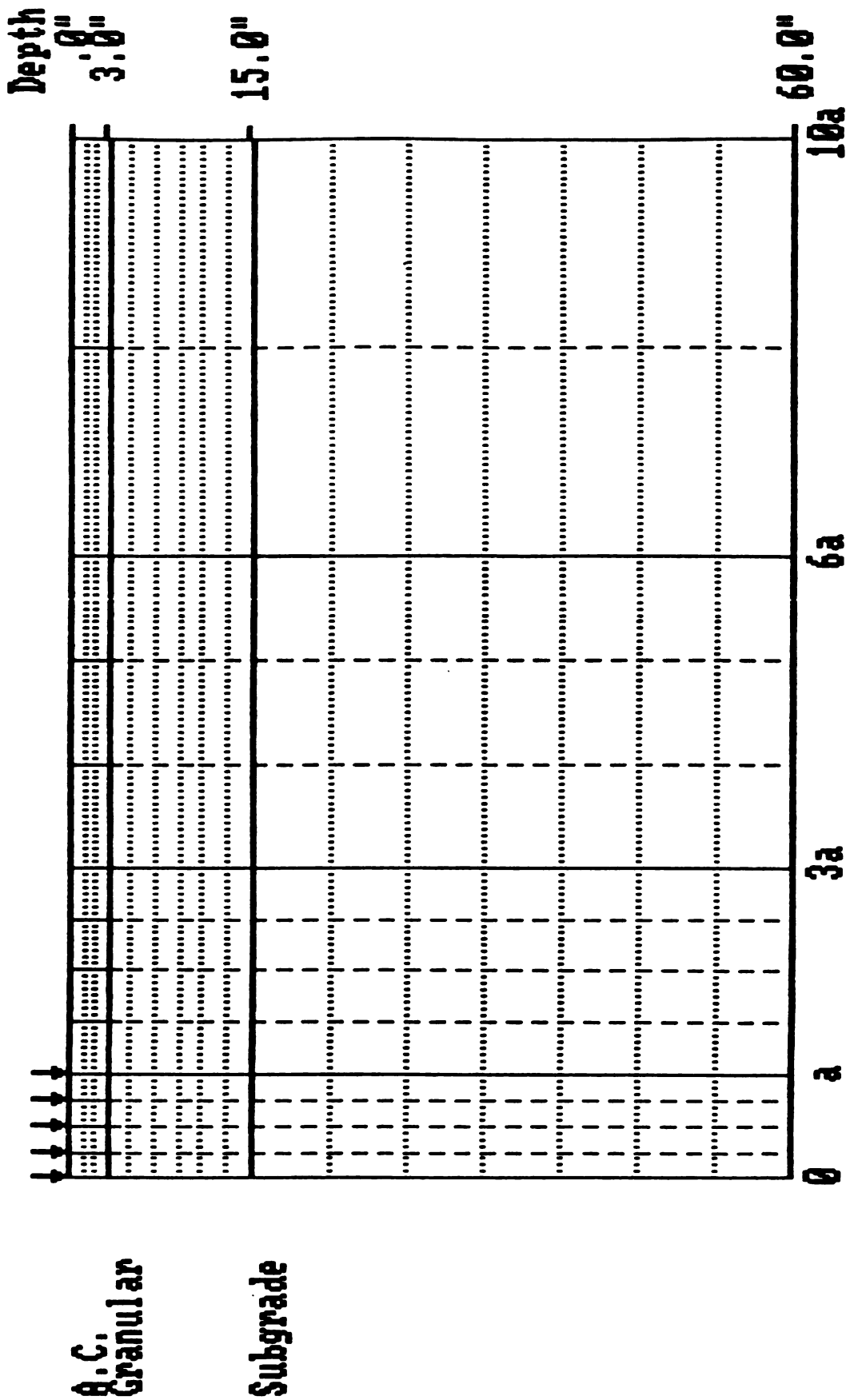

Radial Distance in Radii (Radius of Loaded Area, a = 6 in)
Figure 4-13 : Finite Element Mesh for section 2

will achieve reasonably accurate results. In general, if the flexible boundary is located too close to the top of roadbed soil, then the displacements of elements may still be accurate, but the stresses may not be. If the flexible boundary is placed too deep, the primary advantages of using the flexible boundary is lost. The depth at which the boundary is placed is a function of tire pressure, wheel load, and material properties of each layer. Also, the requirement of how many elements should be used in each layer along the depth is a function of the thickness and material properties of each layer. In general, the thicker the layer, the more elements must be used.

4.4.2 ; Gravity and Lateral Stresses of Pavement Materials

The MICH-PAVE program includes the gravity stress arising from the weight of the materials and considers the lateral stress between elements. At a point at depth z located within the i^{th} layer, the vertical gravity stress is computed as

$$\sigma_g = \sum_{j=1}^{i-1} \gamma_j t_j + (z - \sum_{j=1}^{i-1} t_j)\ \gamma_i \qquad \text{(Eq.4-6)}$$

where γ_j and t_j are the unit weight and thickness of the j^{th} layer.

The lateral stress, σ_h, is calculated from the coefficient of earth pressure at rest, K_0, and vertical gravity stress as (see Figure 4-14)

$$\sigma_h = K_0\ \sigma_g \qquad \text{(Eq.4-7)}$$

The final radial, tangential and vertical stresses are expressed as

$$\begin{aligned} \sigma_r &= \sigma_r' + \sigma_h \\ \sigma_t &= \sigma_t' + \sigma_h \\ \sigma_v &= \sigma_v' + \sigma_g \end{aligned} \qquad \text{(Eq.4-8)}$$

where

σ_r', σ_t' and σ_v' are the radial, tangential, and vertical stresses due to the wheel load, respectively.

In order to account for "locked-in" stresses due to compaction, a value for K_0 higher than the coefficient of earth pressure at rest may be used.

4.4.3 : Recovering Global Stresses from Modified Principal Stresses

As mentioned in Section 4.2, in MICH-PAVE the principal stresses are modified after each iteration to avoid Mohr-Coulomb failure within any element. It is necessary to obtain the stresses in radial, tangential and vertical coordiate directions (global stresses) from the modified principal stresses. The technique used for this for each element is outlined below.

1. Find the angle of rotation from the calculated global stresses to the principal stresses. Since $\tau_{r\theta}$ is zero, we only need to consider the r-z plane since the tangential stress is always a principal stress. (see Figure 4-15). The angle of rotation is

$$\alpha = 0.5 \tan^{-1}(2\tau_{rz}/(\sigma_r - \sigma_z)) \qquad \text{(Eq.4-9)}$$

2. Generate the rotational transformation matrix

$$[R] = \begin{bmatrix} \cos\alpha & 0 & \sin\alpha \\ 0 & 1 & 0 \\ -\sin\alpha & 0 & \cos\alpha \end{bmatrix} \qquad \text{(Eq.4-10)}$$

which relates the global and principal stresses.

3. Modify the principal stresses as outlined in Section 4.2 such that the Mohr-Coulomb failure criterion is not violated. The modified principal stress matrix may be written as

$$[\sigma_p] = \begin{bmatrix} \sigma_1 & 0 & 0 \\ 0 & \sigma_2 & 0 \\ 0 & 0 & \sigma_3 \end{bmatrix} \qquad \text{(Eq.4-11)}$$

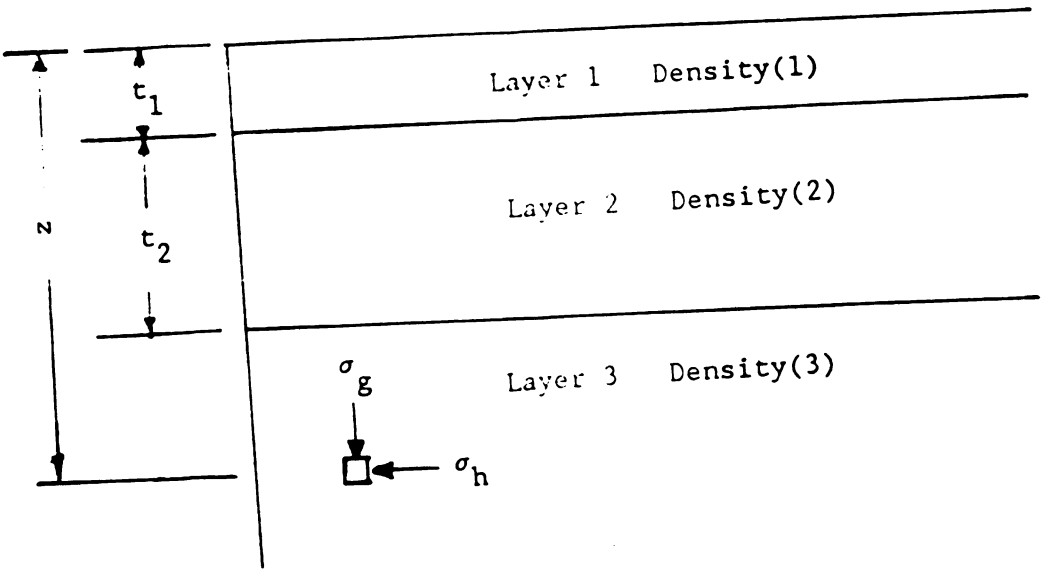

Figure 4-14: **Calculation of Gravity and Lateral Stresses**

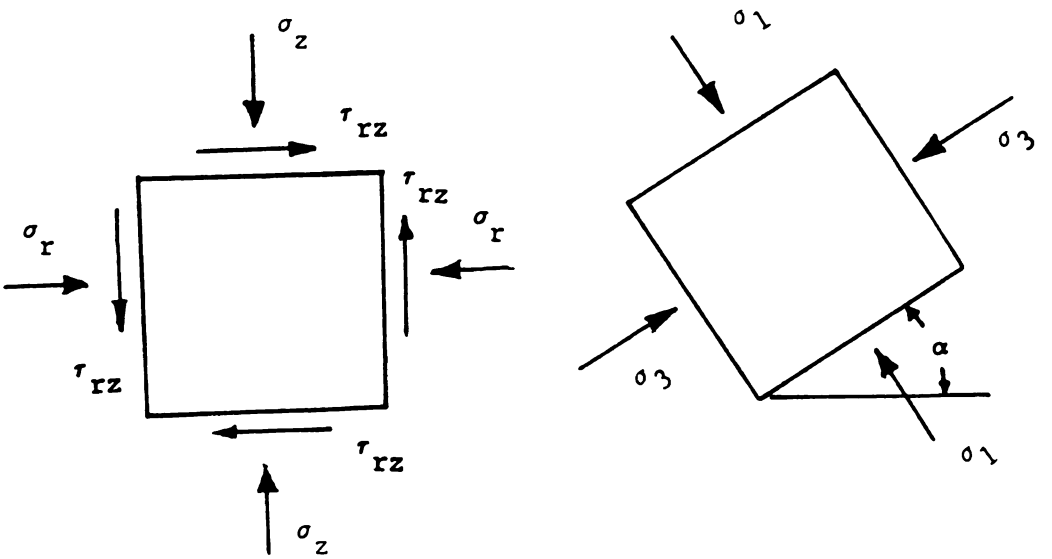

Figure 4-15 : **Stresses and Principal Stresses in r-z Plane**

4. Find the global stress matrix corresponding to $[\sigma_p]$ by using the rotational transformation matrix:

$$[\sigma_s] = [R]^T[\sigma_p][R] \qquad \text{(Eq.4-12)}$$

where

$$[\sigma_s] = \begin{bmatrix} \sigma_r & 0 & \tau_{r\theta} \\ 0 & \sigma_t & 0 \\ \tau_{r\theta} & 0 & \sigma_z \end{bmatrix} = \text{modified global stress matrix} \qquad \text{(Eq.4-13)}$$

and σ_r, σ_t, σ_z, and $\tau_{r\theta}$ are the radial, tangential, vertical, and shear stresses, respectively. Note that since [R] is an orthogonal matrix, i.e., $[R]^{-1} = [R]^T$, the inverse relation of that in Eq. 4-12 is

$$[\sigma_p] = [R][\sigma_s][R]^T \qquad \text{(Eq.4-14)}$$

4.4.4 : Interpolation and Extrapolation of Stresses and Strains at Layer Boundaries

For a pavement section in which different layers are fully bonded (i.e., no slip at layer boundaries), quantities such as the vertical and shear stresses, and the radial and tangential strains should be continuous across layer interfaces. However, due to the low order interpolation functions chosen in the FE method, these quantities are not continous across element boundaries. Thus if these quantities are estimated by FE approach at two adjacent points across an interface, the results will show an apparent discontinuity that is an artifact arising from the error in the FE method. This is undesirable and can be overcome by using interpolation to estimate these quantities at an interface from those at the middle of the adjacent elements. This is illustrated in Figure 4-16 (a). For example, if σ_1 is the stress at the center of an element immediately above the interface and σ_2 is the stress at the

center of an element immediately below the interface, then the stress at the interface obtained by linear interpolation is

$$\sigma_0 = \frac{\sigma_1 z_2 + \sigma_2 z_1}{z_1 + z_2} \qquad \text{(Eq.4-15)}$$

where z_1 and z_2 are the depths of the points at which σ_1 and σ_2 are evaluated.

Since the FE approach gives accurate estimates of stresses and strains at the center of elements, but can yield significant error at element edges, even those stresses and strains at the interfaces that are discontinuous across the interface can deviate significantly. For quantities that are discontinuous across an interface, it is possible to estimate their values at one side of the interface by linear extrapolation of the values from the center of two elements on that side of the interface. For example, if σ_1 and σ_2 are stresses at the center of two adjacent elements below (or above) an interface, then the stress at the lower (upper) side of the interface can be obtained through linear extrapolation as

$$\sigma_0 = \frac{\sigma_2 - \sigma_1}{z_2 - z_1} (z_0 - z_1) + \sigma_1 \qquad \text{(Eq.4-16)}$$

where z_1 and z_2 are the depths of the points at which σ_1 and σ_2 are estimated (see Figure 4-16 (b) and (c)).

Finally, based on prior knowledge of the solution, the surface stresses are arbitrarily set to their proper values in MICH-PAVE. Vertical and shear stresses must be zero at the surface, except for the vertical stress below the wheel load, which must be identical to the tire pressure.

(a): Interpolation for Vertical and Shear Stresses Between Two Layers

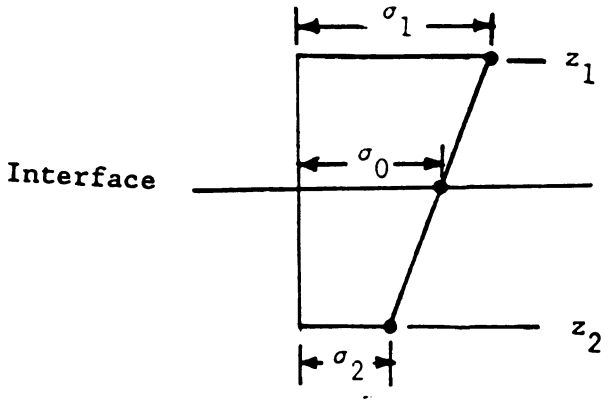

$$\sigma_0 = \frac{\sigma_1 z_2 + \sigma_2 z_1}{z_1 + z_2}$$

(b): Extrapolation for Radial and Tangential Stresses, and Vertical Strain Below the Interface

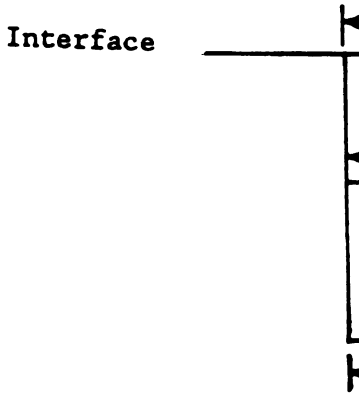

$$z_2\ \sigma_0 = \frac{\sigma_2 - \sigma_1}{z_2 - z_1} \times (z_0 - z_1) + \sigma_1$$

(c): Extrapolation for Radial and Tangential Stresses, and Vertical Strain Above the Interface

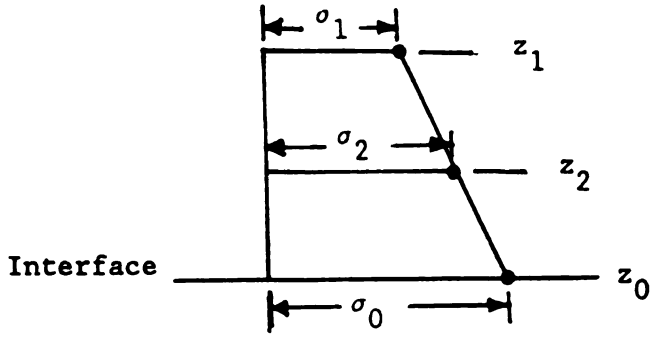

Figure 4-16: Interpolation and Extrapolation of Stresses and Strains at Layer Boundary

The improvement in accuracy through interpolation and extrapolation is illustrated by considering a typical pavement section for linear analysis using the MICH-PAVE and CHEV5L programs. The material properties of the section are given below.

Layer 1: AC - E = 300,000 psi; ν = .4; thickness = 8"

Layer 2: Base - E = 20,000 psi; ν = .38; thickness = 12"

Layer 3: Roadbed soil - E = 8,000 psi; ν = .45; semi-infinite depth

Comparison of stresses and strains between MICH-PAVE (before and after interpolation/extrapolation and adjustment of surface stresses) and CHEV5L are given in Tables 4-7 to 4-10.

Table 4-7 : Comparison of radial and tangential stresses at 67" from the center of the loaded area

Depth (in)	Radial stress (psi)			Tangential stress (psi)		
	Before	After	CHEV5L	Before	After	CHEV5L
0	-199.02	-167.91	-172.8	-199.02	-167.91	-173.0
8(+)	124.65	106.31	111.6	124.65	106.31	111.9
8(-)	1.84	.35	.22	1.84	.35	.24
20(+)	2.53	2.49	3.52	2.53	2.49	3.53
20(-)	-.66	-.47	-.23	-.66	-.47	-.23

Table 4-8 : Comparison of vertical and shear stresses at 67" from the center of the loaded area

Depth (in)	Vertical stress (psi)			Shear stress (psi)		
	Before	After	CHEV5L	Before	After	CHEV5L
0	143.57	100.	99.7	2.62	0.	0.
8(+)	0.	12.25	12.25	3.29	2.31	.55
8(-)	9.15	12.25	12.25	.65	2.31	.55
20(+)	3.03	2.99	3.36	.12	.10	.07
20(-)	1.61	2.99	3.36	.07	.10	.07

Table 4-9 : Comparison of radial and tengential strains at 67" from the center of the loaded area

Depth (in)	Radial strain (micro)			Tangential strain (micro)		
	Before	After	CHEV5L	Before	After	CHEV5L
0	207	207	212	207	207	213
8(+)	231	203	239	231	203	241
8(-)	231	203	239	231	203	241
20(+)	136	124	173	136	124	173
20(-)	136	124	173	136	124	173

Table 4-10 : Comparison of vertical and shear strains at 67" from the center of the loaded area

Depth (in)	Vertical strain (micro)			Shear strain (micro)		
	Before	After	CHEV5L	Before	After	CHEV5L
0	52	108	129	24	164	
8(+)	287	316	339	31	24	
8(-)	528	582	621	90	90	
20(+)	248	242	302	16	14	
20(-)	275	315	394	26	26	

It can therefore be seen that the interpolation and extrapolation used in MICH-PAVE to obtain stresses and strains at layer boundaries results in significant improvement.

CHAPTER 5

COMPARISONS WITH OTHER PROGRAMS

5.1 : COMPARISONS WITH SAP-IV RESULTS

In order to validate the linear elastic part of MICH-PAVE its results were compared with those obtained from the commercial FE program SAP-IV (Bathe, et al., 1973). The mesh used was 100 inches wide in the radial direction and 160 inches deep (see Figure 5-1). The same mesh was used with both programs and the displacements and stresses in every element due to a 31415.9 pound wheel load and 100 psi of tire pressure were computed. The results were essentially identical and the displacements under the load are shown in Table 5-1. Therefore, the FE axsymmetrical model is verified to be correct.

Table 5-1 : Comparisons of the vertical displacements at the center of the loaded area

Depth	Vertical Displacement (in.)	
(in.)	SAP-IV	MICH-PAVE without F.B.*
0.	.043477	.043476
2.5	.043626	.043625
5.0	.043149	.043147
7.5	.042293	.042292
10.	.040974	.040973
17.5	.031967	.031967
25.	.026018	.026018
32.5	.021862	.021863
40.	.018656	.018657
52.5	.013914	.013915

* : F.B. denotes flexible boundary.

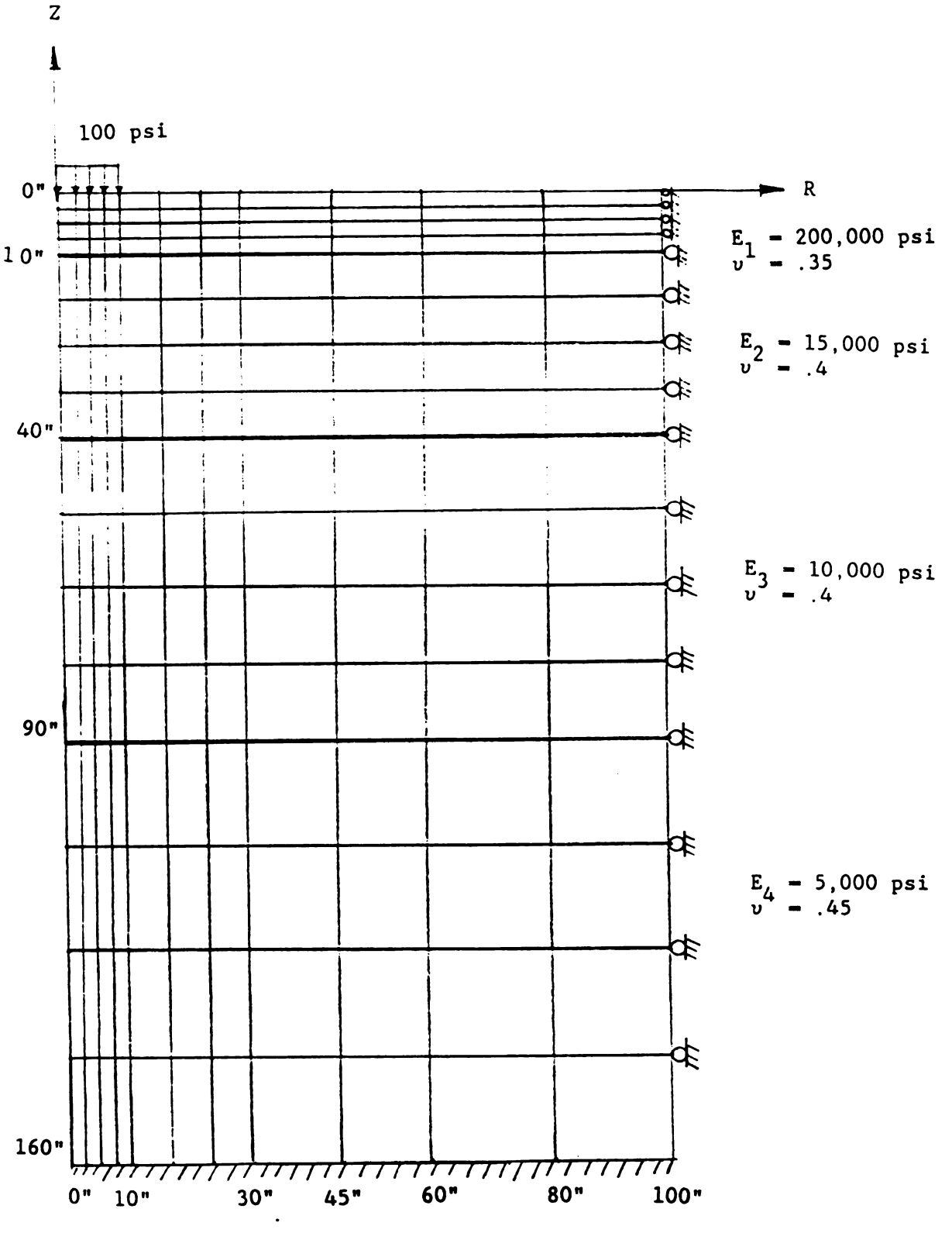

Figure 5-1: **Finite Element Mesh and Material Properties for a Typical Section**

5.2 : COMPARISONS WITH CHEV5L RESULTS

Since the CHEV5L program is a linear elastic layer analysis program, it cannot account for the nonlinear behaviour of granular material and roadbed soils. However, the MICH-PAVE program can account for both linear and nonlinear behavior of granular material and roadbed soils. The linear elastic part of the MICH-PAVE program utilizing the flexible boundary is compared here to the CHEV5L program which gives essentially exact solutions for elastic materials. Also the use of equivalent resilient moduli in the CHEV5L program, which are estimated from the results of the MICH-PAVE program, are investigated.

5.2.1 : Linear Elastic Analysis using the CHEV5L and MICH-PAVE Programs

Two pavement sections, a full-depth asphalt concrete on roadbed soil, and a section with 3 inches of AC and 12 inches of granular material, overlying the roadbed soil, are analyzed. Since the CHEV5L program assumes weightless material, zero material density is also used in the MICH-PAVE program. Tables 5-2 and 5-3 show the basic design data. A wheel load of 9002.55 pound and a tire pressure of 79.6 psi is used.

Table 5-2 : Design data for a 12" full-depth AC on roadbed soil

Layer Type	Thickness (in.)	Elastic Modulus (psi.)	Poisson's Ratio
AC	12	500,000	0.40
Roadbed Soil	Semi-infinite (52)*	8,753	0.45

* : In the MICH-PAVE program, the flexible boundary was placed at a depth of 52 inches.

Table 5-3 : Design data for a 3" AC and a 12" granular material on the roadbed soil

Layer Type	Thickness (in.)	Elastic Modulus (psi.)	Poisson's Ratio
AC	3	500,000	0.40
Granular	12	21,696	0.38
Roadbed Soil	Semi-infinite (60)*	7,387	0.45

Figures 4-12 and 4-13 show the finite element mesh corresponding to Tables 5-2 and 5-3, respectively. Tables 5-4 and 5-5 and Figure 5-2 show comparisons of surface deflections between the two programs.

Table 5-4 : Comparisons of surface deflections between CHEV5L and MICH-PAVE programs for a 12" full-depth AC section

Radial Distance from the Center of the Loaded Area (in.)	Surface Deflections (in.)		Error* (%)
	CHEV5L	MICH-PAVE	
0.	.01322	.01250	-5.5
0.75	.01321	.01247	-5.6
2.25	.01313	.01238	-5.7
3.75	.01295	.01220	-5.8
5.25	.01266	.01188	-6.2
7.25	.01203	.01134	-5.7
10.5	.01158	.01079	-6.8
13.5	.01110	.01036	-6.7
16.5	.01061	.00996	-6.1
21.	.00989	.00940	-5.0
27.	.00896	.00872	-2.7
33.	.00809	.00816	.9
42.	.00692	.00758	9.5
54.	.00562	.00715	27.2

* : The percentage errors are calculated assuming that the CHEV5L results are exact.

Table 5-5 : Comparisons of surface deflections between CHEV5L and MICH -PAVE programs for the three layer section

Radial Distance from the Center of Loaded Area (in.)	Surface Deflections (in.)		Error * (%)
	CHEV5L	MICH-PAVE	
0.	.03496	.03259	-6.8
0.75	.03487	.03237	-7.2
2.25	.03420	.03167	-7.4
3.75	.03291	.03043	-7.5
5.25	.03109	.02870	-7.7
7.25	.02812	.02577	-8.4
10.5	.02384	.02216	-7.0
13.5	.02060	.01916	-7.0
16.5	.01801	.01675	-7.0
21.	.01503	.01413	-6.0
27.	.01219	.01149	-5.7
33.	.01014	.00972	-4.1
42.	.00798	.00825	3.4
54.	.00611	.00724	18.5

Tables 5-4 and 5-5 show that the surface deflections calculated by the MICH-PAVE program are less than those calculated by the CHEV5L program by about 5 to 7 percent. However, at the right vertical boundary region, the error is much higher due to the interaction of the boundary itself.

Tables 5-6 and 5-7, and Figure 5-3 and 5-4 show comparisons of vertical and radial stresses at .75 inch from the center of the loaded area between CHEV5L and MICH-PAVE for the two pavement sections. These tables show that the stresses predicted by both programs are very close.

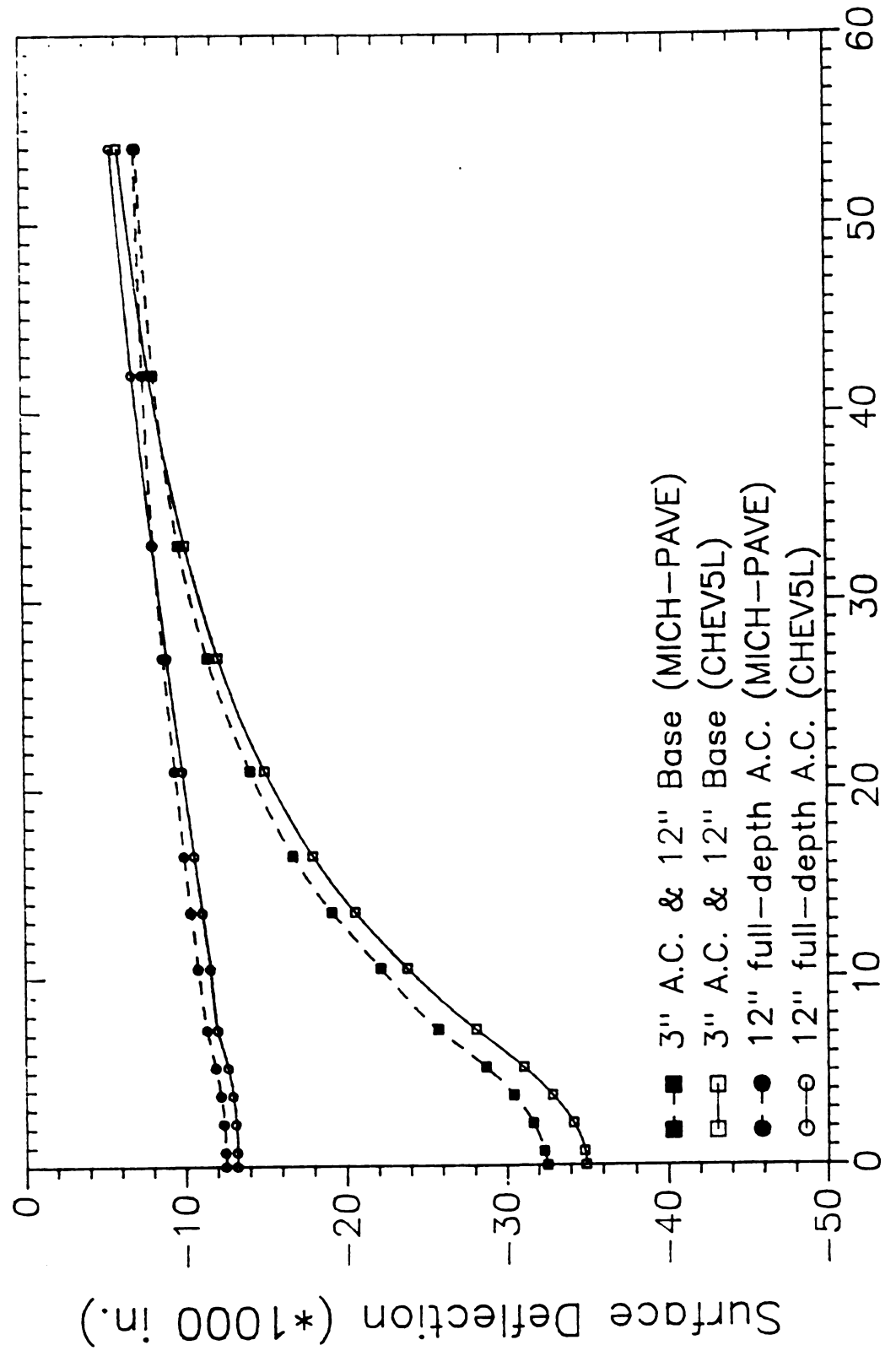

Figure 5-2: Comparison of Surface Deflection between CHEV5L and MICH-PAVE

Table 5-6 : Comparisons of vertical and radial stresses at .75 inch from the center of the loaded area for a 12" full-depth AC section

Depth (in.)	Vertical Stress(psi.)		Error (%)	Radial Stress(psi.)		Error (%)
	CHEV5L	MICH-PAVE		CHEV5L	MICH-PAVE	
0	79.36	79.60	.3	124.7	111.95	-10.7
1	78.73	77.51	- 1.5	95.43	89.25	- 6.5
3	68.49	66.75	- 2.5	47.61	43.96	- 7.7
5	49.59	48.27	- 2.6	15.19	13.54	-10.9
7	30.12	29.22	- 3.	- 9.35	- 8.85	- 5.3
9	14.34	14.01	- 2.3	-32.8	-29.85	- 9.
11	4.06	4.96	11.2	-60.8	-54.97	- 9.6
12(+)	2.82	3.76	64.9	-78.5	-67.53	-14.
12(-)	2.82	3.76	64.9	.77	.65	-15.6
14.9	2.40	2.14	-10.8	.62	.62	0
20.6	1.85	1.64	-11.4	.42	.57	35.7
26.3	1.5	1.31	-12.7	.30	.56	87.
32	1.25	1.11	-11.2	.23	.55	139.
37.7	1.06	.96	- 9.4	.18	.53	200.
43.4	.91	.86	- 5.5	.14	.51	271.
49.1	.79	.76	- 3.8	.12	.47	267.
52	.74	.71	- 4.	.11	.44	264.

(+) and (-) indicate locations just above and just below the interface.

Table 5-7 : Comparisons of vertical and radial stresses at .75 inch from the center of the loaded area for the three layer section

Depth (in.)	Vertical Stress(psi.)		Error (%)	Radial Stress(psi.)		Error (%)
	CHEV5L	MICH-PAVE		CHEV5L	MICH-PAVE	
0.	79.4	79.6	.2	395.5	380.6	- 3.8
.5	76.76	75.52	- 1.6	274.1	267.3	- 2.5
1.5	59.92	58.7	- 2.	44.4	40.7	- 8.4
2.5	41.68	40.64	- 2.5	-183.	-183.7	.4
3.(+)	37.11	36.84	- .7	-301.8	-295.9	- 2.
3.(-)	37.11	36.84	- .7	9.03	7.29	-19.3
4.	32.95	30.77	- 6.6	5.80	5.36	- 7.6
6.	25.3	23.53	- 7.	1.63	1.51	- 7.4
8.	19.	17.67	- 7.	- 1.02	- .88	-13.7
10.	14.2	13.12	- 7.	- 3.16	- 2.74	-13.4
12.	10.5	9.7	- 7.6	- 5.38	- 4.65	-13.6
14.	7.95	7.33	- 7.8	- 8.18	- 7.04	-13.9
15.(+)	7.18	6.37	-11.3	- 9.97	- 8.24	-17.4
15.(-)	7.18	6.37	-11.3	.36	.32	-11.1
18.2	5.63	5.12	- 9.	.22	.27	
24.6	3.72	3.31	-11.	.09	.18	
31.1	2.62	2.32	-11.4	.05	.27	
37.5	1.96	1.73	-11.7	.03	.36	
43.9	1.51	1.36	- 5.6	.03	.40	
50.4	1.20	1.12	- 8.3	.03	.42	
56.8	.98	.93	- 8.2	.03	.39	
60.	.89	.83	-10.1	.03	.38	

It is suggested that stresses in the FEM be computed at the center of each element. This yields the most accurate results.

5.2.2 : Equivalent Resilient Moduli for Linear Analysis

Sometimes, it is desirable to compare the results of the nonlinear FEM with that of elastic layer programs such as CHEV5L. However, the input material constants are different between these two methods. It is therefore necessary to obtain an equivalent resilient modulus which can be used in elastic layer programs from the different resilient moduli in each element of the nonlinear FEM.

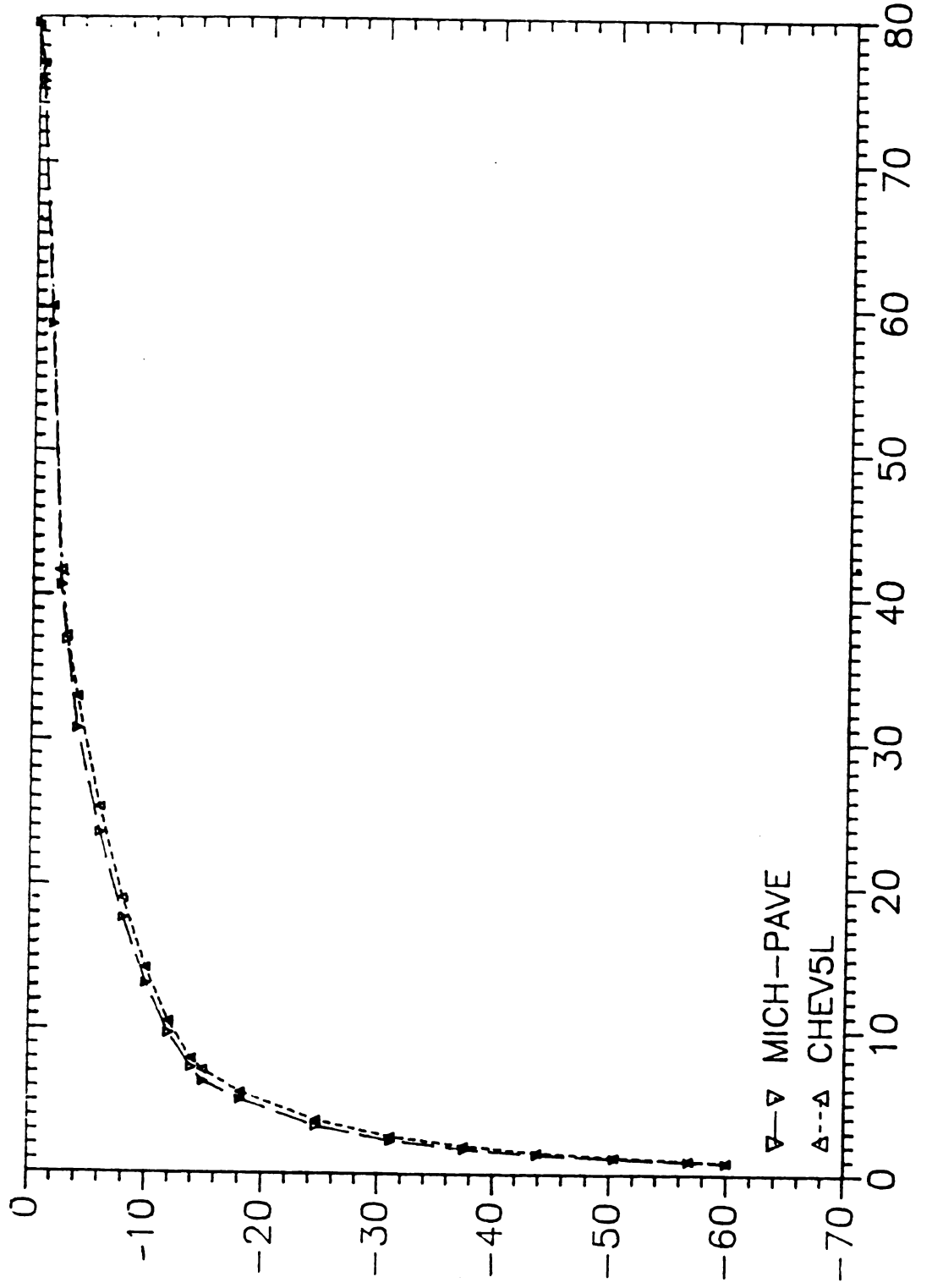

Figure 5-3: Comparison of Vertical Stress between CHEV5L and MICH-PAVE (3" AC and 12" Base)

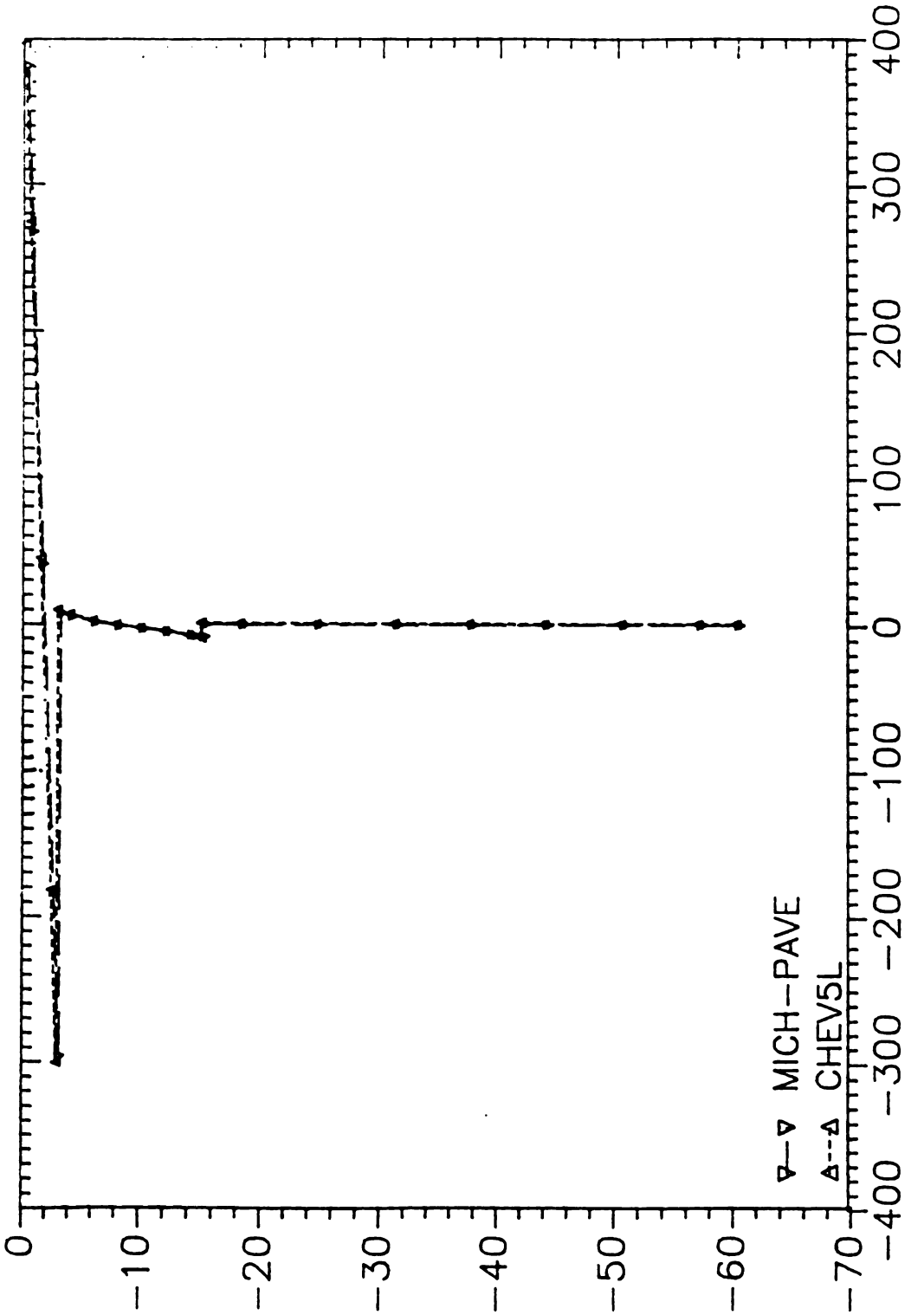

Figure 5-4: Comparison of Radial Stress between CHEV5L and MICH-PAVE (3" AC and 12" Base)

There are different ways in which equivalent resilient moduli for linear analysis can be obtained. Three approachs are discussed here:

1. The equivalent resilient modulus for each layer is obtained as the average of the moduli of the finite elements in the layer that lie within an assumed 2:1 load distribution zone as shown in Figure (5-5). The average moduli of those elements within the regions ABGH, BCFG and CDEF are taken as the equivalent moduli for layers 1, 2 and 3, respectively.
2. The equivalent resilient modulus is taken as the average of the moduli of all elements in each layer. For example, in Figure 5-5 the average moduli in zones ABJI, BCKJ and CDLK are taken as the equivalent moduli for layers 1, 2 and 3, respectively.
3. The equivalent resilient modulus is taken as the average of the moduli of those elements in each layer that lie directly beneath the loaded area on the surface. For example, in Figure 5-5 the average moduli in zones ABMH, BCNM and CDON are taken as the equivalent moduli for layers 1, 2 and 3, respectively.

Comparisons of the equivalent resilient moduli for linear analysis by the above three approachs are given in Table 5-8a, 5-8b for two flexible pavement sections. The two sections are shown in Figures 5-6 and 5-7.

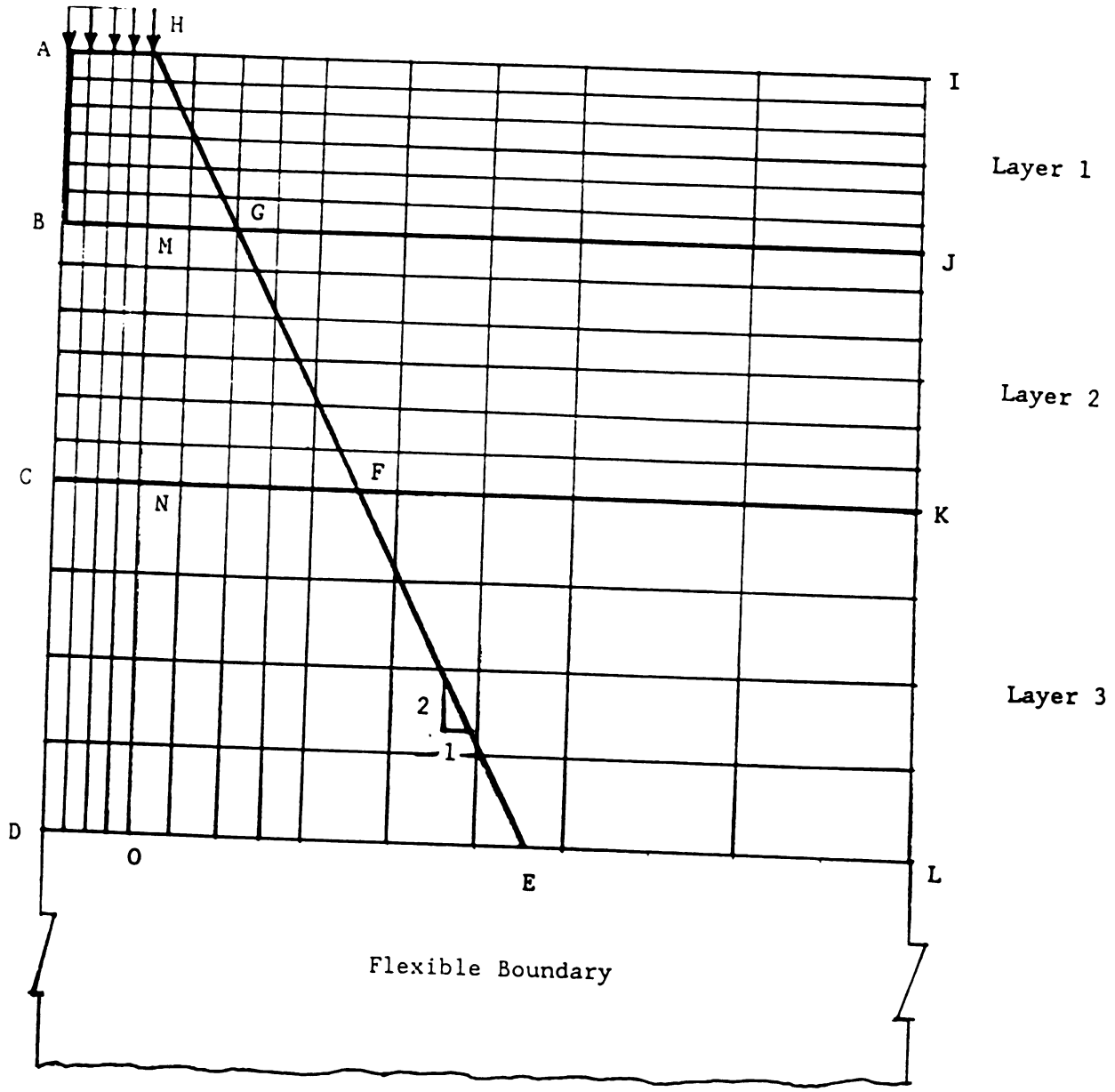

Figure 5-5: **Three Different Approaches to Calculate Equivalent Resilient Moduli**

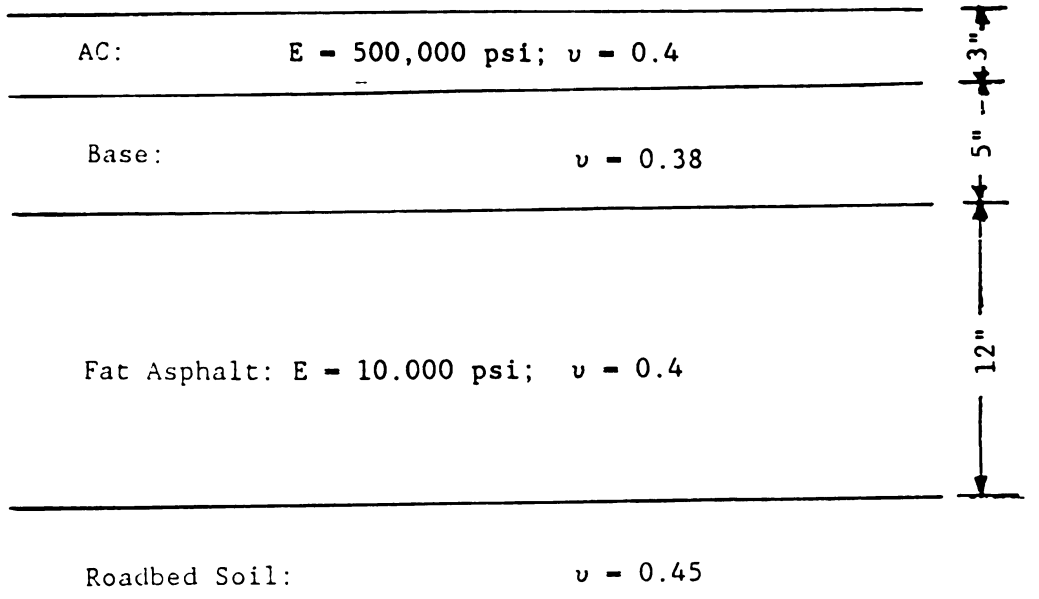

Figure 5-6 : **Material Properties of Pavement Section 1**

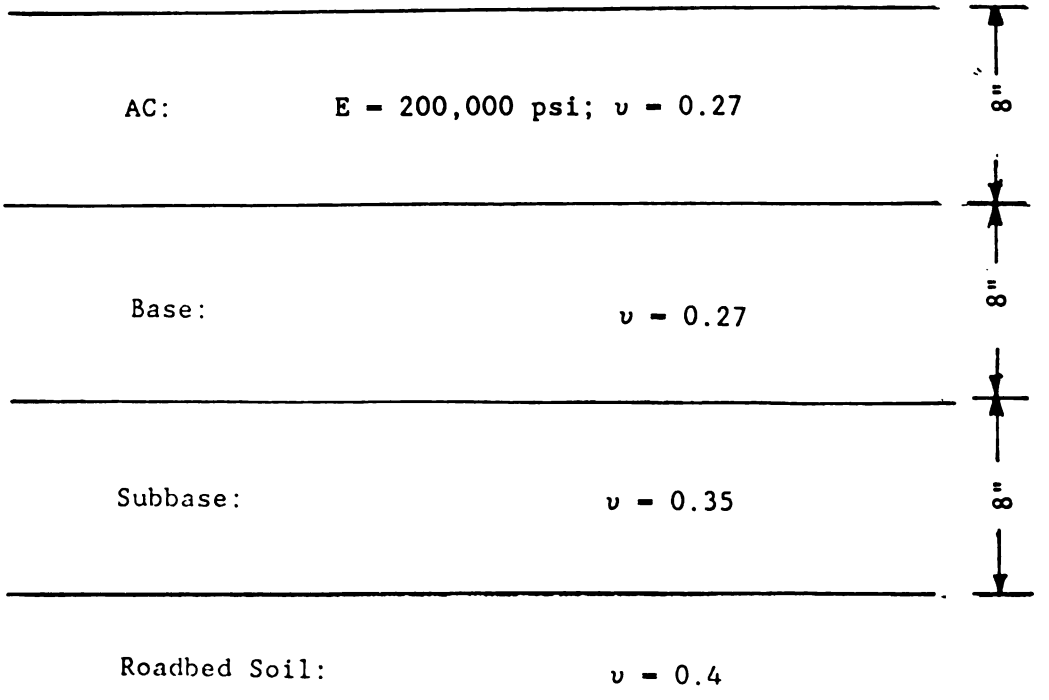

Figure 5-7 : **Material Properties of Pavement Section 2**

Table 5-8a : Comparison of the equivalent resilient moduli for linear analysis by three different approaches (section 1)

Layer Type	Equivalent Resilient Modulus for Linear Analysis (psi)		
	2 to 1 Zone (1)	Whole Layer (2)	Under Loaded Area (3)
AC	500,000	500,000	500,000
Base	26,281	18,283	27,692
Fat Asphalt	10,000	10,000	10,000
Subgrade	7,509	7,719	7,194

Table 5-8b : Comparison of the equivalent resilient moduli for linear analysis by three different approaches (section 2)

Layer Type	Equivalent Resilient Modulus for Linear Analysis (psi)		
	2 to 1 Zone (1)	Whole Layer (2)	Under Loaded Area (3)
AC	200,000	200,000	200,000
Base	28,052	22,881	30,719
Subbase	17,521	16,550	19,050
Subgrade	6,269	6,400	6,132

Tables 5-8a and 5-8b, show that the values of equivalent resilient moduli for linear analysis by using approach 1 are between those obtained using the other two approaches. The first approach considers, approximately, those elements within the loaded region which contribute most to the pavement strength, and is therefore expected to be more reasonable than the other two approaches.

The surface deflections using the CHEV5L program with the equivalent resilient moduli (linear analysis) are compared with those obtained through the nonlinear FEM in Figures 5-8 and 5-9. The computed surface

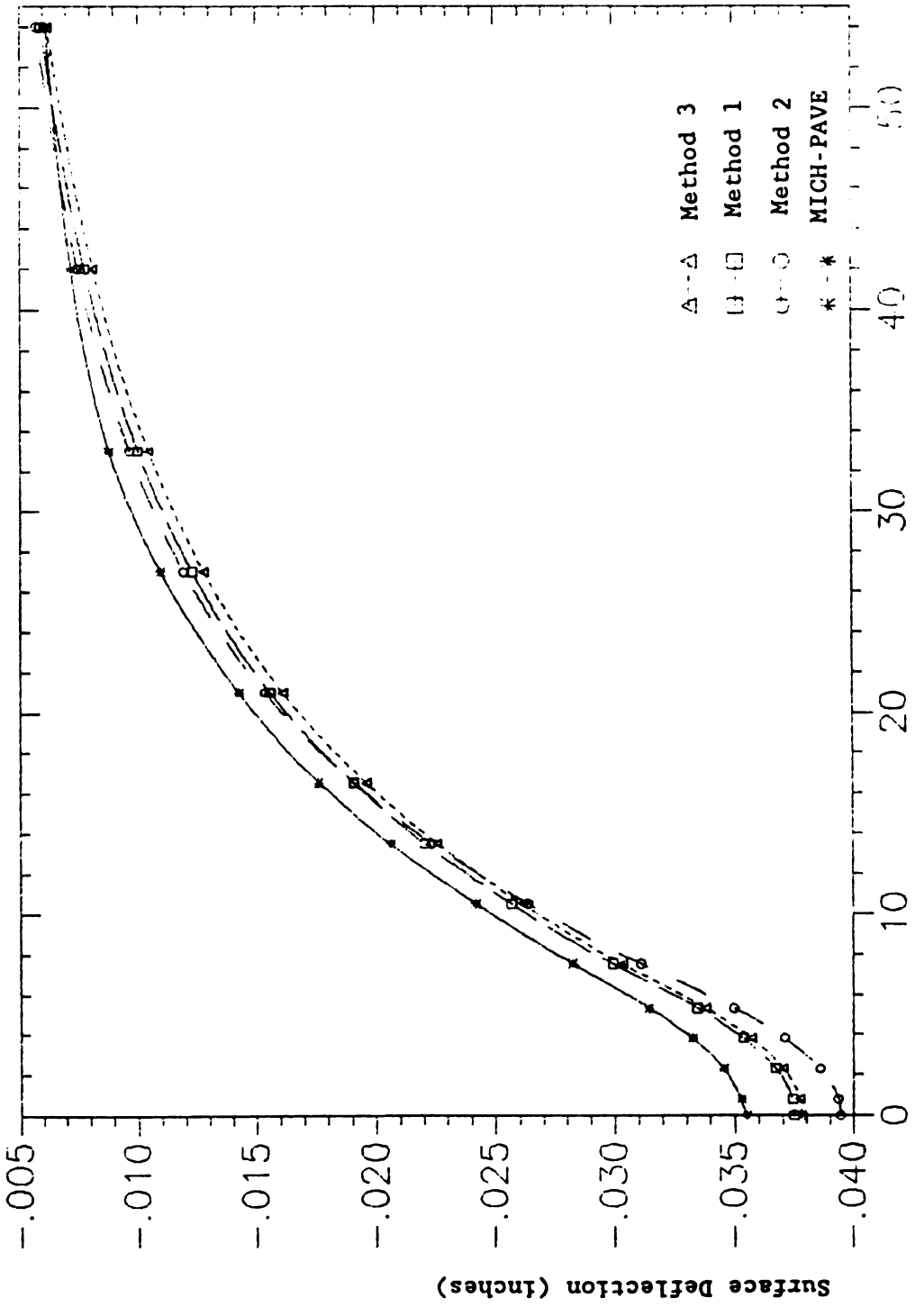

Figure 5-8 : Comparisons of the Surface Deflections Due to the Different Equivalent Resilient Moduli (section 1)

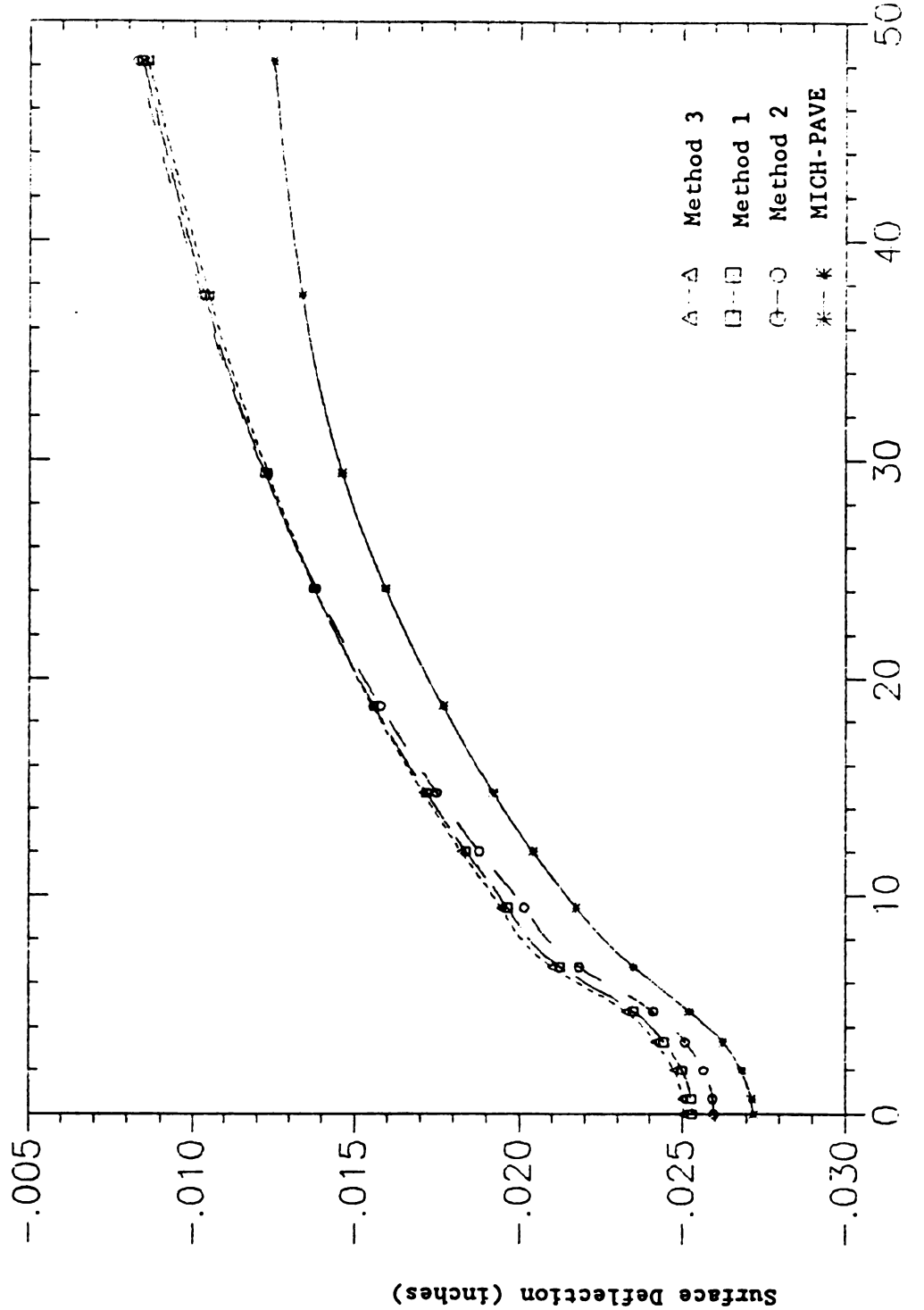

Figure 5-9 : Comparisons of the Surface Deflections Due to the Different Equivalent Resilient Moduli (section 2)

deflections are quite similar for all three sets of equivalent moduli. However, for the reason mentioned earlier, the first approach is recommended for the calculation of equivalent resilient moduli for linear analysis.

The use of equivalent resilient moduli obtained through nonlinear analysis utilizing the MICH-PAVE program, in the CHEV5L program is further investigated through typical examples.

Tables 5-9 and 5-10 show the linear and nonlinear material properties of a 12 inch full-depth AC section and a three layer section with 3 inches of AC and 12 inches of granular material on roadbed soil. The material constants and nonlinear stress-strain model were outlined earlier in section 4-2. A cohesion of 6.45 psi and an angle of friction of 0 were used for the roadbed soil in the full-depth section. For the three layer section, c = 0 psi and $\phi = 45°$ was used for the granular material and c = 6.45 psi and $\phi = 0°$ was used for the roadbed soil .

Table 5-9 : Linear and nonlinear material properties of the 12 inches full-depth AC section

Layer Type	Thickness (in.)	Modulus (psi)	ν	K_0	K_1 (psi)	K_2 (psi)	K_3	K_4	density (pcf)
AC	12	500,000	.4	.67					150
R.S.	40	8,753	.45	.82	6.2	3021	1110	-178	115

Table 5-10 : Linear and nonlinear material properties for three layer section

Layer Type	Thickness (in.)	Modulus (psi)	ν	K_0	K_1 (psi)	K_2 (psi)	K_3	K_4	density (pcf)
AC	3	500,000	.4	.67					150
Gran.	12	21,696	.38	.6	5000	.5			140
R.S.	45	7,387	.45	.82	6.2	3021	1110	-178	115

Figures 5-10 and 5-11 show comparisons of surface deflections for nonlinear analysis using MICH-PAVE and the linear analysis using CHEV5L with equivalent moduli. Figures 5-12 and 5-13 show comparisons of the vertical and radial stresses at .5 inch from the center of the loaded area.

It is clear that there is a greater difference in stresses between the nonlinear and linear analyses. Some of this difference arises because CHEV5L neglects the weight of the material. In particular, CHEV5L can give tensile stresses in the granular material.

5.3 : COMPARISONS WITH ILLI-PAVE RESULTS

Since the finite element meshes between ILLI-PAVE and MICH-PAVE are different, the surface deflection, and vertical and radial stresses between the two programs cannot be computed at every point. The output of the ILLI-PAVE and percentage differences between the results from the two programs are computed here at some identical points. The percentage difference is calculated taking ILLI-PAVE results as the reference value. When the percentage difference is a positive value, then the result calculated by MICH-PAVE is higher than that calculated by ILLI-

PAVE.

Comparisons of surface deflections between the two programs are shown in Figures 5-10 and 5-11, and comparsions of the vertical and radial stresses at .5 inch from the center of the loaded area are shown in Figures 5-12 and 5-13.

Figures 5-12 and 5-13 show that the vertical and radial stresses between the two programs are very close. However, Figures 5-10 and 5-11 show the surface deflections calculated by the MICH-PAVE are about 12 percent higher than those computed by ILLI-PAVE. However, as discussed in Section 4.3.2, the surface displacements in linear analysis are better when a flexible boundary is used, as in MICH-PAVE, than a deep fixed boundary is used, as in ILLI-PAVE (see Figures 3-13 and Table 3-1 in Section 3.4). Extending this observation to the nonlinear case, it is to be expected that MICH-PAVE would yield slightly larger surface displacements than ILLI-PAVE. Further, based on the results for linear analysis, one would be inclined to assume that the surface deflections obtained through MICH-PAVE are more accurate than those obtained by ILLI-PAVE.

5.4 : SUMMARY

Comparison of results obtained from linear elastic analysis using MICH-PAVE with those of SAP-IV, a general purpose finite element program, vertified that the linear elastic part of MICH-PAVE is performing without error. The errors obtained from FE analysis are estimated based on the essentially exact solutions obtained through the CHEV5L linear layer analysis program.

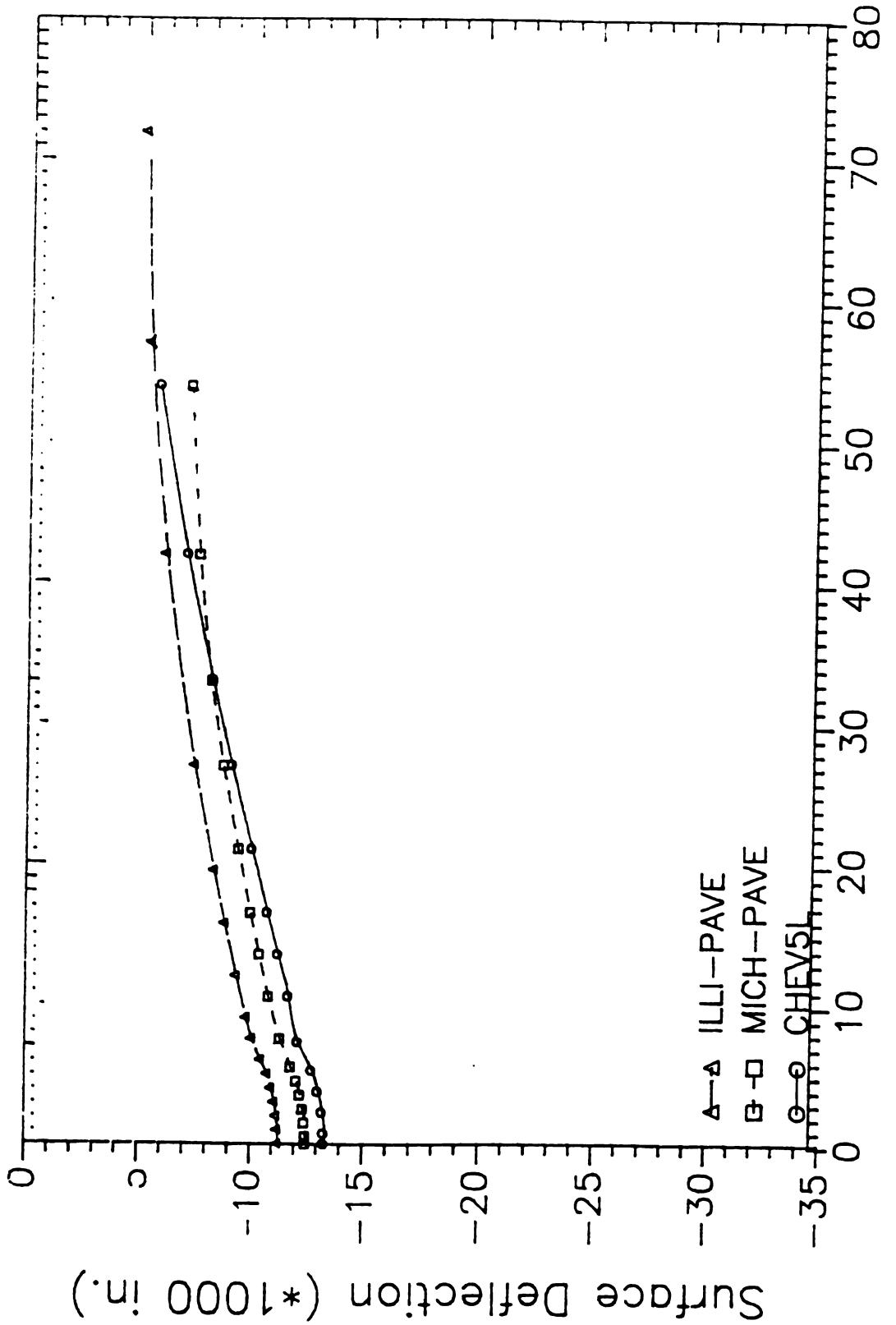

Figure 5-10 : Comparison of Surface Deflection (12" of full-depth AC)

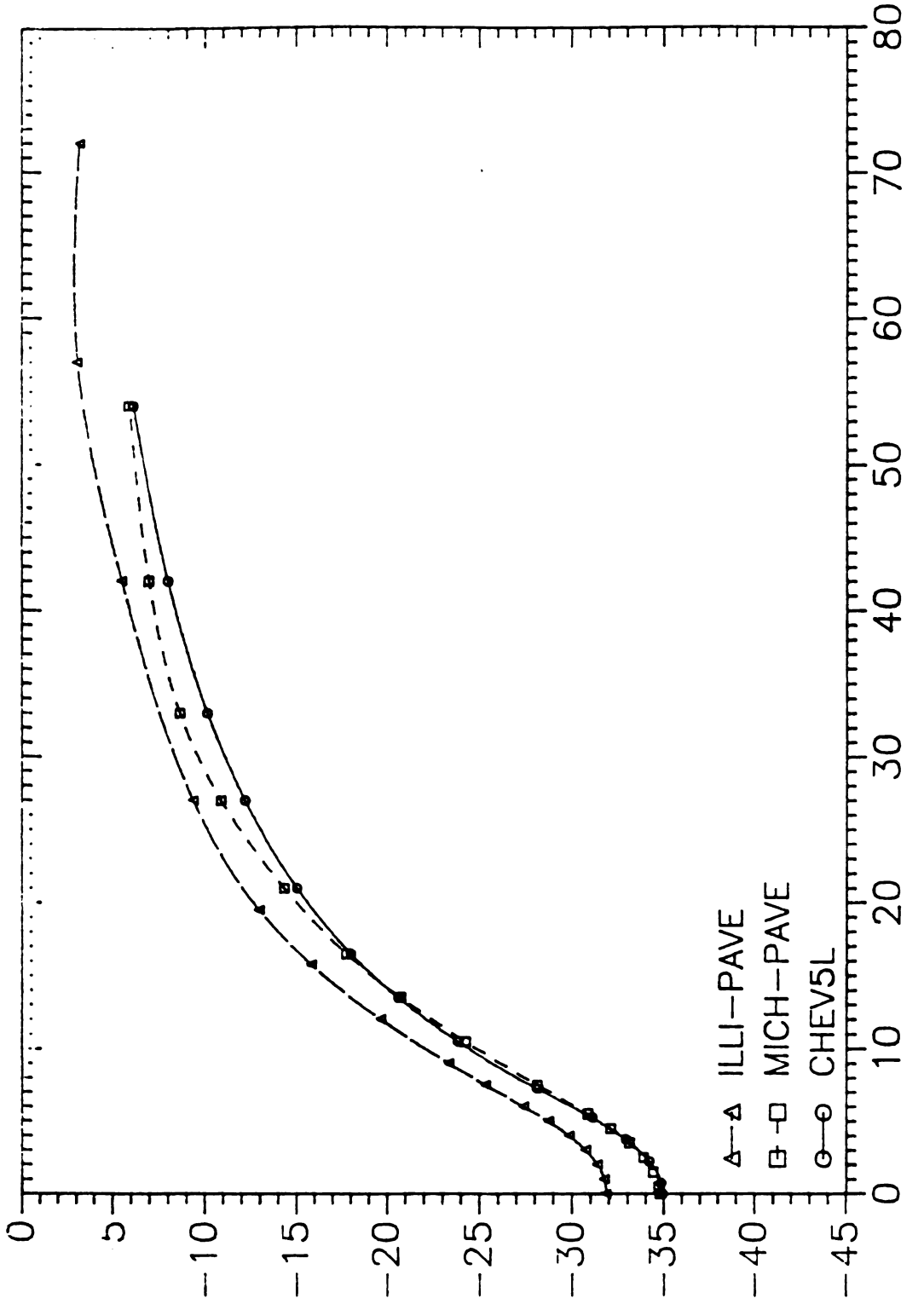

Figure 5-11 : **Comparison of Surface Deflection (3" of AC and 12" of Base)**

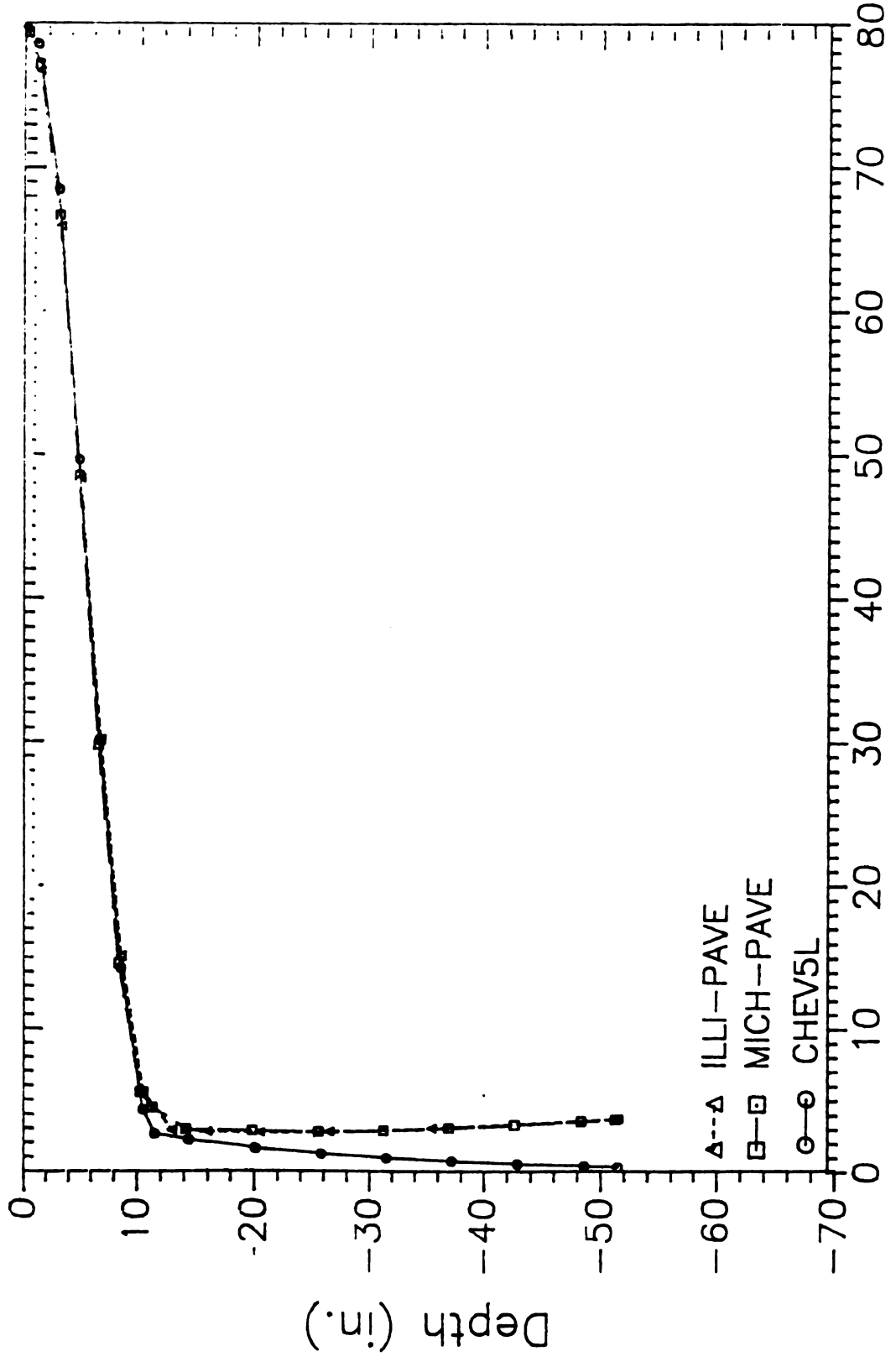

Figure 5-12: Comparison of Vertical Stress along Three Programs (12" of full-depth AC)

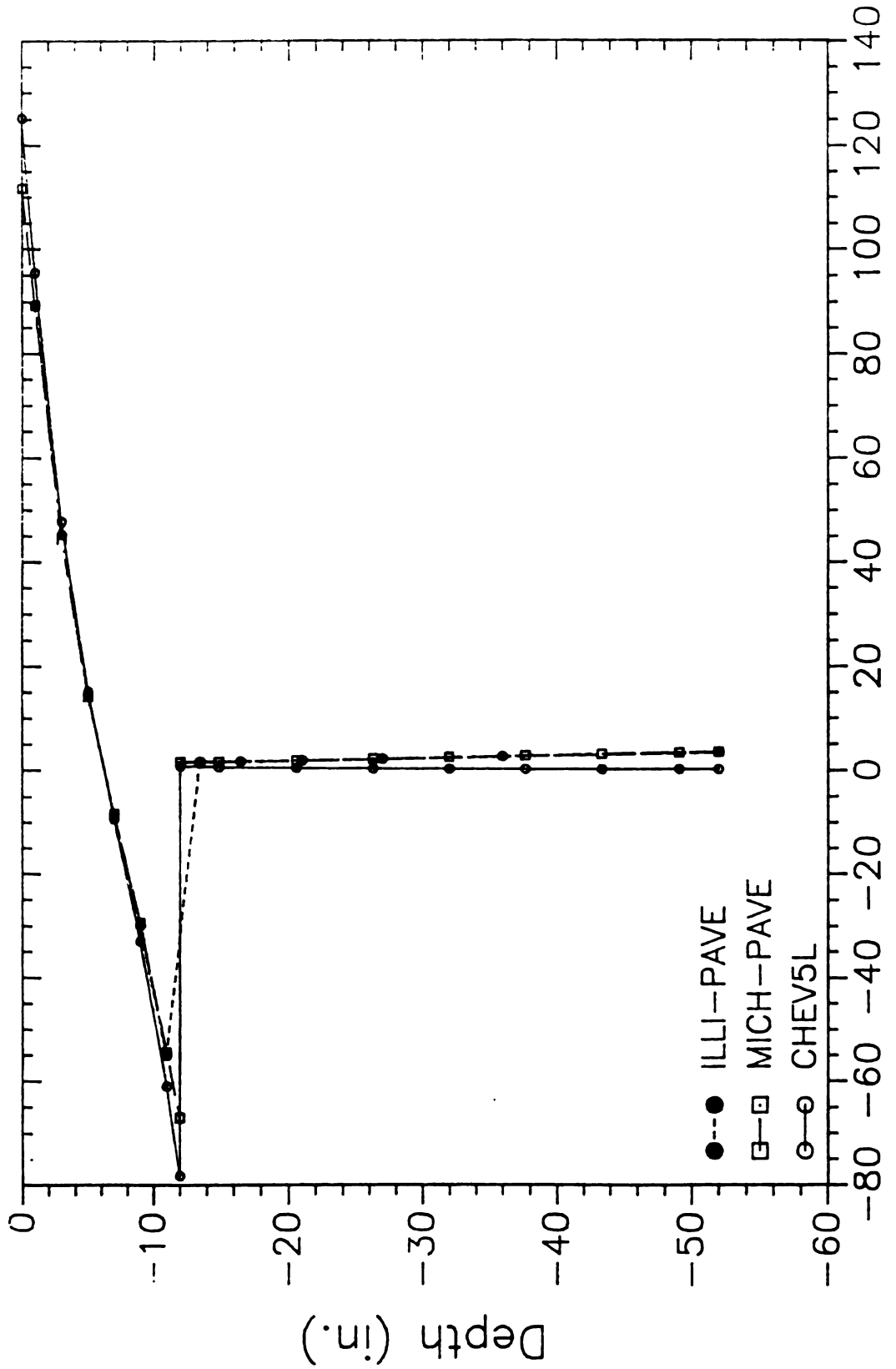

Figure 5-13: **Comparison of Radial Stress along Three Programs (12" of full-depth AC)**

A technique of estimating equivalent elastic moduli of layers from MICH-PAVE for use with linear analysis programs such as CHEV5L is presented. Use of the equivalent moduli in CHEV5L indicate that fairly accurate stresses can be obtained from a linear analysis once the equivalent moduli are known. However, the surface displacements from the linear analysis tend to be about 5 to 7 higher than those obtained through nonlinear analysis. Note, however, that a nonlinear program such as MICH-PAVE is required in order to estimate equivalent moduli for the layers.

Comparison of results from MICH-PAVE and ILLI-PAVE indicate that the stresses obtained from both programs are very close. However, the displacements from MICH-PAVE are about 12 % larger than those from ILLI-PAVE. Based on exact Solutions from linear analysis, the flexible boundary used in MICH-PAVE is expected to give better deflection estimates than the deep fixed boundary used in ILLI-PAVE.

CHAPTER 6

FATIGUE LIFE AND RUT DEPTH MODELS

6.1 GENERAL

Laboratory fatigue life data for asphalt mixes has been accumulated in large quantities since the early 1950's. Traditionally, the data are plotted as stress or strain amplitude versus the resulting life, commonly known as S-N curves. For asphalt mixes, as for most other materials, fatigue life steadily increases with decreasing stress or strain amplitude until the stress or strain level of the fatigue limit is reached, below which the life apparently becomes infinitely long. In general, stresses at or below the fatigue limit cause only elastic strains. It should be emphasized that cyclic and/or cumulative plastic strains are ultimately responsible for fatigue damage and the consequent fatigue failure. In addition, since asphalt mixes are weaker in tension than in compression, the magnitude of the induced tensile strain due to the applied load is typically used to estimate the fatigue life of the mixes.

Two tests are generally used in the laboratory to assess the fatigue life of compacted asphalt mixes: the beam test and the indirect tensile test. For the beam test, the fatigue life of a beam specimen is typically defined by the number of load application at which the flexural modulus of the beam decreases to 50 percent of its original value. For the indirect tensile test, the fatigue life is defined by the number of load applications at which a crack is observed along the vertical diameter of the test specimen (Baladi,et al.,1989).

Using stress-controlled cyclic load indirect tensile tests and Marshall size specimens, Baladi (1989) developed empirical models using statistical methods, relating the fatigue life and the cumulative plastic compressive deformations along the vertical diameter of the test specimens to the various asphalt mix and test variables. These models are presented in equations 6-1 and 6-2.

$$\ln(N_{FL}) = 36.631 - 0.1402 \times TT - 2.300 \times \ln(CL) - 0.5095 \times AV - 0.001306 \times KV + 0.06403 \times ANG \quad \text{(Eq.6-1)}$$

$$\ln(CD1) = -11.615 + 0.07028 \times TT + 0.5000 \times \ln(N) + 1.148 \times \ln(CL) + 0.3326 \times AV - 0.001007 \times KV \quad \text{(Eq.6-2)}$$

where:

ln = natural log;

N_{FL} = fatigue life = number of load applications to fatigue;

CD1 = cumulative plastic deformation along the vertical diameter (inch x 10^{-4});

TT = test temperature (^{o}F);

CL = the magnitude of the cyclic load (pounds);

AV = the percent air voids in the asphalt mix; (AV = 3 to 7);

KV = the kinematic viscosity of the asphalt binder (centistokes); and

ANG = the angularity of the aggregate in the mix, (ANG = 4 for 100% crushed aggregate, 2 for rounded river deposited natural aggregate);

Based on limited field observations of in-service flexible pavements in the States of Michigan and Indiana, Baladi noted that the fatigue life of asphalt pavements is about 20 times larger than that estimated using equation 6-1. He also noted that equations 6-1 and 6-2 can be used to predict the fatigue life and rut depth of in-service pavements

provided that (for each pavement in question) the values of the coefficients in the equations are adjusted to reflect the properties of the different pavement layers and their thicknesses. Based upon these observations, equations 6-1 and 6-2 were empirically calibrated using the modulus of the various pavement layers of several in-service pavements and the outputs (stresses, strains, and surface deflection) obtained from the MICH-PAVE computer program. The calibration process and the resulting fatigue and rut depth models are presented in the next section.

6.2 FATIGUE LIFE MODEL

As noted in the previous section, equation 6-1 was empirically calibrated using the actual modulus and thicknesses of the different pavement layers and the output of the MICH-PAVE computer program. The calibration process was accomplished in four steps as outlined below:

Step 1 - The actual fatigue lives of 10 pavement sections (see table 6-1) with known layer thicknesses and properties were tabulated. The fatigue life of the pavement sections is defined by the estimated number of 18 kips equivalent single axle load (ESAL) that traveled the pavement sections prior to the initiation of low severity alligator cracking (one or two disconnected longitudinal hair cracks in the wheel path). It should be noted that, for most cases, accurate traffic data (ESAL) was not available. Hence, visual trafficcount and several assumptions were made to convert the average daily traffic (ADT) data to ESAL.

Step 2 - In this step, the actual pavement cross section (layer thicknesses and moduli) were used as input to the MICH-PAVE program

and the compressive and tensile strains and stresses in the asphalt concrete were calculated. These values along with the properties of the pavement layers were then correlated to the fatigue life of the 10 pavement sections using the same equation form as that of equation 6-1. This step yielded a fatigue life equation which accurately predicted the actual fatigue life of only four pavement sections. The predicted fatigue life of the remaining six sections, however were not as accurate.

Step 3 - Thirty arbitrary selected pavement sections (see table 6-2) were analyzed using the 1986 AASHTO design guide and the MICH-PAVE program. Using the same equation form as that obtained in step 1 above, the resulting life in terms of ESAL obtained from the 1986 AASHTO design guide were then statistically correlated to the modulus, stresses, and strains of the various pavement layers that were calculated using the MICH-PAVE program. This step resulted in a second fatigue life equation that accurately predicted the life of the 30 arbitrary selected pavement sections. the value of the constants in front of each variable of this last equation were slightly different than those of the previous equation obtained in step 2.

Step 4 - The two equations obtained from steps 2 and 3 were then combined by averaging the values of the constants of each variable from the two equations. Finally, the sensitivity of the fatigue life of the resulting equation to each variable of the equation was studied relative to the sensitivity of equation 6-1 and to the outputs (stresses and strains) of the MICH-PAVE program. The purpose of the study was to make final adjustment in the value of the

constant in front of each variable in the equation to yield similar sensitivity to that of equation 6-1 and to the output of MICH-PAVE program. Equation 6-3 is the final fatigue life equation.

$$\log(ESAL) = -2.416 - 2.799(\log(SD)) + 0.00694(TBEQ) + 0.917(\log(MR_b)) + 0.154(TAC) - 0.261(AV) + 0.0000269(MR_s) - 1.096(\log(TS)) + 1.173(\log(CS)) - 0.001(KV) \quad \text{(Eq.6-3)}$$

where: log = base 10 logarithmic operator;

ESAL = number of equivalent 18 kips single axle load traveling the pavement section prior to failure;

SD = surface deflection under the center of the load (inch);

TBEQ = base thickness plus the equivalent thickness of the subbase (inches); equivalent thickness of the subbase is calculated by multiplying the actual thickness of the subbase by the ratio of the modulus of the subbase to that of the base material;

MR_b = resilient modulus of the base material (psi);

TAC = thickness of the AC layer (inch);

AV = the percent air voids of the AC layer (%);

MR_s = effective resilient modulus of the roadbed soil as defined in the AASHTO 1986 design guide (psi);

TS = the tensile strain at the bottom of the AC layer;

CS = the average compressive strain of the AC layer; and

KV = kinematic viscosity of the asphalt concrete binder (centistrokes).

It should be noted that an average annual air temperature of 75°F was assumed and used in all steps. Nevertheless, the fatigue life calculated using equation 6-3 of the 10 in-service pavement sections and the 30 arbitrary selected sections are listed in tables 6-1 and 6-2, respectively.

Table 6-1: Fatigue lives and rut depths of field data.

Site	TAC/MR_{AC}	TB/MR_b	TSB/Mr_{sb}	MR_s	FL(1)	FL(2)	AASHTO	RD(1)	RD(2)
	in/ksi	in/ksi	in/ksi	ksi	ESAL	ESAL	ESAL	in	in
IN1	4/500	12/60	6/12	6	1900000	2200000	750000	.3	.123
IN1	5/500	12/60	6/12	6	5500000	5300000	1750000	.2	.101
IN1	6/500	12/60	6/12	6	9700000	11500000	3700000	-	.087
IN2	3/150	12/25		4	9000	4245	13500	.2	.303
IN3	3/150	6/30		6	12200	2054	5200	-	.347
IN4	3/150	10/25		4	4000	2226	7000	-	.316
MIU1	4/150	10/20	36/9	3	82000	66589	620000	<.1	.047
MIU2	2.5/150	20/20	10/9	3	41000	26892	280000	<.1	.086
MIU3	6/350	16/20	13/9	3	500000	535550	1000000	.5-1	.029
MIU4	4.5/350	12/20	70/9	3	5475000	4960000	450000000	<.1	.030

IN1 : a pavement which was overlayed twice. Each overlay consist of one inch thick AC;

TAC : thickness of the asphalt concrete course (inch);

TB : thickness of the base layer (inch);

TSB : thickness of the subbase (inch);

MR_{AC} : resilient modulus of the asphalt concrete (ksi);

MR_b : resilient modulus of the base layer (ksi);

MR_{sb} : resilient modulus of the subbase layer (ksi);

MR_s : resilient modulus of the subgrade (ksi);

FL(1): fatigue life of the pavement section (ESAL);

FL(2): calculated fatigue life (ESAL);

RD(1): measured rut depth (inch); and

RD(2): calculated rut depth (inch); for all pavement sections located in Indiana (IN1 through IN4) an average annual air temperature of 75 ^{o}F was used, for Michigan sections (MIU1 through MIU4), 66^{o}F was used.

Table 6-2: Parameters for calibrating the fatigue life and rut depth equations used in MICH-PAVE.

C	TAC (in)	AV (%)	TB (in)	MR_{ac} (ksi)	MR_b (ksi)	MR_s (ksi)	TS	CS	SD (in)	$FL_{(1)}$ AASHTO	$FL_{(2)}$ (ESAL)	Ratio	RD (in)
1	2	7	6	150	25.9	3	532	143	.1074	212	134	.63	0.58
2	4	7	6	150	19.2	3	809	302	.0836	778	631	.81	0.32
3	8	7	6	150	12.0	3	495	318	.0550	8767	9970	1.14	0.22
4	2	7	6	150	73.6	3	-10	57	.0826	1261	*	*	*
5	8	7	6	150	25.0	3	383	320	.0518	23340	30622	1.31	0.18
6	8	7	6	150	38.2	3	304	322	.0497	45325	66288	1.46	0.16
7	2	5	6	300	24.5	3	654	121	.1012	446	328	.74	0.50
8	2	3	6	500	23.2	3	667	98	.0955	835	933	1.12	0.44
9	8	5	6	300	10.1	3	317	164	.0472	47196	32677	.69	0.21
10	8	3	6	500	8.9	3	216	100	.0420	210720	114230	.54	0.19
11	2	7	9	150	24.2	3	444	239	.0955	784	629	.80	0.57
12	2	7	12	150	22.7	3	426	293	.0879	1865	1606	.86	0.54
13	4	7	9	150	56.1	3	239	322	.0599	26190	28509	1.09	0.24
14	4	7	12	150	54.5	3	220	354	.0550	87556	69635	.80	0.22
15	4	7	6	150	57.9	3	300	274	.0677	6051	8318	1.38	0.26
16	2	7	6	150	27.4	6	490	238	.0685	1351	1190	.88	0.58
17	2	7	6	150	28.3	9	474	290	.0533	3631	3891	1.07	0.56
18	8	5	6	300	11.9	9	278	168	.0234	680635	467143	.69	0.17
19	8	3	12	500	10.6	9	194	103	.0199	5.31e6	4.79e6	.90	0.11
20	8	3	12	500	12.7	25	179	105	.0122	59.0e6	66.9e6	1.13	0.10
21	8	3	12	500	35.6	9	146	108	.0176	34.4e6	29.6e6	.86	0.08
22	8	3	12	500	39.2	25	131	112	.0099	444 e6	512 e6	1.15	0.07
23	8	3	18	500	10.6	9	193	103	.0203	8.41e6	11.9e6	1.42	0.10
24	8	3	18	500	11.9	25	184	104	.0129	95. e6	132 e6	1.39	0.08
25	8	3	18	500	33.8	9	139	110	.0172	95.4e6	84.5e6	.89	0.07
26	8	3	18	500	37.2	25	130	112	.0099	2880e6	1286e6	.45	0.06
27	8	5	18	300	23.4	9	213	177	.0207	11.3e6	11.8e6	1.05	0.09
28	8	5	18	300	26.3	25	198	181	.0129	193 e6	148 e6	.77	0.08
29	8	5	18	300	37.4	9	171	183	.0191	44.3e6	30.1e6	.68	0.08
30	8	5	18	300	40.3	25	160	188	.0115	640 e6	399 e6	.62	0.07

Where:

$FL_{(1)}$ = fatigue life calculated using the 1986 AASHTO design guide;
$FL_{(2)}$ = fatigue life calculated using the MICHPAVE program;
TS = tensile microstrain at the bottom of the AC;
CS = average compressive microstrain within the AC;
Ratio = ratio of $FL_{(2)}/FL_{(1)}$;
TB = equivalent base thickness;
RD = rut depth is calculated by Eq.6-4 (in); and
* = pavement failed in shear.

NOTE: The rut depth is calculated at the fatigue life of the pavement section and an average annual temperature of 75 ^{o}F.

6.3 RUT DEPTH MODEL

The rut depth model (equation 6.2) was calibrated using field data from 7 different pavement sections (see table 6-1). First, each section was analyzed using the MICH-PAVE computer program. The calculated stresses, strains, and surface deflection, and the layer thicknesses and properties were then used to calibrate equation 6.2. This resulted in the following model:

$$\log(RD) = -1.6 + .067(AV) - 1.4(\log(TAC)) + .07(AAT) - .000434(KV) + .15(\log(ESAL_t)) - .4(\log(MR_s)) - .50\log(MR_b) + .1(\log(SD)) + .01(\log(CS)) - .7(\log(TBEQ)) + .09(\log(50-(TAC+TBEQ))) \quad \text{(Eq.6-4)}$$

where: RD = rut depth (inches);

$ESAL_t$ = the number of ESAL at time t where the rut depth is being calculated;

AAT = average annual air temperature (^{o}F);

50 -(TAC+TBEQ)) = the affected depth of the roadbed soil; and

all other variables are as before.

It should be noted that since the number of variables in equation 6-4 is higher than the number of pavement sections where rut depth data wereavailable,thevalue of thecoefficient infrontofthe average annual temperature (AAT) term was kept the same as that of equation 6-2. and a constant tire pressure of 100 psi was assumed. In addition, a step-wise statistical analyses were conducted whereby a maximum of 7 variables were used in each step. This resulted in several equations each containing only seven variables beside the AAT. It was noted that for all equations the values of the constants in front of the AV, TAC,

and ESAL were almost the same while the values of the other constants changed slightly from one equation to another. Nevertheless, Equation 6-4 was obtained by averaging the values of each constant in front of each variable obtained from all equations. Measured and calculated (using equation 6-4) rut depths for 7 in-service pavement sections are listed in table 6-1.

6.4 : SENSITIVITY ANALYSIS

6.4.1 Fatigue Model

Sensitivity analysis of the fatigue life equation (Eq. 6-3) has indicated that:

1. The fatigue life of a flexible pavement decreases as the surface deflection at the center of the loaded area increases. Increasing the surface deflection from 0.001 to 0.01 inch causes a decrease in the fatigue life by a factor of 630. It should be noted that the surface deflection is an intrinsic function of the thicknesses and properties of all pavement layers.
2. Increasing the thickness of the granular layer from 6 to 18 inches causes an increase in the fatigue life by a factor of about 6.8.
3. Increasing the modulus of granular layer from 10 to 50 ksi causes an increase in the fatigue life by a factor of about 4.4.
4. Increasing the thickness of AC from 2 to 8 inches causes an increase in the fatigue life by a factor of about 8.4.
5. The fatigue life decreases as the percent air voids in the mix increases. Increasing AV from 3 to 7 percent yields a decrease in the fatigue life by a factor of about 11.

6. Increasing the modulus of roadbed soil from 3 to 25 ksi causes an increase in the fatigue life by a factor of about 4.
7. An increase in the tensile strain at the bottom of AC layer from 90 to 600 micro strain causes a decrease in the fatigue life by a factor of about 8.
8. An increase in the average compressive strain within the AC layer from 100 to 300 micro strain causes an increase in the fatigue life by a factor of about 3.6.
9. Decreasing the kinematic viscosity of the AC from 270 to 159 centistokes causes an increase in the fatigue life by a factor of about 1.3.

6.4.2 Rut Depth Model

Sensitivity analysis of the rut depth equation (Eq. 6-4) has indicated that:

1. Increasing the percent air voids in the mix from 3 to 7 percent yields an increase in the rut depth by a factor of about 1.9.
2. Increasing the thickness of the AC from 2 to 8 inches causes a decrease in the rut depth by a factor of about 7.
3. The rut depth equation is very sensitive to the average annual temperature. Increasing the average annual temperature from 60 to 77^{o}F yields an increase in the rut depth by a factor of about 15.5.
4. Increasing the kinematic viscosity of the AC from 159 to 270 centistokes causes a decrease in the rut depth by a factor of about 1.1. This indicates that the rut depth equation is relatively insensitive to the kinematic viscosity of the AC.

5. Increasing the number of load repetitions from 100,000 to 1,000,000 ESAL causes an increase in the rut depth by a factor of about 1.4.
6. Increasing the modulus of roadbed soil from 3 to 25 ksi causes a decrease in the rut depth by a factor of about 2.3.
7. Increasing the modulus of granular layer from 10 to 50 ksi causes a decrease in the rut depth by a factor of about 2.2.
8. An increase in the pavement surface deflection at the center of the loaded area from 0.001 to 0.01 inch causes an increase in the rut depth by a factor of 1.3.
9. An increase in the average compressive strain within the AC from 100 to 300 micro strain causes an increase in the rut depth by a factor of about 1.01.
10. Increasing the equivalent base thickness from 6 to 18 inches causes a decrease in the rut depth by a factor of about 2.2.
11. Increasing the affected depth of the roadbed soil from 20 to 40 inches causes a increase in the rut depth by a factor of about 1.1.

6.5 : ANALYSIS OF MICH-PAVE INPUT/OUTPUT

The sensitivity of three important outputs (tensile strain at the bottom of the AC layer, compressive strain at the top of the roadbed soil, and pavement surface deflection) of MICH-PAVE computer program to the input variables was studied using several pavement sections. The results of the study are summarized in the following sections.

6.5.1 : Thickness and Modulus of the Asphalt Concrete

The thickness and modulus of the AC course have significant effects upon the tensile strain at the bottom of the AC layer. For example, a 2 inch thick and soft (MR < 150 ksi) AC course located on top of a stiff base layer whose modulus is larger than about one third of that of the AC (i.e., cement or asphalt treated base layer) will cause no tensile strain at the bottom of the AC layer. The reason is that the AC course and the base layer will act as one layer whose nutral axis is located within the base layer (well below the bottom of the AC course). Hence, the entire AC layer will be in compression (see Table 6-3). Figure 6-1 depicts the effect of the thickness of the AC on the tensile strain at the bottom of the AC layer.

Increasing the thickness of the AC surface causes a significant decrease in the compressive strain at the top of the roadbed soil (see Figure 6-2). This is especially true when the modulus of the AC layer is significantly higher than that of the granular base material. Hence, one way to reduce the compressive strain at the top of the roadbed soil (which contributes most to high surface deflection and rut), is to increase the thickness of the AC. Nevertheless, Figure 6-3 shows the pavement surface deflection as a function of the thickness of the AC layer. The numerical results are listed in Table 6-3.

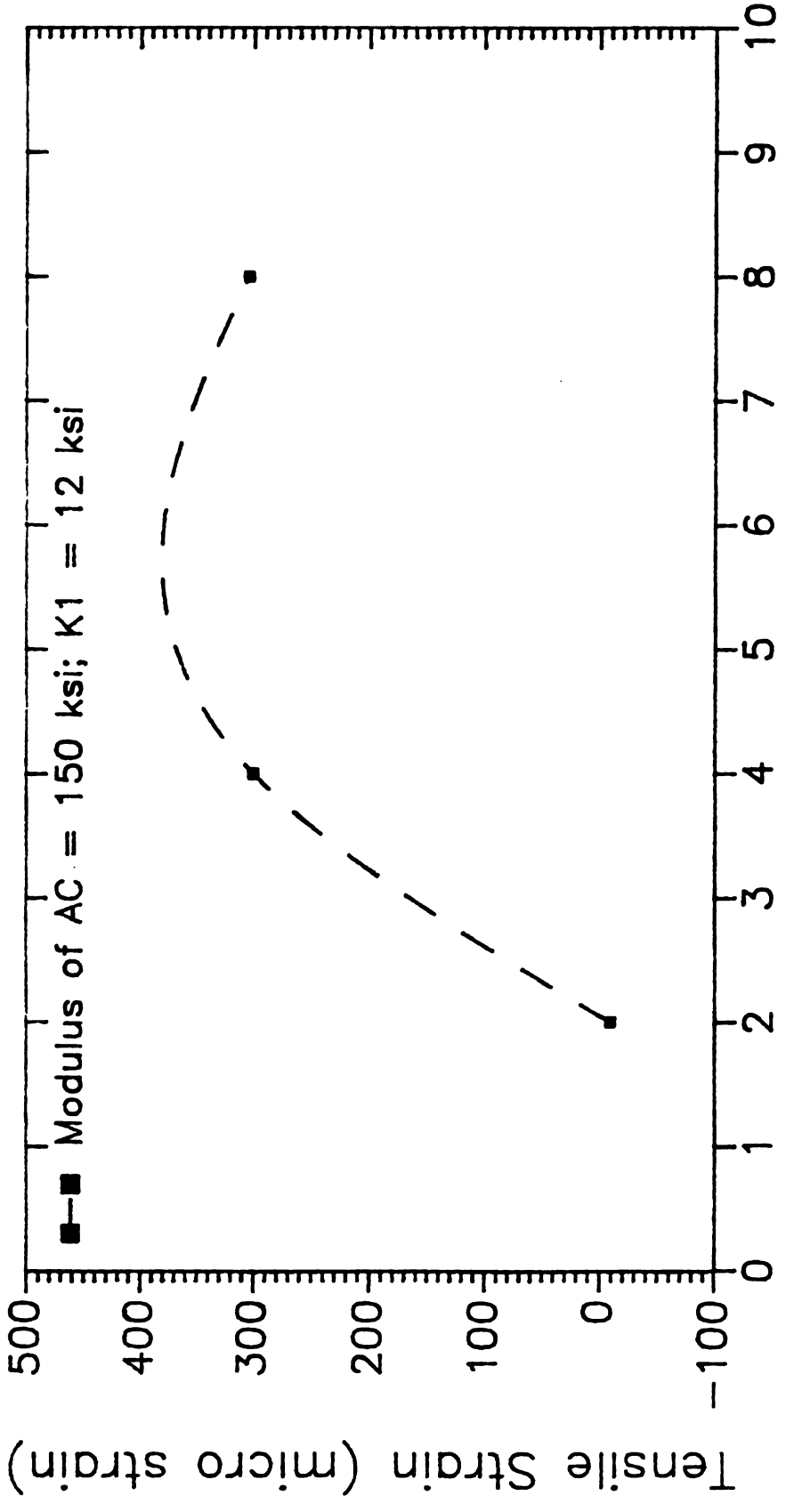

Figure 6-1: Tensile Strain at the Bottom of AC Layer to Thickness of AC

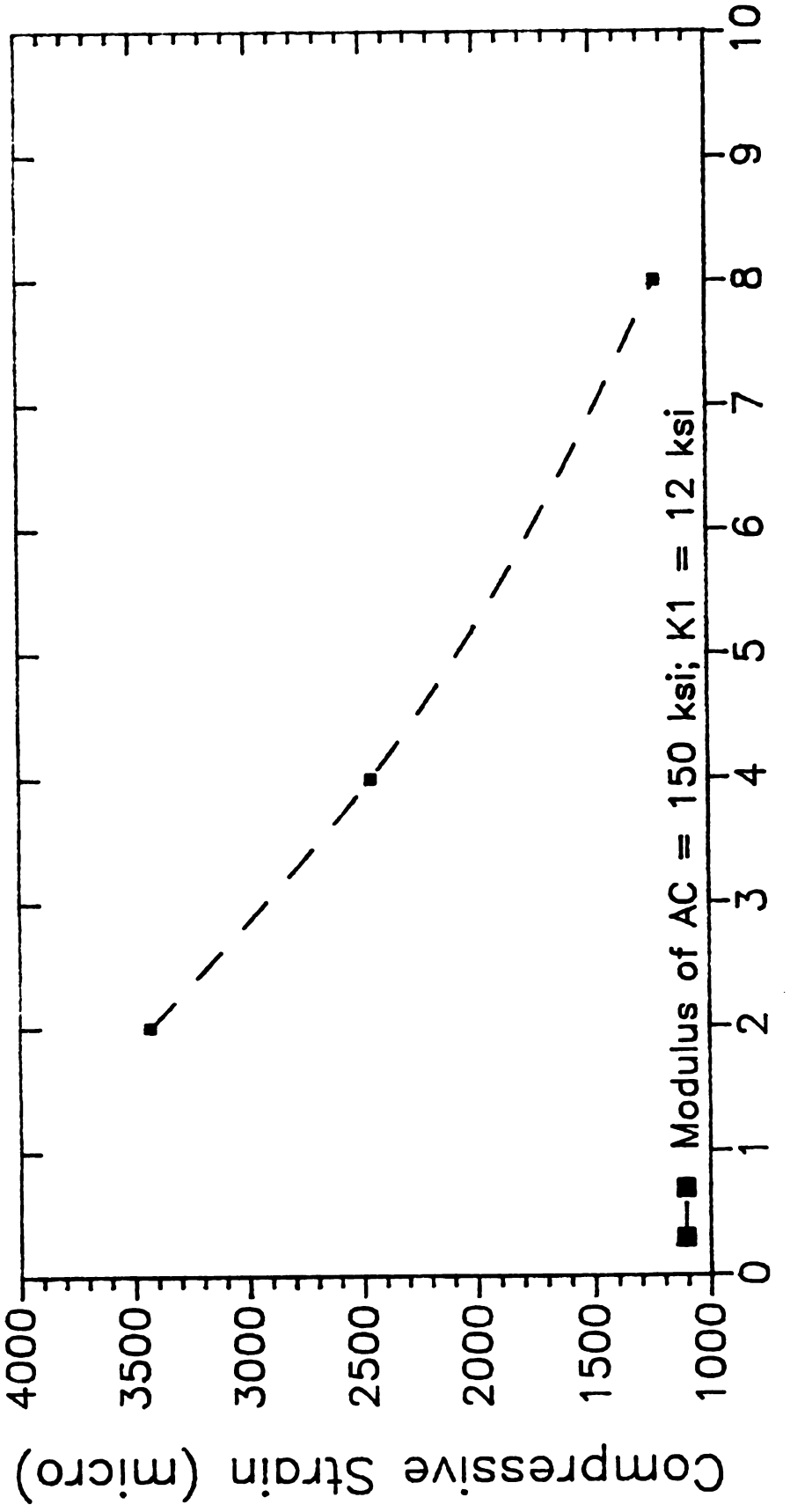

Figure 6—2: Compressive Strain at the Top of Roadbed Soil to Thickness of AC

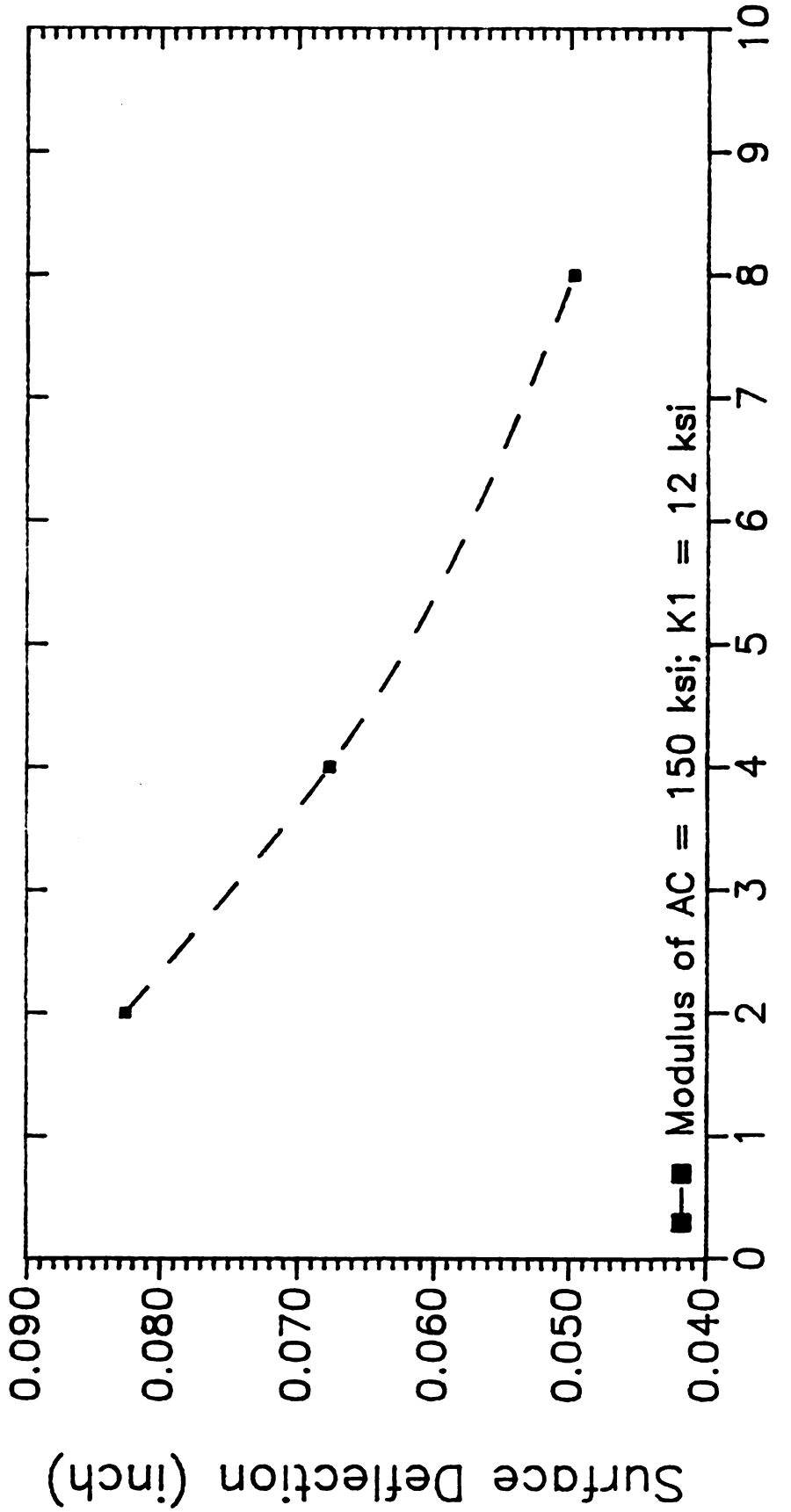

Figure 6—3: Surface Deflection at the Center of Loading to Thickness of AC

Table 6-3: Tensile strain at the bottom of the AC and compressive strain at the top of the roadbed soil for varying AC thicknesses.

Case	Thickness (in)	Tensile Micro Strain	Compressive Micro Strain	Surface Def. (in)
4	2	- 10	3430	0.08258
15	4	300	2462	0.06769
6	8	304	1226	0.04970

6.5.2 : Percent Air Voids in the Asphalt Concrete

For a 2 inch thick AC layer, decreasing the percent air voids from 7 to 3 percent (increasing the modulus from about 150 to about 500 ksi) results in an increase in the tensile strain at the bottom of the AC layer. For an 8 inch thick AC layer (on the other hand), similar decrease in the percent air voids causes a decrease in the tensile strain (see Table 6-4 and Figure 6-4). These observations were expected because of the stress distribution within the AC layer and its flexibility. Thicker AC will spread the load over wider area than thin AC layer. The significant of these observations is that (since the tensile strain is not an independent variable) a successful predictive fatigue model for flexible pavements should not be strictly based on the stiffness of the AC or the percent air voids. It must accounts for all the variables that affect the tensile strain at the bottom of the AC course.

The percent air voids of the AC layer has minor effects upon the compressive strain at the top of the roabed soil as well as on the pavement surface deflection as shown in Figure 6-5 and 6-6, respectively. Again, these observations were expected because surface deflection and compressive strain at the top of the roadbed soil are

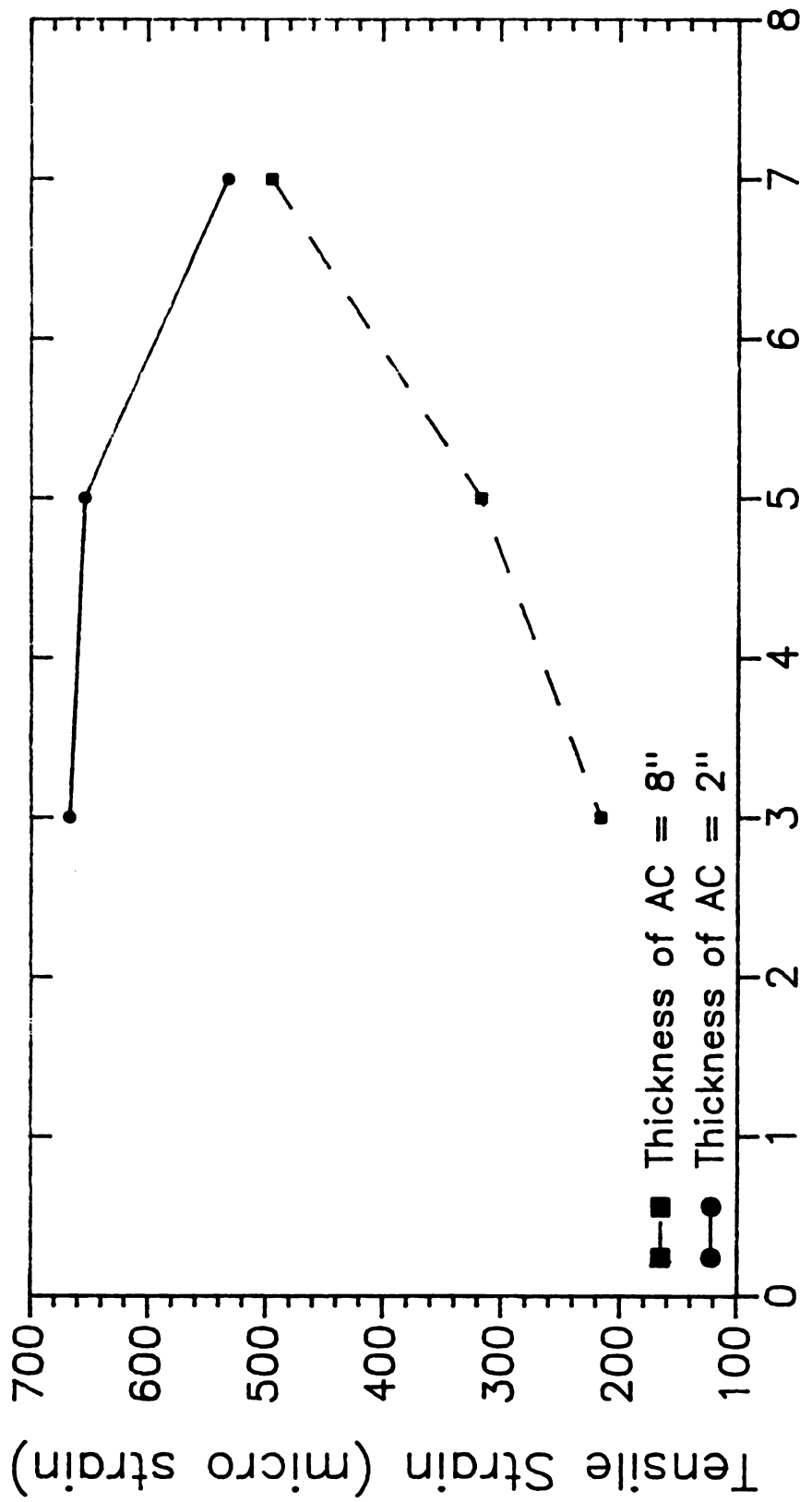

Figure 6–4: Tensile Strain at the Bottom of AC Layer to Air Voids of AC

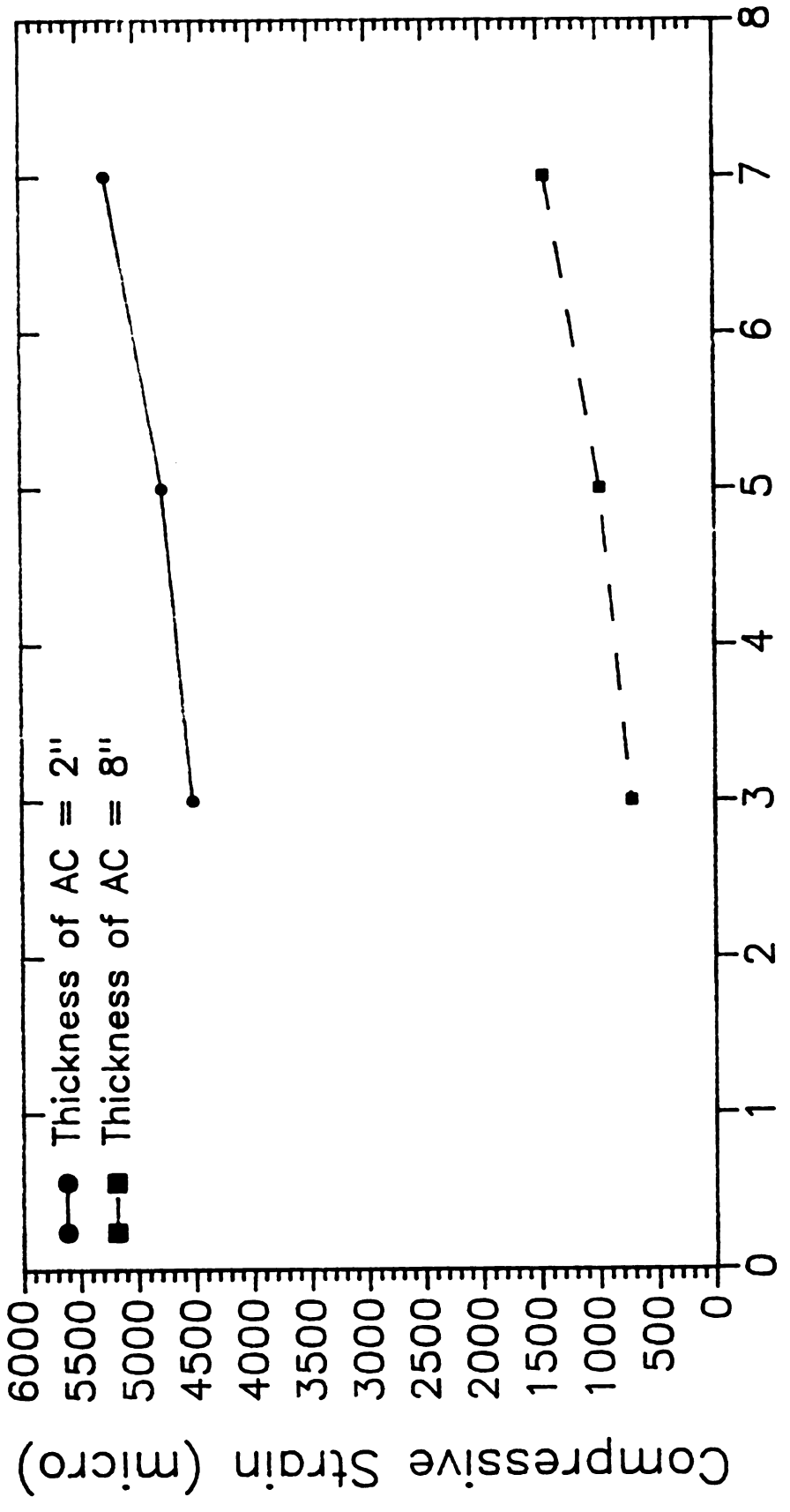

Figure 6—5: Compressive Strain at the Top of Roadbed Soil to Air Voids of AC

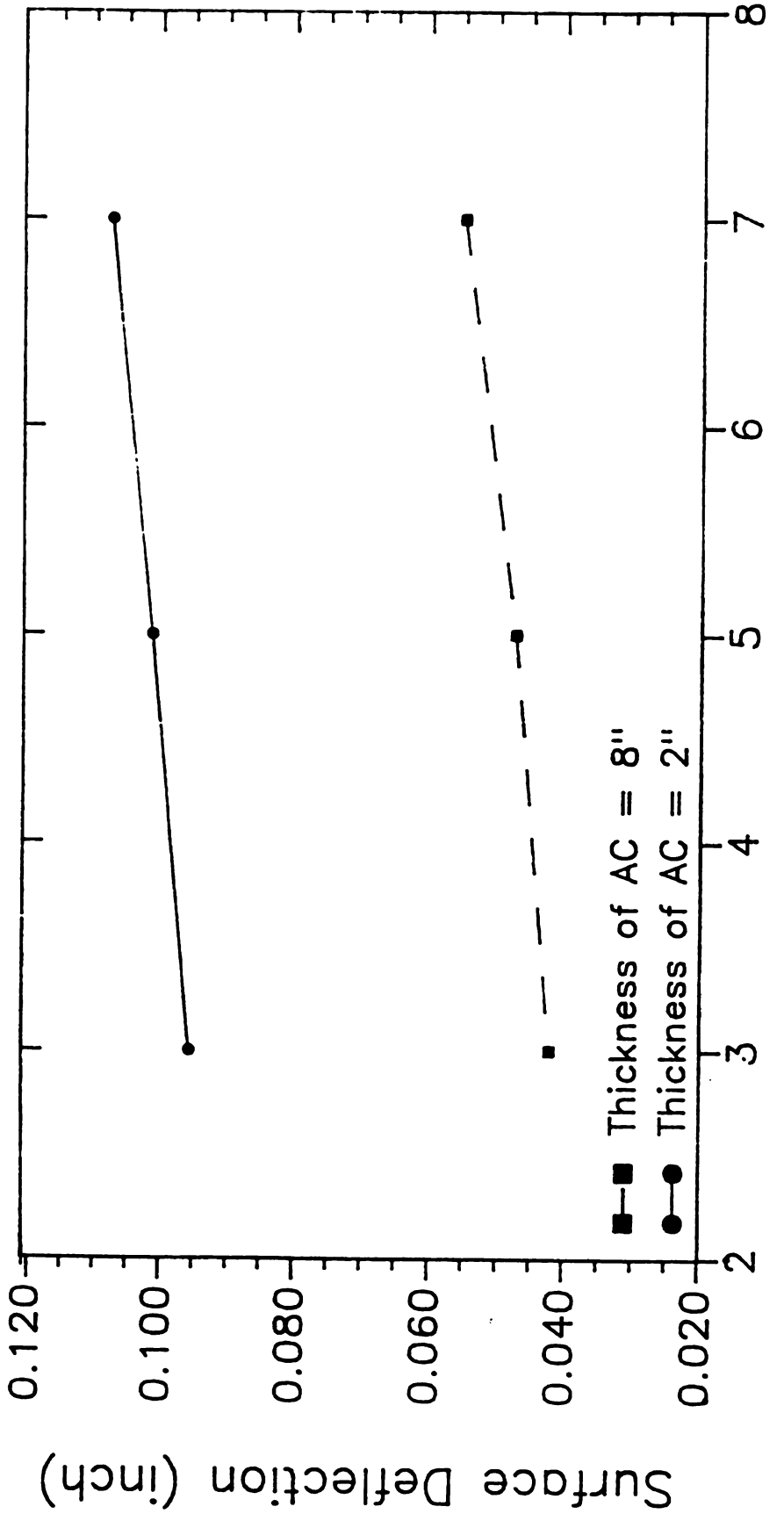

Figure 6—6: Surface Deflection at the Center of Loading to Air Voids of AC

mainly function of the stresses delivered to the roadbed soil. The percent air voids and/or the stiffness of the AC layer will cause no significant increase and/or decrease in the magnitude of these stresses. The stresses delivered to the roadbed soil are significantly affected by the thicknesses of the protective layers (AC, base, and subbase).

Table 6-4: Tensile strain at the bottom of the AC and compressive strain at the top of the roadbed soil for varying values of air voids in the AC.

Case	Air Voids (%)	Modulus (ksi)	Tensile Micro Strain	Compressive Micro Strain	Surface Def. (in)
1	7	150	532	5247	0.1074
7	5	300	654	4767	0.1012
8	3	500	667	4508	0.0955
3	7	150	495	1440	0.0550
9	5	300	317	975	0.0472
10	3	500	216	716	0.0420

6.5.3 : Thickness of Granular Layers

The effects of the thickness of the granular layer upon the tensile strain at the bottom of the AC layer, the compressive strain at the top of the roadbed soil, and the surface deflection were also analyzed using the MICH-PAVE program. The results are listed in Table 6-5 and plotted in Figures 6-7 through 6-9. Examination of these results have indicated that:

1) Increasing the thickness the granular layer causes a reduction in the tensile strain at the bottom of the AC layer (see Figure 6-7) until an optimum thickness is reached beyond which the magnitude of the reduction is insignificant. For example, in reference to Table 6-5, increasing the thickness of the granular layer from 6 to 9 inches causes a 26 percent reduction in the tensile strain.

Adding three more inches result in a decrease of only 8 percent. The optimum thickness of the granular layer for any typical pavement design can be determined using economical analysis. It should be noted that, in general, lower tensile strain yield higher fatigue life).

2) Increasing the thickness of the granular layer from 6 to 9 inches results in a 29 percent decrease in the compressive strain at the top of the roadbed soil (see Table 6-5 and Figure 6-8). Further increase in the thickness of the granular layer from 9 to 12 inches will cause an additional 24 percent decrease. Thus, as far as the compressive strain is concerned, thicker granular layer is beneficial. It should be noted that lower compressive strains at the top of the roadbed soil yield lower rut potential of the soil until the elastic strain limit is reached. This limit is mainly a function of the type of roadbed soil and its degree and time duration of saturation. Hence, the optimum thickness of the granular layer to reduce the rut potential of the roadbed soil should be analyzed on a case by case basis relative to the type of the roadbed soil and drainage conditions.
3) Finally, Figure 6-9 indicates that increasing the thickness of the granular layer from 6 to 12 inches causes a reduction in the surface deflection by about 20 percent. This percentage decrease is about half of that due to an increase in the thickness of the AC from 2 to 8 inches (see section 6.5.1).

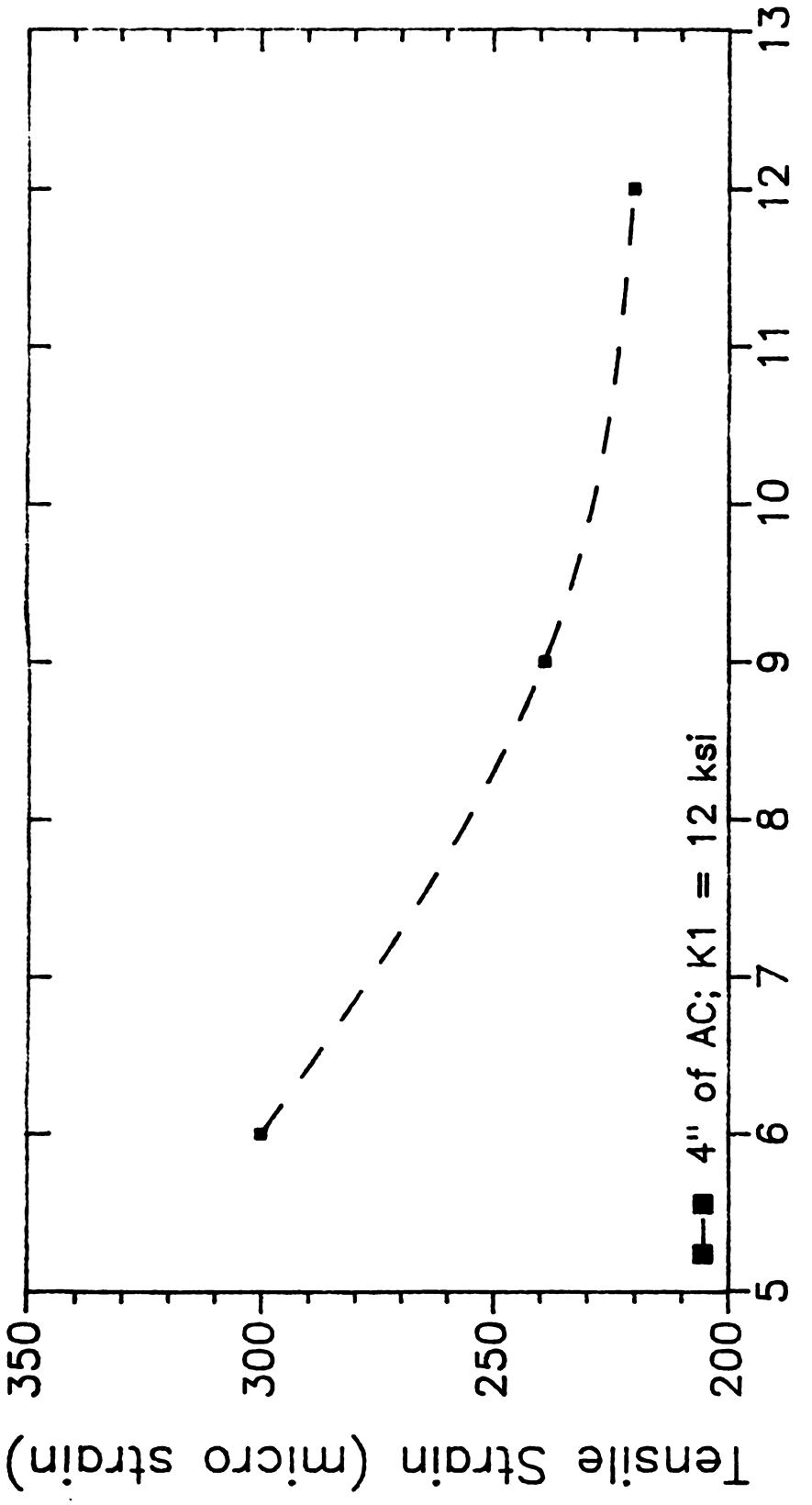

Figure 6—7; Tensile Strain at the Bottom of AC Layer to Thickness of Granular Layer

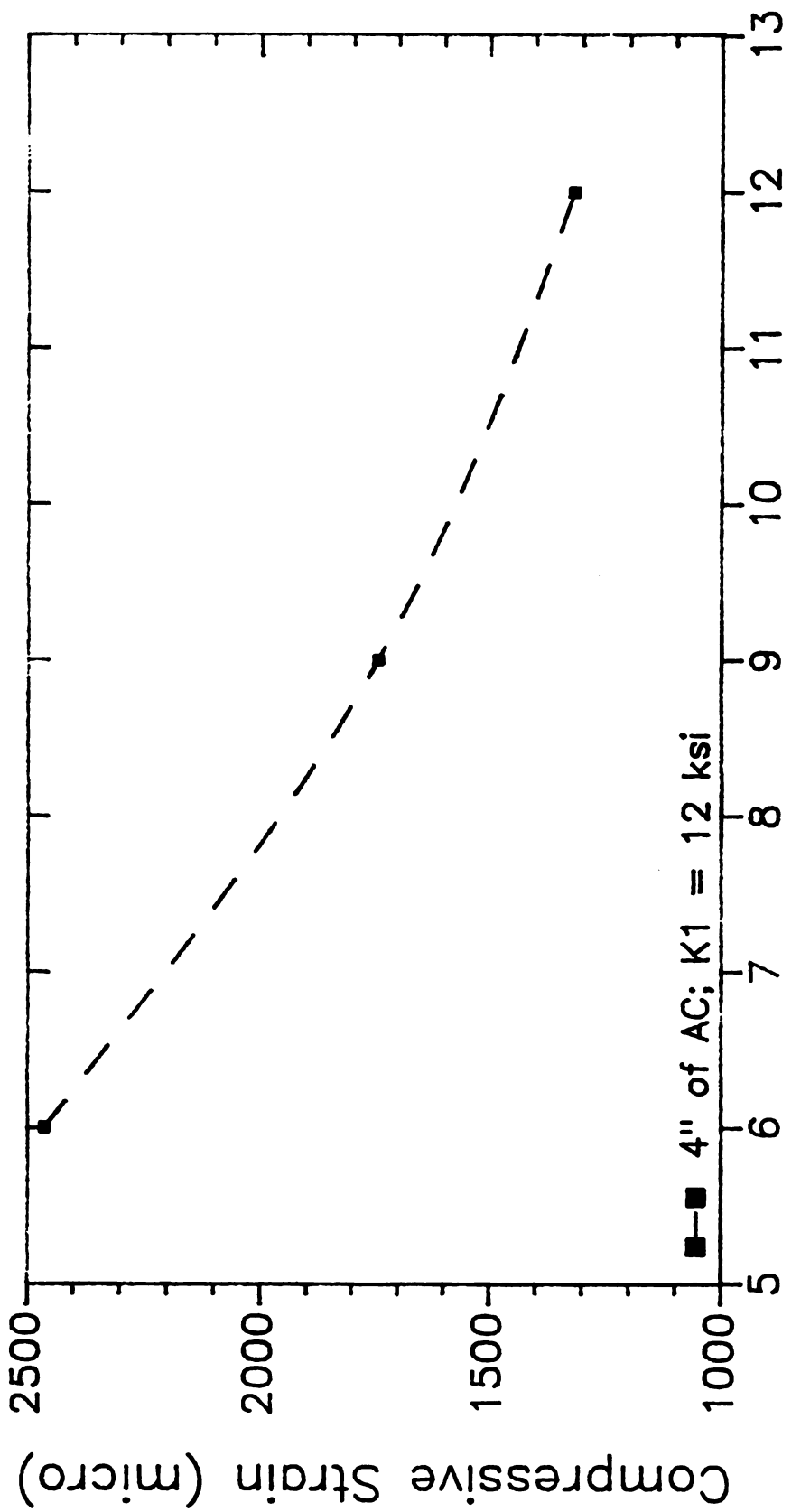

Figure 6—8: Compressive Strain at the Top of Roadbed Soil to Thickness of Granular Layer

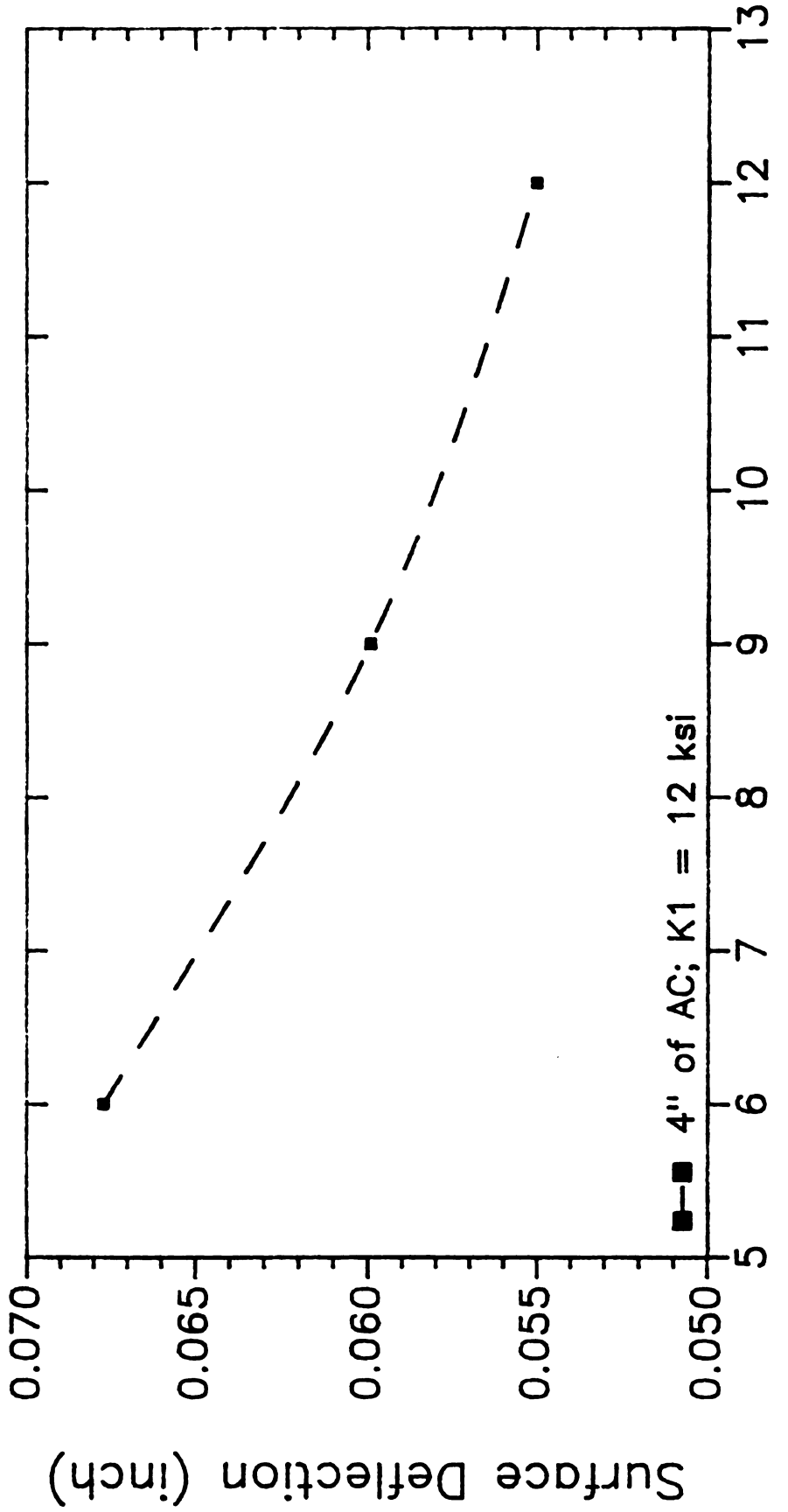

Figure 6—9: Surface Deflection at the Center of Loading to Thickness of Granular Layer

Table 6-5: Tensile strain at the bottom of the AC and compressive strain at the top of the roadbed soil for varying thickness of the granular layer.

Case	Thickness of Base(in)	Tensile Micro Strain	Compressive Micro Strain	Surface Def. (in)
15	6	300	2462	0.0677
13	9	239	1744	0.0599
14	12	220	1317	0.0550

6.5.4 : Modulus of the Granular layer

The effects of the modulus of the granular layer on the tensile strain at the bottom of the AC course, the compressive strain at the top of the roadbed soil, and on the pavement surface deflection vary and depend upon the thickness of the AC and its modulus. Recall that (see section 4-2) the nonlinear behavior of the granular layer was modeled using the $K1(\theta)^{K2}$ equation. The sensitivity of the outputs of MICH-PAVE program to the modulus of the granular layer was studied by varying the value of K1. The results of the study are summarized in Table 6-6 and plotted in Figure 6-10 through 6-12. Examination of the results indicated that:

1) For a pavement with 2 inch thick AC layer, increasing the value of K_1 from 4 to 12 ksi causes the tensile strain at the bottom of the AC layer to become compressive (see Figure 6-10) and causes tensile strain in the granular layer. The reason for this was explained in section 6.5.1 above.
2) For a 4 inch thick AC layer, increasing the K_1 value from 4 to 12 ksi results in a reduction in the tensile strain by a factor of about 2.7 (see Figure 6-10).

3) For an 8 inch thick AC layer, increasing the K_1 value from 4 to 12 ksi causes no significant effects in the tensile strain.

Table 6-6 and Figures 6-11 and 6-12 show that (except in the case of the 2 inch thick AC layer) increasing the K_1 value of the granular layer from 4 to 12 ksi does not significantly reduce the compressive strain or the pavement surface deflection. Therefore, one can concluded that (except for thin asphalt layers) the compressive strain at the top of the roadbed soil and the pavement surface deflection are insensitive to the modulus of the granular layer.

Table 6-6: Tensile strain at the bottom of the AC and compressive strain at the top of the roadbed soil for varying material properties of the granular layer.

Case	K_1 Value (ksi)	Modulus* (psi)	Tensile Micro Strain	Compressive Micro Strain	Surface Def. (in)
1	4	25886	532	5247	0.1074
4	12	73597	- 10	3430	0.0826
2	4	19153	809	3323	0.0836
15	12	57933	300	2462	0.0677
3	4	12002	495	1440	0.0550
5	8	24960	383	1334	0.0518
6	12	38216	304	1226	0.0497

* Modulus represents the equivalent resilient modulus of the granular layer.

6.5.5 : Elastic Modulus of Roadbed Soil

Due to the lack of an appropriate nonlinear model for roadbed soil in the State of Michigan, the nonlinear behavior of the roadbed soil is modeled in the MICH-PAVE program (see section 4-2) using an available model which require four material constants as input. For most State Highway Agency laboratories, these constants cannot be obtained. Therefore for simplicity, the following analyses were conducted using a

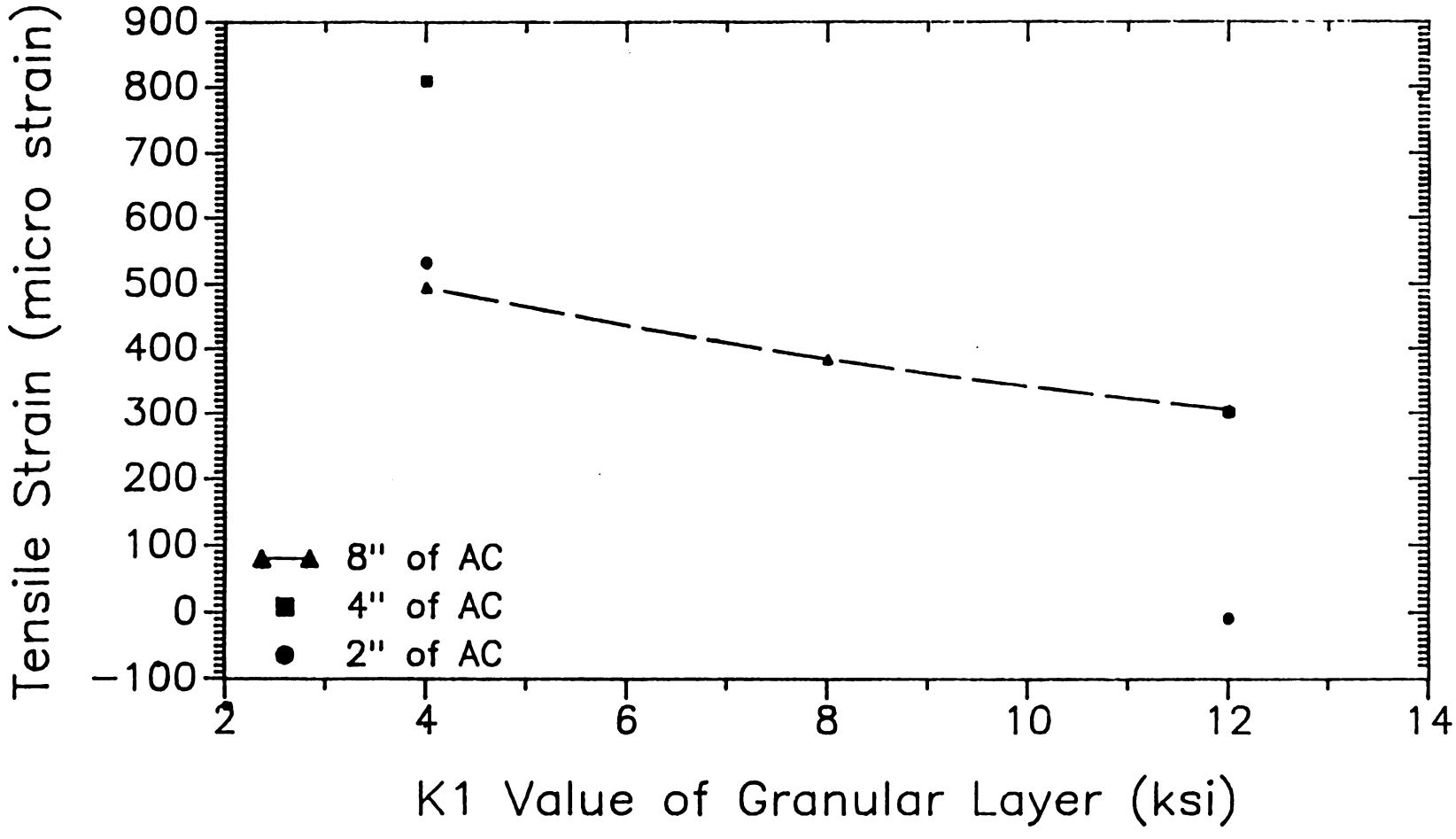

Figure 6–10: Tensile Strain at the Bottom of AC Layer to Material Properties of Granular Layer

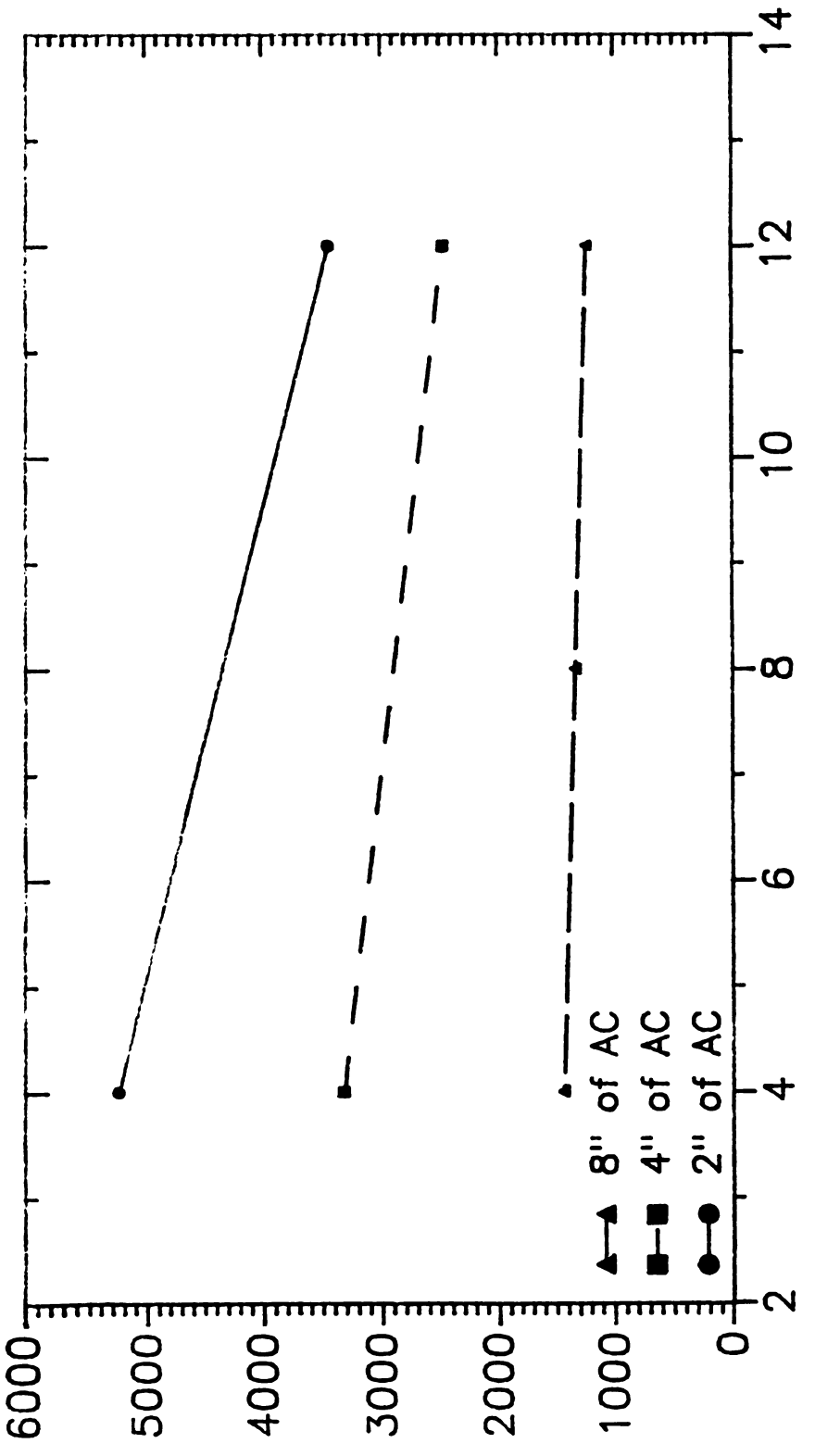

Figure 6—11: Compressive Strain at the Top of Roadbed Soil to Material properties of Granular Layer

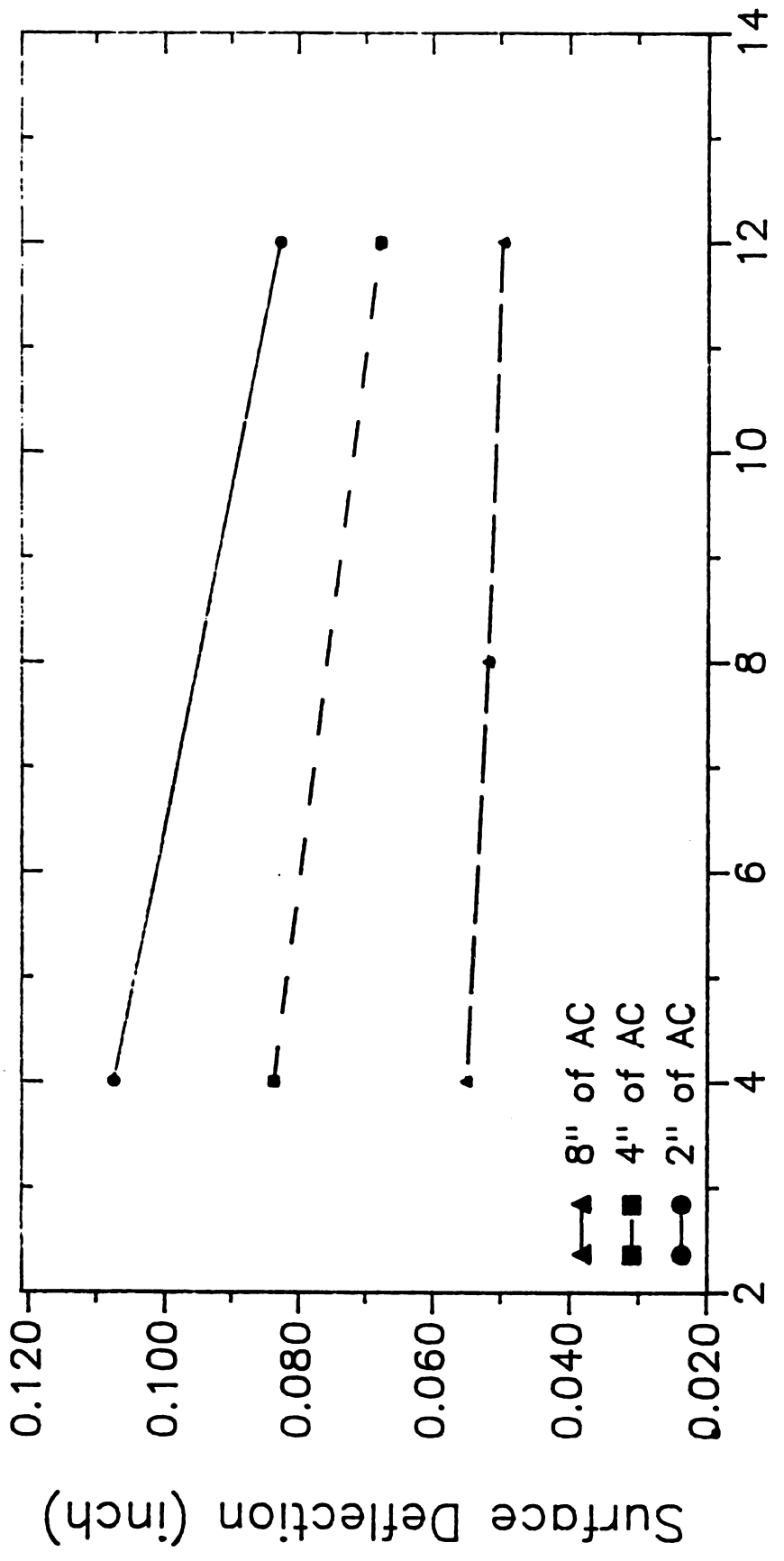

Figure 6–12: Surface Deflection at the Center of Loading to Material Properties of Granular Layer

linear model.

Table 6-7 and Figure 6-13 show that the tensile strain at the bottom of the AC layer is insensitive to variations (from 3 to 9 ksi) in the modulus of the roadbed soil. Figures 6-14 and 6-15, on the other hand, show that the compressive strain at the top of the roadbed soil and the surface deflection are very sensitive to the modulus of the roadbed soil. For example, increasingthe modulus of the roadbed soil from 3 to 9 ksi results in a decrease of about 39 percent in the compressive strain, and a decrease of about 50 percent in the surface deflection. Therefore, the modulus of the roadbed soil and the thickness of the AC layer are the most significant factors affecting the pavement surface deflection.

Table 6-7: Tensile strain at the bottom of th AC and compressive strain at the top of the roadbed soil for varying elastic moduli of the roadbed soil.

Case	Modulus (ksi)	Tensile Micro Strain	Compressive Micro Strain	Surface Def. (in)
9	3	317	975	0.0472
18	9	278	591	0.0230

6.6 : DETAILED ANALYSIS OF THE FATIGUE LIFE EQUATION

The following sections, discuss the influence of the thickness and air voids in the AC, the thickness and modulus of the granular layer, and the modulus of the roadbed soil on the fatigue life of pavements. It should be noted that the fatigue life is always calculated using equation 6-3.

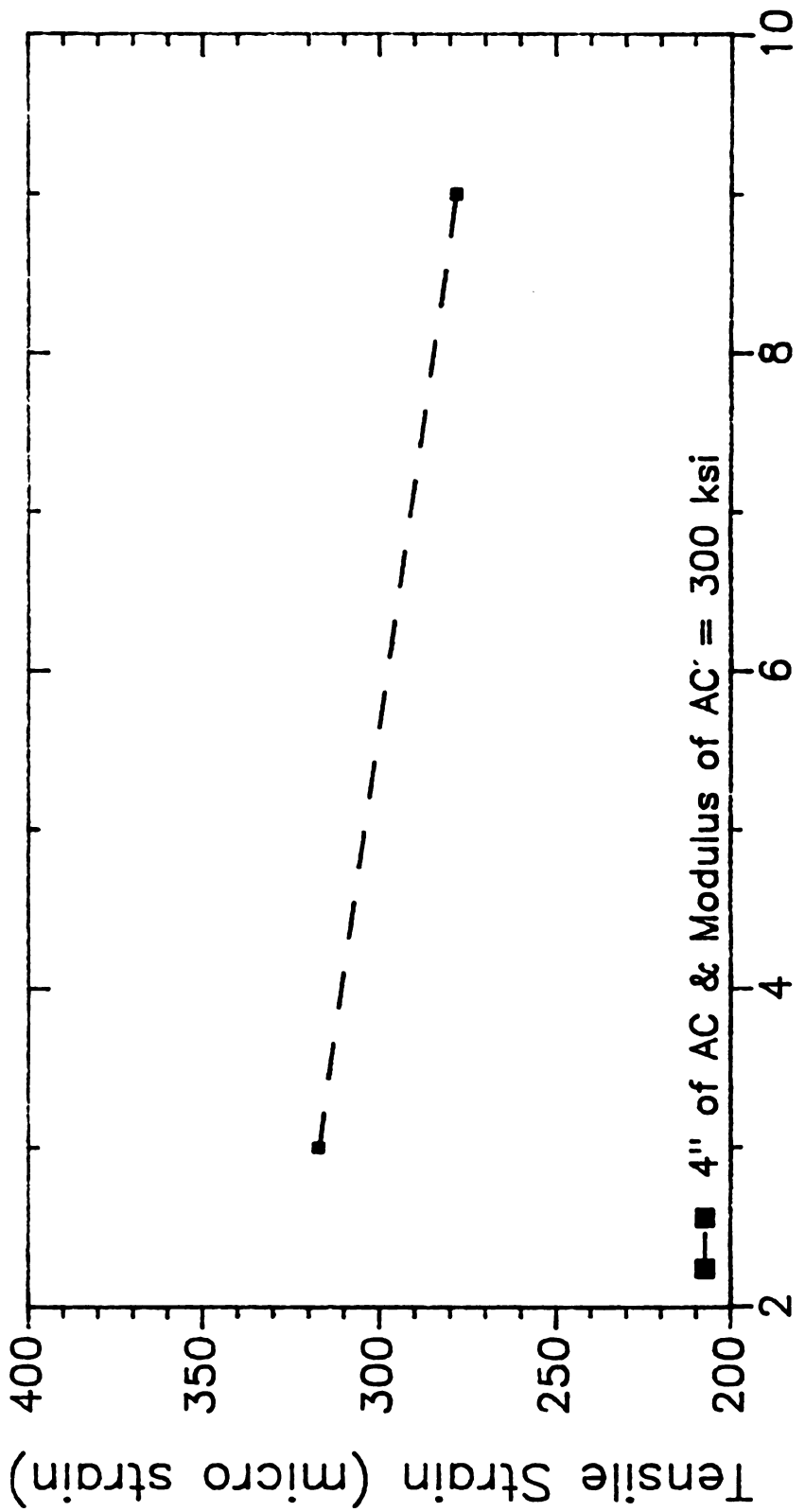

Figure 6—13: Tensile Strain at the Bottom of AC Layer to Elastic Modulus of Roadbed Soil

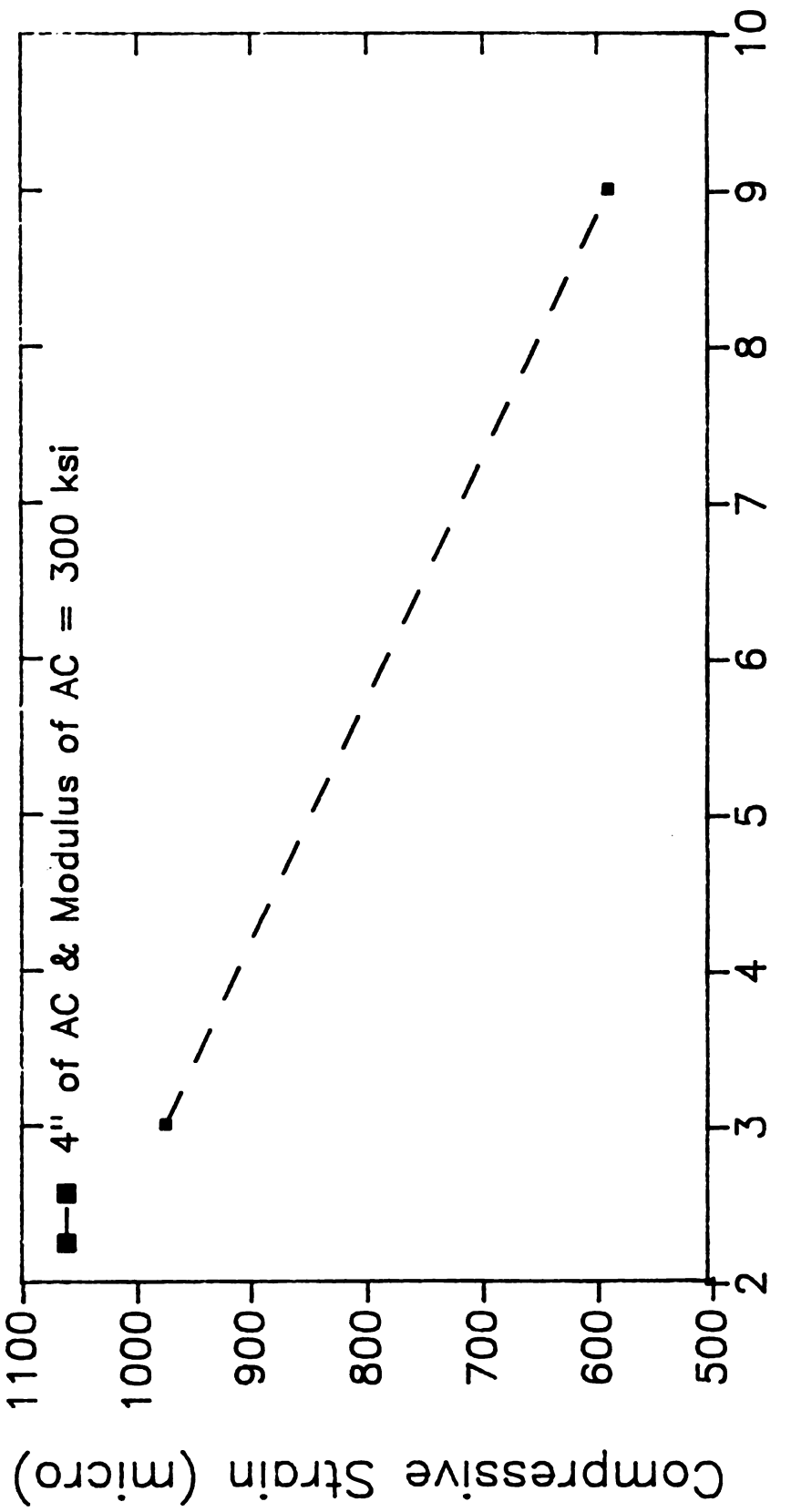

Figure 6—14: Compressive Strain at the Top of Roadbed Soil to Elastic Modulus of Roadbed Soil

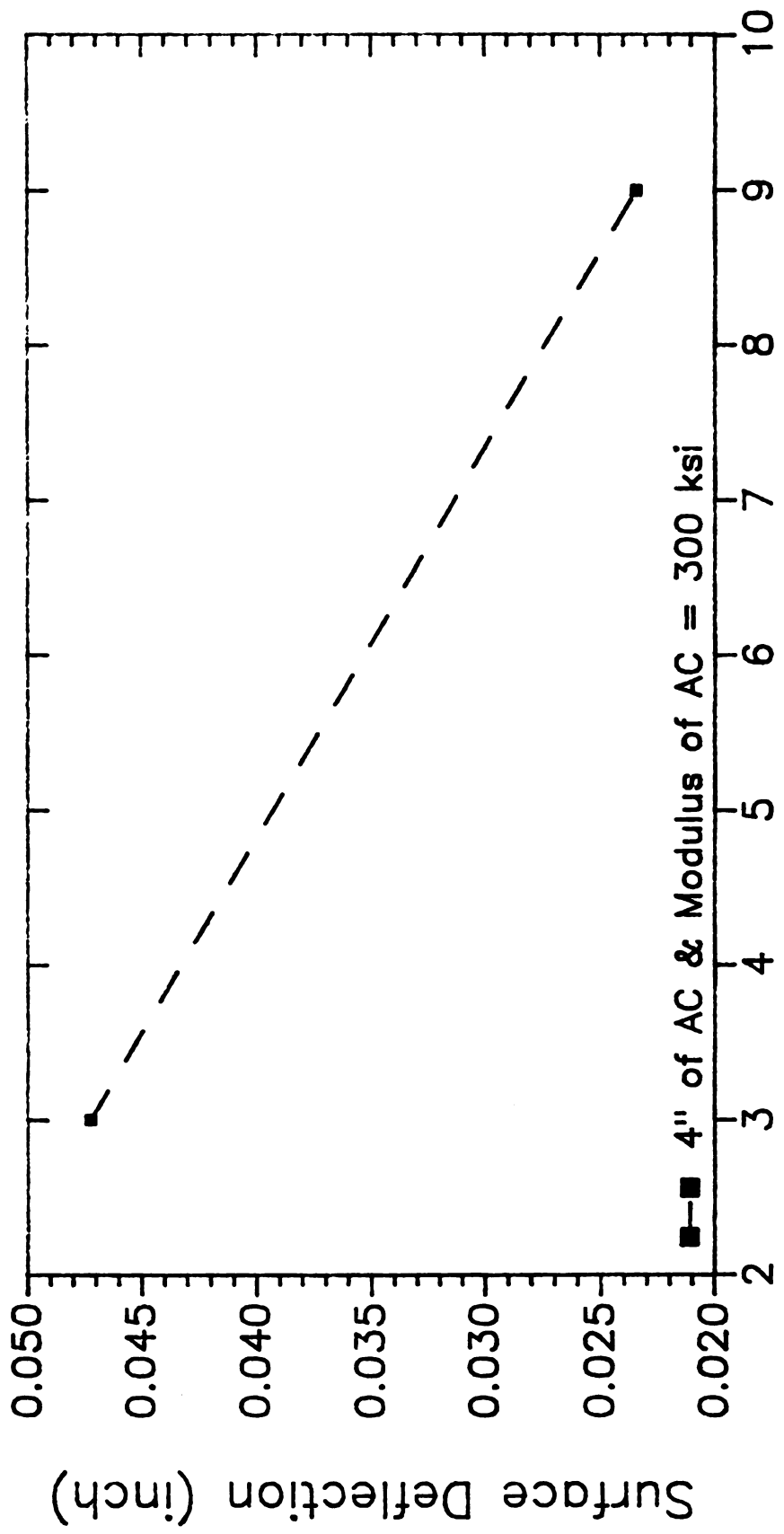

Figure 6-15: Surface Deflection at the Center of Loading to Elastic Modulus of Roadbed Soil

6.6.1 : Thickness of AC

Table 6-8 and Figure 6-16 show that increasing the thickness of the AC from 2 to 8 inches causes an increase in the fatigue life by a factor of about 74 for an AC with 150 ksi modulus, and by a factor of 122 for an AC with 500 ksi modulus. The proper thickness of the AC to be used in any pavement design will naturally depends on the pavement type, traffic level, and economic analysis.

Table 6-8: Effect of the thickness of the AC on the fatigue life of pavements.

Case	Thickness of AC (in)	K_1 value of Granular Layer (ksi)	Fatigue Life (ESAL)**	Factor*
1	2	4	134	
2	4		631	
3	8		9,970	74
7	2	4	328	
9	8		32,677	99.6
8	2	4	933	
10	8		114,230	122

* Factor is calculated by dividing the fatigue life for 8 inches of AC by the fatigue life for 2 inches of AC;

** ESAL represents the 18 kip equivalent single axle load.

6.6.2 : Air Voids in AC

Table 6-9 and Figure 6-17 show that when the thickness of the AC is 2 inches, decreasing its air voids from 7 to 3 percent only results in an increase in the fatigue life by a factor of about 7.0. When the thickness of the AC is 8 inches, decreasing its air voids from 7 to 3 percent causes an increase in the fatigue life by a factor of about 11.4. Since the percent air voids in a typical asphalt mix is mainly a function of compaction, higher fatigue life can be achieved by using

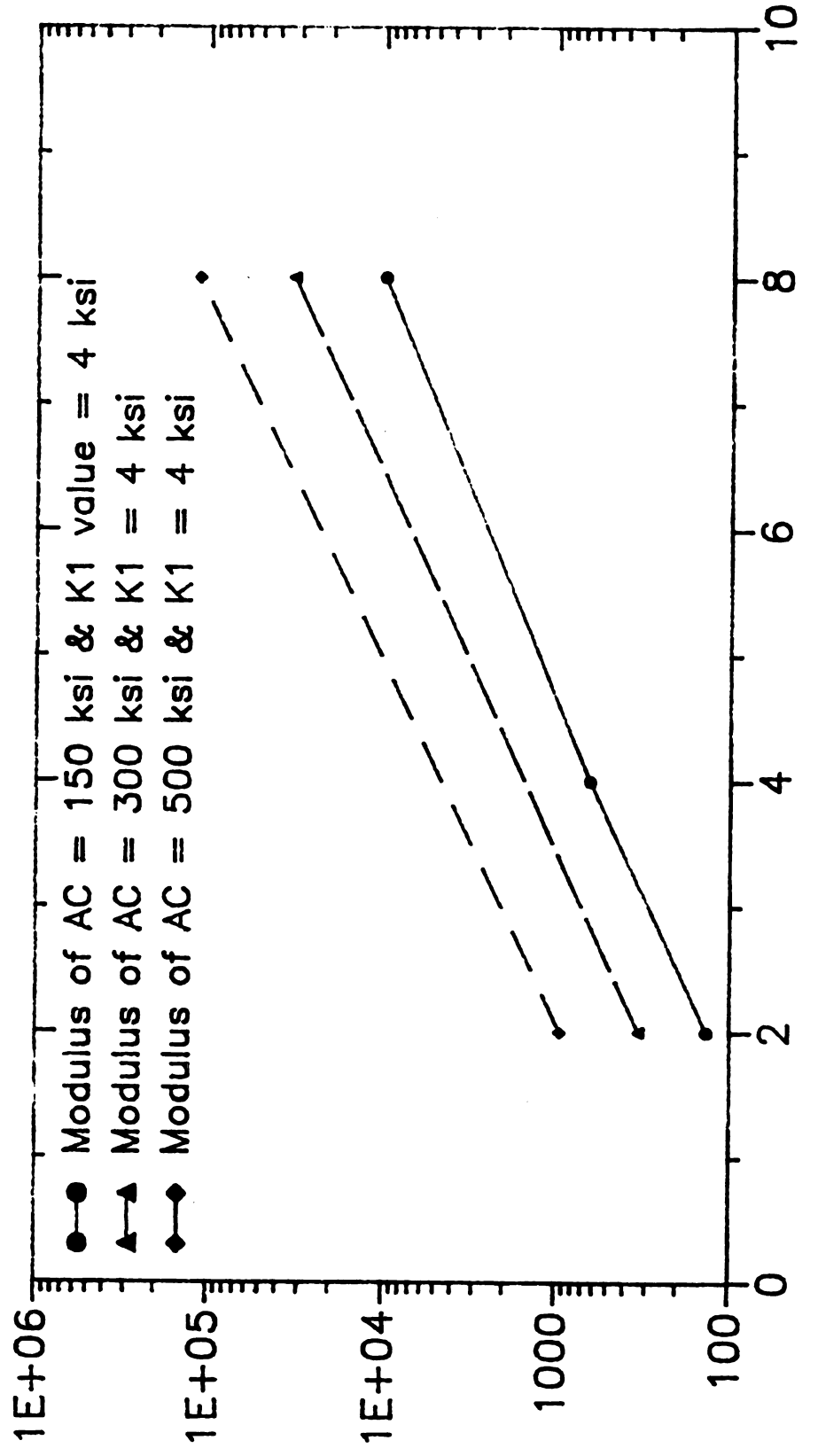

Figure 6—16 : Effect of AC Thickness on Fatigue Life

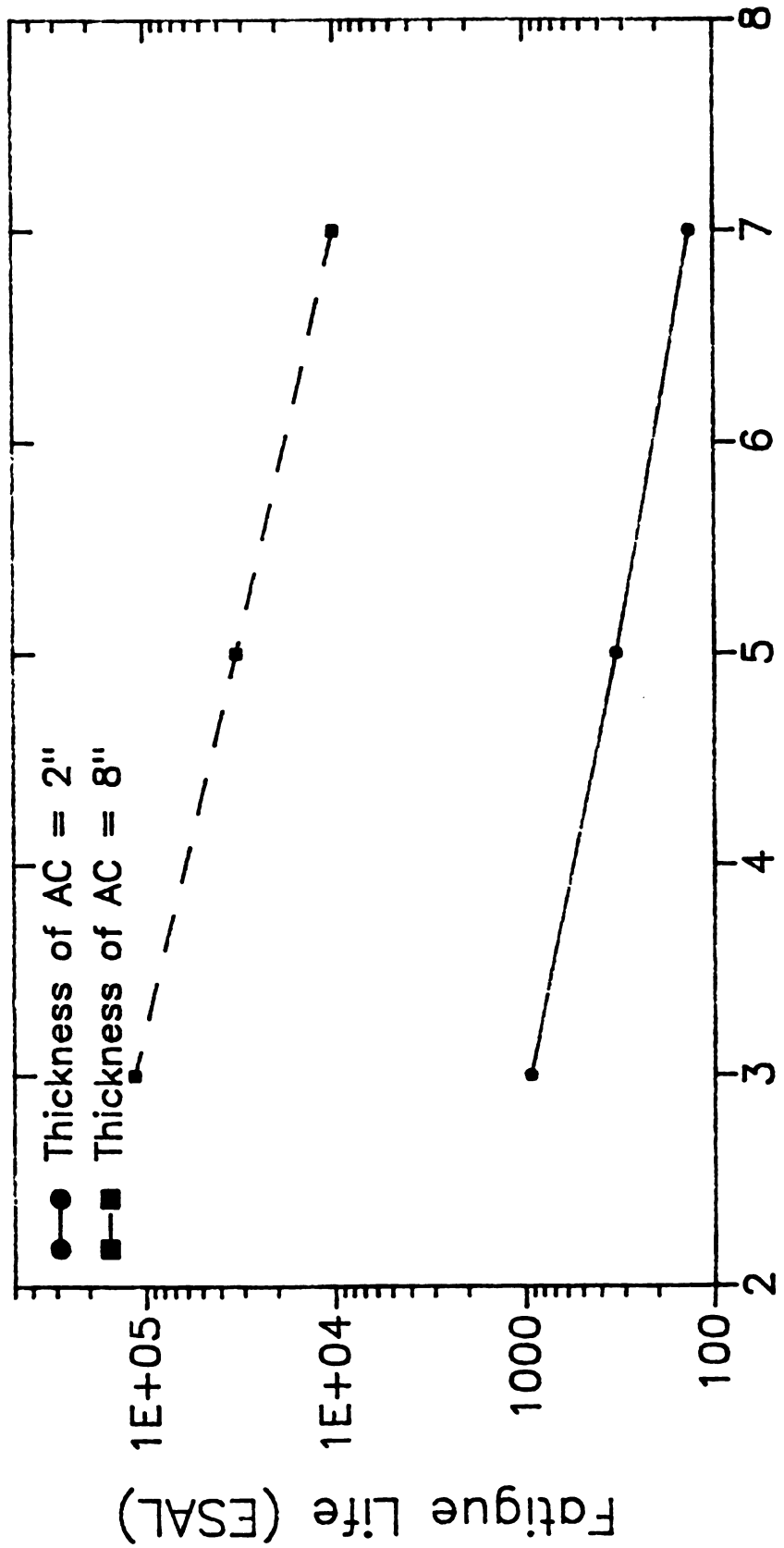

Figure 6—17 : Effect of Air Voids in AC on Fatigue Life

better compaction specifications and quality control.

Table 6-9: Effect of the air voids in the AC on the fatigue life of pavements.

Case	Air Voids of AC (%)	Modulus of AC (ksi)	Thickness of AC (in)	Fatigue life (ESAL)	Factor
1	7	150		134	
7	5	300	2	328	
8	3	500		933	7.0
3	7	150		9,970	
9	5	300	8	32,677	
10	3	500		114,230	11.4

6.6.3 : Thickness of Granular Layer

Figure 6-18 and Table 6-10 show that increasing the thickness of the granular layer from 6 to 9 to 12 inches cause an increase in the fatigue life by factors of 3.4 and 2.4, respectively.

Table 6-10: Effect of the thickness of the granular layer on the fatigue life of pavements.

Case	Thick. of G.L.* (in)	Thick. of AC(in)	E of AC(ksi)	K_1 Value G.L.(ksi)	Fatigue Life (ESAL)	Factor
15	6	4	150	12	8,318	
13	9	4	150	12	28,509	3.4
14	12	4	150	12	69,635	2.4

* G.L. is an abbreviation for the granular layer.

6.6.4 : Resilient Modulus of the Granular Layer

In general, higher resilient modulus of the granular layer causes higher fatigue life. However, the functional relationship between the resilient modulus of the granular material and the fatigue life is dependent upon the thickness of the AC layer. For example, Table 6-11 and Figure6-19 showthat increasing the resilient modulus of the granular material by a factor of 3 causes an increase in the fatigue life of a 4

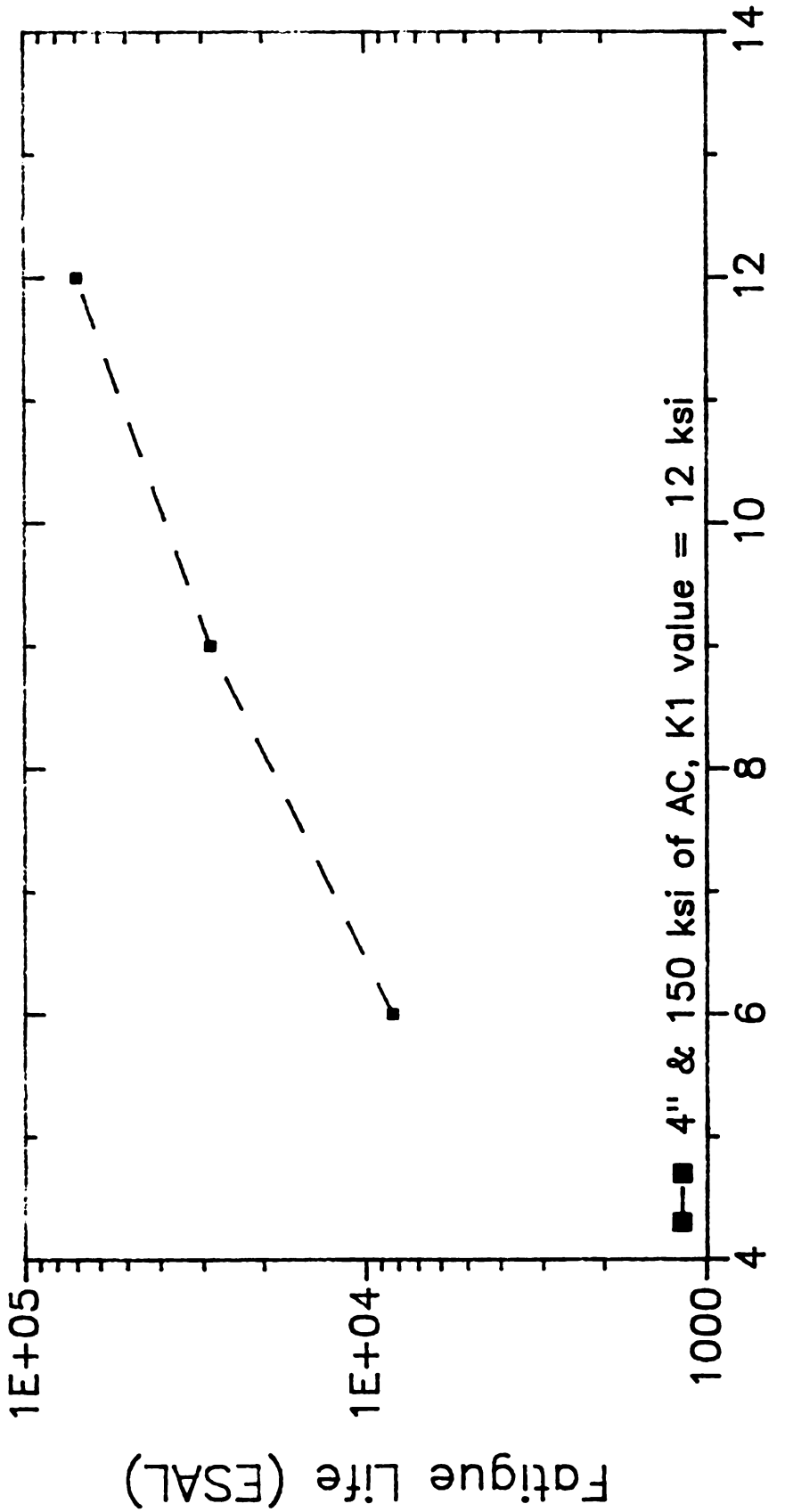

Figure 6—18 : Effect of Granular Layer Thickness on Fatigue Life

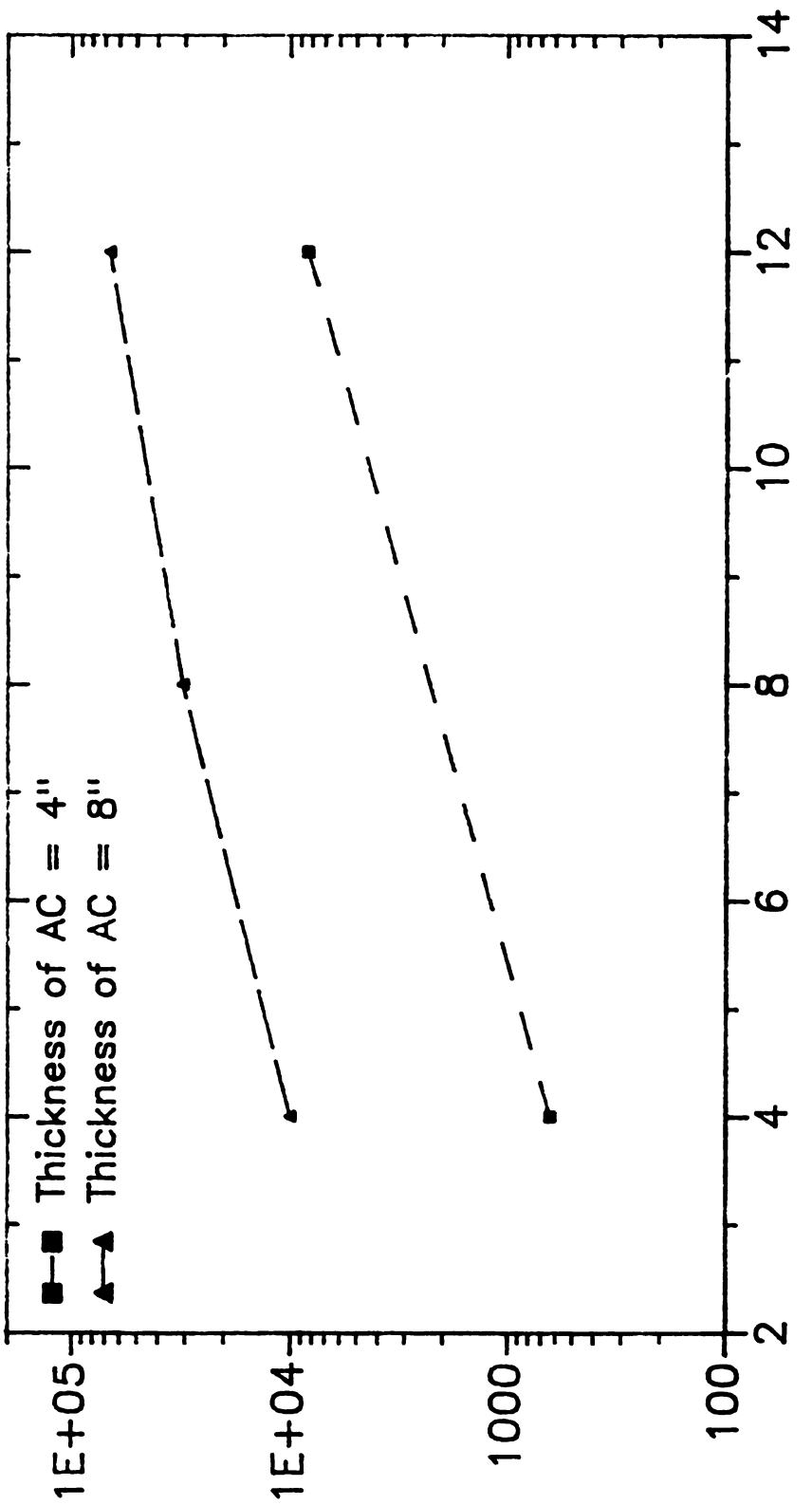

Figure 6—19 : Effect of K1 Parameter of Granular Layer on Fatigue Life

inch thick AC layer by a factor of 13.2 and by a factor of 6.6 for an 8 inch thick AC.

Table 6-11: Effect of the material properties of the granular layer on the fatigue life of pavements.

Case	K_1 Value of G.L. (ksi)	Equiv. MR. of G.L.(psi)	Thick. of AC (in)	Fatigue Life (ESAL)	Factor
2	4	19,153	4	631	
15	12	57,933	4	8,318	13.2
3	4	12,002	8	9,970	
5	8	24,960	8	30,622	
6	12	38,216	8	66,288	6.6

* Equiv. MR represents the equivalent resilient modulus of the granular layer (see section 5.2.2)

6.6.5 : Resilient Modulus of the Roadbed Soil

Although the resilient modulus of the roadbed has no significant effects on the tensile strain at the bottom of the AC layer (see section 6.5.5), it has significant effects on the pavement surface deflection and an the pavement fatigue life. Table 6-12 and Figure 6-20 show that for an 8 inch thick AC layer with 300 ksi modulus, increasing the resilient modulus of the roadbed soil from 3 to 9 ksi causes an increase in the fatigue life by a factor of 14.3. One important point should be noted is that the resilient modulus of the roadbed soil varies from season to season and relative to the moisture content. The resilient modulus to be used as an input to the fatigue life model should be the effective resilient modulus. The AASHTO 1986 design guide for flexible pavements contains detailed explanation concerning the calculation of the effective resilient modulus.

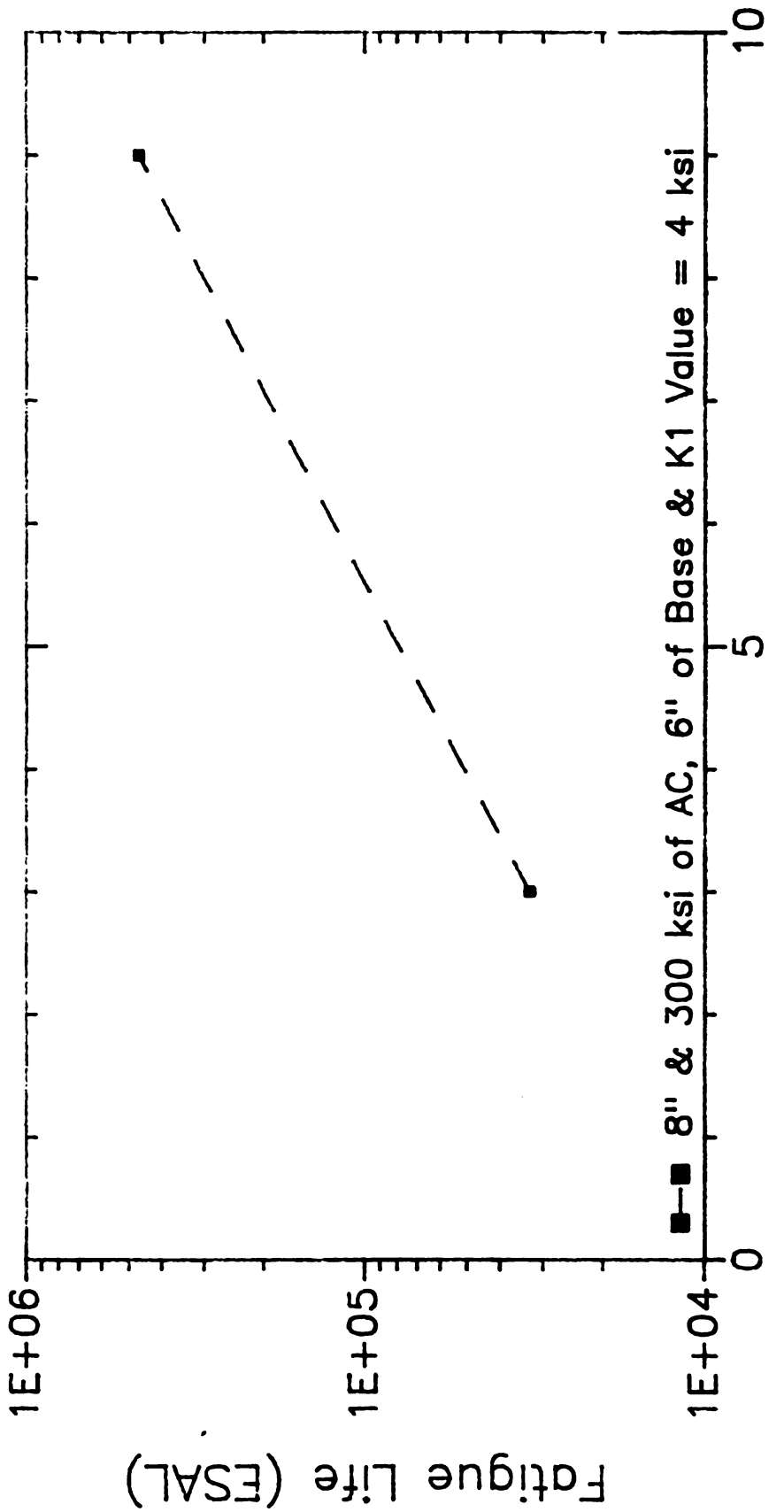

Figure 6–20 : Effect of Roadbed Soil Modulus on Fatigue Life

Table 6-12: Effect of the resilient modulus of the roadbed soil on the fatigue life of pavements.

Case	Modulus of R.S.* (ksi)	Thick. of AC (in)	Modulus of AC (ksi)	Fatigue Life (ESAL)	Factor
9	3	8	300	32,677	
18	9	8	300	467,143	14.3

R.S. represents the roadbed soil.

6.6 : EQUIVALENT WHEEL LOAD FACTOR

An equivalent wheel load factor (ELF) defines the damage per pass caused to a specific pavement section caused by an arbitrary vehicle relative to the damage per pass caused by a selected vehicle with an 18-kip single axle load moving on the same pavement section (Yoder, et al., 1975).

Deacon (1971) and Witczak (1973) showed that the equivalent wheel load factor F_j for any vehicle can be expressed by the following equation:

$$F_j = \left(\frac{\varepsilon_j}{\varepsilon_s} \right)^c \qquad \text{(Eq.6-5)}$$

where : c = constant between 3 and 6 with common values of 4 to 5;

ε_s = the tensile strain at the bottom of the AC under an 18-kip single axle load;

ε_j = the tensile strain at the bottom of the AC course due to any axle load.

Based on elastic layer analysis using CHEV5L program, Eq.6-5 cannot be applied for pavements with very thin AC layers in which the radial strain at the bottom of the AC may be compressive or only marginally

tensile. In addition, the damage delivered to a pavement section by a passing wheel load is functions of the thicknesses and properties of all pavement layers. Since, the pavement surface deflection is also functions of the properties and thicknesses of all pavement layers including the roadbed soil, it was thought that expressing the ELF in terms of the pavement surface deflection will yield more accurate results. Consequently, the surface deflection for several pavement sections and axle loads were calculated using the MICH-PAVE program (see Table 6-13). The results were then correlated to the AASHTO equivalent wheel load factor (EWLF). This resulted in the following equation:

$$ELF = \left(\frac{SD_j}{SD_s} \right)^{4.25} \qquad \text{(Eq.6-6)}$$

where: SD_s = surface deflection of pavement in inches due to an 18 kips single axle load or any other standard axle load;

SD_j = surface deflection of pavement in inches under an arbitrary wheel load.

The data (surface deflection) in Table 6-13 was obtained using the linear CHEV5L computer program with various wheel loads to compute the surface deflections of several pavement sections. The AASHTO equivalent wheel load factors were obtained using the structural number (SN) of each pavement section. Nevertheless, it can be seen that Equation 6-6 compares well with the AASHTO estimate. The advantages of equation 6-6 is that the ELF can be calculated at any time and for any season by simply conducting a nondestructive deflection testing. Since pavement deflection varies from season to season, with moisture content, and with pavement age, the ELF can be obtained for any time and any moisture or

seasonal conditionas. The AASHTO EWLF method, on the other hand, assumes, for each pavement section and axle load, a constant value throughout the pavement life and for all seasonal and/or moisture conditions.

Table 6-13 : Comparison of the equivalent wheel load factor between Equation 6-6 and the AASHTO method.

Case	Axle Load (kip)	Surface Deflection (inch)	EWLF	
			Eq.6-6	AASHO
6	4	0.01291	0.004	0.004
	10	0.02761	0.11	0.12
	18	0.04636	1.	1.
	30	0.07439	7.46	7.94
	40	0.09739	23.4	28.51
23	4	0.00487	0.003	0.003
	10	0.01079	0.097	0.09
	18	0.01868	1.	1.
	30	0.03024	7.75	6.9
	40	0.03957	24.3	21.6
10	4	0.01002	0.0005	0.004
	10	0.02236	0.11	0.1
	18	0.03791	1.	1.
	30	0.06176	7.96	6.83
	40	0.08178	26.2	22.50
14	4	0.01252	0.004	0.004
	10	0.02713	0.12	0.11
	18	0.04455	1.	1.
	30	0.06989	6.78	7.5
	40	0.09062	20.5	25.0
19	4	0.00493	0.003	0.004
	10	0.01088	0.01	0.1
	18	0.01884	1.	1.
	30	0.03053	7.78	6.83
	40	0.03996	24.4	22.50
28	4	0.00345	0.005	0.002
	10	0.00726	0.12	0.08
	18	0.01187	1.	1.
	30	0.01825	6.22	7.79
	40	0.02325	17.4	23.04

6.7 ; SUMMARY

The dominant factor in the fatigue life equation (Eq.6-3) for flexible pavements is the surface deflection under the wheel load rather than the tensile strain at the bottom of the AC. The surface deflection

under the wheel load is an intrinsic function of all input parameters, such as the thickness of the AC, air voids in the AC, thickness of the granular layer, modulus of the granular layer, modulus of the roadbed soil, wheel load, and tire pressure. Of these, the thickness of the AC and the modulus of the roadbed soil are the two dominant factors that affect the surface deflection. A summary of the sensitivity of the tensile strain at the bottom of the AC layer, the compressive strain at the top of the roadbed soil, and the pavement surface deflection due to the various pavement variables are presented in Table 6-14.

Table 6-14 : Sensitivity of some response measures to key properties of pavement sections.

	Tensile Strain	Compressive Strain	Surface Deflection
Thickness of the AC	sensitive	very sensitive	very sensitive
Air Voids in the AC	sensitive	insensitive	insensitive
Thickness of the Granular Layer	sensitive to an optimum thick.	sensitive	sensitive
Modulus of the Granular Layer	sensitive	insensitive	insensitive
Modulus of Roadbed Soil	insensitive	very sensitive	very sensitive

Equations 6-3 and 6-4 are strictly applicable to three- and/or four-layerpavement sections in which the AC is the toplayer that underlain by a granular (base and/or subbase) layer and a roadbed soil. The model should not be applied to pavement sections where a second asphalt layer is sandwiched between the base and subbase layers without verification and calibration. Nevertheless, equations 6-3 and 6-4 can be improved by

further calibration using field data. It is strongly recommended that the equations be checked using field data prior to their uses as predictive models.

When a thin AC layer is used in a pavement section, a compressive radial strain may occur at the bottom of the AC rather than a tensile radial strain. This is contrary to the normal design assumption. For such pavements, it is recommended that a response measure such as the surface deflection be used, instead of the the tensile strain at the bottom of the AC for designing the pavement.

CHAPTER 7

CONCLUSIONS AND RECOMMENDATIONS

7.1 : SUMMARY AND CONCLUSIONS

Two major achievements have been accomplished in this research. First, a new concept of utilizing a flexible boundary in flexible pavement analysis has been introduced, and its characteristics fully investigated. Second, an extremely "user-friendly" nonlinear finite element program for pavement analysis and design, named MICH-PAVE, has been implemented on personal computers.

The main findings of this research are outlined below:

(1) In the linear analysis of a multilayer pavement, the finite element mesh with a flexible boundary results in a decrease in the percentage error of the surface deflection when compared to the results obtained using a finite element mesh yielding about the same level of computational efforts. Other response quantities such as strains and strains are also improved.

(2) Sensitivity studies of the flexible boundary in linear analysis show that:

(a) for normal conditions (9 kip wheel load and 100 psi tire pressure), the optimal location of the flexible boundary is about 3 feet from the top of the roabed soil;

(b). when the tire pressure is increased to 120 psi, the optimal location of the flexible boundary is still about 3 feet from the top of the roadbed soil; and

(c). When the wheel load is increased to 12 kips, the optimal location of the flexible boundary is about 7 feet from the top of the roadbed soil.

Qualitatively, the flexible boundary should be placed deeper when the wheel load is large.

(3) Sensitivity studies of the flexible boundary in nonlinear analysis show that locating it at about 3 feet from the top of the roadbed soil yields the required accuracy (see Tables 4-5 and 4-6). However, It should be noted that when the wheel load was increased up to 12 kips, the MICH-PAVE program did not converge even after 25 iterations. This indicates that this pavement section becomes significantly nonlinear at this very high load, and is too weak for practical purposes. It also indicates that the algorithm being used converges well only for moderate levels of nonlinearity and may not converge for strongly nonlinear problems. This, however, should not be a cause for concern in normal practice.

(4) The axisymmetric finite element model is selected as the basic foundation for the development of a nonlinear finite element program to be implemented on personal computers.

(5) The resilient modulus model is selected to characterize the nonlinearity in granular and cohesive soils. The reasons for this are:

(a) the model reduces the complicated nonlinear response to a simple form and is easy to use;

(b) the resilient moduli of granular materials and roadbed soil can be determined by most state highway agencies; and

(c) the granular materials and roadbed soil still maintain their resilient behavior under repeated loads even after the occurrence of large permanent deformations.

(6) If only the FEM with the resilient modulus model is used, it will converge extremely slowly. Therefore, the Mohr-Coulomb failure criterion is applied with the resilient modulus model. The Mohr-Coulomb failure criterion is used to modify the principal stresses in each element in the granular layers and roadbed soil after each iteration.

(7) In order to minimize the influence of boundary interactions, the equivalent modulus for the halfspace below flexible boundary is calculated by averaging the resilient moduli of all bottom elements except for the three elements which are closest to the right vertical boundary. The equivalent modulus approximately accounts for the displacements of the halfspace.

(8) The MICH-PAVE program automatically generates the finite element mesh along both the radial and vertical directions. The default mesh may, however, be changed by the user.

(9) The MICH-PAVE program includes the gravity stress arising from the weight of the materials and approximately accounts for the lateral "locked in" stress due to compaction.

(10) The MICH-PAVE program uses extrapolation to improve the radial and tangential stresses, and vertical strains at layer boundaries, and uses interpolation to improve the vertical, and shear stresses at layer boundaries (see Section 4.4.4).

(11) An equivalent resilient modulus for each layer is obtained as the average of the moduli of the finite elements in the layer that lie

within an assumed 2:1 load distribution zone. These equivalent moduli may be used in any analyses utilizing linear elastic layer programs.

(12) Comparison of results from the MICH-PAVE and ILLI-PAVE programs indicate that the stresses obtained from both programs are very close. However, the displacements from MICH-PAVE are about 12% larger than those from ILLI-PAVE. Based on exact solutions from linear analysis, the flexible boundary used in MICH-PAVE is expected to give better deflection estimates than the deep fixed boundary used in ILLI-PAVE.

(13) The fatigue life (Eq.6-3) and rut depth (Eq.6-4) equations offer a preliminary concept of how empirical equations may be used together with the FEM to design flexible pavements. At the present time, these equations have only been calibrated on three and four layer pavement sections consisting of an asphalt concrete upper layer, a granular middle layer (base, or base with subbase), and a cohesive roadbed soil bottom layer. It may not be accurate to use these equations for different pavement sections.

(14) The dominant factor in the fatigue life equation (Eq.6-3) of flexible pavements is the surface deflection under the wheel load rather than the tensile strain at the bottom of the AC. The surface deflection under the wheel load is an intrinsic function of all input parameters, such as the thickness of the AC, air voids in the AC, thickness of the granular layer, modulus of the granular layer, modulus of the roadbed soil, wheel load, and tire pressure. Of these, the thickness of the AC and the modulus of the roadbed soil are the two dominant factors that affect the surface deflection. However, in the rut depth equation (Eq.6-3), the average annual temperature is the dominant factor.

(15). When a thin AC layer is used in a pavement section, a compressive radial strain may occur at the bottom of the AC rather than a tensile radial strain. This is contrary to the normal design assumption. For such pavements, it is recommended that a response measure such as the surface deflection be used, instead of the fatigue life, for designing the pavement.

(16). The tensile strain failure model (Eq. 6-5) used to predict the equivalent wheel load factor (EWLF) cannot be applied for the pavement with a very thin AC layer in which the radial strain at the bottom of the AC may be compressive or only marginally tensile. However, a reasonable estimate of the EWLF can still be obtained by using the surface deflection of the pavement section instead of the tensile strain at the bottom of the AC (see Eq. 6-6).

7.2 : RECOMMENDATIONS FOR FUTURE RESEARCH

Based on the results of this research, the following recommendations for future research are suggested.

(1) At the present time, the MICH-PAVE program considers only the linear response of the asphalt concrete. In reality, asphalt concrete is a nonlinear viscoplastic material. It is very difficult to simulate all of the complex behavior of asphalt concrete. However, the viscoelastic model can be used to closely simulate the response of asphalt concrete. Also, temperature is a very important factor affecting the behavior asphalt concrete, but it is not intrinsically considered in the current version of MICH-PAVE. Therefore, it is recommended that the viscoelastic model and a temperature sensitive description of material properties for

the asphalt concrete be incorporated in the future.

(2) The major limitations of the axisymmetric FE model are that it cannot represent the multiple wheel loads and consider the edge effects. Only three-dimensional FE analysis can fully represent these effects. However, a three-dimensional analysis requires large amounts of memory and computational time. If the concept of the flexible boundary is used with the new generation of engineering workstations that are under development, then it may be possible to make available a three-dimensional analysis program for daily use by design engineers.

(3) The shear and volumetric stress-strain relationship (also called the coutour model) is a more accurate material model for granular layers and roadbed soils, because it considers the stress path dependent responses of these materials. However, most state highway agencies do not presently own the sophisticated equipment required to estimate the material constants required for such a model. When suitable equipment becomes available, more sophisticated material models may be used in the analysis.

(4) Both the fatigue life and rut depth equations need to be improved considerably when additional field data becomes available. At the present time, equations 6-3 and 6-4 are strictly applicable to three or four layer pavement sections consisting of an asphalt concrete upper layer, a granular middle layer (base, or base with subbase), and a cohesive roadbed soil bottom layer. It is desirable to have fatigue life and rut depth equations that can be applied on more general pavement sections. Futher research is required to establish these.

APPENDIX

OUTLINE OF COMPUTER PROGRAM

The MICH-PAVE program is written in the FORTRAN language and includes several source files. The source files are written for version 4 of the Microsoft FORTRAN compiler. The graphics part uses the GRAFMATIC package available from Microcompatibles, Inc., 301 Prelude Drive, Silver Spring, Maryland 20901, Phone: (301) 593-0683. The program is made up of two parts. The first contains subroutines for user-friendly screen manipulations, and the second contains subroutines for the finite element analysis. For convenience, a "make" file named **MICHPAVE.MAK** has been prepared to compile each source file into an object file, and to link all object files together into an executable file (MICHPAVE.EXE).

The function of each subroutine is explained in the following section.

Subroutines	Function
1. THE MAIN PROGRAM	Call appropriate subroutines to perform the following functions: 1. Show the overview screen; 2. Create a new data file; 3. Change a current data file; 4. Modified an existing data file; 5. Perform analysis; 6. Type summary results on screen; 7. Plot results on screen; 8. Print results on printer; 9. Exit-return to DOS.

2. FORM — Move cursor to the field IFLD and display alphanumeric keys. It also determines the next field to move to if a cursor movement key is pressed.

3. SCREAD — Read a variable of length LNTH located at screen position (ICOL,IROW).

4. CTGRY — Determine the category of a single keyboard entry.
   Functions = 1;
   Cursor movement (except left and right) = 2;
   Numbers (also ., +, -, e and E) = 3;
   Letters = 4;
   Ins, Del, Backspace, Cursor left and right = 5;
   Others = 0.

5. DRAWMU — Draw boxes and write texts for the called menus.

6. CLEAR — Clear the screen and color it blue.

7. ERROR — Display an error message on the bottom screen line.

8. BOX — Draw a single or double line box.

9. CHKFIL — Check for the existence of an input/output file.

10. CHKDAT — Check the crucial part of the input data before analysis and plotting.

11. CHKLAY — Check the input sequence.

12. INIMU2 — Initialize all input or calculated data.

13. OPENFI — Check whether or not input file is opened.

14. OPENPT — Check whether the data file required for plotting figures on the screen exists.

15. TOPSCR — Show the initial screen.

16. MENU — Generate the main menu.

17. HELP Create the screen showing an overview of the program.
18. PLOTMS Draw the finite element mesh on the screen.
19. INIDA Generate the screens for the required initial data, such as input and output filenames, wheel load, etc., and/or subcreen for the fatigue life and rut depth data.
20. INIDA1 Define the input form for the initial data, such as wheel load, tire pressure, etc..
21. INIDA2 Read the initial data from INIDA1.
22. WRINIDA Write the initial data, such as wheel load, tire pressure, etc., on the screen.
23. FALIFE Define the input form for fatigue life and rut depth data.
24. FTLF2 Read the fatigue life and rut depth data from FALIFE.
25. WRFL Write the data of fatigue life and rut depth on the screen.
26. FTSUM Generate the screen for the results of fatigue life and rut depth.
27. MATTYP Define the layer type for each layer.
28. MATP1 Define the input form for the layer type.
29. MATP2 Read the layer type from MATP1.
30. WRMAT Write the layer type for each layer on the screen.
31. MATPRP Define up to three material properties as outlined below
    1. Subroutine ELSPRP for linear elastic material (generally asphalt concrete);
    2. Subroutine GRAPRP for granular materials (base and subbase);
    3. Subroutine COHPRP for cohesive materials (roadbed soils).

32. COHPRP Define the input form for properties of cohesive materials.

33. COH1PRP Read properties of cohesive materials from COHPRP.

34. WRCOH Write properties of cohesive materials on the screen.

35. GRAPRP Define the input form for properties of granular materials.

37. GRA1PRP Read properties of granular materials from GRAPRP.

38. WRGRA Write properties of granular materials on the screen.

39. RDELPR Read the linear elastic material properties from ELSPRP.

40. ELSPRP Define the input form for linear elastic material properties.

41. WRELS Write properties of linear elastic material on the screen.

42. CROSSVH Generate the menu for the number and locations of required horizontal and vertical sections.

43. WRCRVH Write the number of horizontal and vertical sections on the screen.

44. CROSV Define the input form for the locations of required vertical sections.

45. CROSV1 Read the locations of required vertical sections from CROSV.

46. WRCROV Write the locations of the vertical sections on the screen.

47. CROSH Define the input form for the locations of required horizontal sections.

50. CROSH1 Read the locations of required horizontal sections from CROSH.

51. WRCROH Write the locations of the horizontal sections on the screen.

52. CROSS Define the input form for the number of required horizontal and vertical sections.

53. CRO1 Read the number of horizontal and vertical sections from CROSS.

54. OPTIMAL Find the optimal locations for the required vertical and horizontal sections.

55. MODFM Modify the finite element mesh in the vertical and horizontal directions.

56. MOFMV Define the locations and number of elements in the vertical direction.

57. MOFMV1 Read the number of elements in the vertical direction from MOFMV.

58. WRMFMV Write the number of elements in the vertical direction on the screen.

59. MOFMH Define the locations and number of elements in the horizontal direction.

60. MOFMH1 Read the number of elements in the horizontal direction from MOFMH.

61. WRMFMH Write the number of elements in the horizontal direction on the screen.

62. DEFMESH Define the default values of the finite element mesh.

63. MICHPAVE This is main computation part which reads and writes all necessary data, and performs the analysis.

64. GENTN Calculate the total nodal points, elements, and boundary nodal points of the finite element mesh.

65. EDGELD Convert the wheel load to the equivalent nodal forces.

66. MATERIAL Find the initial elastic moduli and gravity stresses for every element.

67. GRAVITY Calculate the gravity stresses of every element in the asphalt concrete layer.

68. YGM1 Calculate the gravity stresses and initial elastic moduli of every element in granular layers.

69. YGM2 Calculate the gravity stresses and initial elastic moduli of every element in roadbed soils. The initial elastic modulus of each element is set equal to the value of K_2.

70. AUTOGEN FInd the nodes [LNODS(I,J)], nodal coordinates [COORD(I,J)], boundary nodes [NOFIX(I)], boundary conditions [IFPRE(I,J); 0 = free, 1 = fixed], and equation number of every nodes in the FE mesh.

71. BAND Calculate the bandwidth of the global stiffness matrix.

72. PRCALC Calculate Poisson's ratio for every element.

73. SPRING Compute the flexibility and stiffness matrices for a half-space loaded with a finite number of ring loads. The rings are approximated by a thin annulus. Loading on tributary area is used for diagonal terms. The first and last nodes have only a vertical d.o.f., while all other nodes have both radial and vertical d.o.f.

74. SMATINV Invert a real symmetric matrix. Subroutine is adapted from "Computer Program for Filtering and Spectral Analysis," by M.T. Silvia and E.A. Robinson, Elsevier, 1979, pp. 190.

75. SPF Calculate the nodal forces of the flexible boundary, and store those values in the global force vector.

76. DCALC Calculate the material matrix D(4,4).

77. SHAPE Calculate the shape functions and their derivatives, and Jacobian matrix, its inverse and determinant, and [B] matrix in the r-z coordinates.

78. QUAD4 Generate the element stiffness matrix [k], and store it in the array SE.

79. ASSEM Assemble the local element stiffness matrices into the global stiffness matrix [S], and the local force matrices [ELOAD] into the global force vector (RRG). Store the global stiffness matrix in the banded form.

80. ADD Add the flexible boundary stiffness matrix [SPSTIFF] into the global stiffness matrix.

81. GAUSSEL Use Gauss elimination to solve the stiffness equations, and then find the displacement vector (RG).

82. STRMDF Add the gravity stress to the vertical stress, and add the lateral stress to the radial and tangential stresses.

83. AVERE Find the equivalent modulus for the halfspace below the flexible boundary. The modulus is calculated by averaging the resilient moduli of all bottom elements except for the three elements closest to the right vertical boundary.

84. CHECMR Check that the calculated principal stresses don't exceed the Mohr-Coulomb failure criterion.

85. RM Calculate the resilient moduli of all elements in the granular layers.

86. RM1 Calculate the resilient moduli of all elements in the roadbed soils.

87. FORCE Calculate the strain vector {STN}, stress vector {STRS}, and nodal force vector {F} for all elements, and calculate the convergence error.

88. RECSTR Recover the global stresses which are used in subroutines FORCE, STR1, and STR2, from the modified principal stresses.

89. PRST Calculate the principal stresses and the principal directions in one element.

90. STR1 Calculate the displacements, stresses, and strains at the middle point of elements for the selected horizontal sections.

91. STR2 Calculate the displacements, stresses, and strains at the middle point of elements and at layer boundaries for the selected vertical sections.

92. EXTRAPO Use extrapolation to modify the radial and tangential stresses, and vertical strains at interfaces.

93. INTERPO Use interpolation to modify the vertical and shear stresses.

94. STRCAL Calculate the displacements, stresses, and strains at a specific point in the selected vertical sections.

95. EAVER Use the 2:1 load distribution zone to calculate the equivalent resilient moduli of granular layers and roadbed soils.

96. PLINE Draw a horizontal line in the output file.

97. FATIGUE Use the empirical equations to calculate the fatigue life and rut depth of the design pavement section.

98. PLOTVH Generate the screen menu for plotting the results of required vertical and horizontal sections.

99. PLOTV Generate the screen submenu for plotting the stresses, strains, and displacements along the vertical sections.

100. PLOTH Generate the screen submenu for plotting the stresses, strains, and displacements along the horizontal sections.

101. PLTVERT Read the stresses, strains, and displacements along the vertical sections from data files.

102. PLTHORI Read the stresses, strains, and displacements along the horizontal sections from data files.

103. PLTHSD Plot the stresses, strains, and displacements along the horizontal sections.

104. STRSSPLT Plot the displacements, stresses, and strains along the selected vertical sections.

105. AUTOSCL Determine the starting and ending values to be used in subroutines STRSSPLT and PLTHSD.

List of References

American Association of State Highway Officials, " AASHO Intermin Guide For Design of Pavement Structures 1972," *AASHO, AASHO committee on Design*, Wahington, D. C., 1972.

American Association of State, Highway, and Transportation Officials, "AASHTO Guide for Design of Pavement Structures," *AASHTO*, Washington, D. C., 1986.

American Association of State, Highway, and Transportation Officials, "DNPS86, a Computer Program to Perform the AASHTO Design Procedure, 1986," *AASHTO*, Wahington,D.C., 1986.

Baladi, G.Y., "In-Service Performance of Flexible Highway Pavement," *International Air Transportation Conference*, Vol. 1, ASCE, 1979, PP. 16-32.

Baladi, G., "Fatigue Life and Permanent Deformation Characteristics of Asphalt Concrete Mixes," *Transportation Research Board*, 68th Annual meeting, Page No. 880497, January 1989.

Baladi, G.Y., and Snyder, M., "Highway Pavements," *A Four Week Course Developed for the FHWA*, January, 1989.

Barksdale, R.D., and Hicks, R.G., "Material Characterization and Layered Theory for Use in Fatigue Analysis," *Highway Research Board*, Special Report 140, 1973, PP. 20-49.

Bathe, K.J., Wilson, E.L., and Peterson, F.E., " SAP IV: A Structural Analysis Program for Static and Dynamic Response of Linear Systems," University of California, Berkeley, 1973.

Bathe, K.J., and Wilson, E.L., "Numerical Methods in finite Element Analysis," *Prentice - Hall*, Englewood Cliffs, N. J., 1976.

Boyer, R.E., "Predicting Pavement Performance Using Time-Dependent Transfer Functions," *Joint Highway Research Project*, Prudue University and Indiana State Highway Commission, September, 1972.

Brown, S.F., and Pappin, J.W., "Analysis of Pavements with Granular Bases", *Transportation Research Record* 810, 1981, PP. 17-23.

Chen, W.F. and Saleeb, A.F., "Constitute Equations for Engineering Materials," *John Wiley & Sons, Inc.*, Vol. 1, New York, 1982, PP. 516-525.

Chou, Y.T., "An Interative Layered Elastic Computer Program for Rational Pavement Design," *Federal Aviation Administration*, FAA-RD-75-226, Feburary 1976.

Claessen, A.I.M., Edwards, J.M., Sommer, P., and Uge, P., "Asphalt Pavement Design, The Sell Method," *Proceedings of Fourth International Conference on the Structural Design of Asphalt Pavements*, Vol. 1, University of Michigan, August 1977.

Cook, R.D., "Concepts and Applications of Finite Element Analysis," *John Wiley & Sons, Inc.*, Second Ed., New York, 1981. PP. 29-45, 113-124.

Corps of Engineers, "Revised Method of Thickness Design for Flexible Highway Pavements at Military Installations," *Waterways Experiment Station*, Technical Resport 3-582, August, 1961.

Deacon, J.A., "Equivalent Passages of Aircraft with Respect to Fatigue Distress of Flexible Airfield Pavements," *Proceedings*, AAPT, Vol. 40, 1971.

Dehlen, G.L., and Monismith, C.L., "Effect of Nonlinear Material Response on the Bahaviour of Pavements under Traffic," *Highway Research Board* 310, Wahington, D. C., 1970.

De Jong, D.L., Peutz, M.G.F., and Korswagen, A.R., "Computer Program BISAR Layered Systems under Normal and Tangential Surface Loads," *Kominklijke/Shell-Laboratorium*, Amsterdam, External Report AMSR.0006.73, 1973.

Duncan, J.M., Monismith, C.L., and Wilson, E.L., "Finite Element Analysis of Pavements," *Highway Research Record*, No. 228, Highway Research Board, Washington, D. C., 1968, PP. 18-33.

Duncan, J.M., and Chang, C.Y., "Nonlinear Analysis of Stress and Strain in Soils," *Journal of the Soil Mechanics and Foundation*, Proceeding of the American Society of Civil Engineers, September 1970, PP. 1629-1653.

Dysli, M., and Fontana, A., "Deformations around the Excavations in Clayey Soil," *International Symposium on Numerical Mehtods in Geomechanics*, September 1982, PP. 634-642.

ERES Consultants, Inc. etc., "Pavement design Principal and Practices," *ERES Consultants, Inc.*, Champaign, Illinois, *National Highway Institute*, Washington, D. C., 1987.

Harichandran, R., and Yeh, M.S., "Flexible Boundary in Finite Element Analysis of Pavements," *Transportation Research Board*, 67th Annual Meeting, Paper No. 870116, January 1988.

Haynes, H.J., and Yoder, E.J., "Effects of Repeated Loading on Gravel and Crushed Stone Base Course Materials Used in the AASHO Road Test," *Highway Research Record*, No. 39, Highway Research Board, Washington, D. C., 1963, PP. 82-96.

Hicks, R.G., and Monismith, C.L., "Prediction of the Resilient Response of Pavements Containing Granular Layers Using Non-Linear Elastic Theory," *Proceedings of Third International Conference on the Structural Design of Asphalt Pavements*, London, English, 1972.

Highter, W.H., and Harr, M.E., "Predicting Pavement Performance," *Journal of Transportation*, ASCE, May, 1974.

Huffred, W.L., and Lai, J.S., "Analysis of N-Layered Viscoelastic Pavement System," Report No. FHWA-RD-78-22, *Federal Highway Administration*, Washington, D. C., January 1978.

Ioannides, A.M., and Donnelly, J.P., "Three-Dimensional Analysis of Slab on stress dependent Foundation," *Transportation Research Board*, 67th Annual Meeting, Paper No. 870092, January 1988.

Janbu, N., "Soil Compressibility as Determined By Oedometer and Triaxial Tests," *Proceedings European Conference on Soil Mechanics and Foundation Engineering*, Wiesbaden, Germany, Vol. 1, 1963, PP. 19-25.

Ko, H.Y., and Masson, R.M., "Nonlinear Characterization and Analysis of Sand," *Numberical Methods in Geomechanics*, Vol. 1, Edited by Desai, C. S., 1976. PP. 294-305.

Kopperman, S., Tiller, G., and Tseng, M.T., "ELSYM5 Interactive Microcomputer Version, User's Manual, IBM-PC and Compatible Version," *FHWA*, Final Report, Contract No. DTFH61-85-C-00051, September, 1985.

Kujawski, J., and Wibery, N.E., "Thick Plates on Multi-Layered Soil, a semianalytical 3D FEM - Solution," *International on Numerical Models in Geomechanical*, Zurich, September 1982, PP. 693-702.

National Crushed Stone Association, "Flexible Pavement Design Guide for Highways", *NCSA* Publication, Washington, D. C., 1972.

Poulos, H.S., and Davis, E.H., "Elastic Solutions for Soil and Rock Mechanics," *Wiley*, New York, 1974.

Raad, L., and Figueroa, J.L., "Load Response of Transportation Support System," *Transportation Engineering Journey*, ASCE, Vol. 106,1980, PP. 111-128.

Seed, H.B., Chan, C.K., and Lee, C.E., "Resilience Characteristics of Subgrade Soils and Their Relation to Fatigue Failures in Asphalt Pavements," *Proceedings*, First International Conference on the Structural Design of Asphalt Pavements, Ann Arbor, August 1962, PP. 77-113.

Soussou, T.E., Moavenzadeh, F., and Findakly, H.K., "Synthesis of Rational Design of Flexible Pavements," *Civil Engineering Dept. Report, Massachusetts Institute of Technology*, January 1973.

Swami, S.A., , Goetz, W.H., and Harr, M.E., "Time and Load Independent Properties of Bituminous Mixtures," *Highway Research Board* 313, 1970, PP. 63-78.

The Asphalt Institute, "Thickness Design-Asphalt Pavements for Highways and Streets," *The Asphalt Institute*, Manual Series No. 1 (MS-1), September 1981.

The Asphalt Institute, "Computer Program DAMA: User's Manuel," *The Asphalt Institute*, CP-1, October, 1983.

Thompson, M.R., "ILLI-PAVE, User's Manual," *Transportation Facilities Group, Dept. of Civi Engineering, University of Illinois*, November 1986.

Witczak, M. W., "Prediction of Eqvivalent Damage Repetitions from Aircraft Traffic Mixtures for Full Depth Airfield Pavements," *Proceedings", AAPT, Vol. 42, 1973.*

Yoder, E.J., and Witczak, M.W., "Principal of Pavement Design," *John Wiley and Sons, Inc.*, 2nd. Edition, New York, 1975.

Young, M.A., and Baladi, G.Y., "Repeated Load Triaxial Testing, State of the Art," *Michigan State University*, March 1977.